

Dissertation zur Erlangung des Doktorgrades
der Fakultät für Chemie und Pharmazie
der Ludwig-Maximilians-Universität München

Influence of the Chemical Structure on the Fluorescence Lifetime of Dicarboxylic Imides and Oligothiophenes

Thorben Schlücker

aus

München, Deutschland

2016

Erklärung

Diese Dissertation wurde im Sinne von § 7 der Promotionsordnung vom 28. November 2011 von Herrn Prof. Dr. Heinz Langhals betreut.

Eidesstattliche Versicherung

Diese Dissertation wurde eigenständig und ohne unerlaubte Hilfe erarbeitet.

München, 21. Oktober 2016

Thorben Schlücker

Dissertation eingereicht am 21.10.2016

1. Gutachter: Prof. Dr. Heinz Langhals
2. Gutachter: Prof. Dr. Manfred Heuschmann

Mündliche Prüfung am 16.12.2016


Acknowledgement

Seneca vermeldete er sei dankbar, nicht weil es vorteilhaft sei, sondern weil es Freude mache. Mit eben dieser Freude danke ich allen, die mich auf dem Weg meiner Promotion begleitet und diese eben dadurch erst möglich gemacht haben.

Die vorliegende Arbeit entstand in der Zeit von Mai 2012 bis Dezember 2016 am Department Chemie und Pharmazie der Ludwig-Maximilians-Universität München unter Anleitung von Herrn Prof. Dr. Heinz Langhals. Zuvorderst bedanke ich mich herzlichst bei Ihnen, Herr Prof. Dr. Heinz Langhals, für die freundliche Aufnahme in Ihren Arbeitskreis, die interessante Themenstellung und ausgezeichnete fachliche Unterstützung. Ihre dauernde Diskussionsbereitschaft und große Nähe zu Ihren Mitarbeitern haben mich beeindruckt und sehr gefreut. Mein Dank geht auch an Prof. Dr. Manfred Heuschmann für die freundliche Übernahme des Co-Referats. Ebenfalls danke ich den übrigen Mitgliedern der Prüfungskommission Prof. Dr. Konstantin Karaghiosoff, Dr. Henry Dube, Prof. Dr. Rudolf Knorr und Dr. Dina Fattakhova-Rohlfing für Ihre Zeit und Mühe. Ich bedanke mich bei allen Mitarbeitern des Arbeitskreises für ihr kollegiales Verhalten und ihre Hilfsbereitschaft. Im Besonderen möchte ich mich bei meinen Laborkollegen Dr. Dominik Zgela, Moritz Eberspächer und Markus Herman, aber auch bei Ludwig Huber und Kevin Weiland für die angenehme Atmosphäre bedanken, die so manchen langen Labortag kurz erscheinen ließ. Für die zahlreichen Analysen und Messungen bedanke ich mich bei Claudia Dubler und Dr. David Stephenson für die Aufnahme der NMR-Spektren und bei Susanne Sauerer und Robert Eicher für die Elementaranalysen. Brigitte Breitenstein, Carola Draxler, Dr. Werner Spahl und besonders Sonja Kosak danke ich herzlich für die äußerst schnelle Durchführung der Massenspektrometrie. Dr. Moritz Ehrl und Prof. Dr. Pablo Docampo danke ich für die freundliche Unterstützung in technischen Belangen zur Messung von Fluoreszenzlebensdauern. Außerdem möchte ich meine Dankbarkeit gegenüber allen Bachelor- und PraktikumsstudentInnen aussprechen, die mich zumindest stets Geduld und Nachsicht gelehrt haben, ohne deren Engagement die Arbeit aber sicher auch weniger Freude und Kurzweil bedeutet hätte. Nicht zuletzt danke ich allen Projektpartnern und Co-Autoren für ihre durchweg kooperative Arbeitsweise. Hervorzuheben sind hier Prof. Dr. Hans Poisel, Dr. Alexander Bachmann und Florian Winkler.

Mein ganz persönlicher Dank geht auch an meine langjährigen Freunde Tim Büsch, Josef Rossa und Maximilian Legat. Ihr habt mir viele schöne und interessante Tage und Abende verschafft und mich so auch immer wieder motiviert. Ich möchte meiner Familie aus tiefstem Herzen danken, dass sie mir mein Studium ermöglicht und mir stets sowohl finanziell als auch moralisch geholfen hat. Ich weiß zu schätzen, dass ihr immer hinter mir steht und mich in allem was ich mache unterstützt. Abschließend danke ich meiner lieben Freundin Dr. Ksenia Fominykh für alles. Fachlich wie moralisch hat mir Deine Liebe immer neue Kraft gegeben und dadurch wesentlich mehr als nur diese Arbeit erst ermöglicht.





Es suchten lang vor uns die Alten
nach Raum und Zeit und den Gestalten
Doch Zeit, so kommt es einem vor
die lernt man erst in dem Labor.
Nun weiß man was davon zu halten



Table of Contents

I	List of Abbreviations and Physical Quantities	I
II	List of Figures	III
III	List of Schemes	VIII
IV	List of Tables	X
V	List of Equations	XI
VI	List of Compounds	XII
1	General and Theoretical Section	1
1.1	Fundamentals of Fluorescence	2
1.2	Fluorescent Dyes	9
1.3	Objectives	12
2	Results and Discussion	13
2.1	Modifications of Perylene Diimides: Shortening the Fluorescence Lifetime via Intramolecular Interactions in Axial-Linked Di- and Trichromophores	15
2.2	Influence of Intramolecular Dynamics on Fluorescence Properties	29
2.2.1	Intramolecular Dynamics of 4-Aryl Naphthalimides	30
2.2.2	Synthesis and Characterization of Substituted Anthracene Dicarboximides	51
2.2.2.1	<i>N</i> -Substituted 10-Aminoanthracene-1,9-dicarboximides	54
2.2.2.2	Transition Metal-Free Homo-Coupling Reactions of Anthracen- and Naphthalene Dicarboximides	65
2.3	Concentration Dependency of the Fluorescence Lifetime: Long-Range Electromagnetic Molecular Interactions Indicated by the Process of Light Emission	69
2.4	Efficient Recycling of Unmarked Polymers by Means of their Auto-Fluorescent Decay	81
2.4.1	Development of an Optical Method for the Recycling of Unmarked Polymers	82
2.4.2	Studies on the Fluorescence of Ce(IV). A Universal Probe for Sorting Polymers	94
2.5	Synthesis and Characterization of Oligothiophenes with Short Fluorescence Lifetimes and High Stokes' Shifts	99
2.5.1	Adamantyl Substituted Oligothiophenes	100
2.5.2	Alkyl and Aryl Substituted Oligothiophenes	109
3	Summary	117
4	Experimental Section	121

Table of Contents

4.1	General Working Techniques	121
4.2	Analytical Methods and Instruments	122
4.3.1	9,9'-(2,3,5,6-Tetramethyl-1,4-phenylene)bis(2-(nonadecan-10-yl)anthra[2,1,9- <i>def</i> :6,5,10- <i>d'e'f'</i>])diisoquinoline-1,3,8,10(2 <i>H</i> ,9 <i>H</i>)-tetraone) (9)	123
4.3.2	2,9-Bis(4-amino-2,3,5,6-tetramethylphenyl)anthra[2,1,9- <i>def</i> :6,5,10- <i>d'e'f'</i>])diisoquinoline 1,3,8,10(2 <i>H</i> ,9 <i>H</i>)-tetraone (12)	124
4.3.3	9,9'-((1,3,8,10-Tetraoxo-1,3,8,10-tetrahydroanthra[2,1,9- <i>def</i> :6,5,10- <i>d'e'f'</i>])diisoquinoline-2,9-diyl)bis(2,3,5,6-tetramethyl-4,1-phenylene))bis(2-(tridecan-7-yl)anthra[2,1,9- <i>def</i> :6,5,10- <i>d'e'f'</i>])diisoquinoline-1,3,8,10(2 <i>H</i> ,9 <i>H</i>)-tetraone) (13)	125
4.3.4	1,2,4,5-Tetrakis(bromomethyl)benzene (15)	126
4.4.1.1	6-(4-Cyanophenyl)-2-(tridecan-7-yl)-1 <i>H</i> -benzo[<i>de</i>]isoquinoline-1,3(2 <i>H</i>)-dione (30)	127
4.4.1.2	8-Methoxy-4-methyl-1,2-dihydronaphthalene (precursor of 28)	128
4.4.1.3	1-Methoxy-5-methylnaphthalene (precursor of 28)	129
4.4.2.1	Aceanthrylene-1,2-dione (38)	130
4.4.2.2	1 <i>H</i> ,3 <i>H</i> -Dibenzo[<i>de,h</i>]isochromene-1,3-dione (39)	131
4.4.2.3	2-(Tridecan-7-yl)-1 <i>H</i> -dibenzo[<i>de,h</i>]isoquinoline-1,3(2 <i>H</i>)-dione (40)	132
4.4.2.4	7-(Hexylamino)-2-(tridecan-7-yl)-1 <i>H</i> -dibenzo[<i>de,h</i>]isoquinoline-1,3(2 <i>H</i>)-dione (41)	133
4.4.2.5	7-((2-Aminoethyl)amino)-2-(tridecan-7-yl)-1 <i>H</i> -dibenzo[<i>de,h</i>]isoquinoline-1,3(2 <i>H</i>)-dione (42)	134
4.4.2.6	7-(Phenylamino)-2-(tridecan-7-yl)-1 <i>H</i> -dibenzo[<i>de,h</i>]isoquinoline-1,3(2 <i>H</i>)-dione (43)	135
4.4.2.7	7-(Methyl(2-(methylamino)ethyl)amino)-2-(tridecan-7-yl)-1 <i>H</i> -dibenzo[<i>de,h</i>]isoquinoline-1,3(2 <i>H</i>)-dione (44)	136
4.4.2.8	7-(Piperidin-1-yl)-2-(tridecan-7-yl)-1 <i>H</i> -dibenzo[<i>de,h</i>]isoquinoline-1,3(2 <i>H</i>)-dione (45)	137
4.4.2.9	7-(1 <i>H</i> -Indol-1-yl)-2-(tridecan-7-yl)-1 <i>H</i> -dibenzo[<i>de,h</i>]isoquinoline-1,3(2 <i>H</i>)-dione (46)	138
4.4.2.10	7-(3,4,6,7-Tetrahydropyrrolo[1,2- <i>a</i>]pyrimidin-1(2 <i>H</i>)-yl)-2-(tridecan-7-yl)-1 <i>H</i> -dibenzo[<i>de,h</i>]isoquinoline-1,3(2 <i>H</i>)-dione (47)	140
4.4.2.11	7-Hydroxy-2-(tridecan-7-yl)-1 <i>H</i> -dibenzo[<i>de,h</i>]isoquinoline-1,3(2 <i>H</i>)-dione (48)	141
4.4.2.12	2,9-Di(tridecan-7-yl)tetrapheno[8,9- <i>ab</i>]benzo[5,6,7- <i>def</i> :10,11,12- <i>d'e'f'</i>])diisoquinoline-1,3,8,10(2 <i>H</i> ,9 <i>H</i>)-tetraone (49a)	142
4.4.2.13	2,9-di(Tridecan-7-yl)tetrapheno[5,6,7- <i>def</i>]isoquinoline[10,11,12- <i>d'e'f'</i>][[7,8- <i>a,b</i>]benzoisoquinoline-1,3,8,10(2 <i>H</i> ,9 <i>H</i>)-tetraone (49b)	143

Table of Contents

4.4.2.14	2-(Tridecan-7-yl)-1 <i>H</i> -benzo[<i>de</i>]isoquinoline-1,3(2 <i>H</i>)-dione (50)	144
4.4.2.15	5-Amino-2-(tridecan-7-yl)-1 <i>H</i> -benzo[<i>de</i>]isoquinoline-1,3(2 <i>H</i>)-dione (51)	145
4.4.2.16	5,13-Di(tridecan-7-yl)-8,16-dihydrodiisoquinolino[5,4- <i>ab</i> :5',4'- <i>hi</i>]phenazine-4,6,12,14(5 <i>H</i> ,13 <i>H</i>)-tetraone (52)	146
4.5.1.1	5,5 ^{'''} -Di(adamantan-1-yl)-2,2':5',2 ^{''} :5'',2 ^{'''} -quaterthiophene (59a)	148
4.5.1.2	5,5 ^{''''} -Di(adamantan-1-yl)-2,2':5',2 ^{''} :5'',2 ^{'''} :5''',2 ^{''''} :5''''-sexithiophene (59b)	149
4.5.1.3	5,5 ^{''''''} -Di(adamantan-1-yl)-2,2':5',2 ^{''} :5'',2 ^{'''} :5''',2 ^{''''} :5''''-octithiophene (59c)	150
4.5.2.1	2,2':5',2 ^{''} -Terthiophene (60)	151
4.5.2.2	General procedure for the preparation of 1,1'-([2,2':5',2 ^{''} -terthiophene]-5,5''-diyl)bisketones (61-62)	152
4.5.2.3	1,1'-([2,2':5',2 ^{''} -Terthiophene)-5,5''-diyl]bis(propan-1-on) (61a)	154
4.5.2.4	1,1'-([2,2':5',2 ^{''} -Terthiophene)-5,5''-diyl]bis(butan-1-on) (61b)	155
4.5.2.5	1,1'-([2,2':5',2 ^{''} -Terthiophene)-5,5''-diyl]bis(pentan-1-on) (61c)	156
4.5.2.6	1,1'-([2,2':5',2 ^{''} -Terthiophene)-5,5''-diyl]bis(2,2-dimethylpropan-1-on) (61d)	157
4.5.2.7	1,1'-([2,2':5',2 ^{''} -Terthiophene]-5,5''-diyl]bis(phenylmethanon) (61e)	158
4.5.2.8	1-([2,2'-Bithiophen]-5-yl)-2,2,3,3,4,4,4-heptafluorbutan-1-on (62a)	159
4.5.2.9	1-([2,2':5',2 ^{''} -Terthiophen]-5-yl)-2,2,3,3,4,4,4-heptafluorbutan-1-on (62b)	160
4.6	Preparation of Solid Poly(methyl methacrylate) Samples	161
4.6.1	Standard Polymerization Reaction for the Preparation of Dye-Doped Poly(methyl methacrylate) (PMMA)	161
4.6.2	Preparation of Dye-Doped Poly(methyl methacrylate) (PMMA) Films	161
5	References	163



I List of Abbreviations and Physical Quantities

Å	Ångström (10^{-10} m)
abs.	absolute
ATR	attenuated total reflexion
a.u.	arbitrary units
°C	temperature in degrees Celsius
calc.	calculated
CHCl₃	chloroform
cm⁻¹	wavenumber in reciprocal centimeters
δ	chemical shift in ppm
DFT	desity functional theory
DMF	dimethylformamide
ε	molar attenuation coefficient / absorbance
E	attenuation (extinction)
EI	electron ionization
eq.	equivalent
EtOAc	ethyl acetate
H	hours
HCl	hydrochloric acid
HOMO	highest occupied molecular orbital
HRMS	high resolution mass spectrometry
Hz	Hertz (s^{-1})
I	intensity
IR	infrared

IUPAC International Union of Pure and Applied Chemistry

J coupling constant

λ wavelength in nm

λ_{exc} excitation wavelength

LUMO lowest unoccupied molecular orbital

M molar (mol L⁻¹)

MALDI matrix-assisted laser desorption/ionization

mg milligram (10⁻⁶ kg)

min. minute

mL milliliter (10⁻⁶ m³)

MMA methyl methacrylate

mol% mol percent

MS mass spectrometry

NMR nuclear magnetic resonance (spectroscopy)

Φ fluorescence quantum yield

PMMA poly(methyl methacrylate)

ppm parts per million

R_f retardation factor

rt room temperature

τ fluorescence lifetime

THF tetrahydrofuran

TMS tetramethylsilane

UV ultraviolet

UV/Vis absorption spectroscopy in the ultraviolet and visible spectral region

II List of Figures

- Figure 1** Schematic Jablonski diagram. Caused by absorption of a photon an electron is electronically excited into the singlet 1E_1 -state (blue). Usually an internal conversion from an elevated vibronic state into the vibronic ground state takes place. Subsequently, the excited electron relaxes (red) by emission of fluorescence light into an excited vibronic state of the electronic ground state 1E_0 . Phosphorescence occurs after intersystem crossing of the excited electron into the triplet 3E_1 -state under spin inversion. The spin-forbidden relaxation into the ground state (grey) causes the emission of phosphorescence radiation. **3**
- Figure 2** Franck-Condon energy diagram. Schematic wave functions (red) are given for anharmonic oscillators E_0 (electronic ground state) and E_1 (1st electronically excited state) representing the energy potential of the chemical bond, respectively. Absorption (blue) and fluorescence (grey) take place vertically. **4**
- Figure 3** Fluorescence decay of *N,N'*-bis(tridecan-7-yl)perylene-3,4:9,10-tetracarboxylic diimide (**1**) in chloroform. Logarithmic scaled excitation pulses (grey), fluorescence decay (red) and monoexponential fit (black, mainly covered by decay). Insert: Normalized monoexponential fit and resulting fluorescence lifetime of 3.92 ns. **8**
- Figure 4** Absorption (left) and fluorescence (right) spectra of perylene diimide dichromophore **9** (red) vs. those of *S*-**13** (grey) in chloroform. **20**
- Figure 5** Absorptivity of the two main maxima of dichromophore **9** in a dilution series from 3 to 27 x 10⁻⁷ mol L⁻¹ in chloroform. Both maxima at 530.0 nm (red) and 492.0 nm (grey) display linear behavior. **21**
- Figure 6** Absorption (left) and fluorescence (right) spectra of perylene diimide trichromophore **13** (red) vs. those of *S*-**13** (**1**) (grey) and trichromophore **8** (black) in chloroform. **22**
- Figure 7** Absorptivity of the main maxima of trichromophore **13** in a dilution series from 1.7 to 13 x 10⁻⁷ mol L⁻¹ in chloroform. All maxima at 527.0 nm (red), 491.0 nm (grey) and 589 nm (black) display linear behavior. Insert: Detail of the spectrum emphasizing the linear dependency of the absorptivity on the concentration. **23**
- Figure 8** a) UV/Vis absorption (left) and fluorescence (right) spectra of **23** in various solvents. From left to right: hexane (thick solid red), tetradecane (dotted blue), toluene (dashed grey), chloroform (solid black), undecanol (dotted dashed turquoise) DMF (diffuse yellow), 1-butanol (double dotted dashed green). b) Linear relationship of the solvatochromism (E_T) of **23** (diamonds), **24** (triangles) and **37** (circles), respectively to the $E_T(30)$ solvent polarity scale. Closed symbols: Aprotic solvents; open symbols: protic solvents, neglected for regression. c) Aryl naphthalene carboximides **23-30**, **32** and **34** in CHCl₃ under UV-light (366 nm). From left to right: **32**, **30**, **24**, **34**, **23**, **29**, **28**, **27**, **26**, **25**. **38**

- Figure 9** UV/Vis absorption (left) and fluorescence (right) spectra of **27** in various solvents. From left to right: hexane (thick solid red), tetradecane (dotted blue), toluene (dashed grey), chloroform (thin solid black), undecanol (dotted dashed turquoise) DMF (diffuse yellow), 1-butanol (double dotted dashed green). 40
- Figure 10** Comparison of **27** and **28**. a) Absorption (left) and fluorescence spectra of **27** (black) and **28** (red); b-e) Optimized structures of **27** and **28** (B3LYP 6-311**G); b) Electronic ground state of **27**; c) Electronically excited state of **27**; d) Electronic ground state of **28**; e) Electronically excited state of **28**. 41
- Figure 11** Linear correlations of the Stokes' shift $\nu_{\text{abs}} - \nu_{\text{flu}}$ (in 1000cm^{-1}) of **23-30** and **34** versus f_{BK} to obtain m_1 and of the sum $\lambda_{\text{abs}} + \lambda_{\text{flu}}$ versus $f_{\text{BK}} + 2g_{\text{BK}}$ to obtain m_2 . 46
- Figure 12** Time resolved anisotropy of naphthalimides **24**, **27** and **28** in PMMA films. a) Anisotropy (red), parallel fluorescence decay (black) and perpendicular fluorescence decay (grey) of **24**; b) Anisotropy (red), parallel fluorescence decay (black) and perpendicular fluorescence decay (grey) of **27**; c) Anisotropy (red), parallel fluorescence decay (black) and perpendicular fluorescence decay (grey) of **28**; d) Comparison of the anisotropy of **24** (black), **27** (red) and **28** (grey). 49
- Figure 13** Temperature dependent fluorescence spectra of **32** in diethylene glycol diethyl ether. Temperatures approx. 25 °C (grey), 100 °C (black), 200 °C (red). 50
- Figure 14** Absorption (red) and fluorescence (grey) spectra of *N*-(tridecan-7-yl)anthracene dicarboximide (**40**) in chloroform. 53
- Figure 15** Positions of the fluorescence maxima of *N*-(tridecan-7-yl)anthracene dicarboximide (**40**) in different solvents in relation to the $E_{\text{T}}(30)$ -values^[56] of the respective solvent. 54
- Figure 16** Reaction of *N*-(tridecan-7-yl)anthracene dicarboximide (**40**) in 0.1 M DMF with selected amines after different reaction times at room temperature. From top to bottom: a) Directly after addition; b) after 1 h; c) after 4 h; d) after 1 week. From left to right: 4-Amino-*N*-methylphthalimid, aniline, triethylamine, diethylamine, pyrrolidine, (*S*)-proline, (*S*)-lysine, 1-hexylamine, 1,2-diaminoethane. 57
- Figure 17** UV/Vis absorption (left) and fluorescence (right) spectra of the amination products from 1-aminohexane (**41**) (red) and 1,2-diaminoethane (**42**) (grey) in chloroform. 10-(phenylamino)anthracene dicarboximide (**43**) exhibited no fluorescence but absorption (black) only. 58
- Figure 18** UV/Vis absorption (left) and fluorescence (right) spectra of amines **44** (red), **45** (grey) and **46** (black) in chloroform. The yellow spectrum displays the unstable σ adduct with pyrrolidine. 59
- Figure 19** UV/Vis-absorption (red) and fluorescence (grey) spectra of amine **47** in chloroform. 60
- Figure 20** UV/Vis absorption (red) and fluorescence (grey) spectra of **48** in chloroform. 64
- Figure 21** UV/Vis (left) and fluorescence (right) spectra of *trans*-aceanthrene green **49a** (red), *cis*-aceanthrene green **49b** (grey) and dihydrophenazine **52** (black) in chloroform. 68

- Figure 22** UV/Vis absorption spectra of **1** in chloroform with increasing dilution. Insert: Verification of Lambert-Beer's law by the linear correlation of the absorptivity E as a function of the concentration c ; circles: 527 nm, slope $0.810 \times 10^5 \text{ L mol}^{-1}$, standard deviation 0.0049, correlation number 0.99995, coefficient of determination 0.9999, 7 measurements) and diamonds: 490 nm (slope $0.504 \times 10^5 \text{ L mol}^{-1}$, standard deviation 0.0044, correlation number 0.99988, coefficient of determination 0.9998, 7 measurements). **71**
- Figure 23** Fluorescence spectra of **1** in chloroform with optical excitation at 490 nm and increasing dilution. Insert: Linear correlation of the intensity of fluorescence as a function of the concentration of **1**; diamonds: Slit for excitation 2.5 nm (slope $3.38 \times 10^8 \text{ L mol}^{-1}$, standard deviation 3.1, correlation number 0.9995, coefficient of determination 0.9991, 11 measurements) and steep line, circles: Slit for excitation 10 nm (slope $4.11 \times 10^9 \text{ L mol}^{-1}$, standard deviation 0.33, correlation number 0.999998, coefficient of determination 0.999997, 8 measurements). **72**
- Figure 24** Concentration dependency of the fluorescence lifetime of fluorophores **1** (red), **53** (blue), **54** (green) and **55** (violet). **74**
- Figure 25** Dependence of the fluorescence lifetime τ of **1** in chloroform on the concentration c (circles; see Table 1). Insert: Linear correlation according to equation (8) ($E_D = 1.17 \text{ ns}$, $c^* = 1.17 \cdot 10^5 \text{ mol L}^{-1}$ and $\tau_0 = 3.77 \text{ ns}$), (standard deviation 0.015, correlation number 0.9992, coefficient of determination 0.9984, 11 measurements). **76**
- Figure 26** Optical properties of Nile blue (**53**) in ethanol. a) Concentration dependent fluorescence lifetime. b) Dilution series of **53** in ethanol. c) Linear correlation between concentration and absorptivity in agreement with Lambert-Beer's law. **77**
- Figure 27** Dependency of the fluorescence lifetime τ of S-13 (**1**) doped PMMA nanoparticles on the concentration (represented by attenuation E). Applied nanoparticles (rounded average values): 25 ppm **1**, 200 nm (black); 25 ppm **1**, 300 nm (red); 100 ppm **1**, 200 nm (grey); 300 ppm **1**, 200 nm (yellow); 300 ppm **1**, 300 nm (blue). **78**
- Figure 28** Fluorescence spectra of the auto fluorescence of Luran® (blue, dotted curve), Delrin® (red, dashed curve) and Ultramid® (black, solid curve) with optical excitation at 365 nm. **83**
- Figure 29** Fluorescence decay of polymers (excitation: 356 nm, detection: 460 nm) in linear (left) and logarithmic scales (right). Mono-exponentially fitted functions of decay as solid lines (mainly covered by actual measurement points). Fluorescence decay of Luran® (red), Delrin® (grey) and Ultramid® (black). **85**
- Figure 30** Time-resolved fluorescence spectra of selected polymers: HDPE (red), Delrin® (black), PC (yellow), PET (blue), PMMA (green) and Tectosil® (violet) Light curves represent the time slots from 2 ns to 3 ns, solid curves those from 4 ns to 100 ns. **86**
- Figure 31** Fluorescence lifetimes τ in ns of technical polymers. Reproducibility is given within $\pm 1\%$. **86**
- Figure 32** For determination of τ_1 and τ_2 the decay was split in two branches, one representing the short relaxation processes from t_{\max} to $t_{\max}+3$ (black). IRF (grey line) and non-relevant measuring points (light grey) are given for completion. **91**

- Figure 33** Two-dimensional characterization of polymers by means of their constants τ_1 and τ_2 attained by bi-exponential evaluation of the fluorescence decay. Filled circles: polyethylenes LDPE, HDPE and UHDPE; squares: PET; diamonds: Silicones; triangles: silicone elastomer Tectosil®. **92**
- Figure 34** Fluorescence lifetimes τ of pre-treated PET; expanded range. **93**
- Figure 35** Two-dimensional characterization of PET with various pre-treatment by means of their constants τ_1 and τ_2 after bi-exponential evaluation of the fluorescence decay. **93**
- Figure 36** Fluorescence spectra of highly disperse silica excited at 405 nm. Colors indicate the applied dispersant: Neat film (**red**), water (**grey**), methanol (**yellow**), DMF (**blue**), toluene (**green**), hexane (**violet**). The top respective curve is for Cab-o-sil® from Merck (Acros), the accompanying bottom curve for HDK® H 15 from Wacker. The bottom black curve represents the spectrum of Ludox® from sigma aldrich, a highly pure aqueous silica standard for optical scattering. **95**
- Figure 37** Fluorescence spectra of cerium(IV)sulfate in aqueous solution at different concentrations. Lighter colors represent lower concentration. The excitation wavelength was set to 405 nm. **96**
- Figure 38** Correlation of relative fluorescence intensities and concentration of aqueous solutions of cerium(IV)sulfate. Very high concentrations completely quench fluorescence (**grey**). At lower concentrations (**red**) the relative intensity of the fluorescence band at 460 nm increases. **97**
- Figure 39** UV/Vis-Spectra in chloroform (for **59a**) or $C_2H_2Cl_4$ (for **59b-c**). **Blue 59a** ($n = 4$), **red 59b** ($n = 6$), **green 59c** ($n = 8$). Left absorption spectra with scale $E_{rel.}$, right fluorescence spectra with scale I . **103**
- Figure 40** UV/Vis-Spectra in chloroform. **Blue 57b** ($n = 2$), **red 57c** ($n = 3$), **green 57d** ($n = 4$). Left absorption spectra with scale $E_{rel.}$, right fluorescence spectra with scale I . **105**
- Figure 41** Schematic process causing the increased Stokes' shifts. i) Vertical transition by light absorption ($h\nu$) from the electronic ground state S_0 (top left) to reach the electronically excited state S_1 . ii) Relaxation to a geometrically more favorable, energetically lower excited state S_1' . iii) Bathochromically shifted fluorescence ($-h\nu'$) from S_1' to S_0' . iv) Relaxation to the energetically more favored initial state from S_0' to S_0 . **106**
- Figure 42** UV/Vis-Spectrum (**blue**), fluorescence excitation spectrum (**red**) and fluorescence spectrum (**green**) of **57d** in solid PMMA. Absorption spectrum with scale $E_{rel.}$, Fluorescence spectra with scale I . **107**
- Figure 43** Comparison of optical spectra of **57d**. a) Absorption (**grey**), fluorescence excitation (**red**) and fluorescence (black) spectra in chloroform; b) Fluorescence lifetime in chloroform. Excitation pulse (**grey**), decay (**red**) and mono-exponential deconvolution fit (black). Insert: Logarithmic decay; c) Fluorescence excitation (**red**) and fluorescence (black) spectra in PMMA; b) Fluorescence lifetime in PMMA. Excitation pulse (**grey**), decay (**red**) and mono-exponential deconvolution fit (black). Insert: Logarithmic decay. **108**
- Figure 44** Left: Absorption (right) and fluorescence (left) spectra of **61a** (black), **61d** (red) and **61e** (grey) in chloroform; Right: Fluorescence lifetime of **61d** in chloroform. IRF (**grey**), fluorescence decay (**red**), deconvolutional fit (black). Insert: Exponential fit of **61d** resulting in a fluorescence lifetime of 0.403 ns. **112**

- Figure 45** Quantumchemical calculations of **61d** (B3LYP 6-311**G and CAM-B3LYP 6-311**G). Left: Planar structure of the electronic ground state (bottom) and the electronically excited state (top) in either of the applied methods. Right: Calculated HOMO and LUMO of **61d**. **113**
- Figure 46** Crystal structure of terthiophenediyl bisketone **61d**. The thiophene units are twisted to each other with dihedral angles of about 10°. **113**
- Figure 47** Left: Absorption (in chloroform, grey), fluorescence excitation (in PMMA, black) and fluorescence (in PMMA, red) spectra of **61d**; Right: Fluorescence lifetime of **61d** in PMMA fiber. IRF (grey), fluorescence decay (red), deconvolutional fit (black). Insert: Exponential fit of **61d** in PMMA resulting in a fluorescence lifetime of 0.388 ns. **114**
- Figure 48** PMMA fluorescent optical fiber (FOF) with 35 ppm of **61d**. **115**

III List of Schemes

Scheme 1	Alkaline hydrolysis of perylene diimide 1 . The resulting <i>N,N'</i> -bis(tridecan-7-yl)perylene-3,4-dicarboximide-9,10-dicarboxylic anhydride (2) can be condensed with various functional amines.	10
Scheme 2	Orthogonally fixed perylene diimide – benzoperylene triimide dichromophore 3 (left). The chromophores are linked via an aromatic 2,3,5,6-tetramethylphenylene moiety. Below the linearly <i>N-N'</i> -linked perylene diimide – perylene diimide dichromophore 4 consisting of the same subunit.	11
Scheme 3	General preparation procedure for <i>N-N'</i> -linked perylene diimide based di- and trichromophores according to the literature. ^[32]	17
Scheme 4	Preparation of 2,3,5,6-tetramethylbenzene-linked perylene diimide di- and trichromophores 9 and 13 .	19
Scheme 5	Investigated reaction pathways to obtain 1,2,4,5-tetrapentylbenzene (20).	24
Scheme 6	Pentylated tetramer 21 consisting of durene units. Constitutional isomers are not considered, the given structure is the sterically most favorable.	25
Scheme 7	Representative schematic section of the discussed polymer from the <i>Grignard</i> reaction of 15 and 17 .	26
Scheme 8	Synthesis of arylated naphthalene carboximides 23-30 . a) 4-(Trimethylsilyl)phenylboronic acid and 4-cyanophenylboronic acid was used for 29 and 30 , respectively.	31
Scheme 9	Bromination of 26 and subsequent cross-coupling with MeZnCl gives 32 (top); cyanation and Negishi cross-coupling of 33 leads to 34 . 30 was alternatively obtained via Pd-catalyzed cyanation (bottom).	32
Scheme 10	4-Amino- <i>N</i> -methylphthalimide (35) and 4-methoxy- <i>N</i> -methylphthalimide (36) as reference for fluorescence data comparison.	37
Scheme 11	Two possible mesomeric resonance structures indicate the electrophilicity of anthracene-1,9-dicarboximide in C-10 position.	52
Scheme 12	Synthesis of <i>N</i> -(tridecan-7-yl)anthracene dicarboximide (40) starting from anthracene (37) in 3 steps. ^[55]	52
Scheme 13	Proposed reaction mechanism for the formation of amine 47 .	60
Scheme 14	Proposed <i>Chichibabin</i> -like reaction mechanism of amines with <i>N</i> -(tridecan-7-yl)anthracene imide. Two possible reactions either form the product (red) or lead to the collapse of the σ -adduct to recover starting material (yellow).	61
Scheme 15	Isolated products of the reaction of anthracene dicarboximide with the corresponding amines (appr. No. for reference in Table 11).	63
Scheme 16	Reaction of KOH or KO ^t Bu with anthracene dicarboximide to 10-hydroxyanthracene dicarboximide 48 .	64
Scheme 17	Synthesis of <i>N,N'</i> -aceanthrene green tetracarboxylic diimide 49 .	66
Scheme 18	Structure of 5,13-bis(tridecan-7-yl)-8,16-dihydrodiisoquinolino[5,4- <i>ab</i> :5',4'- <i>hi</i>]phenazine-4,6,12,14(5 <i>H</i> ,13 <i>H</i>)-tetraone (52).	67
Scheme 19	Chemical structures of the applied fluorophores 53-55 .	73

- Scheme 20** Determination of a time-resolved emission spectrum with custom time slots. The range from TimeGate1First to TimeGate1Last was set up for control of the short fluorescent components. The second time range in red considers all components with lifetimes of the excited state of more than 4 ns. The top limit of 100 ns is set to a value where all molecules are estimated to have already relaxed. **87**
- Scheme 21** Preparation of 1-adamantyl substituted oligothiophenes **57a-c** ($n = 1-3$) via Negishi cross coupling reactions. Further bromination with NBS leads to the readily soluble 5-bromo oligothiophenes **58a-c**. **101**
- Scheme 22** Preparation of higher homologues ($n = 4,6,8$) of (1-adamantyl)oligothiophene. The well soluble mono-alkylated quaterthiophene **57d** was obtained via a Negishi cross-coupling reaction of 2-thienylzinc chloride with 5''-(1-adamantyl)-5-bromoterthiophene (**58c**). Treatment of mono-(1-adamantyl)oligothiophenes ($n = 2-4$) with FeCl₃ leads to the respective mirror symmetrical coupling products **59a-c**. **102**
- Scheme 23** Synthesis of ([2,2':5',2''-terthiophene]-5,5''-diyl)bisketones **61a-e** under two different conditions. **110**
- Scheme 24** Synthesis of bi- and terthienylheptafluorobutanone **62a-b**. **110**

IV List of Tables

Table 1	Elementary analysis of the polymer forming at low temperatures. The indicated hydroxyl group can also be interpreted as non-covalent aqueous inclusion.	26
Table 2	Fluorescence quantum yields and lifetimes of naphthalimides 23-30 and 34 .	34
Table 3	Absorption and fluorescence maxima of naphthalimides 23-30 and 34 .	35
Table 4	FWHM*-values of absorption and fluorescence spectra of naphthalimides 23-30 and 34 in nm.	36
Table 5	FWHM*-values of absorption and fluorescence spectra of naphthalimides 23-30 and 34 in eV.	36
Table 6	Solvatochromism of the fluorescence of the dicarboxylic imides 23-30, 32 and 34-36 .	39
Table 7	Quantumchemical calculations of 23-30, 32 and 34 .	42
Table 8	Comparison of quantum chemically calculated optical values with experimental results.	44
Table 9	Slopes m_1 and m_2 .	45
Table 10	Calculated parameters XYZ_0 , s , d , a and b by means of least square fits of the experimental E_T -values of fluorescence according to equation (12). Solvents: 1-Butanol, <i>N,N</i> -dimethylformamide, chloroform, toluene, <i>n</i> -hexane.	47
Table 11	Optimized parameters A_0 , b , c , d and e of equation (13) by means of least square fitting of the experimental E_T -values of the fluorescence of 3 in the solvents 1-butanol, 1-undecanol, <i>N,N</i> -dimethylformamide, chloroform, toluene, <i>n</i> -hexane, <i>n</i> -tetradecane (<i>N,N</i> -dimethylformamide was excluded for 3c because of lack of fluorescence).	48
Table 12	Overview on the applied amines and the most appropriate reaction conditions used for the conversion with <i>N</i> -(tridecan-7-yl)anthracene dicarboximide 40 .	55
Table 13	Optical data of isolated amino compounds 41 – 47 .	62
Table 14	Fluorescence lifetimes τ of 1 in chloroform depending on the concentration c and the calculated average molecular distance d , respectively. Fluorescence excitation at 490 nm and detection at 535 nm.	75
Table 15	Fluorescence lifetimes τ of 53 in ethanol depending on the concentration c . Fluorescence excitation at 628 nm and detection at 667 nm.	77
Table 16	Fluorescence lifetimes of the studied polymers Luran [®] , Delrin [®] and Ultramid [®] .	84
Table 17	Time constants for the auto-fluorescence decay of technical polymers.	90
Table 18	Fluorescence lifetimes of different silica dispersions.	98
Table 19	Optical properties of (1-adamantyl)oligothiophenes.	104
Table 20	Ketoterthiophenes 61 and 62 . Spectroscopic measurements in chloroform.	111

V List of Equations

Equation (1)	$\Phi = \frac{k_r}{k_r + k_n}$	5
Equation (2)	$I(t) = I_0 e^{-\frac{t}{\tau}}$	6
Equation (3)	$\tau = \frac{1}{k_r + k_n}$	6
Equation (4)	$\tau_n = \frac{1}{k_r}$	6
Equation (5)	$k_r = \frac{1}{\tau_n} \cong 2.88 \text{ s}^{-1} \times 10^{-9} n^2 \frac{\int I(\sigma) d\sigma}{\int I(\sigma) \sigma^{-3} d\sigma} \int \frac{\varepsilon(\sigma)}{\sigma} d\sigma$	7
Equation (6)	$\Phi = \frac{\tau}{\tau_n}$	7
Equation (7)	$E_T = \frac{28591 \text{ kcal nm mol}^{-1}}{\lambda_{max}}$	37
Equation (8)	$E_T = a E_T(30) + b$	37
Equation (9)	$f_{BK} = \frac{2n^2 + 1}{n^2 + 2} \left(\frac{\varepsilon - 1}{\varepsilon + 2} - \frac{n^2 - 1}{n^2 + 2} \right)$	45
Equation (10)	$g_{BK} = \frac{3}{2} \frac{n^4 - 1}{(n^2 + 2)^2}$	45
Equation (11)	$\frac{\mu_e}{\mu_g} = \frac{ m_1 + m_2 }{ m_2 - m_1 }$	46
Equation (12)	$E_T = XYZ = XYZ_0 + s(\pi^* + d\delta) + a\alpha + b\beta$	47
Equation (13)	$E_T = A = A_0 + bSA + cSB + dSP + eSdP$	47
Equation (14)	$r = \frac{I_{\parallel} - G I_{\perp}}{I_{\parallel} + 2 G I_{\perp}}$	48
Equation (15)	$E = \log \frac{I_0}{I} = \varepsilon c d$	71
Equation (16)	$\tau = E_D \ln \left(\frac{C}{C^*} + 1 \right) + \tau_0$	76

VI List of Compounds

All chemical compounds discussed in this work are listed below named according to IUPAC standards with support of the chemical software ChemDraw 13[®]. Within the main text, trivial names published in literature are used referring to the core chromophore for more clarity.

- 1** 2,9-Di(tridecan-7-yl)anthra[2,1,9-*def*:6,5,10-*d'ef'*]diisoquinoline-1,3,8,10(2*H*,9*H*)-tetraone
- 2** 9-(Tridecan-7-yl)-1*H*-isochromeno[6',5',4':10,5,6]anthra[2,1,9-*def*]isoquinoline-1,3,8,10(9*H*)-tetraone
- 3** *N*²,*N*³-Bis(tridec-7-yl)-*N*¹-[*N*-(tridec-7-yl)-*N'*-(2,3,5,6-tetramethylphenyl-4-yl)perylene-3,4:9,10-tetracarboxylic bisimide]benzo[ghi]perylene-2,3:8,9:11,12-hexacarboxylic trisimide
- 4** 9,9'-Di(tridecan-7-yl)-1*H*,1'*H*-[2,2'-bisanthra[2,1,9-*def*:6,5,10-*d'ef'*]diisoquinolin]-1,1',3,3',8,8',10,10'(9*H*,9'*H*)-octaone
- 5** Anthra[2,1,9-*def*:6,5,10-*d'ef'*]diisochromene-1,3,8,10-tetraone
- 6** 2-Amino-9-(tridecan-7-yl)anthra[2,1,9-*def*:6,5,10-*d'ef'*]diisoquinoline-1,3,8,10(2*H*,9*H*)-tetraone
- 7** 9-Amino-9'-(tridecan-7-yl)-1*H*,1'*H*-[2,2'-bianthra[2,1,9-*def*:6,5,10-*d'ef'*]diisoquinolin]-1,1',3,3',8,8',10,10'(9*H*,9'*H*)-octaone
- 8** 9,9''-Di(tridecan-7-yl)-1*H*,1''*H*-[2,2':9',2''-teranthra[2,1,9-*def*:6,5,10-*d'ef'*]diisoquinoline]-1,1',1'',3,3',3'',8,8',8'',10,10',10''(9*H*,9''*H*)-dodecaone
- 9** 9,9'-(2,3,5,6-Tetramethyl-1,4-phenylene)bis(2-(nonadecan-10-yl)anthra[2,1,9-*def*:6,5,10-*d'ef'*]diisoquinoline-1,3,8,10(2*H*,9*H*)-tetraone)
- 10** 2,3,5,6-Tetramethylbenzene-1,4-diamine
- 11a** 9-(Tridecan-7-yl)-1*H*-isochromeno[6',5',4':10,5,6]anthra[2,1,9-*def*]isoquinoline-1,3,8,10(9*H*)-tetraone
- 11b** 9-(Nonadecan-10-yl)-1*H*-isochromeno[6',5',4':10,5,6]anthra[2,1,9-*def*]isoquinoline-1,3,8,10(9*H*)-tetraone
- 12** 2,9-bis(4-amino-2,3,5,6-tetramethylphenyl)anthra[2,1,9-*def*:6,5,10-*d'ef'*]diisoquinoline-1,3,8,10(2*H*,9*H*)-tetraone
- 13** 9,9'-((1,3,8,10-tetraoxo-1,3,8,10-tetrahydroanthra[2,1,9-*def*:6,5,10-*d'ef'*]diisoquinoline-2,9-diyl)bis(2,3,5,6-tetramethyl-4,1-phenylene))bis(2-(tridecan-7-yl)anthra[2,1,9-*def*:6,5,10-*d'ef'*]diisoquinoline-1,3,8,10(2*H*,9*H*)-tetraone)
- 14** 1,2,4,5-Tetramethylbenzene
- 15** 1,2,4,5-Tetrakis(bromomethyl)benzene

- 16 1,2,4,5-Tetrakis(methylenmagnesium bromide)benzene
- 17 Butylmagnesiumbromide
- 18 Benzene-1,2,4,5-tetracarbonitrile
- 19 1,1',1'',1'''-(Benzene-1,2,4,5-tetra-yl)tetrakis(pentan-1-one)
- 20 1,2,4,5-Tetrapentylbenzene
- 21 1,2-Bis(2,5-dipentyl-4-(2,4,5-tripentylphenethyl)phenyl)ethane
- 22 6-Bromo-2-(tridecan-7-yl)-1*H*-benzo[*de*]isoquinoline-1,3(2*H*)-dione
- 23 6-Phenyl-2-(tridecan-7-yl)-1*H*-benzo[*de*]isoquinoline-1,3(2*H*)-dione
- 24 6-(4-Methoxyphenyl)-2-(tridecan-7-yl)-1*H*-benzo[*de*]isoquinoline-1,3(2*H*)-dione
- 25 6-(4-(Dimethylamino)phenyl)-2-(tridecan-7-yl)-1*H*-benzo[*de*]isoquinoline-1,3(2*H*)-dione
- 26 2-(Tridecan-7-yl)-6-(3,4,5-trimethoxyphenyl)-1*H*-benzo[*de*]isoquinoline-1,3(2*H*)-dione
- 27 6-(4-Methoxynaphthalen-1-yl)-2-(tridecan-7-yl)-1*H*-benzo[*de*]isoquinoline-1,3(2*H*)-dione
- 28 6-(4-Methoxy-8-methylnaphthalen-1-yl)-2-(tridecan-7-yl)-1*H*-benzo[*de*]isoquinoline-1,3(2*H*)-dione
- 29 2-(Tridecan-7-yl)-6-(4-(trimethylsilyl)phenyl)-1*H*-benzo[*de*]isoquinoline-1,3(2*H*)-dione
- 30 4-(1,3-Dioxo-2-(tridecan-7-yl)-2,3-dihydro-1*H*-benzo[*de*]isoquinolin-6-yl)benzotrile
- 31 6-(2,6-Dibromo-3,4,5-trimethoxyphenyl)-2-(tridecan-7-yl)-1*H*-benzo[*de*]isoquinoline-1,3(2*H*)-dione
- 32 2-(Tridecan-7-yl)-6-(3,4,5-trimethoxy-2,6-dimethylphenyl)-1*H*-benzo[*de*]isoquinoline-1,3(2*H*)-dione
- 33 6-(4-Iodophenyl)-2-(tridecan-7-yl)-1*H*-benzo[*de*]isoquinoline-1,3(2*H*)-dione
- 34 6-(4'-Methoxy-[1,1'-biphenyl]-4-yl)-2-(tridecan-7-yl)-1*H*-benzo[*de*]isoquinoline-1,3(2*H*)-dione
- 35 5-Amino-2-methylisoindoline-1,3-dione
- 36 6-Methoxy-2-methyl-1*H*-benzo[*de*]isoquinoline-1,3(2*H*)-dione
- 37 Anthracene
- 38 Aceanthrylene-1,2-dione
- 39 1*H*,3*H*-Dibenzo[*de,h*]isochromene-1,3-dione
- 40 2-(Tridecan-7-yl)-1*H*-dibenzo[*de,h*]isoquinoline-1,3(2*H*)-dione
- 41 7-(Hexylamino)-2-(tridecan-7-yl)-1*H*-dibenzo[*de,h*]isoquinoline-1,3(2*H*)-dione
- 42 7-((2-Aminoethyl)amino)-2-(tridecan-7-yl)-1*H*-dibenzo[*de,h*]isoquinoline-1,3(2*H*)-dione
- 43 7-(Phenylamino)-2-(tridecan-7-yl)-1*H*-dibenzo[*de,h*]isoquinoline-1,3(2*H*)-dione

- 44** 7-(Methyl(2-(methylamino)ethyl)amino)-2-(tridecan-7-yl)-1*H*-dibenzo[*de,h*]isoquinoline-1,3(2*H*)-dione
- 45** 7-(Piperidin-1-yl)-2-(tridecan-7-yl)-1*H*-dibenzo[*de,h*]isoquinoline-1,3(2*H*)-dione
- 46** 7-(1*H*-Indol-1-yl)-2-(tridecan-7-yl)-1*H*-dibenzo[*de,h*]isoquinoline-1,3(2*H*)-dione
- 47** 7-(3,4,6,7-Tetrahydropyrrolo[1,2-*a*]pyrimidin-1(2*H*)-yl)-2-(tridecan-7-yl)-1*H*-dibenzo[*de,h*]isoquinoline-1,3(2*H*)-dione
- 48** 7-Hydroxy-2-(tridecan-7-yl)-1*H*-dibenzo[*de,h*]isoquinoline-1,3(2*H*)-dione
- 49a** 2,9-Di(tridecan-7-yl)tetrapheno[8,9-*ab*]benzo[5,6,7-*def*:10,11,12-*d'ef'*]diisoquinoline-1,3,8,10(2*H*,9*H*)-tetraone
- 49b** 2,9-di(Tridecan-7-yl)tetrapheno[5,6,7-*def*]isoquinoline[10,11,12-*d'ef'*]([7,8-*a,b*]benzoisoquinoline-1,3,8,10(2*H*,9*H*)-tetraone
- 50** 2-(Tridecan-7-yl)-1*H*-benzo[*de*]isoquinoline-1,3(2*H*)-dione
- 51** 5-Amino-2-(tridecan-7-yl)-1*H*-benzo[*de*]isoquinoline-1,3(2*H*)-dione
- 52** 5,13-Di(tridecan-7-yl)-8,16-dihydrodiisoquinolino[5,4-*ab*:5',4'-*hi*]phenazine-4,6,12,14(5*H*,13*H*)-tetraone
- 53** Bis(9-(diethylamino)-5*H*-benzo[*a*]phenoxazin-5-iminium) sulfate
- 54** Disodium 2-(6-oxido-3-oxo-3*H*-xanthen-9-yl)benzoate
- 55** *N*-(9-(2-Carboxyphenyl)-6-(diethylamino)-3*H*-xanthen-3-ylidene)-*N*-ethylethanaminium chloride
- 56a** 2-Bromothiophene
- 56b** 5-Bromo-2,2'-bithiophene
- 56c** 5-Bromo-2,2':5',2''-terthiophene
- 57a** 2-(Adamantan-1-yl)thiophene
- 57b** 5-(Adamantan-1-yl)-2,2'-dithiophene
- 57c** 5-(Adamantan-1-yl)-2,2':5',2''-terthiophene
- 57d** 5(Adamantan-1-yl)-2,2':5',2'':5'',2'''-quaterthiophene
- 58a** 2-(Adamantan-1-yl)-5-bromothiophene
- 58b** 5-(Adamantan-1-yl)-5'-bromo-2,2'-dithiophene
- 58c** 5-(Adamantan-1-yl)-5''-bromo-2,2':5',2''-terthiophene
- 59a** 5,5'''-Di(adamantan-1-yl)-2,2':5',2'':5'',2'''-quaterthiophene
- 59b** 5,5''''-Di(adamantan-1-yl)-2,2':5',2'':5'',2''':5''',2''''-sexithiophene
- 59c** 5,5''''''-Di(adamantan-1-yl)-2,2':5',2'':5'',2''':5''',2''''':5''''',2''''''-octithiophene

- 60** 2,2':5',2''-terthiophene
- 61a** 1,1'-([2,2':5',2''-terthiophene]-5,5''-diyl)bis(propan-1-one)
- 61b** 1,1'-([2,2':5',2''-terthiophene]-5,5''-diyl)bis(butan-1-one)
- 61c** 1,1'-([2,2':5',2''-terthiophene]-5,5''-diyl)bis(pentan-1-one)
- 61d** 1,1'-([2,2':5',2''-terthiophene]-5,5''-diyl)bis(2,2-dimethylpropan-1-one)
- 61e** [2,2':5',2''-terthiophene]-5,5''-diylbis(phenylmethanone)
- 62a** 1-([2,2'-bithiophen]-5-yl)-2,2,3,3,4,4,4-heptafluorobutan-1-one
- 62b** 1-([2,2':5',2''-terthiophen]-5-yl)-2,2,3,3,4,4,4-heptafluorobutan-1-one

1 General and Theoretical Section

*Everybody gets so much information
all day long that they lose their common sense.*

– Gertrude Stein

Our modern information and communication society relies more and more on constantly increasing data volumes.^[1] No matter whether in public or private networks, in the automotive or industrial section – the demand for higher data flow increases.^[2] Whereas ten to twenty years ago local storage space was a main concern, nowadays most data are located decentralized and data processing is dominated by cloud computing.^[3] The interaction between the separated devices requires very high Bit rates to ensure real-time communication. Thus, the demand for high-speed data transmission promotes the development of optoelectronic solutions based on the interaction of matter with light, due to the high frequency of light. For these devices themselves applications such as for organic semiconductors, i.e. organic light-emitting diodes (OLED),^[4] are still at the research stage^[5] whereas the connection between the computing units are widely spread realized through optical fiber technology. In the field of telecommunication glass fibers already represent a significant percentage of the network in OECD countries.^[6] For home applications, polymer optical fibers^[7] are of increasing interest.^[8] The high mechanical flexibility and very low production costs propose polymer optical fibers to short-range data transmission and sensor technology.^[9]

Besides those advantages, polymer host materials can be doped with primarily organic fluorescent dyes to create fibers with enhanced optical properties. Those fluorescent optical fibers are widely disseminated as ion sensors,^[10] or wavelength shifter.^[11] Furthermore, fluorescent optical fibers display one characteristic difference to undoped light guides: The light as the information carrier does not need to be launched from the terminal closing edge such as in glass fibers but can be injected from all directions and then be absorbed. The penetrating light excites the fluorescence dyes which subsequently emit fluorescence

radiation isotropically in all directions. A significant share is now trapped inside the fiber due to the laws of refraction. The operating principle corresponds to that of fluorescence solar collectors^[12] and enables contactless transmission of information in versatile, particularly rotating, devices. Such optical slip rings have potential for implementation in the automotive sector or medical technology such as computed tomography scanners.

The performance of optical slip rings is mainly equated with the data transmission rate. This in turn is physically limited by the fluorescence properties of the applied dyes. Particularly the fluorescence lifetime determines the data rates as the maximum pulse frequency is limited by the fluorescence decay time of the fluorophore. Most fluorescent dyes exhibit fluorescence lifetimes of about 5 ns.^[13-14] As a consequence, a slip ring with 100 Mbit s⁻¹ already could be realized using many fluorescent dyes such as Nile Blue as the fluorophore. With sub-nano second fluorescence lifetimes data rates of more than 1 GBit s⁻¹ are feasible. The development of such customized fluorescent dyes and for many more special applications requires a profound understanding of both, the basic physical processes as well as the relation between chemical structure and optical properties.

1.1 Fundamentals of Fluorescence

The emission of light from any substance is called luminescence. It occurs from electronically excited states and can formally be divided in two categories; fluorescence and phosphorescence, depending on the nature of the excited state. If the excited electron is paired to the electron in the corresponding ground state orbital by opposed spin we observe singlet states causing fluorescence. The return of the electron into the ground state is spin-allowed and takes place rapidly by emission of a photon (Figure 1). Phosphorescence conversely describes the light-emitting process from triplet states.^[14-15]

Following light absorption, several processes may occur. A fluorophore is usually excited to some higher vibrational level of 1E_1 . With a few rare exceptions, molecules rapidly relax to the lowest vibrational level of 1E_1 . This process is called internal conversion and occurs within 10^{-12} s or less. Since fluorescence lifetimes are typically near 10^{-8} s, internal conversion is generally complete prior to emission. Hence, fluorescence emission results from a thermally equilibrated excited state, that is, the lowest energy vibrational state of 1E_1 . Return to the

electronic ground state typically occurs to a higher excited vibrational ground state level, which then quickly (10^{-12} s) reaches thermal equilibrium (Figure 1). The fluorescence spectrum is commonly a mirror image of the absorption spectrum of the $^1E_0 - ^1E_1$ transition. This similarity occurs because electronic excitation does not importantly alter the nuclear geometry. Hence the spacing of the vibrational energy levels of the excited states is similar to that of the ground state. As a result, the vibrational structures seen in the absorption and the emission spectra are mirror-type very similar. Some molecules in the 1E_1 state can also undergo a spin conversion to the first triplet state 3E_1 . Emission from that state is termed phosphorescence, and is generally shifted to longer wavelengths (lower energy difference) relative to the fluorescence. The conversion of 1E_1 to 3E_1 is called intersystem crossing. Transition from the triplet to the singlet ground state is spin-forbidden and as a result the rate constants for triplet emission are several orders of magnitude smaller than those for fluorescence resulting in longer excited lifetimes. Molecules containing heavy atoms such as bromine and iodine are frequently phosphorescent. The heavy atoms facilitate intersystem crossing and thus enhance phosphorescence quantum yields.^[14]

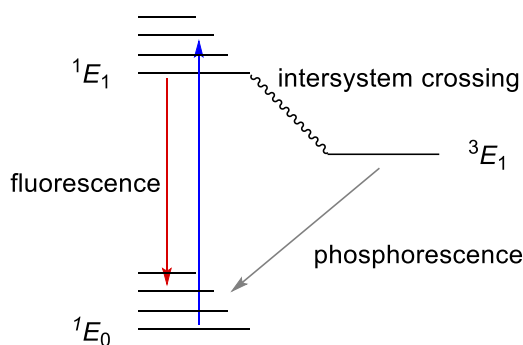


Figure 1: Schematic Jablonski diagram. Caused by absorption of a photon an electron is electronically excited into the singlet 1E_1 -state (blue). Usually an internal conversion from an elevated vibronic state into the vibronic ground state takes place. Subsequently, the excited electron relaxes (red) by emission of fluorescence light into an excited vibronic state of the electronic ground state 1E_0 . Phosphorescence occurs after intersystem crossing of the excited electron into the triplet 3E_1 -state under spin inversion. The spin-forbidden relaxation into the ground state (grey) causes the emission of phosphorescence radiation.

A more quantum chemical view on vibronic (simultaneously electronic and vibrational) transitions is represented by the *Franck-Condon-Scheme*(Figure 2). The respective electronic states are represented by anharmonic oscillators visualizing the potential energy (ordinate) of a chemical bond (or more complex approximations such as *Morse potential*) in relation to the nuclear coordinates (abscissa). Vibrational states are represented by their respective wave function. The principle presumes a significant difference between the time needed for electronic transitions (about 10^{-15} s) and that required for changes in the nuclear coordinates (approx. 10^{-12} s). Thus, the transition occurs vertically and the probability of a specific transition depends on the electron probability density of the respective vibrational state.

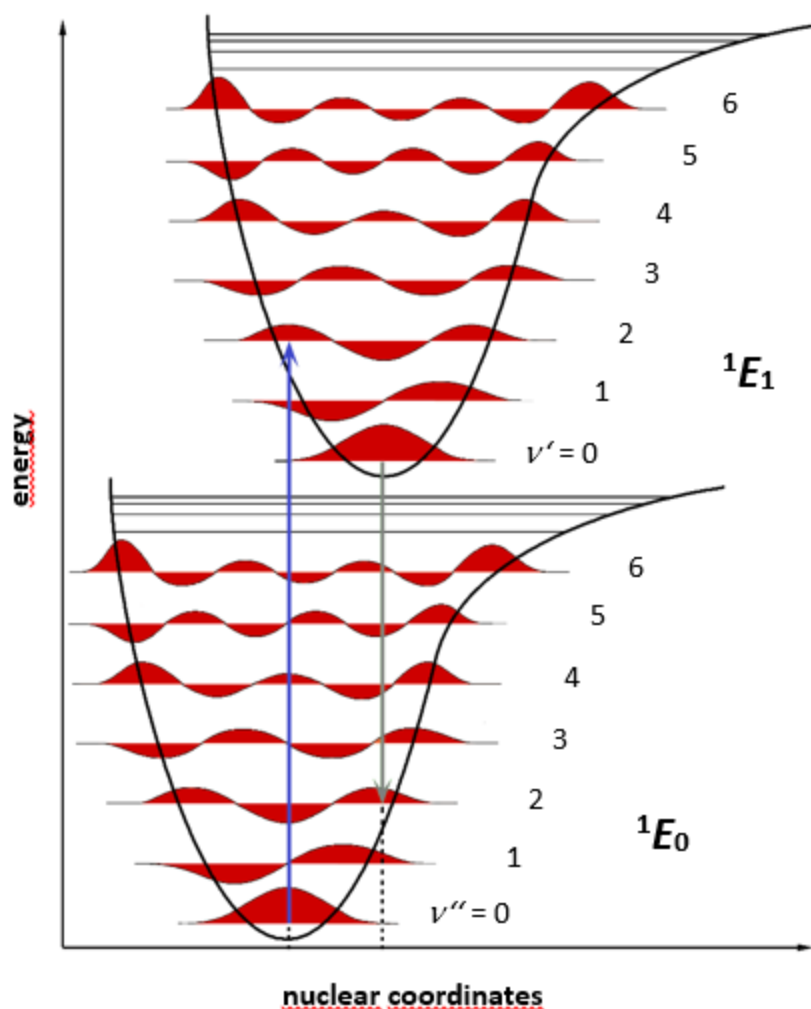


Figure 2: *Franck-Condon* energy diagram. Schematic wave functions (red) are given for anharmonic oscillators E_0 (electronic ground state) and E_1 (1st electronically excited state) representing the energy potential of the chemical bond, respectively. Absorption (blue) and fluorescence (grey) take place vertically.

The International Union of Pure and Applied Chemistry (IUPAC) defines: “Classically, the Franck–Condon principle is the approximation that an electronic transition is most likely to occur without changes in the positions of the nuclei in the molecular entity and its environment. The resulting state is called a Franck-Condon state, and the transition involved, a vertical transition. The quantum mechanical formulation of this principle is that the intensity of a vibronic transition is proportional to the square of the overlap integral between the vibrational wavefunctions of the two states that are involved in the transition.”^[16]

The wavelength of the absorption depends on the energy difference between the ground state 1E_0 and the excited singlet state (generally the 1st, called 1E_1). A relation between that difference and the chemical structure is given by *König* and *Ismailsky* for the majority of dyes.^[17] According to Figures 1 and 2, fluorescence occurs slightly shifted to longer wavelengths. This observation was first described by *Stokes* in 1852^[18] and is now called Stokes’ shift. Usually it describes the difference between the global maxima of absorption and fluorescence and is given in nm (non-linear scale) or eV (linear scale).

There are two further important characteristics besides the wavelength of fluorescence spectra, the fluorescence quantum yield Φ and the fluorescence lifetime τ . The first indicates the quotient of the number of emitted photons divided by the number of absorbed photons, see equation (1). Substances with high quantum yields close to unity, such as rhodamines or perylendiimides, display colors under common scattered daylight dominated by their fluorescence. The rate constants k_r (radiative) and k_n (non-radiative) both depopulate the excited state. A fluorescence quantum yield according to equation (1) can be close to $\Phi = 1.00$, in this case the non-radiative constant is negligible and all absorbed photons are re-emitted as fluorescence radiation.

$$\Phi = \frac{k_r}{k_r + k_n} \quad (1)$$

The lifetime of the excited state is defined by the time a molecule spends in the excited state prior to return to the ground state. The fluorescence decay is an exponential function of the number of relaxing photons versus time t . For single exponential behavior the fluorescence

lifetime τ is described by equation (2). The number of electrons relaxing by fluorescence in a specific time interval equals the intensity I of the emitted light. In a variant form of presentation as in equation (3) the fluorescence lifetime can be expressed reciprocal to the sum of k_r and k_n .

$$I(t) = I_0 e^{-\frac{t}{\tau}} \quad (2)$$

$$\tau = \frac{1}{k_r + k_n} \quad (3)$$

The fluorescence lifetime of a dye in theoretical absence of non-radiative processes is called intrinsic or natural lifetime τ_n and is given in equation (4). Analogously to equation (3), the natural lifetime equals the reciprocal radiative rate constant k_r .

$$\tau_n = \frac{1}{k_r} \quad (4)$$

Theoretically, the natural lifetime can be calculated from the absorption spectrum, molar attenuation coefficient ε (also called molar extinction coefficient) and emission spectrum of a fluorescent compound. According to *Strickler and Berg*,^[19] the radiative decay k_r can be determined using equation (5). The integrals refer to those below the spectra plotted on the wavenumber (cm^{-1}) scale, $I(\sigma)$ is the fluorescence spectrum whereas $\varepsilon(\sigma)$ describes the absorption spectrum of the 1E_0 to 1E_1 transition. The refractive index of the solvent is represented by n . When roughly neglecting the shape of the spectra, the integral of the absorption spectrum is represented by the molar attenuation coefficient ε . Thus, the qualitative predication of this equation is the reciprocal correlation between the fluorescence lifetime t and the molar absorptivity ε . Furthermore, the fluorescence lifetime τ proportionally depends on the ratio of these spectra given by the fluorescence quantum yield Φ . This interrelation is expressed in equation (6).

$$k_r = \frac{1}{\tau_n} \cong 2.88 \text{ s}^{-1} \times 10^{-9} n^2 \frac{\int I(\sigma) d\sigma}{\int I(\sigma) \sigma^{-3} d\sigma} \int \frac{\varepsilon(\sigma)}{\sigma} d\sigma \quad (5)$$

$$\Phi = \frac{\tau}{\tau_n} \quad (6)$$

Whereas the results of equation (5) match the measured value very good for some classes of dyes, particularly annulated aryls such as perylene, many fluorophores do not behave according to that prediction. Hence, there is often poor agreement between the value of τ_n calculated from equation (6) and that calculated from its absorption and emission spectra, see equation (5). These discrepancies occur for a variety of unknown and known reasons, such as a fraction of the fluorophores located next to quenching groups, which sometimes occurs for tryptophan residues in proteins.^[14] The quantum yields and fluorescence lifetimes can be modified by factors that affect either of the rate constants (k_r or k_n) or the molar absorptivity ε . Thus, quenching processes (internal or external) efficiently shorten the fluorescence lifetime^[20] but also reduce the quantum yield to the same extent. This enables application for sensors and fluorescence bio-imaging but refuses any use for i.e. signal processing or display technology where high emission intensities are required.

Fluorescence lifetimes are measured with means of time resolved photon counting detectors. Very short light pulses, particularly laser pulses, excite the molecules of the sample in solution or solid state. Subsequently, the fluorescence radiation is detected orthogonally at longer wavelengths. With modern technologies such as time-correlated single photon counting (TCSPC) and pulsed lasers as light sources high resolutions with less than 25 ps and good signal to noise ratios can be obtained. Even poorly emitting samples may be analyzed in acceptable measurement periods. The fluorescence decay of *N,N'*-bis(tridecan-7-yl)perylene-3,4:9,10-tetracarboxylic diimide (**1**) (abbreviated as *S-13*) is depicted in Figure 3.

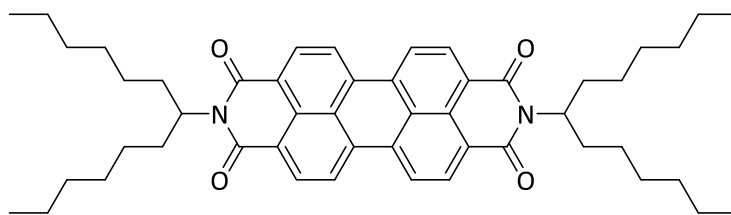
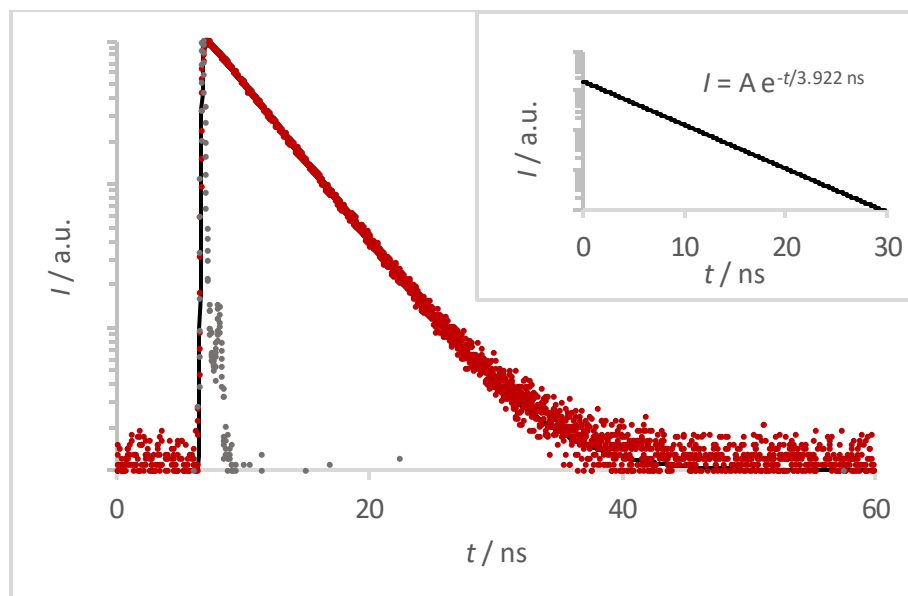
**1**

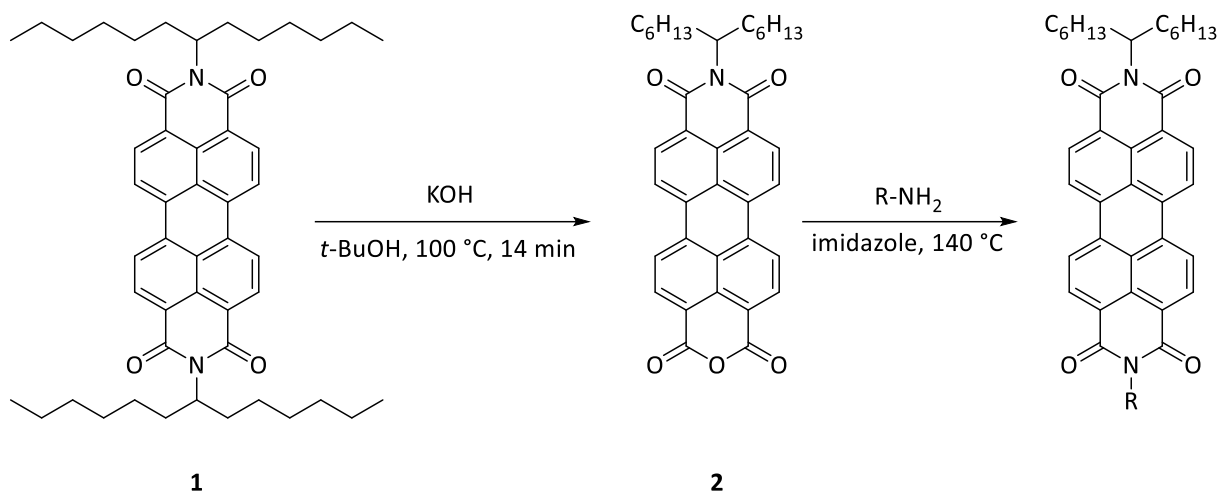
Figure 3: Fluorescence decay of *N,N'*-bis(tridecan-7-yl)perylene-3,4:9,10-tetracarboxylic diimide (**1**) in chloroform. Logarithmic scaled excitation puls (grey), fluorescence decay (red) and monoexponential fit (black, mainly covered by decay). Insert: Normalized monoexponential fit and resulting fluorescence lifetime of 3.92 ns.

1.2 Fluorescent Dyes

A fluorescent dye or fluorophore is a chemical compound that efficiently re-emits light upon optical excitation. Whereas light emitting structures can consist of a variety of elements such as metals or metalloids and their compounds^[21], the term fluorescent dye refers generally to organic molecules. The efficiency of fluorescence depends on the chemical structure of the chromophore. A rigid geometry is required to avoid non-radiative relaxation. Moreover, intersystem crossing processes leading to triplet states are promoted by heavy atoms in particular and have to be avoided. Thus, typical fluorophores consist of annulated aromatic rings and highly inflexible moieties within the actual chromophoric system.

The usage of fluorophores is diverse and ranges from simple aesthetic effects to specialized applications in research and technology. Prominent representatives are the xanthene derivatives fluorescein (**54**) and rhodamine B (**55**). Both are water-soluble and thus, are applied in fluorescence bio-imaging.^[22] Various other classes such as coumarins^[23], cyanines^[24], oxazines^[25] or biomolecules like the green fluorescent protein (GFP)^[26] are used as probes for analytical purposes. However, for long-term applications most fluorescent dyes are far too unstable.

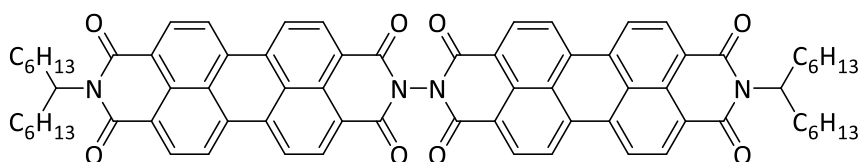
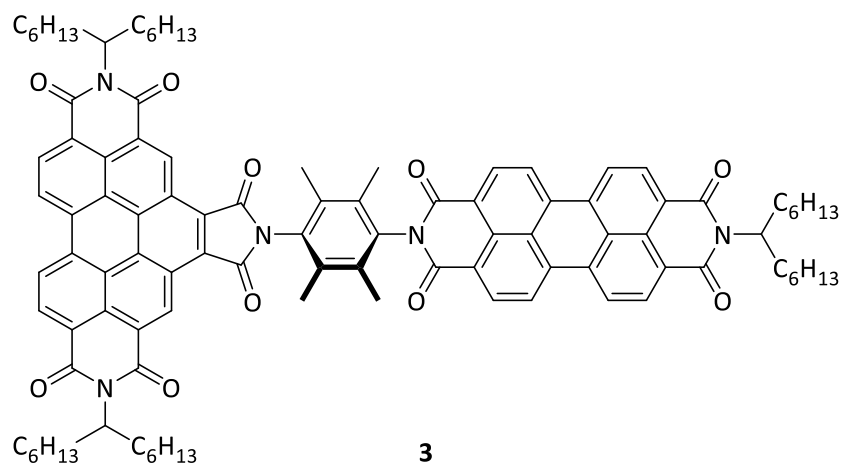
Highly long-term stable and lightfast fluorophores with quantum yields close to unity are perylenediimides. To prevent the expanded aryl system from π -stacking enabling good solubility, sterically demanding flexible alkyl chains are attached to the nitrogen of the imide. Very good results are obtained for secondary alkyls such as tridecan-7-yl moieties.^[27] The resulting perylene diimide **1** excels with a high molar attenuation coefficient of $\epsilon = 87\ 000$ and a fluorescence quantum yield of $\Phi = 0.99$. Hence, it serves as fluorescence standard^[28] and starting material for further derivatization.



Scheme 1: Alkaline hydrolysis of perylene diimide **1**. The resulting *N,N'*-bis(tridecan-7-yl)perylene-3,4-dicarboimide-9,10-dicarboxylic anhydride (**2**) can be condensed with various functional amines.

The molecular structure of perylene diimides displays interesting effects on the optical spectra. Quantum chemical calculations^[29] have shown that in both, HOMO and LUMO of the molecule, the imide nitrogen atoms are located on nodal planes. Thus, derivatization does not influence the absorption or fluorescence spectra. This enables asymmetric substitution without affecting the optical properties.

Particularly multichromophores based on perylene diimides (Scheme 2) display interesting optical behavior. Orthogonally arranged and rigid molecules such as **3** were proved^[30] to exhibit fluorescence resonance energy transfer (FRET)^[31] rates of nearly 1.00. This contradicts present theory and requires additional studies. Dyads with linear geometry such as **4** display increased values for the molar absorptivity caused by exciton effects.^[32] This in turn affects the fluorescence lifetime and motivates for further investigation.



4

Scheme 2: Orthogonally fixed perylene diimide – benzoperylene triimide dichromophor **3** (left). The chromophores are linked via an aromatic 2,3,5,6-tetramethylphenylene moiety. Below the linearly *N-N*-linked perylene diimide – perylene diimide dichromophore **4** consisting of the same subunit.

1.3 Objectives

- **Linear perylene diimide multichromophores and their optical characterization**
 - Development of a synthetic strategy for perylene based multichromophores
 - Preparation of short and stable linkers with solubilizing alkyl moieties
 - Characterization of the optical properties mainly focused on the molar attenuation coefficient and the fluorescence lifetime
- **Dynamic effects in naphthalene dicarboximides and anthracene dicarboximides with electron rich substituents**
 - Investigation of fluorescent solvatochromism in substituted 4-arylnaphthalimides resulting in large Stokes' shifts
 - Conclusions on the geometrical intramolecular dynamics
 - Synthesis and optical characterization of derivatives of 10-aminoanthracene dicarboximides and studies on the reaction conditions
 - Studies on homo-coupling reactions of carboxylic imides to larger aromatic π -systems under metal-free conditions
- **Long-range electromagnetic molecular interactions indicated by fluorescence**
 - Determination of fluorescence lifetimes depending on the concentration
 - Development of a theoretical model
- **Efficient recycling of unmarked polymers by means of the fluorescence decay**
 - Investigation of auto-fluorescence in technical polymers
 - Development of a method for detection of the fluorescence decay for reliable identification of different polymers
- **Oligothiophenes with short fluorescence lifetimes**
 - Synthesis of highly soluble 2,5-substituted oligothiophenes
 - Studies on the optical properties, particularly the fluorescence lifetime
 - Synthesis of long-term stable derivatives of bisketoterthiophenes with large Stokes' shift and very short fluorescence lifetimes

2 Results and Discussion

The following section discusses optical investigations such as absorption, fluorescence and fluorescence lifetime spectroscopy. All measurements were carried out in concentrations below 10^{-5} mol L⁻¹ if not stated otherwise, where reabsorption or quenching effects are generally accepted to be negligible. Particularly in the case of fluorescence lifetimes it was found, that the concentration of the sample severely affects the obtained values. However, for better comparability the reported lifetimes are given as simple numbers because within the range of differences between the respective dilutions the results can be assumed as constant. For more detailed evaluation of the data the concentration of the respective measurement is given in the experimental section. For identical compounds, the same solution was applied for fluorescence decay measurements and for the determination of the fluorescence quantum yield. Thus, the actual concentration of the sample can be extracted from the report on fluorescence quantum yields in Chapter 4.

2.1

Modifications of Perylene

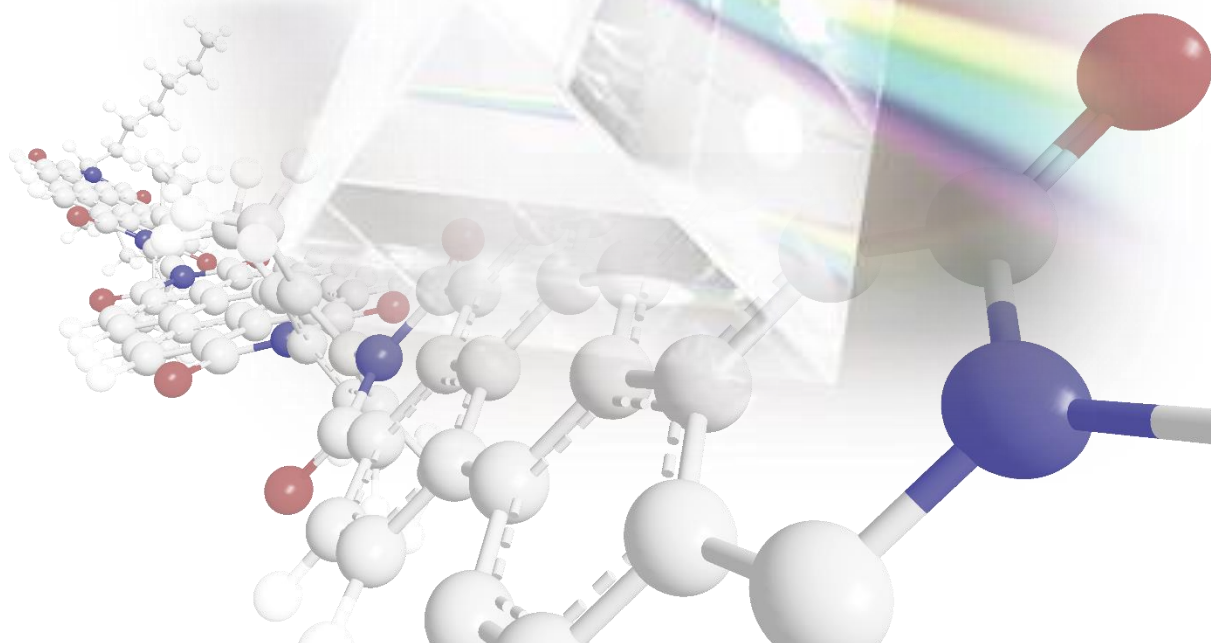
Diimides:

Shortening the Fluorescence

Lifetime via Intramolecular

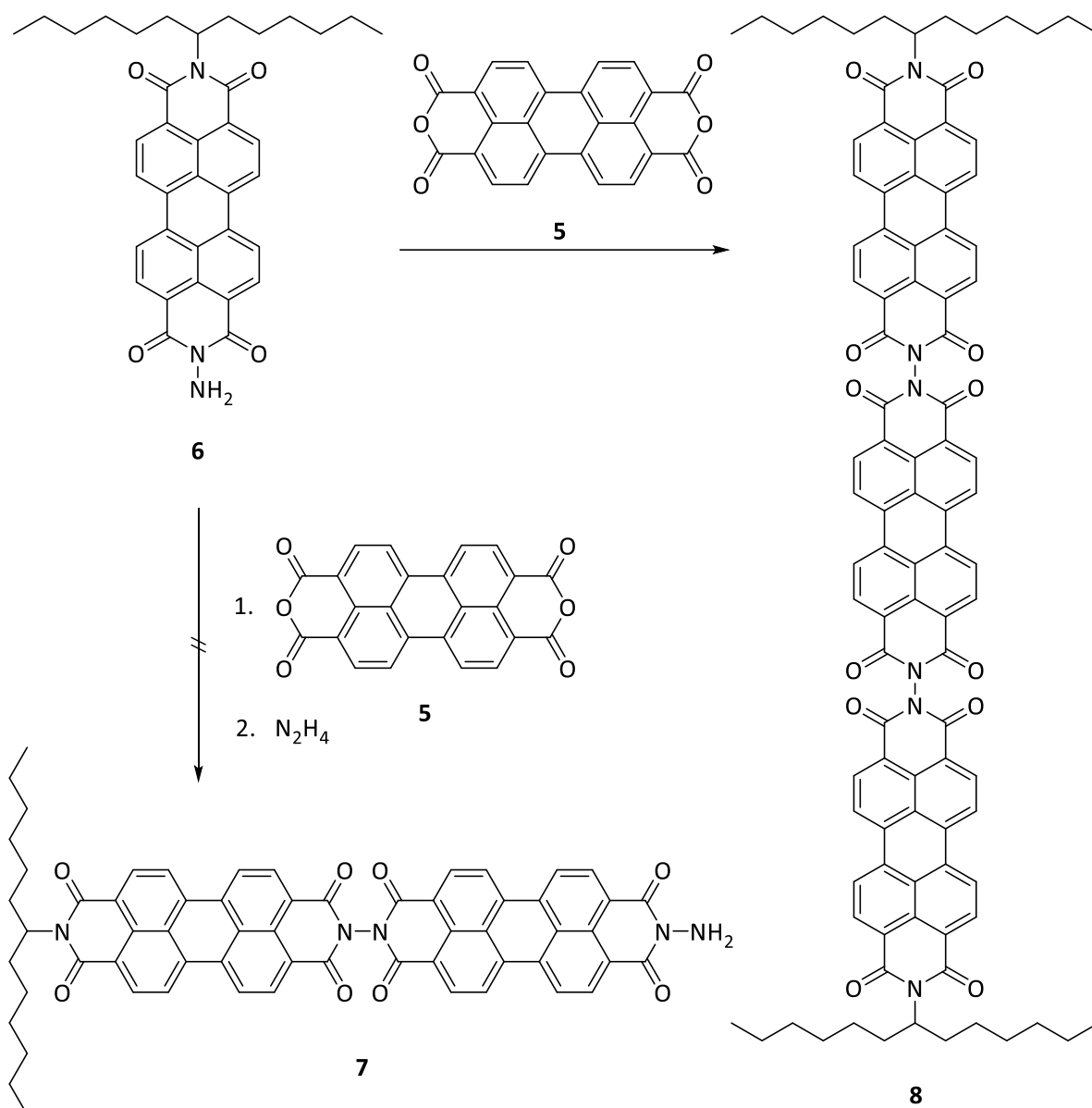
Interactions in Axial-Linked

Di- and Trichromophores



For applications such as data transmission the crucial property of an applied fluorescent dye is the fluorescence lifetime. However, little thereof is known and converted into significant theories. In the literature, many data were reported but mostly as simple facts. More detailed investigation is carried out for special applications or bio-environmental performance. Examinations of fluorescence quenching effects are often limited to one chromophore^[33]. There are two equations describing the dependency of the fluorescence decay from assessable and measurable parameters. First, the proportional correlation of the fluorescence quantum yield to the fluorescence lifetime, expressed in equation (6). Second, the reciprocal dependency of the latter from the electronic transition probability expressed in the molar attenuation coefficient ε , see equation (5). Both theories are valid, but they proved to be limited to considerations within the same substance or at least, class of substances. Moreover, no concept exists describing the relation between fluorescence lifetime and molecular structure, i.e. as there is such for the correlation of absorption wavelengths and molecular structure.^[17] Hereinafter, the known theories were assigned to perylene diimides, a well-studied class of fluorescent dyes. Very high fluorescence quantum yields close to unity and a high light-fastness are advantageous properties for studying structural influences on opto-physical processes.

According to equation (5), the fluorescence lifetime of perylene diimides is indirectly proportional to the oscillator strength indicated by the molecular absorptivity ε . *Langhals* and *Jona*^[32] describe the superelevation of the molar absorptivity caused by exciton effects in perylene diimide di- and trichromophores. This in turn leads to shorter fluorescence lifetimes of about 2.4 ns compared to about 3.95 ns for *N,N'*-bis(tridecan-7-yl)perylene-3,4,9,10-tetracarboximide (**1**). Increasing the number of perylene units to more than $n = 3$ should even further decrease the fluorescence decay.

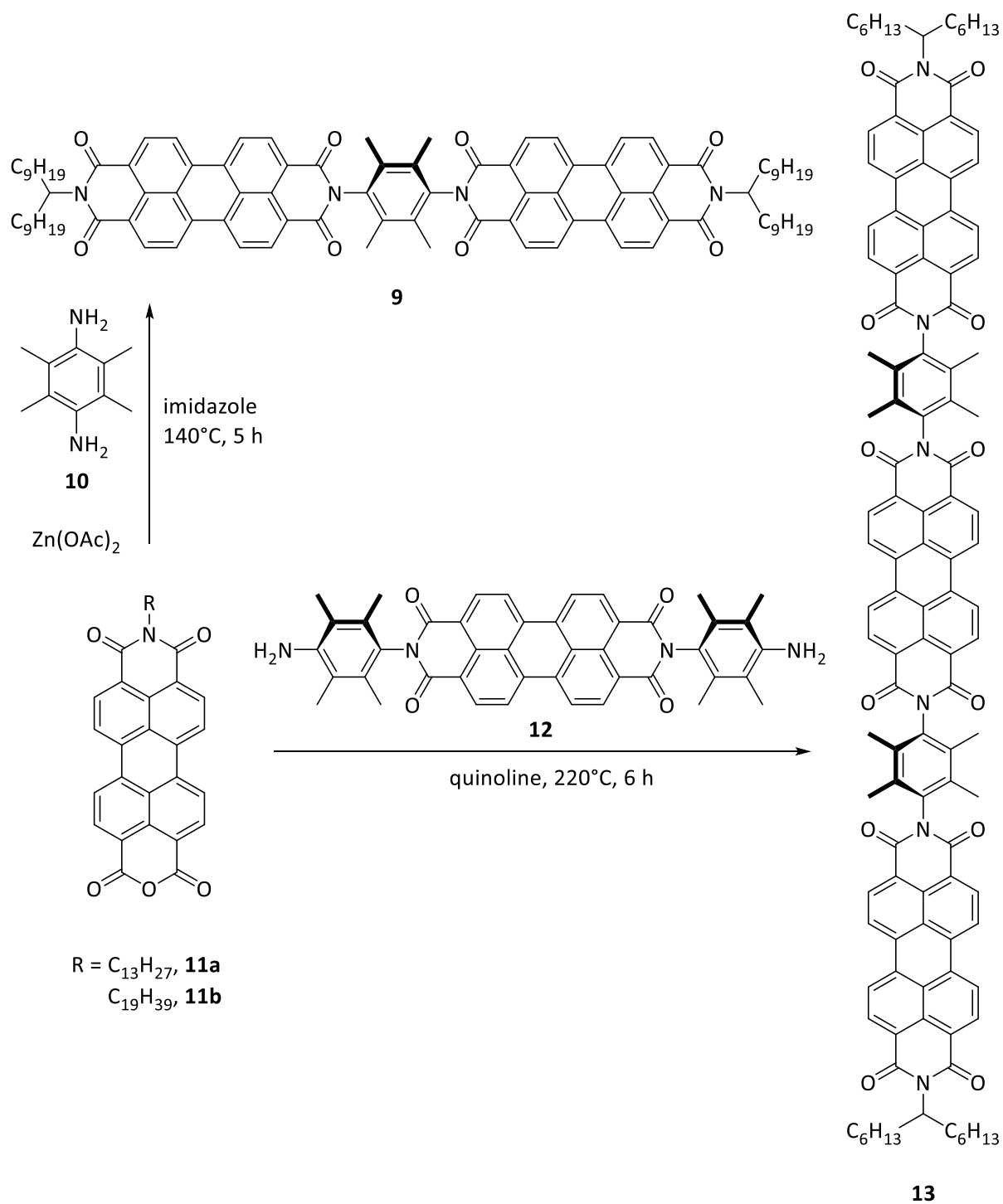


Scheme 3: General preparation procedure for *N-N'*-linked perylene diimide based di- and trichromophores according to the literature.^[32]

Additional prolongation to higher oligomers according to this approach is described to fail (Scheme 3). Hydrolysis of the inward carboximides is favored^[32] over the terminal ones of **8**. Obviously, the electron-withdrawing effect of the carbonyl groups on the second imide moiety dominates over the steric hindrance. In further experiments the stepwise construction of **8** via **7** in single reactions was studied. Unfortunately, hydrazine displays an antagonistic behavior between its nucleophilic and basic attributes. The condensation which is enhancing the growth process to higher oligomers competes with the degrading alkaline hydrolysis. Again, the *N-N*-junction between the chromophores is hydrolyzed and only the starting

material could be detected besides newly formed *N*-aminoperylene-3,4-carboximide-9,10-dicarboxylic anhydride as byproduct.^[32] Hence, in this study an approach was followed using more sterical hindered but still short linkers for the connection of the single dyes. 1,4-Diamino-2,3,5,6-tetramethylbenzol (**10**) is an easily accessible building block for linked carboximides.^[34] To increase the solubility of the multichromophore product, a prolonged secondary “swallow-tail” alkyl chain^[27] containing 19 carbon atoms was introduced for most approaches.

Double condensation of two units of perylene monoimide mono anhydride **11b** with the above mentioned amine **10** yields 47% of the corresponding dichromophore **9** (Scheme 4). The target compound was isolated via column chromatography and the structure verified by means of *MALDI* and *FAB* mass spectrometry and ¹H NMR spectroscopy. A precise elemental analysis failed indicating minor impurities.



Scheme 4: Preparation of 2,3,5,6-tetramethylbenzene-linked perylene diimide di- and trichromophores **9** and **13**.

The absorption maxima (Figure 4) were found at 492.2 and 529.6 nm. Thus, they are slightly shifted to longer wavelengths compared to the basic monochromophore^[35] (*N,N*-bis(nonadecan-10-yl)perylene-3,4:9,10-tetracarboxylic (*S*-19) imide, 489 and 526 nm). The determined molar attenuation coefficient at 529.6 nm displays a value of 183 000 L mol⁻¹ cm⁻¹ which equals more than twice the absorptivity of *S*-19^[35] with 87 100 L mol⁻¹ cm⁻¹. A factor of 2.1 points to the same effects described for **8** by Langhals and Jona^[32]. Although the molecular attenuation coefficient is not absolutely conclusive for not highly pure compounds, byproducts are expected to lead to smaller values. As the opposite effect is observed the result unambiguously shows analogy to the superelevation of the absorptivity of **8**. The measured fluorescence lifetime of $\tau = 3.73$ ns for **9** is in very good agreement with equation (5) and the expected exciton effects. Moreover, the possible influence of aggregating effects could be excluded in a simple dilution series. The results shown in Figure 5 display a linear behavior in the respective range of concentration indicating no aggregation. The fluorescence maxima were found at 536.0 and 577.9 nm (Figure 4). A fluorescence quantum yield of $\Phi > 0.99$ equals that of *S*-13 (**1**) and would be ideal for any applications or use for standards. These results motivated for the synthesis of higher multichromophores.

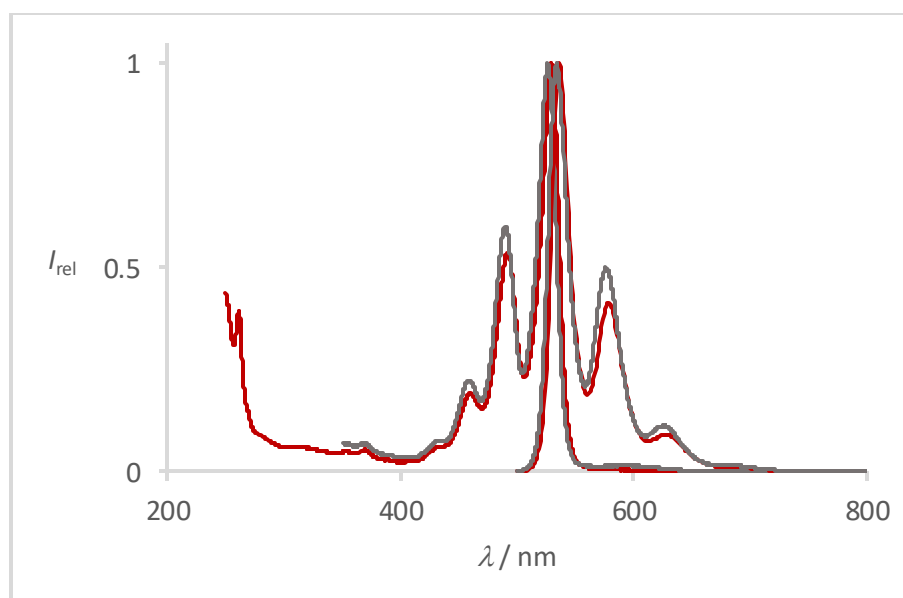


Figure 4: Absorption (left) and fluorescence (right) spectra of perylene diimide dichromophore **9** (red) vs. those of *S*-13 (grey) in chloroform.

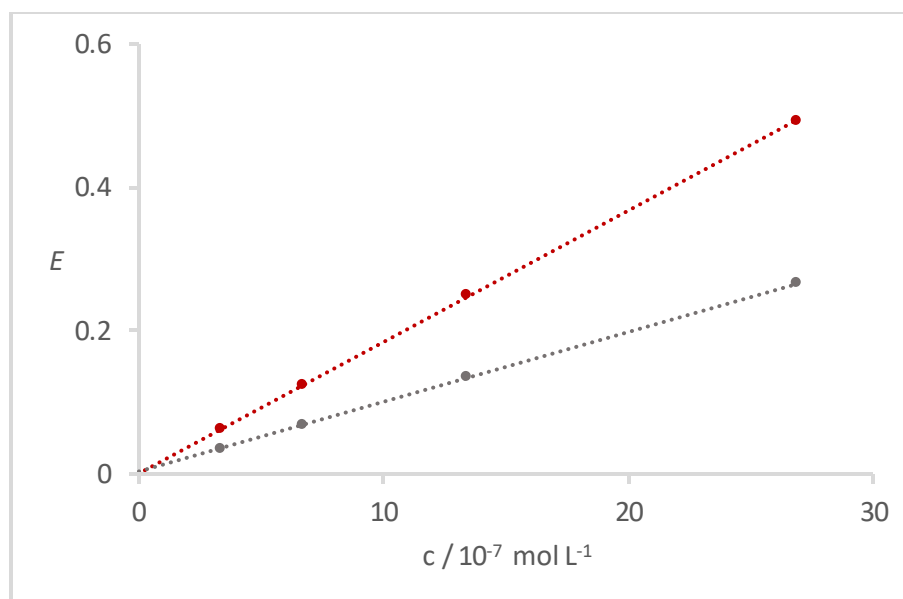


Figure 5: Absorbance of the two main maxima of dichromophore **9** in a dilution series from 3 to $27 \times 10^{-7} \text{ mol L}^{-1}$ in chloroform. Both maxima at 530.0 nm (red) and 492.0 nm (grey) display linear behavior.

Further increase of the number of perylene units to the trichromophore **13** was realized by the condensation of 5 equivalents *N,N'*-bis(tridecan-7-yl)perylene monoamide **11a** with *N,N'*-bis(4-amino-2,3,5,6-tetramethylphenyl)perylene-3,4:9,10-tetracarboxylic imide^[36] **12**. Using harsh conditions in quinolone at 220 °C for 6 h lead to only 7% yield. More moderate conditions as for the bichromophore **9** did not succeed in any product. The isolation of the trichromophore proved to be very challenging due to the low solubility of the product. Aggregation on the column during chromatography seems to impede the formation of well-defined fractions. Furthermore, the ^1H NMR spectrum displays a multitude of broad signals. Hence, a determination of the purity via NMR spectroscopy failed. The product was verified by *MALDI* mass spectroscopy and exhibited a single spot in thin layer chromatography on silica and aluminum oxide in highly diluted chromatograms.

The absorption of **13** (Figure 6) exhibits maxima at 490.8 and 527.2 nm, respectively. Compared to *S*-13 (**1**), the minima are slightly bathochromically shifted. The molar attenuation coefficient ($154\,200\text{ L mol}^{-1}\text{ cm}^{-1}$) displayed values considerably below the expected threefold absorptivity of *S*-13 (**1**) (about $260\,000\text{ L mol}^{-1}\text{ cm}^{-1}$). First, this can be attributed to the notable impurities. Second, the respective absorption bands are not only broadened compared to both, the *N*-*N'*-trichromophore **8** and even *S*-13 (**1**) there is also a significant further absorption band at 589.0 nm. This is typical for the formation of *J*-type aggregates^[37] explaining the band-shape and the low absorptivity at shorter wavelengths. Moreover, aggregation might be the key problem of the chromatographical purification where no distinct fractions could be obtained. To investigate the aggregation a dilution series down to concentrations of less than $2 \times 10^{-7}\text{ mol L}^{-1}$ was measured (Figure 7). Surprisingly, the intensities of all maxima, even that at 589.0 nm exhibits linear behavior. Thus, aggregation seems to occur even in highly diluted solutions and application for fiber-doping is disadvantageous. The fluorescence displays maxima at 534.8 and 577.6 nm, respectively and a quantum yield of $\Phi = 0.86$. The lower fluorescence strength compared to **9** is also in good agreement with the results indicating aggregation.

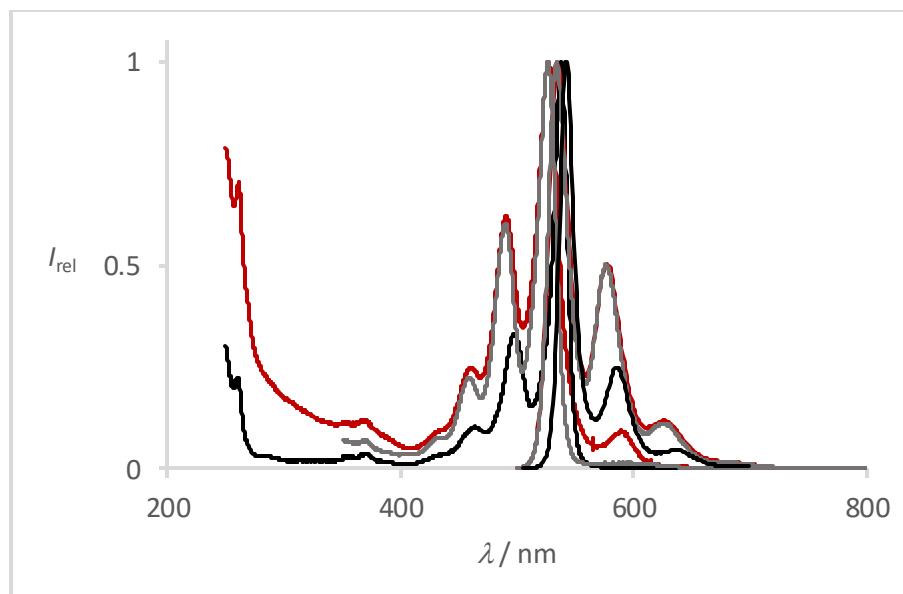


Figure 6: Absorption (left) and fluorescence (right) spectra of perylene diimide trichromophore **13** (red) vs. those of *S*-13 (**1**) (grey) and trichromophore **8** (black) in chloroform.

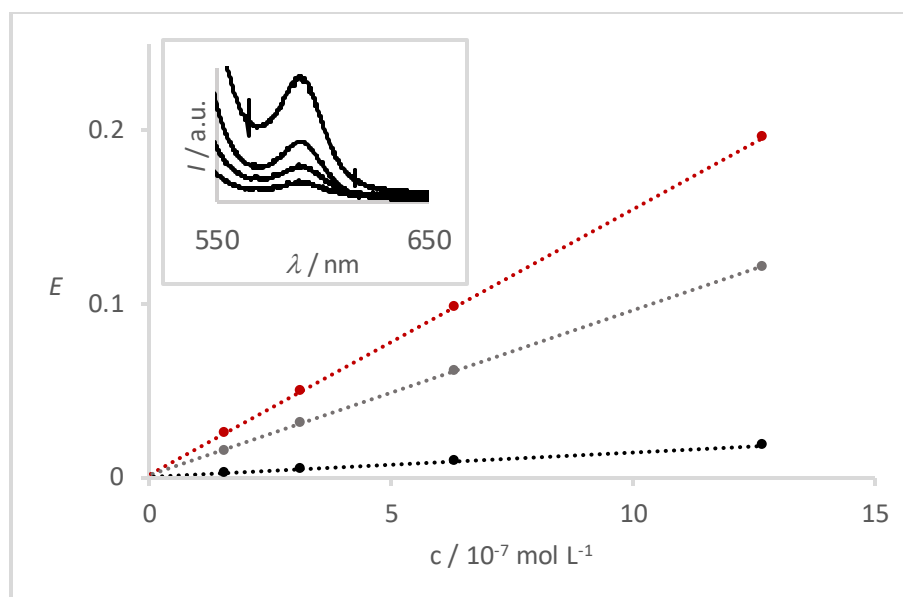


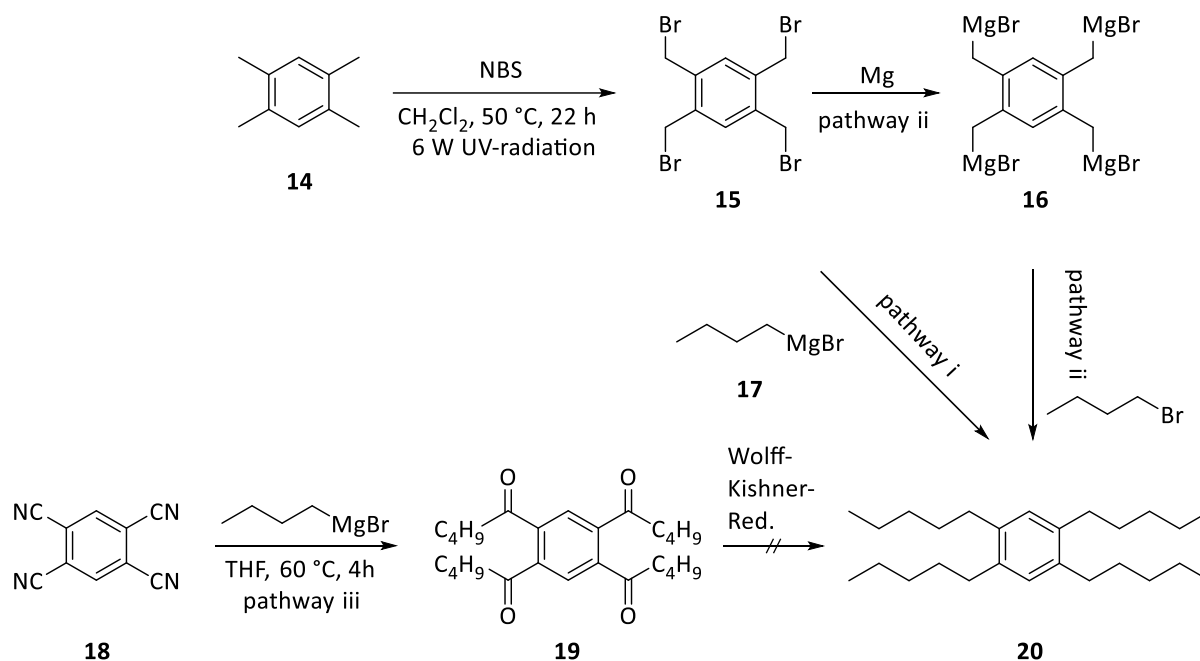
Figure 7: Absorbivity of the main maxima of trichromophore **13** in a dilution series from 1.7 to $13 \times 10^{-7} \text{ mol L}^{-1}$ in chloroform. All maxima at 527.0 nm (red), 491.0 nm (grey) and 589 nm (black) display linear behavior. Insert: Detail of the spectrum emphasizing the linear dependency of the absorbivity on the concentration.

Countering the problem of aggregation the introduction of a more solubilizing spacer is a promising approach to better accessible multichromophores. Not only the optical properties should improve and the purification might be simplified, but also the reactivity of those compounds could be increased to result in higher yields. Sticking to a *p*-phenylenediamine moiety sustains a short but stable spacer which can be functionalized in opposed, in case *para*-positions. The methyl groups of the 2,3,5,6-tetramethylphen-1,4-diyl moiety in the approach described above can be substituted with longer alkyl chains causing higher steric requirements and thus, less aggregation.

The idea was to prolong the alkyl chains in a *Grignard* reaction^[38] to yield compound **20** (Scheme 5). Nitration with nitric acid in either concentrated sulfuric acid or a mixture of acetic acid and acetic anhydride would lead to 1,4-dinitro,2,3,5,6-tetrapentylbenzene which would be reduced to give the corresponding 1,4-diamino derivative.

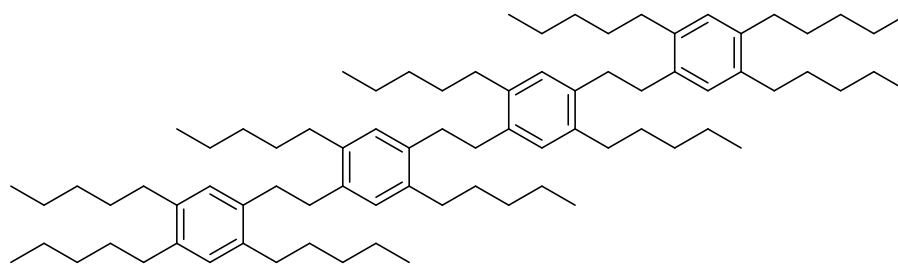
The preparation of the 1,2,4,5-tetrapentylbenzene **20** via *Grignard* reactions was studied in several pathways under different conditions, in total six different approaches. Starting with 1,2,4,5-tetramethylbenzene (**14**), a UV-induced bromination in benzylic position with *N*-bromosuccinimide^[39] lead to the fourfold substituted compound **15**. The product was

obtained elementary analytically pure in 46% yield and served as starting material in the first approaches.



Scheme 5: Investigated reaction pathways to obtain 1,2,4,5-tetrapentylbenzene (20).

Pathway i: A freshly prepared solution of 10 equivalents butylmagnesium bromide (17) in THF was added to a solution of 1,2,4,5-tetra(bromomethyl) benzene 14 in THF slowly at -78°C . Under copper iodide catalysis^[40] the reaction mixture was allowed to warm to room temperature, stirred for 17 h and subsequently heated to 80°C for additional 7 h. The reaction was quenched with 1 M aqueous hydrochloric acid, extracted with chloroform and purified via multiple column chromatography on aluminum oxide. The product was found in significant percentage in ^1H NMR and mass spectra. However, impurities of oligomers were also found and could not be removed chromatographically. Obviously, an intermolecular metal exchange took place to form a *Grignard* species of the durene moiety which reacted with other bromodurenes left. In *EI-MS*, peaks for the di-, tri, and tetramer 21 (Scheme 6) were found at $m/z = 602, 846$ and 1090 . Higher homologues might also form but are outside the detectable range of the analytical method.

**21**

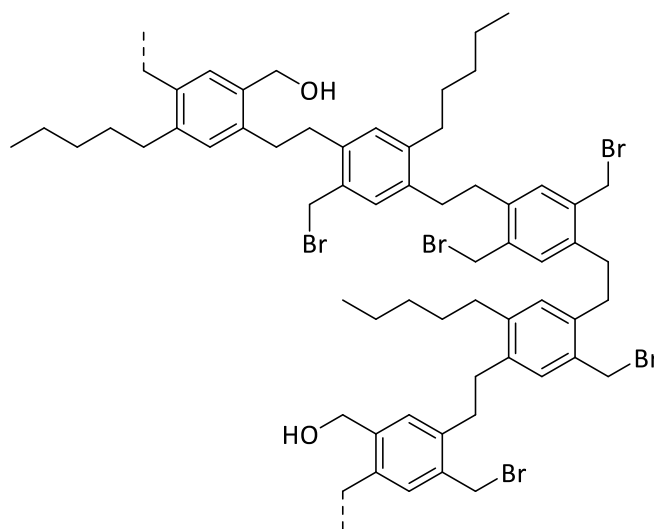
Scheme 6: Pentylated tetramer **21** consisting of durene units. Constitutional isomers are not considered, the given structure is the sterically most favorable.

To prevent metal exchange, the following approach was carried out adding the reagents in opposite order. When tetrabromo durene **15** is added to a solution of butylmagnesium bromide (**17**), an excess of the Grignard reagent is ensured during the addition process. Thus, a competition between exchange and substitution might favor the latter. Moreover, the temperature was kept below $-70\text{ }^{\circ}\text{C}$ for the entire reaction time. A few minutes after the complete addition, the reaction mixture started to precipitate and was kept at $-70\text{ }^{\circ}\text{C}$ for 1 h. Then the temperature was allowed to rise with about $10\text{ }^{\circ}\text{C}$ per hour to room temperature and the mixture was worked up as described before. A colorless, solid polymer was obtained and analyzed by elementary analysis. As known from the mass spectrometry of the earlier approach, each durene unit is linked to two more aryls. It is plausible, that for steric reasons only two aryl units can react with one durene group, most likely in *para*-position. Deriving from the elemental analysis (Table 1), each durene unit is still brominated in one benzylic position while in average only every second unit is substituted with the alkyl chain (Scheme 7). The remaining positions seem to be hydroxylated which could be attributed to substitution during basic work up. As the mass of the polymer is unknown, only a rough estimation of its composition was successful. Slightly different but qualitative same results are obtained when water inclusions inside the bulk material are assumed. In summary, the reduced temperature could not prevent from the magnesium exchange but supporting it in relation to the aimed substitution. The formed polymer precipitates after exceeding a specific length. While still in solution, substitution with butylmagnesium bromide (**17**) takes place but once a critical length is approached, the polymer coils, precipitates and prevents the remaining bromomethyl moieties from further reaction.

Table 1: Elementary analysis of the polymer forming at low temperatures. The indicated hydroxyl group can also be interpreted as non-covalent aqueous inclusion.

Elemental analysis	C	H	Br
Calc. for $(C_{10}H_{10})^a(C_4H_9)_{0.4}Br_{1.1}(OH)_{0.5})_n$	55.86	5.70	35.24
found	54.66	5.81	35.23

a) Durene units are estimated to form a polymer chain. Two positions per unit are occupied with either a butyl, bromo or hydroxyl group.



Scheme 7: Representative schematic section of the discussed polymer from the *Grignard* reaction of **15** and **17**.

As a consequence, the reaction temperature was increased to 80 °C. Thus, the thermodynamically favored substitution is promoted. Both variants were performed, addition of the butyl-*Grignard* reagent to the tetrabromodurene and vice versa. In both cases a highly viscous oil was obtained indicating the formation of oligomers which were discarded.

Pathway ii: The results discussed above suggest the benzylmagnesium bromide to be energetically more favored compared to the alkyl *Grignard* compound. Switching the roles of electrophile and nucleophile, a fourfold magnesium insertion was performed to obtain **16**. Subsequently, an excess of bromobutane was slowly added at 80 °C. The reaction was stirred at 80 °C for 90 minutes and quenched with 1 M hydrochloric acid. Again, a solid polymer was isolated and investigated by means of elemental analysis. The percentage of bromine was found at 14.72% whereas the values for carbon and hydrogen increased to 62.70% and 7.87%,

respectively. Compared to the product in pathway i at low temperatures, the aimed reaction is more favored. However, metal exchange takes place in both directions significantly. Thus, the strategy of coupling two bromo moieties was not further pursued.

Pathway iii: 1,2,4,5-Tetracyanobenzene (**18**) is a low-cost and well available precursor. The cyano groups are good electrophiles concerning primary alkylmagnesium bromides. Moreover, no metal insertion is possible and thus, no homo-coupling is anticipated. After protic-aqueous treatment of the product the corresponding tetraketone should be obtained. A *Wolff-Kishner* type reduction leads to the respective tetraalkylbenzene.

Two equivalents of a freshly prepared solution of butylmagnesium bromide (**17**) in THF were treated with a solution of tetracyanobenzene (**18**) in THF at 0 °C. The reaction was heated to 60 °C and first turned green at room temperature, later red at elevated temperatures (> 50 °C). The reaction was quenched with 1 M hydrochloric acid and extracted with chloroform. After chromatographic purification on silica the product **19** could be verified with mass spectrometry (*EI* and *MALDI*) and ¹H NMR spectroscopy. Whereas most byproducts were removed, an isolation of **19** from the less converted compounds such as 1-cyano-2,4,5-tripentanoylbenzene did not succeed due to the very similar behavior in column chromatography. A consecutive *Wolff-Kishner*-reaction of the obtained mixture failed.

Transmetallation, particularly *Negishi* zinc insertion did not succeed particularly due to the reduced reactivity. Generally, the fourfold reaction requires highly reactive species to obtain acceptable yields. Furthermore, the separation of the product from various similar but less substituted byproduct proved to be extremely difficult. A distillation could not be performed under the given circumstances with an aromatic compound of that molecular weight.

Conclusion

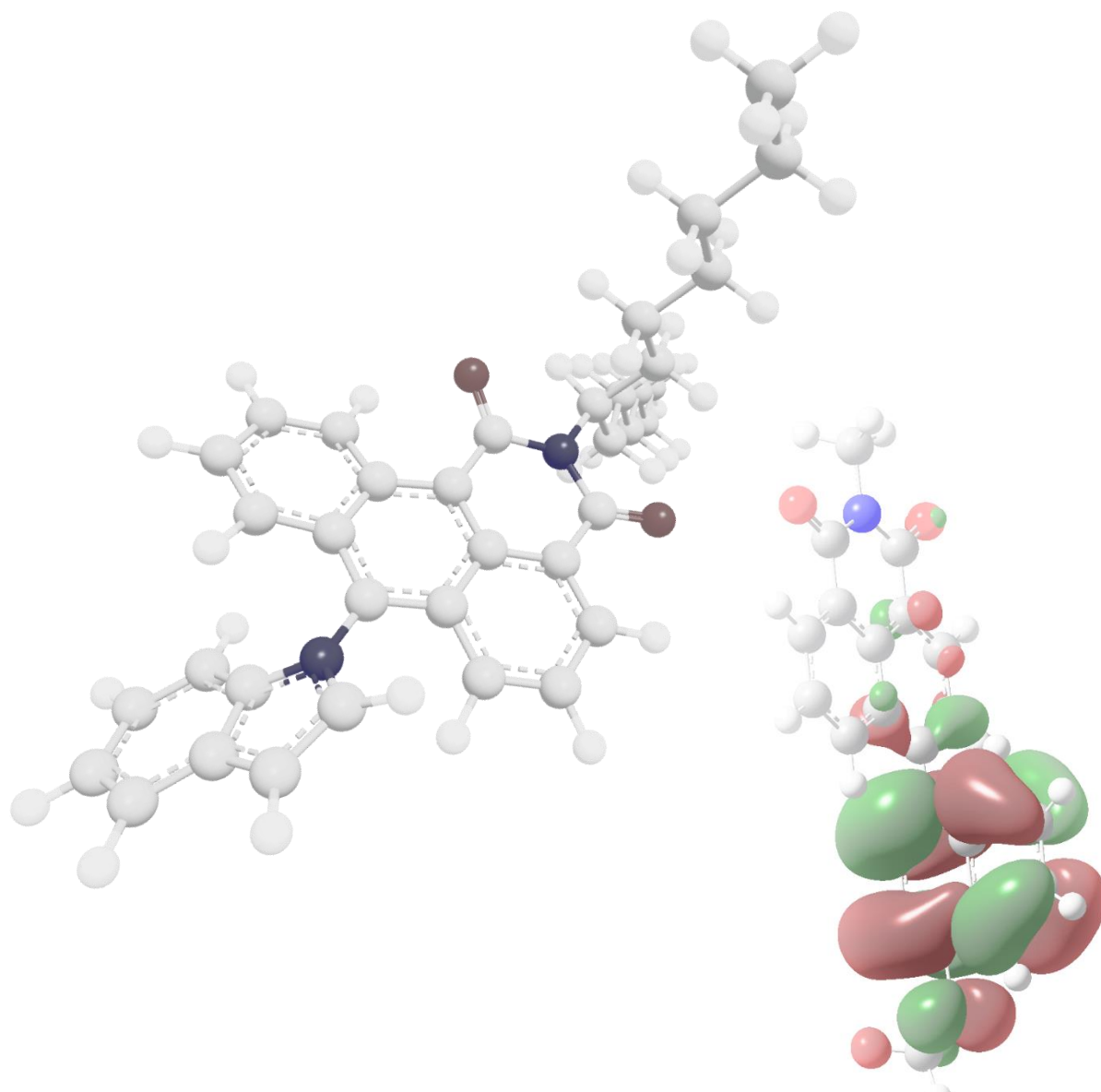
The approach to reduce the fluorescence lifetime by increasing the molar attenuation coefficient by exciton effects resulted in two main recognitions. The concept presented by *Langhals* and *Jona*^[32] can be transferred to longer-range spacers. Although the relative orientation of the chromophores is different (parallel vs. orthogonal along the lateral axis), same results are found for the dichromophores. The trichromophore **13** however, evades from any comparison as it displays significant aggregation. Introduction of sterically more demanding spacers failed. In most approaches the reaction itself leads to product. Multi-site

reactions are impeding good yields and purification via column chromatography was not successful as no distinct spots are obtained.

The poor solubility of the dyads complicated the handling of these compound and is a huge disfavor for isolation and futher reactions. Thus, the focus shifted from perylene diimide mulitchromophores to smaller fluorophores.

2.2

Influence of Intramolecular Dynamics on Fluorescence Properties



H. Langhals, T. Schlücker, R. Greiner, D. Zgela, *Ger. Offen.* DE 102016004396.2 (Apr. 7th 2016).

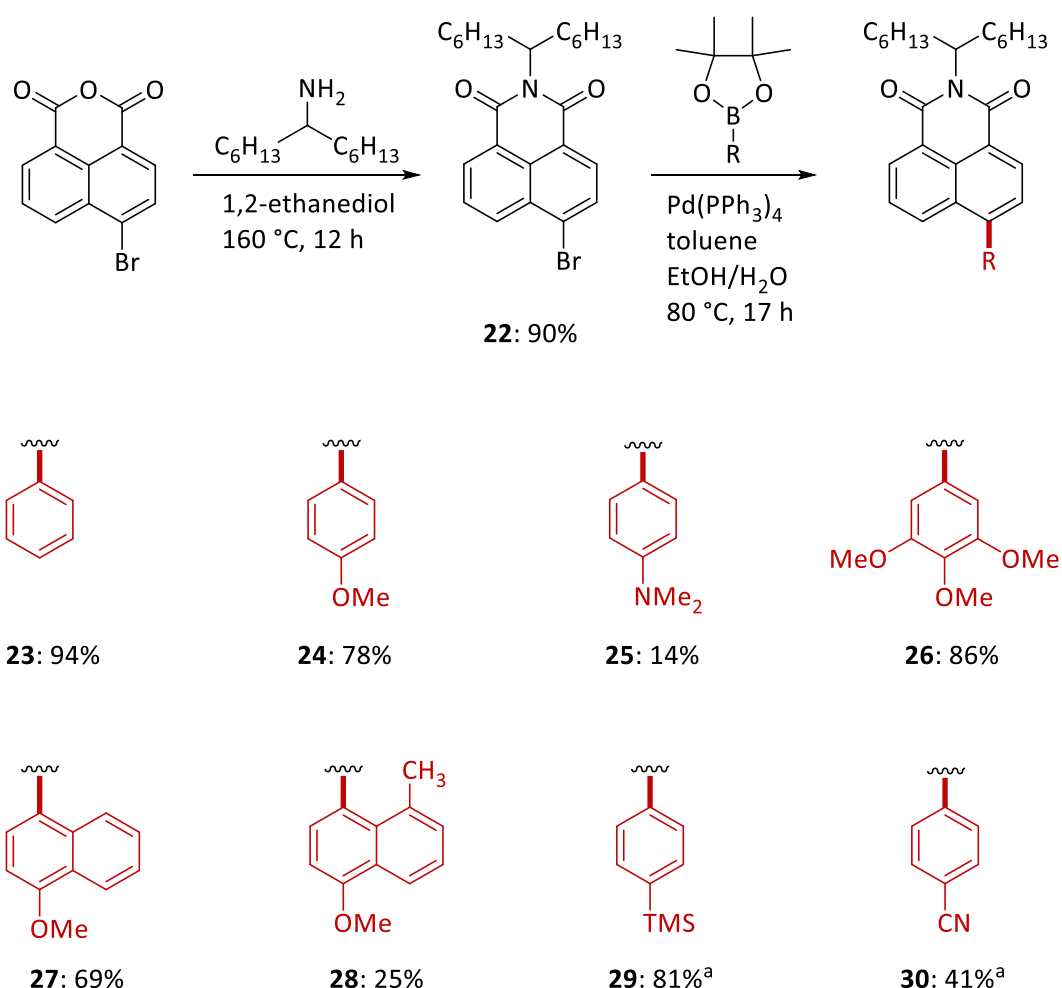
Intramolecular dynamics and high fluorescence quantum yield usually contradict each other. In most cases, dynamic processes are caused by rotational degrees of freedom preventing any detectable fluorescence. However, in some cases this intramolecular motion can be limited in its range and, more important, controlled by the interaction with light. This results in two different arrangements, one for the ground state and one for the excited state. Both geometric situations, particularly the one of the electronically excited state, can be rigid enough to exhibit fluorescence. *Langhals* and *Hofer* demonstrated^[41] a C-C-coupled perylene dichromophore with an increased Stokes' shift of 70.3 nm (0.277 eV) and a quantum yield of $\Phi > 0.99\%$. The fluorescence lifetime was found to be $\tau = 3.76$ ns and thus slightly below the value of *S-13* (3.95 ns). Regarding the dynamic impact on the fluorescence key properties, Stokes' shift and fluorescence lifetime, investigations on molecular dynamics and its effects on the optical properties were intensified.

2.2.1 Intramolecular Dynamics of 4-Aryl Naphthalimides

N-alkyl naphthalene-1,8-dicarboxylic imides are the simplest representatives of well soluble *peri*-arylene imides. Substitution with aryl moieties in *peri*-position introduces an extended aromatic π -system, however steric repulsion between the hydrogen atoms of the subunits in *ortho*- or *peri*-position induce considerable twists interfering good orbital overlap. Hence, the dihedral angle should depend on the electronic state of the molecule. There are two concepts concerning this dynamics, in particular for push-pull chromophores. *Langhals et al.* presented a theory^[41] where the dihedral angle diminishes after excitation. The electron deficiency in the HOMO results in a shorter C-C bond and a more planar geometry between the subunits. This effects a large Stokes' shift due to better delocalization of the π -electrons in the excited state. In contrast, the TICT-theory^[42] (twist induced charge transfer) predicts a orthogonalization caused by electronic excitation. This twist in turn induces a charge transfer from the donor to the acceptor moiety. Also a large Stokes' shift is obtained but quantum yields are usually below $\Phi = 0.3$ due to competing non-radiative relaxation.

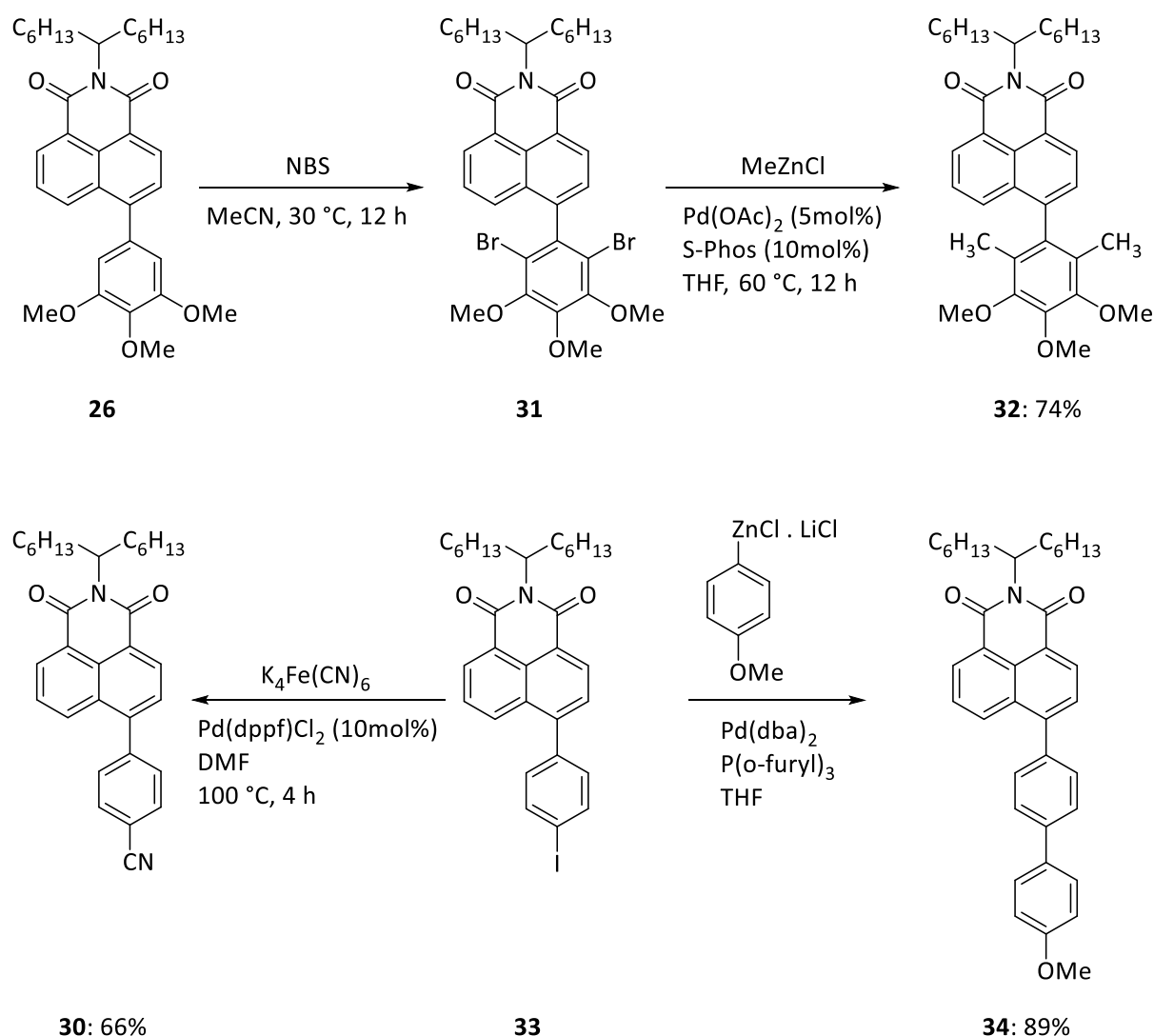
In 4-arylnaphthalimides, a photo-induced shift of electron density from the donor to the carboximide is responsible for inducing a large dipole moment. Sensitivity of the energy of the excited state towards solvation with polar solvents causes a bathochromic shift of the fluorescence. This process corresponds to the positive solvatochromism of 4-amino-*N*-

methylphthalimide applied for Zelinski's^[43] solvent polarity *S* scale. An even more pronounced solvatochromism of naphthalimides should be obtained caused by the introduction of extended electron rich aryl moieties. The fluorescent solvatochromism is expected to increase with the photo-induced dipole moment depending on the distance of the separated charges. Thus, aryl groups were inserted as conjugating spacers between donor groups and the naphthalimide acceptor moiety by means of transition metal catalysed cross-coupling reactions. To obtain highly soluble dyes, we started with a condensation of readily available 4-bromonaphthalic anhydride with 7-aminotridecane^[27] giving the highly soluble key intermediate **22** (Scheme 8). The *Suzuki* cross-coupling^[44] reaction of **22** with various aryl dioxaborolanes attained the corresponding arylated derivatives **23-30**.



Scheme 8: Synthesis of arylated naphthalene carboximides **23-30**. a) 4-(Trimethylsilyl)phenylboronic acid and 4-cyanophenylboronic acid was used for **29** and **30**, respectively.

Substitution with the sterically hindered 2,6-dimethyl phenyl boronate failed where synthesis could be alternatively realised by stepwise peripheral introduction of the demanding methyl groups. The easily accessible trimethoxy derivative **26** was brominated with *N*-bromosuccinimide to give **31** and then further treated with methylzinc chloride under typical Negishi cross-coupling conditions^[45] to provide **32** (Scheme 9). Since also the borylation of more complex aryl halides proved to be difficult, we converted the trimethylsilyl derivative **29** to the corresponding aryl iodide **33** in order to extend the conjugated system.



Scheme 9: Bromination of **26** and subsequent cross-coupling with MeZnCl gives **32** (top); cyanation and Negishi cross-coupling of **33** leads to **34**. **30** was alternatively obtained via Pd-catalyzed cyanation (bottom).

A typical Negishi cross-coupling of **33** with *p*-anisylzinc chloride^[46] (prepared from the reaction of 4-iodoanisole with *i*PrMgCl·LiCl, followed by ZnCl₂) gave the methoxy biphenyl derivative **34** in very good yield of 89%. Further, the cyanation of **33** led to the corresponding aryl naphthyl cyanide **30** in an improved yield (Scheme 9).

Fluorescence lifetimes of naphthalimides **23-30** and **34** were determined and found to depend on both, the chemical structure and on the applied solvent (Table 2). In chloroform, fluorescence lifetimes of about 3-4 ns were found. Strong donor groups such as *N,N*-dimethylaminophenyl (**25**) and trimethoxyphenyl (**26**) increase the fluorescence lifetime to nearly 7 ns whereas electron withdrawing groups (**29-30**) decrease these values. The prolonged compound **34** also exhibits shorter lifetimes which is attributed to the higher molar attenuation coefficient in accordance to equation (5). However, comparison of highly fluorescent compounds such as **24** with the weaker emitting **27-28** reveal that the fluorescence lifetime is not strictly predictable with equation (5). The absorption is nearly same in intensity and spectral shape (Figures 8a and 9-10) however, the natural lifetimes τ_n (according to equation (6)) are significantly different to each other. In fact the measured lifetimes are comparable which raises the question if fluorescence lifetimes τ are more dependant on the chemical structure than strictly on optical spectra. Moreover, taking into account the discussed properties of *S*-13 (**1**) one can see the similarity of the fluorescence lifetime while absorbance (approx. factor 5) and quantum yields (factor 1-2) are very different and far from compensating each other. This confirms the assumption that the fluorescence lifetime is mainly of structural significance. Equations (5) and (6) are valid (at least qualitatively, see Table 2) but limited to comparisons within a narrow field of structural quite similar compounds.

The fluorescence lifetimes of naphthalimides **23-30** and **34** rely on their chemical structure and can be adjusted by substitution. However, there is no distinct difference between the actual values of τ for different substituent which could be assigned to molecular dynamics. Although different lifetimes were obtained in diverse solvents, this is mainly attributed to fluorescence quenching according to equation (5). Much more intense impact of solvent effects were found for the wavelength of fluorescence (Table 3, FWHM given in Tables 4-5). A pronounced positive fluorescent solvatochromism was observed and associated with molecular dynamics and geometry.

Table 2: Fluorescence quantum yields and lifetimes of naphthalimides **23-30** and **34**.

		CHCl ₃	C ₁₄ H ₃₀	C ₆ H ₁₄	C ₄ H ₉ OH	C ₁₁ H ₂₃ OH	DMF	Toluene
23	ε^a	17100	17600	16800	19000	18500	17700	16900
	Φ^b	0.78	0.094	0.076	0.95	0.76	0.74	0.50
	τ^c	3.21			3.85		3.62	
	τ_n^d	4.11			4.06		4.89	
24	ε^a	16900	15800	15700	17100	16700	16400	16400
	Φ^b	0.83	0.79	0.65	0.83	0.83	0.82	0.75
	τ^c	4.11	3.12	2.65	5.18	4.78	5.24	3.50
	τ_n^d	4.95	3.95	4.07	6.24	5.76	6.39	4.67
25	ε^a	11200	16500	12300	10300	11800	10700	10800
	Φ^b	0.64	0.73	0.70	0.013	0.14	0.0037	0.65
	τ^c	6.99	3.61	3.47	3.50	5.51		5.12
	τ_n^d	10.9	4.95	4.96	269	39.3		7.88
26	ε^a	15900	17100	16500	16600	16900	16500	17000
	Φ^b	0.65	0.51	0.41	0.022	0.26	0.0065	0.71
	τ^c	6.62	2.78	2.03	0.208	1.75	0.119	5.40
	τ_n^d	10.2	5.45	4.95	9.44	6.71	18.2	7.61
27	ε^a	15300	16200	14900	16200	18800	15200	16000
	Φ^b	0.39	0.34	0.33	0.088	0.23	0.13	0.18
	τ^c	4.07	1.83	1.70	1.80	4.85	3.85	1.53
	τ_n^d	10.4	5.37	5.16	20.5	21.1	29.6	8.51
28	ε^a	17100	16000	16800	18100	15900	17000	16900
	Φ^b	0.40	0.34	0.34	0.047	0.28	0.055	0.19
	τ^c	4.14	1.89	1.88	1.05	3.10	3.01	1.59
	τ_n^d	10.4	5.56	5.54	22.5	11.1	54.7	8.36
29	ε^a	18600	18800	17400	18600	19100	17900	18200
	Φ^b	0.79	0.18	0.14	0.89	0.85	0.64	0.51
	τ^c	3.08	5.08		3.63	3.81	3.38	2.03
	τ_n^d	3.90	28.2		4.07	4.48	5.29	3.98
30	ε^a	23700	26400	22600	24100	24600	22800	22400
	Φ^b	0.54	0.54	0.53	0.70	0.71	0.55	0.51
	τ^c	1.34	0.99	1.02	2.21	2.12	2.15	1.16
	τ_n^d	2.48	1.84	1.93	3.16	2.99	3.92	2.27
34	ε^a	27500	29300	28300	27500	26800	28300	27500
	Φ^b	0.67	0.50	0.50	0.16	0.56	0.15	0.40
	τ^c	2.93	1.43	1.35	1.05	3.21	1.91	1.40
	τ_n^d	4.37	2.86	2.71	6.57	5.72	12.7	3.51

a) Molar attenuation coefficient in L mol⁻¹ cm⁻¹; Fluorescence quantum yields relative to S-13 (**1**) with $\Phi = 1.00$ c) Fluorescence lifetime in ns; c) Natural fluorescence lifetime in ns, calculated according to equation (6).

Table 3: Absorption and fluorescence maxima of naphthalimides **23-30** and **34**.

		CHCl ₃	C ₁₄ H ₃₀	C ₆ H ₁₄	C ₄ H ₉ OH	C ₁₁ H ₂₃ OH	DMF	Toluene
23	λ_{Abs}^a	355.4	343.4	342.2	355.2	353.4	355.2	346.8
	λ_{Fluo}^b	420.0	402.3	402.7	429.1	420.6	427.2	410.6
24	λ_{Abs}^a	364.8	356.4	354.2	366.2	365.6	368.0	364.2
	λ_{Fluo}^b	459.6	427.8	424.0	498.1	476.4	497.2	443.2
25	λ_{Abs}^a	426.2	403.8	401.2	430.2	428.6	433.8	418.2
	λ_{Fluo}^b	578.4	469.8	462.7	638.4	610.0		532.4
26	λ_{Abs}^a	362.2	357.0	354.8	361.4	362.6	365.6	360.8
	λ_{Fluo}^b	525.1	442.3	440.2	572.1	526.4	618.8	492.4
27	λ_{Abs}^a	325.0	322.6	322.6	323.6	323.8	323.8	324.0
	λ_{Fluo}^b	509.7	431.7	427.1	576.8	532.4	581.8	478.0
28	λ_{Abs}^a	329.0	327.2	326.6	327.8	329.0	328.8	328.8
	λ_{Fluo}^b	522.7	440.2	434.8	570.1	537.0	597.8	487.0
29	λ_{Abs}^a	356.0	344.4	343.4	357.6	355.0	356.0	353.4
	λ_{Fluo}^b	425.4	407.0	406.7	434.2	430.6	432.7	416.7
30	λ_{Abs}^a	366.4	356.2	355.6	367.8	365.8	367.8	364.6
	λ_{Fluo}^b	447.4	410.8	407.4	480.0	457.5	478.3	427.5
34	λ_{Abs}^a	364.4	357.6	354.0	366.0	369.4	369.0	364.8
	λ_{Fluo}^b	492.2	436.7	426.8	556.6	518.2	583.4	454.6

a) UV/Vis-absorption maximum in nm; b) Fluorescence maximum in nm.

Table 4: FWHM*-values of absorption and fluorescence spectra of naphthalimides **23-30** and **34** in nm.

	Hexane		Tetradecane		Toluene		Chloroform		Undecanol		Butanol		DMF	
	Abs. ^a	Fluo. ^b	Abs. ^a	Fluo. ^b	Abs. ^a	Fluo. ^b	Abs. ^a	Fluo. ^b	Abs. ^a	Fluo. ^b	Abs. ^a	Fluo. ^b	Abs. ^a	Fluo. ^b
23	48.4	58.5	51.6	59.6	52.0	60.2	52.2	63.2	51.8	67.4	48.8	67.7	52.2	66.4
24	54.4	64.5	53.6	64.4	60.2	70.8	60.4	74.0	58.2	88.0	64.8	90.9	62.8	93.1
25	76.4	66.2	79.0	70.8	88.4	83.8	85.0	101.0	92.4	164.1	109.4	205.0	93.2	
26	54.0	70.4	59.6	71.2	62.8	86.6	64.0	104.1	61.8	134.9	66.8	160.1	68.0	
27	83.8	66.4	76.2	67.1		77.8	81.2	91.6		122.3	83.4	141.5		135.5
28	79.2	68.2	81.8	67.3		83.5	82.4	95.6	50.6	123.5	82.0	150.0		143.0
29	50.2	59.2	52.2	60.2	53.0	62.4	53.2	65.9	53.8	70.9	52.2	69.4	53.8	68.2
30	56.4	57.1	53.2	57.9	52.8	60.7	54.6	71.9	57.9	87.0	58.8	89.0	60.2	90.7
34	56.4	65.9	57.6	66.6	60.2	74.7	60.4	90.9	63.8	127.1	63.6	154.6	64.2	152.7

*Full width at half maximum, experimental determination. a) FWHM of absorption in eV; b) FWHM of fluorescence in nm.

Table 5: FWHM*-values of absorption and fluorescence spectra of naphthalimides **23-30** and **34** in eV.

	Hexane		Tetradecane		Toluene		Chloroform		Undecanol		Butanol		DMF	
	Abs. ^a	Fluo. ^b	Abs. ^a	Fluo. ^b	Abs. ^a	Fluo. ^b	Abs. ^a	Fluo. ^b	Abs. ^a	Fluo. ^b	Abs. ^a	Fluo. ^b	Abs. ^a	Fluo. ^b
23	0.518	0.452	0.552	0.456	0.537	0.434	0.530	0.436	0.531	0.460	0.496	0.444	0.530	0.442
24	0.546	0.443	0.529	0.435	0.580	0.433	0.571	0.419	0.544	0.466	0.612	0.446	0.590	0.454
25	0.617	0.360	0.629	0.374	0.657	0.354	0.589	0.359	0.649	0.558	0.781	0.642	0.627	
26	0.540	0.426	0.594	0.423	0.614	0.429	0.626	0.450	0.593	0.580	0.653	0.606	0.656	
27	1.011	0.420	0.926	0.419		0.411	0.974	0.423		0.520	1.014	0.518		0.482
28	0.972	0.415	1.018	0.404		0.426	0.983	0.420	0.547	0.533	0.982	0.553		0.494
29	0.531	0.445	0.547	0.448	0.542	0.440	0.534	0.441	0.546	0.472	0.526	0.443	0.541	0.444
30	0.576	0.403	0.531	0.403	0.512	0.395	0.514	0.434	0.547	0.511	0.559	0.471	0.566	0.479
34	0.567	0.436	0.569	0.433	0.576	0.435	0.568	0.451	0.600	0.584	0.598	0.603	0.601	0.548

*Full width at half maximum, experimental determination. a) FWHM of absorption in eV; b) FWHM of fluorescence in eV.

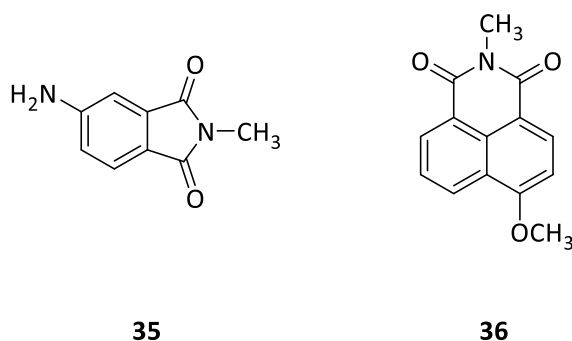
From UV/Vis and fluorescence measurements it can be clearly recognized that naphthalimides **23-30** and **34** are moderately solvatochromic in absorption and strongly solvatochromic in fluorescence as shown for the simple phenyl derivative **23** (Figure 8a). This indicates an optical excitation-induced increase of the dipole moment and was subject of further investigations. The molar energies of fluorescence light of various carboximides were calculated by means of equation (10) where λ_{\max} is the fluorescence maximum of the individual dye in the tested solvent (E_T values^[46] are in kcal/mol for comparison with previously reported values in literature to avoid confusion; these may be multiplied by 4.2 to obtain SI units). The

solvatochromism of the carboximides was compared both with *Dimroth and Reichardt's* $E_T(30)$ polarity scale^[47] representing mainly the effect of dynamic solvation and with *Brooker's* χ_R scale^[48] indicating mostly for the polarisability of the solvent. The spectroscopic data of dyes **23-30** and **34** were compared to reported data to evaluate the solvent sensitivity of the fluorescence. The highly solvatochromic 4-amino-*N*-methylphthalimide (**35**) as the basis of Zelinski's universal *S* solvent polarity scale^[43] served as reference as well as the simple donor substituted 4-amino-*N*-methylphthalimide (**35**) (Scheme 10). The E_T values of **25** were calculated from literature data for various solvents. A linear free energy relation (LFER)^[49] of these E_T values with the $E_T(30)$ polarity scale according to equation (8) gave appreciably better results (correlation number $r=0.95$ for $n=14$ solvents) than with Brooker's χ_R scale^[48] ($r=0.90$ for $n=14$).

$$E_T = \frac{28591 \text{ kcal nm mol}^{-1}}{\lambda_{max}} \quad (7)$$

$$E_T = a E_T(30) + b \quad (8)$$

Similar results were obtained for the solvatochromism of the fluorescence of **23-30** and **34** (Table 3). As a consequence we conclude that the solvent effects by polar dynamic orientation of the solvent molecules dominate for the reported carboximides and agreed with the $E_T(30)$ scale as most appropriate comparison.



Scheme 10: 4-Amino-*N*-methylphthalimide (**35**) and 4-methoxy-*N*-methylphthalimide (**36**) as reference for fluorescence data comparison.

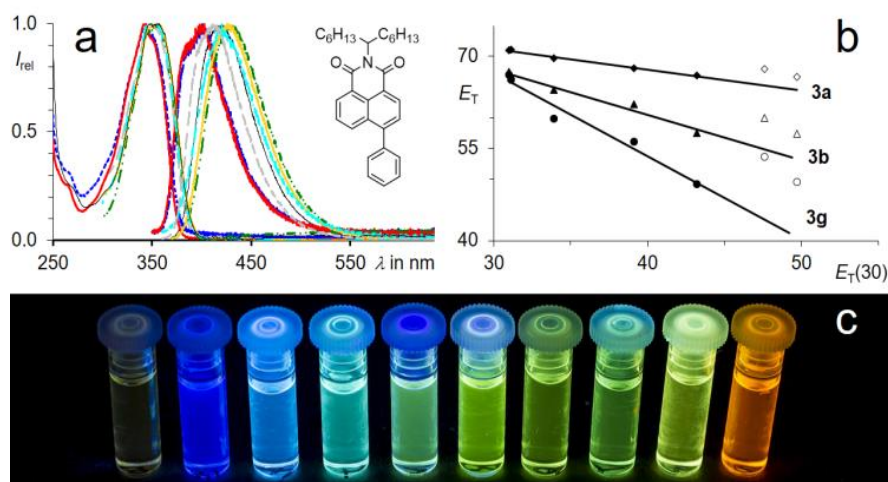


Figure 8: a) UV/Vis absorption (left) and fluorescence (right) spectra of **23** in various solvents. From left to right: hexane (thick solid red), tetradecane (dotted blue), toluene (dashed grey), chloroform (solid black), undecanol (dotted dashed turquoise), DMF (diffuse yellow), 1-butanol (double dotted dashed green). b) Linear relationship of the solvatochromism (E_T) of **23** (diamonds), **24** (triangles) and **37** (circles), respectively to the $E_T(30)$ solvent polarity scale. Closed symbols: Aprotic solvents; open symbols: protic solvents, neglected for regression. c) Aryl naphthalene carboximides **23-30**, **32** and **34** in CHCl_3 under UV-light (366 nm). From left to right: **32**, **30**, **24**, **34**, **23**, **29**, **28**, **27**, **26**, **25**.

The solvents *n*-tetradecane, *n*-hexane, toluene, chloroform, *N,N*-dimethyl formamide (DMF), 1-undecanol and 1-butanol were investigated for an overview of solvent effects where the two protic solvents were applied for studying the influence of hydrogen bonds. Linear correlations of the E_T values with the $E_T(30)$ values were obtained. Larger deviations to higher E_T were observed for hydrogen bond-donating solvents such as 1-butanol and 1-undecanol indicating the specific influence of such interactions; the solvent viscosity seems to have a minor influence (compare hexane with tetradecane and 1-butanol with 1-decanol) and large Stokes' shifts are even observed in a solid glassy matrix of PMMA. As a consequence, the further discussion was concentrated on the non-hydrogen bond-donating solvents.

Table 6: Solvatochromism of the fluorescence of the dicarboxylic imides **23-30**, **32** and **34-36**.

Dye	α^a	r^b	ϑ^c	ϑ_{ex}^d	E_{HOMO}^e	E_{LUMO}^e	$E_{HOMO}(E_1)^f$	$E_{LUMO}(E_1)^f$	Dipole ^g	Dipole _{E1} ^h
23	-0.34	-0.99	57.80	39.64	-6.667	-2.884	-8.027	0.082	5.52	7.75
24	-0.74	-0.99	55.61	35.86	-6.395	-2.803	-7.771	0.166	6.40	9.82
25	-1.49	-0.96	51.35	31.43	-5.606	-2.667	-7.211	0.354	9.20	14.86
26	-1.43	-0.98	57.34	35.67	-6.340	-2.857	-7.837	0.082	6.77	9.22
27	-1.36	-0.98	71.60	43.34	-6.095	-2.830	-7.510	0.245	6.47	12.21
28	-1.37	-0.99	75.38	44.94	-5.987	-2.830	-7.347	0.272	6.03	12.20
29	-0.34	-0.99	57.31	36.39	-6.640	-2.857	-7.946	0.082	6.01	8.53
30	-0.80	-0.99	57.95	36.57	-6.993	-3.184	-8.354	-0.327	0.47	1.66
32			87.42	89.36	-6.531	-2.857	-8.296	0.199	6.08	7.22
34	-1.33	-0.98	56.66 39.56 ⁱ	32.24 31.92 ⁱ	-6.177	-2.857	-7.592	0.082	6.94	11.26
35	-0.60	-0.95			-6.384	-2.466	-8.485	0.700	5.20	8.92
36	-0.27	-0.89			-6.515	-2.723	-8.113	0.411	6.29	7.96

Applied solvents: *n*-tetradecane, *n*-hexane, toluene, chloroform, dimethylformamide (DMF); a) Slope α of the linear regression; b) Coefficient r of correlation for applications of equation (2); c) Calculated dihedral angle ϑ between the naphthalimide and the aryl substituent in the electronic ground state (DFT B3LYP 6-311**G); d) Calculated dihedral angle ϑ between the naphthalimide and the aryl substituent in the first electronically excited state (CIS B3LYP 6-311**G); e) Calculated energy of HOMO and LUMO in eV in the electronic ground state, respectively (CIS 6-311**G); f) Calculated energy of HOMO and LUMO in eV in the electronically excited state, respectively (CIS B3LYP 6-311**G); g) Dipole moment of the electronic ground state in Debye; h) Dipole moment of the electronically excited state in Debye; i) dihedral angle between phenyl moieties.

A slope α of -0.60 is found for 4-amino-*N*-methylphthalimide (dye **35**, Table 6) and characterises the sensitivity of this highly solvatochromic fluorescent dye to polar solvent effects. In comparison, this interaction is appreciably lower for the methoxynaphthalimide **36** ($\alpha = -0.27$) and indicates a smaller alteration of the molecular dipole moment with optical excitation. An extension of the conjugated system of the naphthalimide with a phenyl group in **23** increases the slope slightly to $\alpha = -0.34$ (Figure 8b). Further introduction of a donor group into the *p*-position of the phenyl substituent to obtain **24** establishes a donor acceptor system between the methoxy- and the carbonyl groups and enhances the sensitivity ($\alpha = -0.74$) to exceed the solvatochromism of **35** by far. The dimethylamino group of derivative **25** causes an even higher sensitivity towards solvents, however, the fluorescence quantum yield strongly decreases in polar solvents. Multiple donor groups as in **26** also display a remarkably high

solvatochromism with comparably high fluorescence quantum yields; even though weak fluorescence was still observed in polar DMF. A substitution with larger aryl groups like the 4-methoxynaphthyl moiety leads to **27** which displays a very distinct solvatochromism ($\alpha = -1.36$) while still exhibiting high fluorescence quantum yields in polar solvents. Further extension of the conjugated framework to the methoxybiphenyl derivative **34** also induces such a pronounced fluorescent solvatochromism ($\alpha = -1.33$) exceeding that of the anisyl-substituted species **24**. Finally, the effect of the donor acceptor motif in **24**, was further tested with **30** where the electron donating methoxy group was exchanged by an electron withdrawing cyano group. There is still a comparably high sensitivity to solvent polarity ($\alpha = -0.80$), but as expected, the effect of the donor-substituted derivatives was not reached (Table 6).

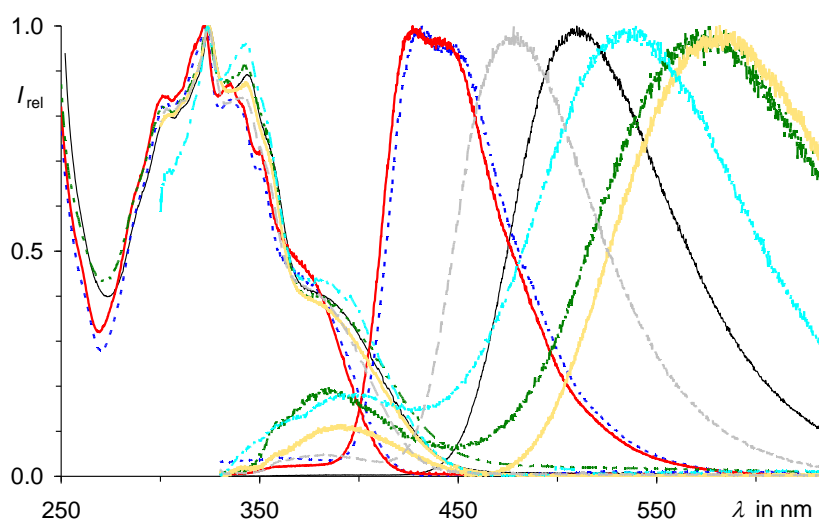


Figure 9: UV/Vis absorption (left) and fluorescence (right) spectra of **27** in various solvents. From left to right: hexane (thick solid red), tetradecane (dotted blue), toluene (dashed grey), chloroform (thin solid black), undecanol (dotted dashed turquoise) DMF (diffuse yellow), 1-butanol (doubledotted dashed green).

The electronic properties of the 4-methoxynaphthyl derivative **27** are comparable to those of compound **24**. However, the slope parameter α is found to be nearly twice as much. This observation made us focussing more intensely on the geometrical arrangement of the chromophores and prompted us to investigate the influence of steric hindrance on mesomerism. In comparison, the optical properties of **27** (Figure 9) and its methylated analogue **28** are only slightly different from each other (Figure 10a). This indicates a similar

intramolecular geometry. A skew arrangement of the aromatic systems seems to be mainly influenced by *peri* hydrogen atoms of the naphthalene subunits. These findings were further confirmed by quantum-chemical calculations (DFT B3LYP 6-311**G, *N*-alkyl was replaced by methyl) as shown in Figure 10b-e. Hence, the steric influence of the methyl group in **28** is only subordinated (dihedral angle 75.38°) and does not affect the geometry significantly (71.60° for **27**). Comparison of the 3,4,5-trimethoxyphenyl naphthalimides **26** (57.34°) and **32** exhibits much more pronounced effects. The absorption properties of both trimethoxy-derivatives display comparable behavior with maxima at 362.2 nm ($\epsilon = 15900 \text{ L mol}^{-1} \text{ cm}^{-1}$) and 344.8 nm ($\epsilon = 16200 \text{ L mol}^{-1} \text{ cm}^{-1}$). Steric repulsion of the methyl groups in **32** arranges the two aromatic systems statically fixed. The nearly orthogonal geometry (87.42°) results in a strong quenching of the fluorescence. This is attributed to the lack of orbital overlap. Calculated structures and molecular orbitals are depicted in Table 7.

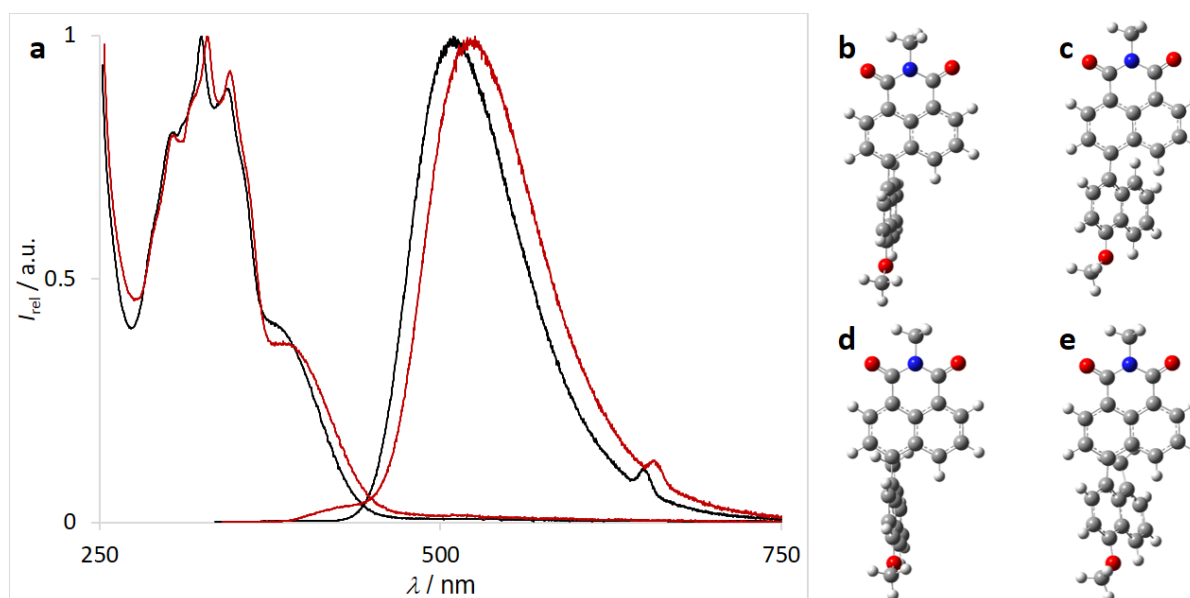
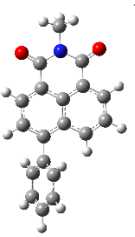
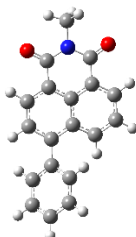
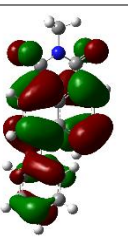
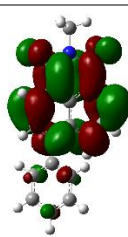
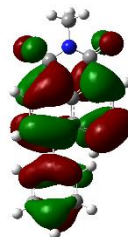
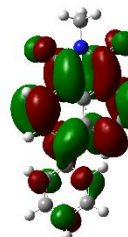
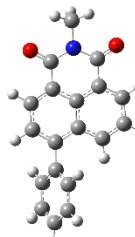
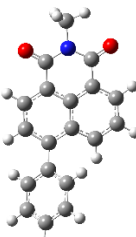
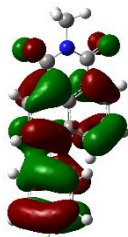

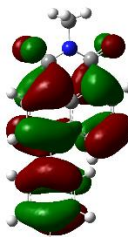
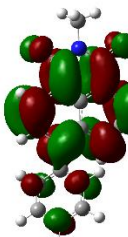
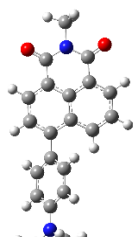
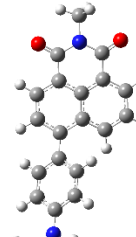
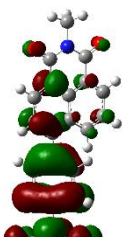

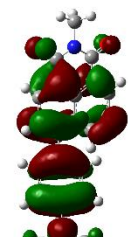
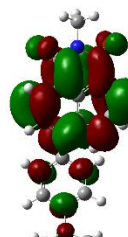
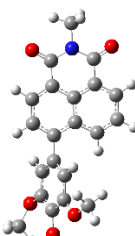
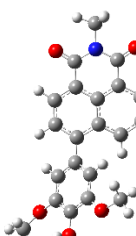
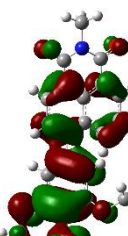

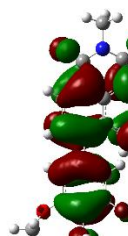
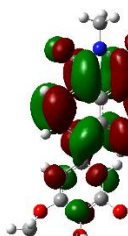


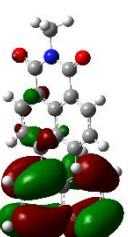
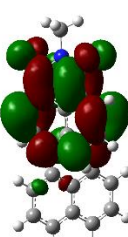
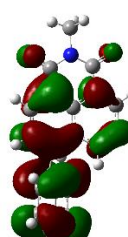
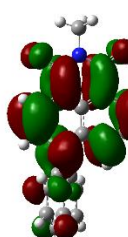
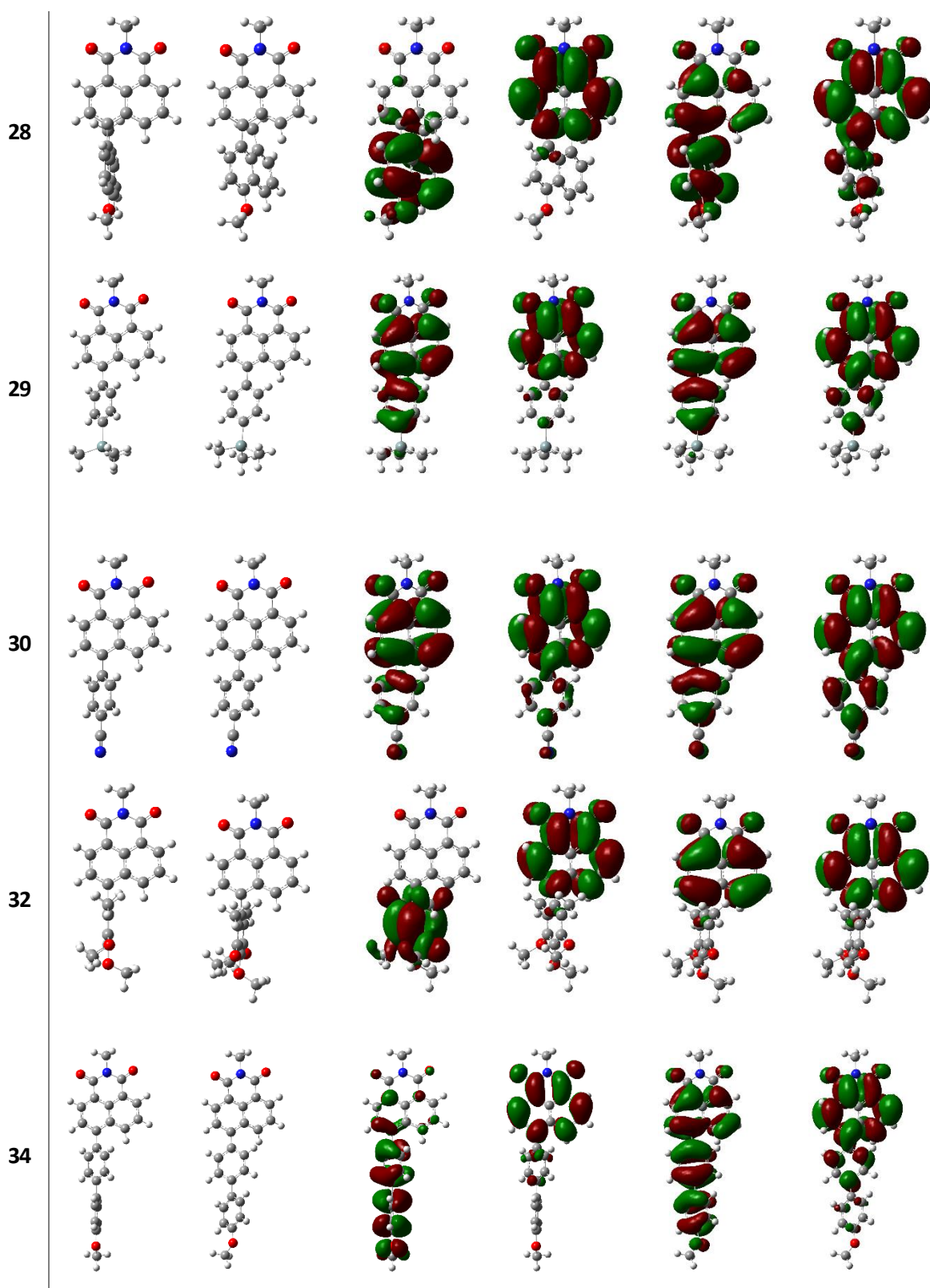


Figure 10: Comparison of **27** and **28**. a) Absorption (left) and fluorescence spectra of **27** (black) and **28** (red); b-e) Optimized structures of **27** and **28** (B3LYP 6-311**G); b) Electronic ground state of **27**; c) Electronically excited state of **27**; d) Electronic ground state of **28**; e) Electronically excited state of **28**.

Table 7: Quantumchemical calculations of **23-30, 32** and **34**.

	Struct. E_0^a	Struct. E_1^b	HOMO E_0^c	LUMO E_0^d	HOMO E_1^e	LUMO E_1^f
23						
24						
25						
26						
27						



Optimized structures and electron density of HOMO and LUMO (DFT B3LYP and CIS 6-311**G basis set). a) Optimized structure in electronic ground state; b) Optimized structure in electronically excited state; c) HOMO in electronic ground state; d) LUMO in electronic ground state; e) HOMO in electronically excited state; f) LUMO in electronically excited state.

The proposed planarization of the molecule in the excited state is supported by DFT calculation (CIS 6-311G**) and summarized in Table 6-7. Differences of the dihedral angles of up to 24° (**34**) are calculated for phenyl-substitution. Naphthyl derivatives **27** and **28** exhibit stronger planarization with angle differences of 28° and 30°. The quantum chemical calculations are in good agreement to the expectations from measured optical spectra. Changes in dipole moments also fit the experimental data. A qualitative tendency associates large changes in the dipole moment with large experimental Stokes' shifts and pronounced fluorescent solvatochromism. However, values of **26** and **30** are too small to explain the observed strong solvatochromism of the fluorescence. Furthermore, the calculated orbital energies were compared to experimental optical data in Table 8. Whereas absorption is represented quite well within the range of unpredicted influences such as solvent effects, fluorescence energy values would exceed the respective energies of the band gap in the ground state by far. Thus, calculated MO energies were not regarded for dynamic analysis.

In addition to analysis according to the $E_T(30)$ concept of *Dimroth* and *Reichardt* and *Brooker's* χ_R scale above the concepts of *Kawski*^[50], *Kamlet*, *Taft* and *Abboud*^[51] and *Catalán*^[52] were applied.

Table 8: Comparison of quantum chemically calculated optical values with experimental results.

	E_{abs}^a	$\lambda_{abs} (calc.)^b$	$\lambda_{abs} (meas.)^c$
23	3.782	327.8	355.4
24	3.592	345.2	364.8
25	2.939	421.9	426.2
26	3.483	356.0	362.2
27	3.265	379.7	325.0
28	3.157	392.8	329.0
29	3.782	327.8	356.0
30	3.810	325.5	366.4
32	3.674	337.5	344.8
34	3.320	373.5	364.4

a) Calculated HOMO-LUMO difference in eV (DFT B3LYP 6-311**G); b) Calculated HOMO-LUMO difference in nm; c) Experimentally determined absorption maxima in chloroform.

The solvatochromism of the series of naphthalimides was analysed with the method reported by *Kawski* and coworkers.^[50] The function f_{BK} was established by means of equation (9) and the function g_{BK} by means of equation (10), respectively, where n is the index of refraction of the solvent and ε the relative permittivity.

$$f_{BK} = \frac{2n^2 + 1}{n^2 + 2} \left(\frac{\varepsilon - 1}{\varepsilon + 2} - \frac{n^2 - 1}{n^2 + 2} \right) \quad (9)$$

$$g_{BK} = \frac{3}{2} \frac{n^4 - 1}{(n^2 + 2)^2} \quad (10)$$

Characteristic indicators for solvent effects are m_1 obtained as the slope of a linear plot of the Stokes' shift $\nu_{abs} - \nu_{flu}$ (in kK as wavenumbers 1000 cm^{-1}) versus f_{BK} and m_2 as the slope (Figure 11) of the sum of the wavenumbers of the maxima of UV/Vis absorption and fluorescence $\nu_{abs} + \nu_{flu}$ versus $f_{BK} + 2g_{BK}$. The results are reported in Table 9.

Table 9: Slopes m_1 and m_2 .

Nr.	m_1^a	$r_{(m1)}^b$	m_2^a	$r_{(m2)}^b$	μ_e/μ_g^c
23	0.51	0.917	-3.00	-0.976	1.4
24	3.06	0.989	-5.11	-0.979	4.0
25	5.24	0.928	-10.21	-0.959	3.1
26	5.89	0.960	-7.56	-0.978	8.0
27	6.69	0.956	-7.21	-0.975	26.7
28	6.32	0.957	-6.93	-0.977	21.7
29	0.69	0.911	-2.94	-0.930	1.6
30	3.24	0.989	-5.29	-0.975	4.2
34	5.80	0.998	-8.01	-0.992	6.2

Applied solvents: 1-Butanol, 1-undecanol, *N,N*-dimethylformamide, toluene, *n*-hexane, *n*-tetradecane; chloroform was not applied because of unfavourable solvent effects. a) in kK as wavenumbers 1000 cm^{-1} ; b) correlation number; c) Calculated ratio of dipole moments in electronically excited μ_e and the ground state μ_g , according to equation (3).

The ratio μ_e/μ_g according to equation (11) indicates the alteration of the dipole moment in the electronically excited state μ_e and the ground state μ_g for parallel transition moments. μ_e/μ_g was applied according to equation (11) as a measure for the solvent influence on the

electronic spectra. A clear maximum was found for **27** verifying the concept of twisted donor acceptor systems enhancing strong fluorescent solvatochromism. The value of **27** exceeds even the effect of the prolonged electronic system in **34** due to higher intra-molecular dynamics. The linear correlations on the basis of f_{BK} and g_{BK} are reported in Figure 11.

$$\frac{\mu_e}{\mu_g} = \frac{|m_1| + |m_2|}{|m_2| - |m_1|} \quad (11)$$

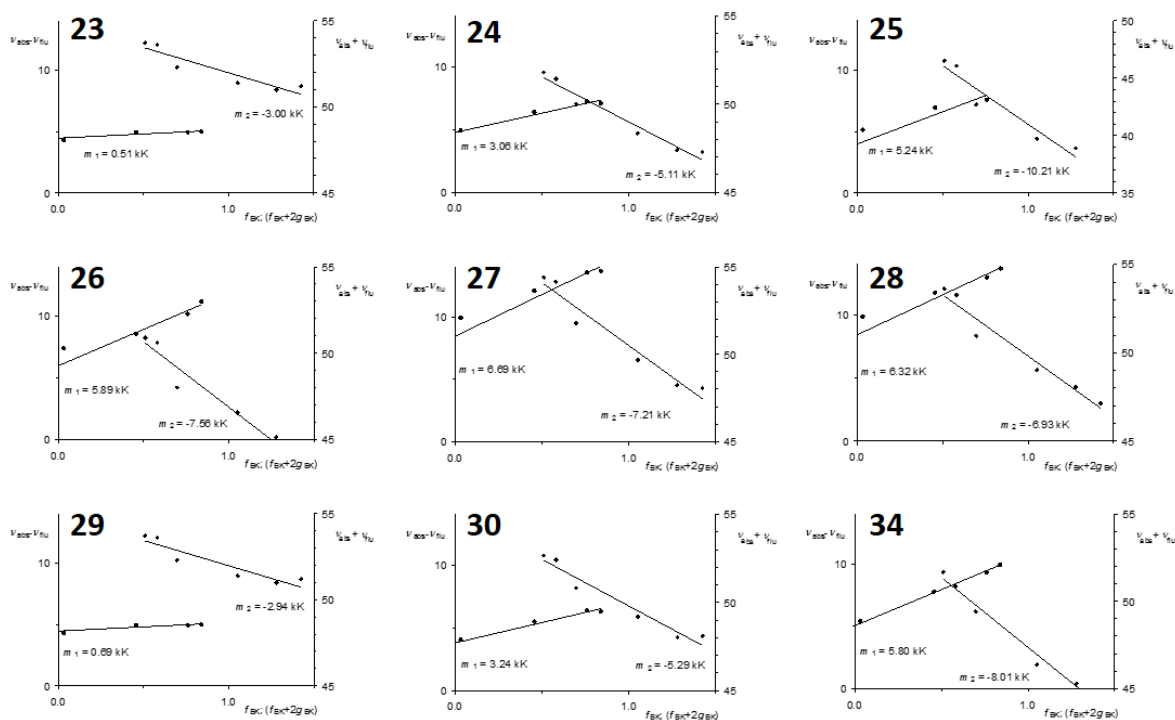


Figure 11: Linear correlations of the Stokes' shift $\nu_{\text{abs}} - \nu_{\text{flu}}$ (in 1000 cm^{-1}) of **23-30** and **34** versus f_{BK} to obtain m_1 and of the sum $\lambda_{\text{abs}} + \lambda_{\text{flu}}$ versus $f_{BK} + 2g_{BK}$ to obtain m_2 .

The series of *peri*-aryl naphthalimides was further analysed by means of the multi parameter approach of equation (12) developed by Kamlet, Taft and Abboud^[51] where solvent effects were generalized to any solvent-dependent property XYZ. The sensitivity to dipolar-polarizability term is characterized by s where a correction d concerns the polarizability. The parameters a and b are attributed to hydrogen acceptor and donor properties. Equation (12) was applied to the E_T values (see equation(7)) of the fluorescence of **23-30** and **34** and we optimized the parameters of equation (12) by least square fitting. The results are reported in Table 10 where the values s indicates a generally pronounced sensitivity to solvent effects.

Large s -values were found for the intensively discussed **27** as well as for **26**, **28** and **34**. A minor variation is found for the parameter d except for the dimethylaminophenyl derivative **25**. A high value of a is found for the latter as one may expect for acceptors of hydrogen bonds. There are only minor variations for the other values of a and b in accordance with the lack of pronounced effects of hydrogen bonds.

$$E_T = XYZ = XYZ_0 + s(\pi^* + d\delta) + a\alpha + b\beta \quad (12)$$

Table 10: Calculated parameters XYZ_0 , s , d , a and b by means of least square fits of the experimental E_T values of fluorescence according to equation (12). Solvents: 1-Butanol, *N,N*-dimethylformamide, chloroform, toluene, *n*-hexane.

Nr.	XYZ_0	s	d	a	b
23	70.71	-3.64	-0.27	-2.30	-0.83
24	66.85	-7.32	-0.28	-3.25	-4.20
25	61.29	-6.29	0.60	-14.37	-3.80
26	63.62	-16.68	-0.23	-3.26	-3.95
27	65.80	-14.22	-0.17	-6.00	-6.02
28	64.48	-15.94	-0.20	-4.92	-3.80
29	70.00	-3.75	-0.20	-2.24	-0.91
30	69.51	-8.41	-0.27	-4.25	-3.38
34	65.77	-15.18	-0.39	-4.12	-4.94

Finally, the multi parameter approach of equation (13) of Catalán^[52] with the generalized solvent effect A was applied to the E_T -values (equation (7)) of the solvatochromism of fluorescence of the naphthalimides **23-30** and **34**.

$$E_T = A = A_0 + bSA + cSB + dSP + eSdP \quad (13)$$

Equation (13) was applied and the parameters A_0 , b , c , d and e were optimized by means of least square fitting (Table 11).

Table 11: Optimized parameters A_0 , b , c , d and e of equation (13) by means of least square fitting of the experimental E_T -values of the fluorescence of **3** in the solvents 1-butanol, 1-undecanol, *N,N*-dimethylformamide, chloroform, toluene, *n*-hexane, *n*-tetradecane (*N,N*-dimethylformamide was excluded for **3c** because of lack of fluorescence).

Nr.	A_0	b	c	d	e	r^a
23	72.6	-5.53	-0.10	-2.46	-3.72	0.9987
24	68.7	-6.02	-3.62	-2.07	-7.36	0.9991
25	72.6	16.33	-13.69	-12.67	-17.60	1.0000
26	71.6	-2.02	-4.99	-10.11	-14.93	0.9984
27	77.3	-12.74	-4.77	-16.11	-12.93	0.9989
28	77.4	-7.30	-5.19	-18.05	-12.80	0.9995
29	74.5	-5.10	-1.07	-6.41	-2.87	0.9953
30	72.9	-8.83	-2.43	-4.37	-8.22	0.9998
34	66.1	-1.74	-7.49	1.15	-13.48	0.9966

a) Correlation number.

The parameter e can be applied as a measure of the sensitivity concerning the dipolarity of the solvent SdP where high negative values were found for the donor-substituted derivatives **25-28** and **34**. The effect of a simple 4-methoxyphenyl group in **24** is appreciably smaller. The parameter d for the solvent polarizability SP is found to be strongly negative for **25-28** indicating a boosting solvent effect of dipolarity and polarizability for these compounds. The parameters b and c concerning solvent acidity SA and solvent basicity SB are not pronounced except of b for **25** because of the hydrogen-bonding ability of the dimethylamino group. The b -value for **27** is remarkably strong negative indicating a further cooperative solvent effects. The results are in agreement to the previous analysis.

The dynamic effect concluded from experimental and quantum chemical results were investigated by means of fluorescence anisotropy spectroscopy. The same instrumental setup used for fluorescence lifetime determination was equipped with a polarizer and the anisotropy r was calculated according to equation (14), where I_{\parallel} is the intensity for parallel polarization of the excitation and emission and I_{\perp} that for orthogonal arrangement. G is an instrument dependent factor which equals the ratio orthogonal intensity divided by parallel intensity for the respective wavelength.

$$r = \frac{I_{\parallel} - G I_{\perp}}{I_{\parallel} + 2 G I_{\perp}} \quad (14)$$

Measurements in solution did not display any specific behaviour because rotation of the molecules influences their global orientation and results in a fast decay of the measured anisotropy. Thus, naphthalimides **24**, **27** and **28** were incorporated in PMMA-films with thicknesses of several 100 μm to prevent rotation. The time-resolved anisotropy of **24**, **27** and **28** is compared in Figure 12.

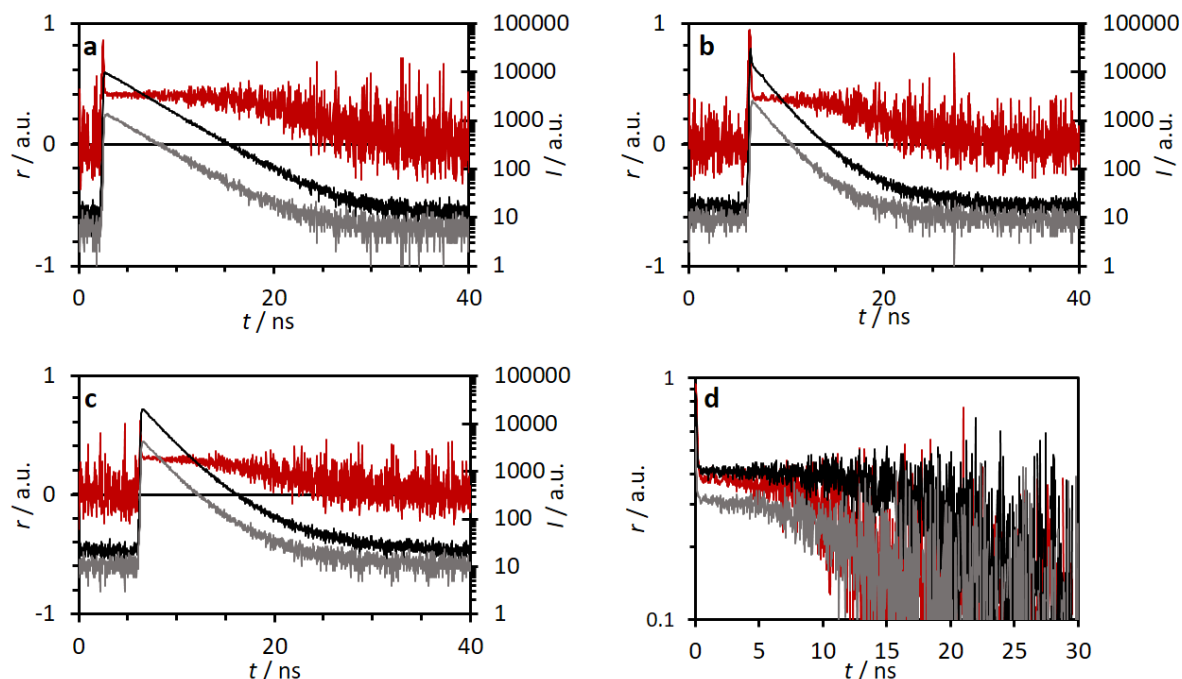


Figure 12: Time resolved anisotropy of naphthalimides **24**, **27** and **28** in PMMA films. a) Anisotropy (red), parallel fluorescence decay (black) and perpendicular fluorescence decay (grey) of **24**; b) Anisotropy (red), parallel fluorescence decay (black) and perpendicular fluorescence decay (grey) of **27**; c) Anisotropy (red), parallel fluorescence decay (black) and perpendicular fluorescence decay (grey) of **28**; d) Comparison of the anisotropy of **24** (black), **27** (red) and **28** (grey).

The fluorescence anisotropy starts with the intrinsic anisotropy at the maximum at $t = 0$ (Figure 12d). Typical values between 0.3 and 0.4 are observed. The methylated naphthylimide **28** displays slightly lower anisotropy. The methoxyphenyl derivative **24** exhibits much longer persistence of the initial anisotropy than the methoxynaphthyl derivatives **27-28**. This is attributed to longer fluorescence lifetimes in comparably low polar PMMA (Table 2) which were determined to be 3.63 ns (**24**), 1.56 ns (**27**) and 1.67 ns (**28**). There is no reason to assume higher mobility of the structural comparable and even larger naphthylimides **27-28**. Hence, a slight tendency of lower fluorescence anisotropy values for more twisted molecules can be observed but is insufficient for validation and analysis of molecular dynamics.

A twisted geometry between the donor and the acceptor seems to promote charge transfer causing strong solvatochromism in fluorescence and large Stokes' shifts while preserving high fluorescence quantum yields. However, a complete orthogonalisation (**32**) quenches fluorescence where an obviously essential residual orbital overlap is lacking. We further confirmed this concept by heating a solution of **32** in diethylene glycol diethyl ether to 200°C where the very weak fluorescence reversibly becomes intensified by a factor of 2 (Figure 13).^[53] This was attributed to thermally induced vibronic perturbation of the nearly orthogonal arrangement enabling fluorescence.

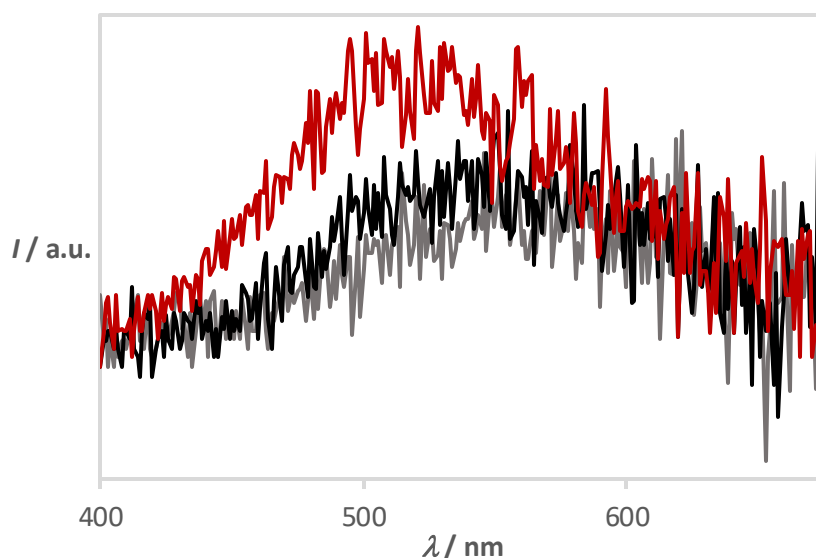


Figure 13: Temperature dependent fluorescence spectra of **32** in diethylene glycol diethylether. Temperatures approx. 25 °C (grey), 100 °C (black), 200 °C (red).

The proposed geometrical requirements for a distinct charge transfer is related to the TICT theory.^[42] However, our results imply that orthogonal arrangements between donor and acceptor completely quench the fluorescence. Thus, significant fluorescence is attributed to skew conformations. By tuning the molecular geometry we could obtain a series of chromophores with TICT-like fluorescence and quantum yields up to more than 80%.

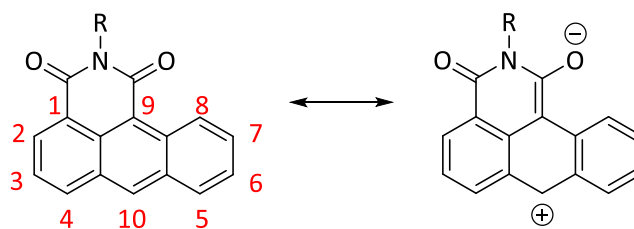
Conclusion

Readily soluble and highly fluorescent derivatives of naphthalene-1,8-dicarboximides were synthesized by Pd-catalyzed arylation in *peri*-position. These compounds display a pronounced solvatochromic fluorescence. Optical data were evaluated according to several approaches described in literature. A combination of electronic and dynamic effects is made

responsible for these properties and was confirmed by quantum chemical calculations. The photo-induced charge transfer from the electron rich aryl moiety to the naphthalimide is enhanced in polar solvents and causes a bathochromic shift of the fluorescence. This in turn strongly depends on the molecular geometry of the fluorophore. The intramolecular arrangement influences the intensity of the charge transfer. A skew geometry between donor and acceptor still allows high fluorescent quantum yields and favours a more pronounced charge transfer resulting in both, distinct solvatochromism and large Stokes' shifts, corresponding to the TICT mechanism. However, nearly orthogonal orientation leads to strongly quenched fluorescence being attributed to a lack of orbital overlap. Thus, an opposed mechanism is found to be more likely where the electronic ground state exhibits high dihedral angles that planarize in the excited state. Still, the sensitivity toward solvent polarity is caused by intra-molecular charge transfer and a geometric twist occurs after excitation. However, the mechanism works vice versa to common TICT theory. This interplay of electronic and geometric effects results in highly fluorescent compounds such as **24** and **27** with easily adjustable emission spectra controlled by medium effects. This provides very large Stokes' shifts exceeding 200 nm (approx. 1.6 eV) being of interest for various applications such as for frequency converters, fluorescence optical fibers and highly tunable light sources.

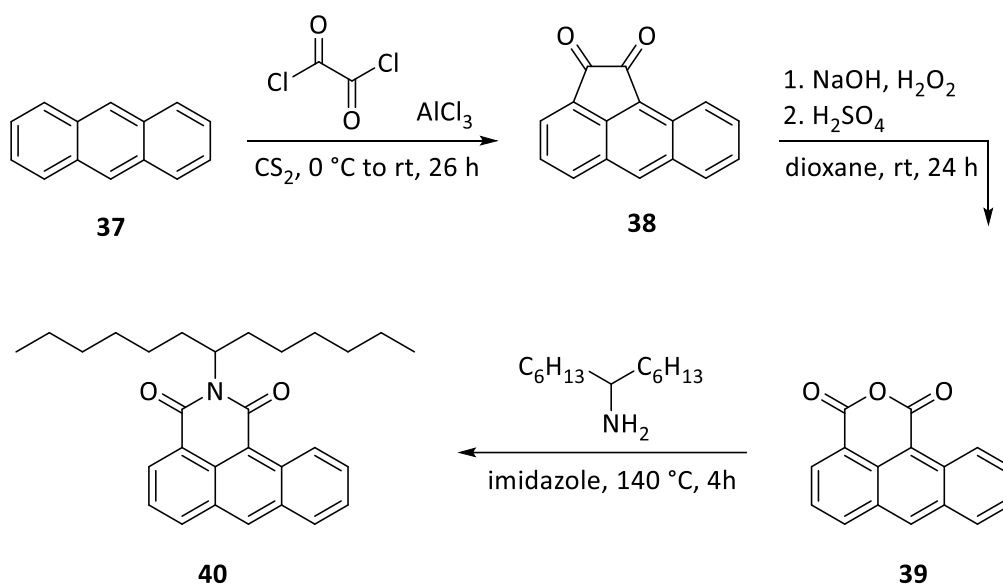
2.2.2 Synthesis and Characterization of Substituted Anthracene Dicarboximides

Langhals et al. report on amination reactions of perylene tetracarboxylicdiimides at low temperatures.^[54] The same behavior was investigated in this work for smaller annulated aryls to result in geometrically and electronically dynamic asymmetrical fluorophores. Anthracen-1,9-dicarboximides are readily accessible fluorescent dyes. This class of dyes was chosen due to its high reactivity and the structural comparability to well-studied annulated aryls such as perylenes. However, the smaller aromatic π -system causes less aggregation and thus enables a wider range of modifications. Nevertheless, the absorption extends to the visible region. A highly reactive site in anthracene dicarboximide is found at the C-10 carbon atom enabling substitution reactions under mild conditions, shown in Scheme 11. A mesomeric resonance structure induces a positive partial charge increasing the electrophilicity in that position.



Scheme 11: Two possible mesomeric resonance structures indicate the electrophilicity of anthracene-1,9-dicarboximide in C-10 position.

To ensure good solubility, *N*-(tridecan-7-yl)anthracene-1,9-dicarboximide^[55] (**40**) was prepared from anthracene (**37**) (Scheme 12). A *Friedel-Crafts* acylation with oxalyl chloride lead to aceantrylene-1,2-dione (**38**) in 69% yield. Subsequent oxidative ring expansion with hydrogen peroxide under basic conditions (*Baeyer-Villiger* oxidation) gave 83% anthracene dicarboxylic anhydride (**39**). After condensation with 7-aminotridecane anthracene imide **40** was obtained in 87% yield.



Scheme 12: Synthesis of *N*-(tridecan-7-yl)anthracene dicarboximide (**40**) starting from anthracene (**37**) in 3 steps.^[55]

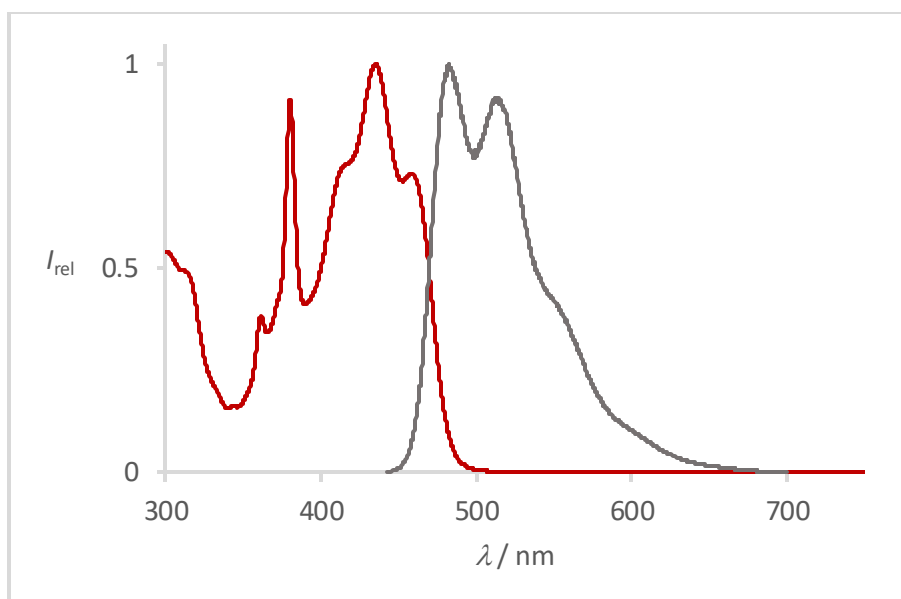


Figure 14: Absorption (red) and fluorescence (grey) spectra of *N*-(tridecan-7-yl)anthracene dicarboximide (**40**) in chloroform.

The absorption maximum of anthracene imide **40** is found at 435.2 nm (Figure 14). The compound displays a structured fluorescence with peaks at 482.5 nm and 512.8 nm. The Stokes' shift is comparably pronounced with 47.3 nm (0.273 eV). This can be attributed to the polarizability promoted by the anthraquinoid resonance structure presented in Scheme 11. This causes different dipole moments for the ground state and the excited state. The same electronic behavior results a moderate solvatochromism of the fluorescence illustrated in Figure 15.

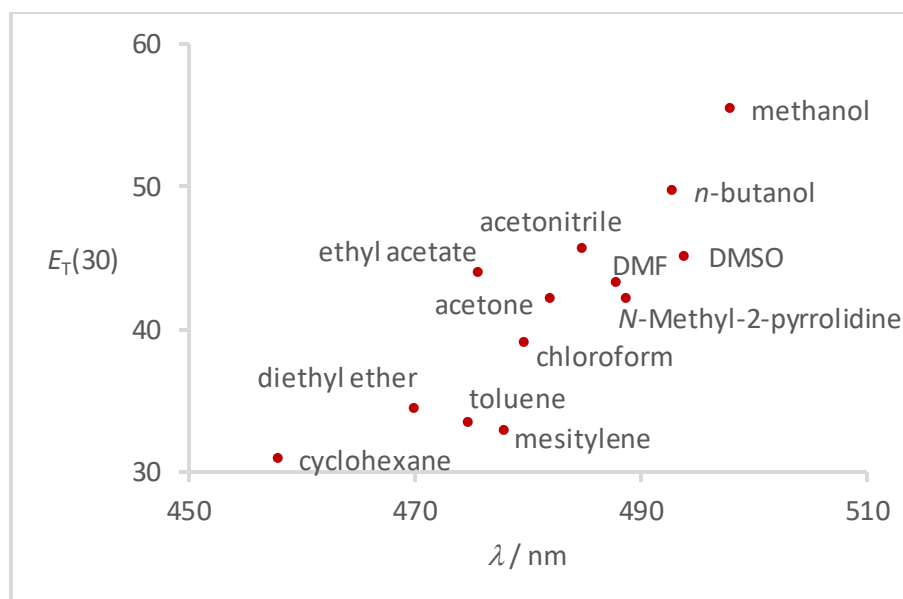


Figure 15: Positions of the fluorescence maxima of *N*-(tridecan-7-yl)anthracene dicarboximide (**40**) in different solvents in relation to the $E_T(30)$ -values^[56] of the respective solvent.

2.2.2.1 *N*-Substituted 10-Aminoanthracene-1,9-dicarboximides

Substitution of anthracene imide **40** in position 10 would lead to more distinct solvatochromic effects. An electron donating groups forms a narrow push-pull system with the opposed electron withdrawing carbonyl moiety. Particularly amines can not only serve as electron donors, but also take part in dynamic effects. Analogously to the highly solvatochromic 4-amino-*N*-methylphthalimide as the basis of *Zelinski's* universal *S* solvent polarity scale^[43] and 4-methoxynaphthalene dicarboximide^[57] electronic excitation induces an alteration of the dipole moment resulting in large *Stokes'* shifts.

Several amines were converted with anthracene imide **40** (summarized in Table 12). The reaction conditions were varied between 0 °C and 120 °C but did not seem to influence the reactions or yields significantly. As a consequence, most reactions were performed at room temperature for 1.5 h up to 14 d. Reactions were carried out with and without additional base (K_2CO_3 or $KOtBu$). When no differences between the conditions were recognized the more moderate option was studied. Liquid amines were used under solvent free conditions whereas solid amines were dissolved in a minimum amount of DMF.

Table 12: Overview on the applied amines and the most appropriate reaction conditions used for the conversion with *N*-(tridecan-7-yl)anthracene dicarboximide **40**.

No.	Amine	Chemical structure	Reaction conditions	Yield	Product
1	(<i>S</i>)-Isoleucine		rt, 3 d, K ₂ CO ₃ , DMF		
2	(<i>S</i>)-Lysine		rt, 3 d, K ₂ CO ₃ , DMF		
3	(<i>S</i>)-Proline		rt, 3 d, K ₂ CO ₃ , DMF		
4	(<i>S</i>)-Phenylalanine		rt, 3 d, K ₂ CO ₃ , DMF		
5	1-aminohexane		rt, 24 h, UV exclusion, solvent free	49%	41
6	1,2-Diaminoethan		rt, 48 h, UV exclusion, solvent free		42
7	Aniline		rt, 6 d, UV exclusion, solvent free	8%	43
8	Diethylamine		rt, 3 d, UV exclusion, solvent free		
9	<i>N,N'</i> -Dimethyl-1,2-diaminoethan		rt, 4 d, UV exclusion, solvent free	6%	44
10	Pyrrolidine		rt, 6 d, UV exclusion, solvent free		
11	Piperidine		rt, 6 d, UV exclusion, solvent free	21%	45
12	Indole		120 °C, 1.5 h, KOtBu, toluene	45%	46
13	1,5-Diazabicyclo[4.3.0]non-5-ene		rt, 3 d, DMF		47
14	Triethylamine		rt, 14 d, DMF		
15	1,4-Diazabicyclo[2.2.2]octane		120 °C, 4.5 h, DMF, under argon		

The reactive behavior of four of the 20 proteinogenic amino acids was analyzed under different conditions. The applied amino acids represent one example of each subset; hydrophobic isoleucine, polar and basic lysine, cyclic secondary proline and aromatic

phenylalanine. The reactions were performed in DMF and ethanol, in each case with and without potassium carbonate addition. In both approaches, temperatures were varied between room temperature and 120 °C (for DMF) or 80 °C (for ethanol), respectively. The reaction times were kept between 1 h and 3 d. In all reactions a slight intensification of the yellow color was observed. However, neither of these approaches succeed in a reaction.

Terminal and aromatic primary amines were applied without solvent and display a more pronounced reactivity towards anthracene carboximide **40**. Both, 1-aminohexane and 1,2-diaminoethan turn red directly after addition at room temperature without solvent or auxiliary base. The reaction with aniline was more slowly, first discoloration was recognized after a few minutes. After 1-6 d at room temperature water was added to all batches followed by extraction with chloroform and purification via column chromatography. For all three batches, red solids were obtained (Scheme 15) and analyzed with mass spectrometrie and optical spectroscopy (Figure 17). However, they seem to decompose within severals days under UV-radiation. Hence, the reactions and isolation steps were carried out under UV exclusion.



Figure 16: Reaction of *N*-(tridecan-7-yl)anthracene dicarboximide (**40**) in 0.1 M DMF with selected amines after different reaction times at room temperature. From top to bottom: a) Directly after addition; b) after 1 h; c) after 4 h; d) after 1 week. From left to right: 4-Amino-*N*-methylphthalimid, aniline, triethylamine, diethylamine, pyrrolidine, (*S*)-proline, (*S*)-lysine, 1-hexylamine, 1,2-diaminoethane.

After mixing both reactants, a change of the color from yellow to deep red is observed (Figure 16). When the reaction is quenched with aqueous solutions or diluted with organic solvents such as methanol, chloroform or DMF, the red color disappears mostly and the starting material can be recovered. However, after some hours reaction time a small percentage of product, particularly in case of 10-(hexylamino)anthracene dicarboximide could be isolated. Column chromatography was performed, but caused for most of the product decomposition into the starting material. The instability cannot be explained for a common covalent C-N-bond. More likely the main fraction of the product contains some kind of stable *Meisenheimer*

adduct. Surprisingly, most species exhibited significant fluorescence. The exact fluorescence quantum yield could not be determined but are rated in the area of approximately 0.10. Optical spectra of the isolated compounds were reported in Figure 17. Further reactions below will be discussed regarding these aspects.

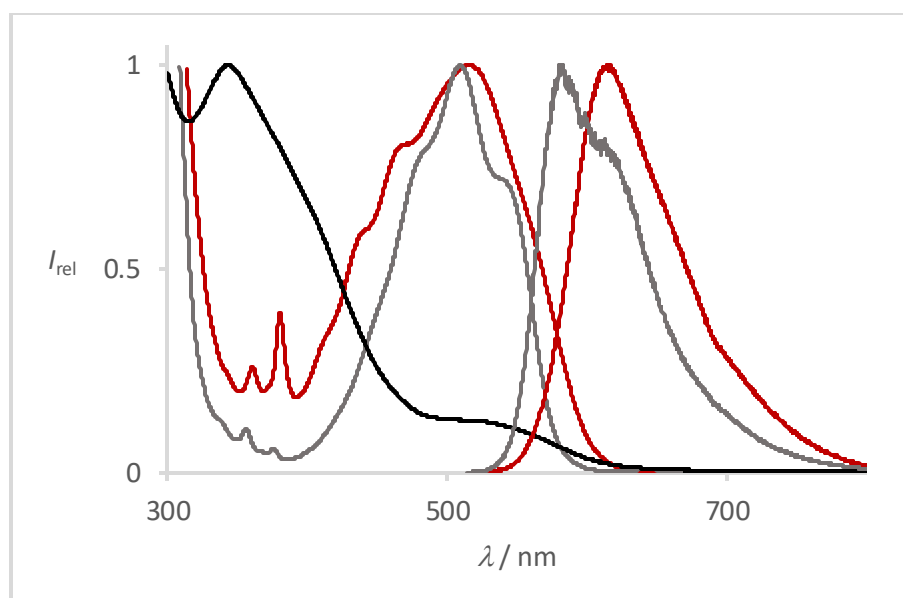


Figure 17: UV/Vis absorption (left) and fluorescence (right) spectra of the amination products from 1-aminohexane (**41**) (red) and 1,2-diaminoethane (**42**) (grey) in chloroform. 10-(phenylamino)anthracene dicarboximide (**43**) exhibited no fluorescence but absorption (black) only.

For secondary amines, the same observations were made as for primary ones. Simple diethylamine and *N,N'*-dimethyl-1,2-diaminoethane (DMEDA) were applied as aliphatic amines. As cyclic representatives pyrrolidine, piperidine and the partial aromatic indole were investigated. All reactions took place at room temperature for 3-6 d, except the solid indole had to be dissolved in toluene and was treated with potassium *tert*-butoxide and heated to 120 °C for 90 min. Changes in color were observed for every approach after a short period of time. After treatment with water or dilution with organic solvents mostly the starting materials were recovered. In case of DMEDA, piperidine and indole, the respective products (Scheme 15) could be isolated in moderate yields and were verified via mass spectrometry. Optical spectra are given in Figure 18.

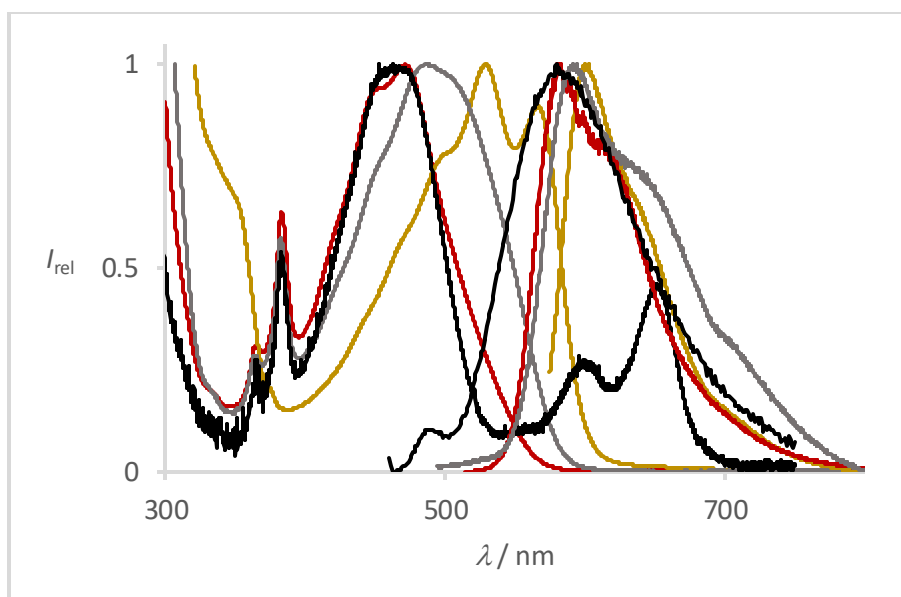
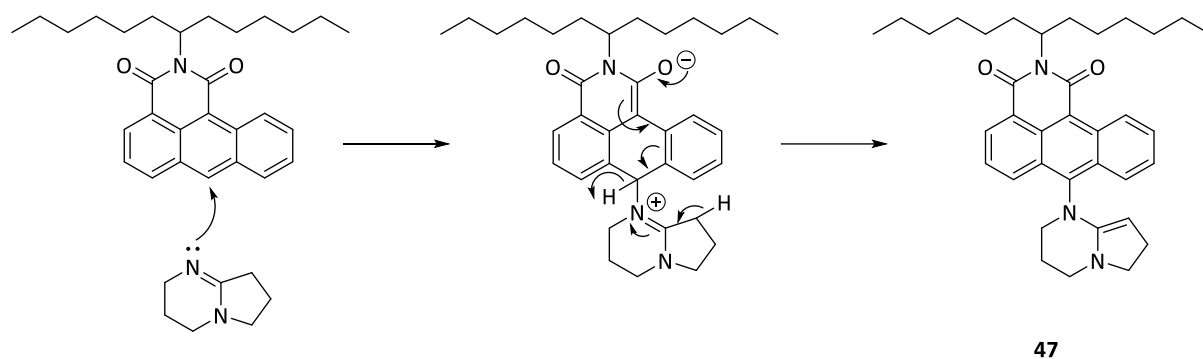


Figure 18: UV/Vis absorption (left) and fluorescence (right) spectra of amines **44** (red), **45** (grey) and **46** (black) in chloroform. The yellow spectrum displays the unstable σ -adduct with pyrrolidine.

Reactions of anthracene dicarboximide **40** with tertiary amines such as 1,5-Diazabicyclo[4.3.0]non-5-ene (DBN), triethylamine or 1,4-Diazabicyclo[2.2.2]octane (DABCO) also exhibit a strong color shift (Figure 16). However, only in the first example the strongly fluorescent ($\Phi = 0.96$ in chloroform, 0.63 in methanol) product **47** (Scheme 15) could be isolated and analyzed.

The reactivity of tertiary amines is generally very different compared to primary or secondary amines. The lone pair still acts for a nucleophile. Thus, if steric hindrance does not occur, the formation of a *Meisenheimer* σ -adduct is also possible. The absence of an abstractable proton impedes the rearomatization of the anthracene unit and thus the reaction. In the reaction with DBN, the cleavage of H_2 can be realized alternatively (Scheme 13) and might be a reason that only this tertiary amine was converted successfully. The optical spectra are shown in Figure 19.



Scheme 13: Proposed reaction mechanism for the formation of amine **47**.

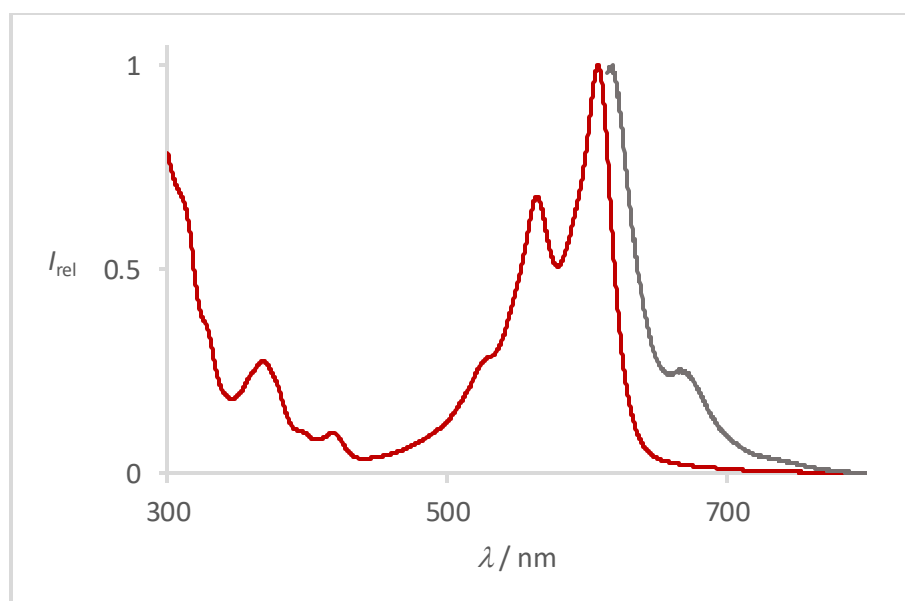
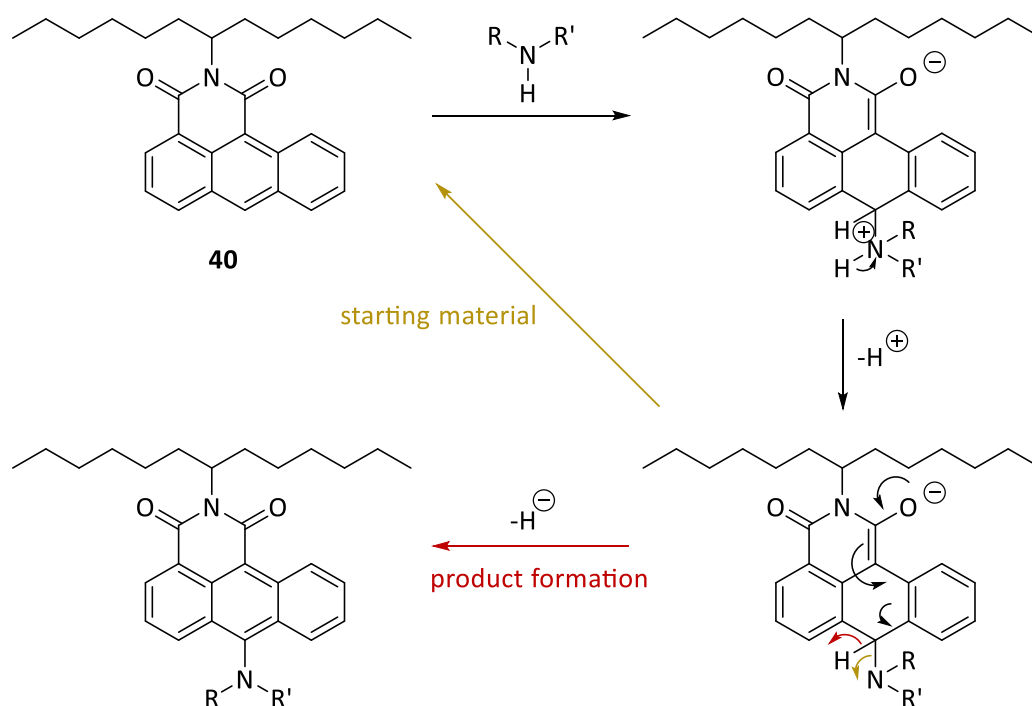


Figure 19: UV/Vis-absorption (red) and fluorescence (grey) spectra of amine **47** in chloroform.

All approaches except those using amino acids (Table 12) have some key behavior in common. Mixing anthracene dicarboximide **40** with different amines results in a bathochromic change of the color. The obtained color is brilliant (Figure 16) indicating a single substance. Addition of water or organic solvent causes the disappearance of that color shift and mostly the starting materials are recovered. This pleads for adduct formation such as a *Meisenheimer* σ -adduct (Scheme 14) being responsible for the observed color. *Novikov et al.* report evidence for electron transfer^[58] in such adducts by the examples of simple *N*-heteroarenes such as pyridine and quinoline. Radical scavengers inhibit the formation which can be an explanation for the failure of any reaction of amino acids with anthracene dicarboximide **40**.

The reaction of amines with anthracene imides proceeds most probably in a *Chichibabin*-like mechanism^[59]. The lone pair of the amine (or nucleophile in general) attacks the partially positive C-10 carbon of the anthracene imide. With the exclusion of redox reactions, in particular under inert gas, H₂ must be lost and may evolve. In contrast to the standard *Chichibabin* reaction a neutral amine attacks the aryl, not an amide anion. The favorable mesomeric resonance of the anthracene imide favors the formation of a σ -adduct under these conditions. Opposed to most described mechanisms^[58], hydride cleavage is hindered under these circumstances as two positive charges (at least partial positive at C-10 due to mesomeric resonance) would be directly next to each other. Furthermore, successful reaction at low temperatures (room temperature) contradicts most empirical descriptions. Thus, the H₂ evolution would be concerted or starts with the abstraction of the *N*-proton. Basic self-catalysis would develop a formal amide in agreement with the initial hydride cleavage described in literature. However, addition of supplemental base did not seem to interfere with the reaction (except for amino acids to recover the nitrogen lone pair in zwitter-ionic structure).



Scheme 14: Proposed *Chichibabin*-like reaction mechanism of amines with *N*-(tridecan-7-yl)anthracene imide. Two possible reactions either form the product (red) or lead to the collapse of the σ -adduct to recover starting material (yellow).

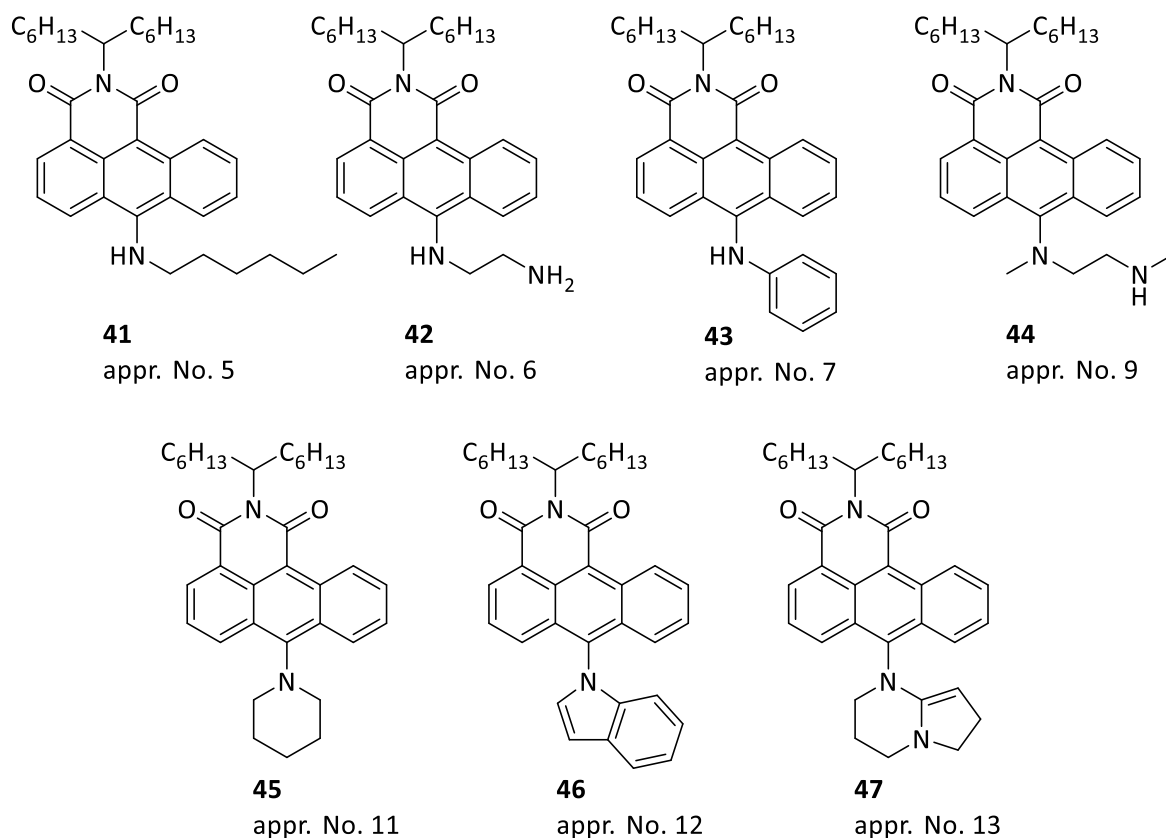
Furthermore, the formation of the *Meisenheimer* adduct also takes place for tertiary amines such as triethylamine (compare Figure 16). Addition of water causes the protonation of the amine subunit and/or oxygen atom of the enolate at the imide and thus, induces the elimination of the amine from the aryl skeleton. However, mass spectrometry proofed the molecular mass of the isolated oxidized fully aromatic products. When quenched, the reaction might have two options to evolve (Scheme 14). One is the described collapse into the starting materials, the other is the thermodynamically favored, but, due to the formation of hydride, kinetically hindered formation of the C-N bond.

The isolated and characterized compounds resulted from reaction approaches no. 5-7,9 and 11-13 (compare Table 12). The corresponding products are listed in Scheme 15. Optical data of the UV-sensitive compounds can be found in Table 13.

Table 13: Optical data of isolated amino compounds **41** – **47**.

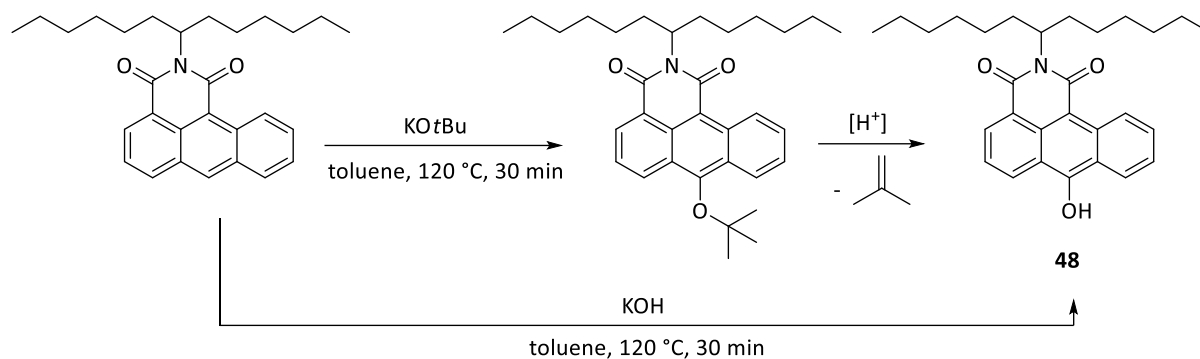
Compound	Abs. ^a λ / nm (I_{rel})	Fluo. ^b λ / nm (I_{rel})
41	515.4 (1.00)	614.0 (1.00)
42	509.4 (1.00)	583.1 (1.00)
43	343.2 (1.00), 518.2 (0.13)	-
44	471.4 (1.00)	577.9 (1.00)
45	486.2 (1.00)	591.2 (1.00)
46	452.8 (1.00), 596.2 (0.28), 653.2 (0.46)	580.0 (1.00)
47	526.4 (0.28), 564.2 (0.68), 608.0 (1.00)	618.1 (1.00), 666.1 (0.25)

a) Relative maxima of absorption, b) relative maxima of fluorescence.



Scheme 15: Isolated products of the reaction of anthracene dicarboximid with the corresponding amines (appr. No. for reference in Table 12).

An analogue type of addition-elimination reaction was observed for *O*-nucleophiles, particularly potassium hydroxide and potassium *tert*-butoxide. The reactions were performed in toluene at 120 °C for 30 min under the exclusion of water. Both resulted in the same product, 10-hydroxy-anthracen dicarboximid (**48**). The UV-sensitive product was obtained in only <5% yield in case of using KOH, whereas application of KO*t*Bu resulted in 56%. Minor traces of the corresponding 10-*tert*-butoxy derivative were found in mass spectrometry. The dealkylation is supposed to be an acid induced *iso*-butene elimination due to the remaining water content of the potassium-*tert*-butylate or induced during the quenching process using 2 M hydrochloric acid (Scheme 16).



Scheme 16: Reaction of KOH or KOtBu with anthracene dicarboximide to 10-hydroxyanthracene dicarboximide **48**.

The UV-Vis absorption maximum (Figure 20) of **48** in chloroform is found to be at 473.2 nm and therefore considerably bathochromically shifted compared to anthracene dicarboximide **40**. However, the shift is slightly less pronounced than in the *N*-alkyl substituted derivatives above due to oxygen being the weaker electron donor. A significant fluorescence is detected at 541.0 nm with a second peak at 565.8 nm ($I_{\text{rel}} = 0.85$). The fluorescence quantum yield was determined to be $\Phi = 0.30$.

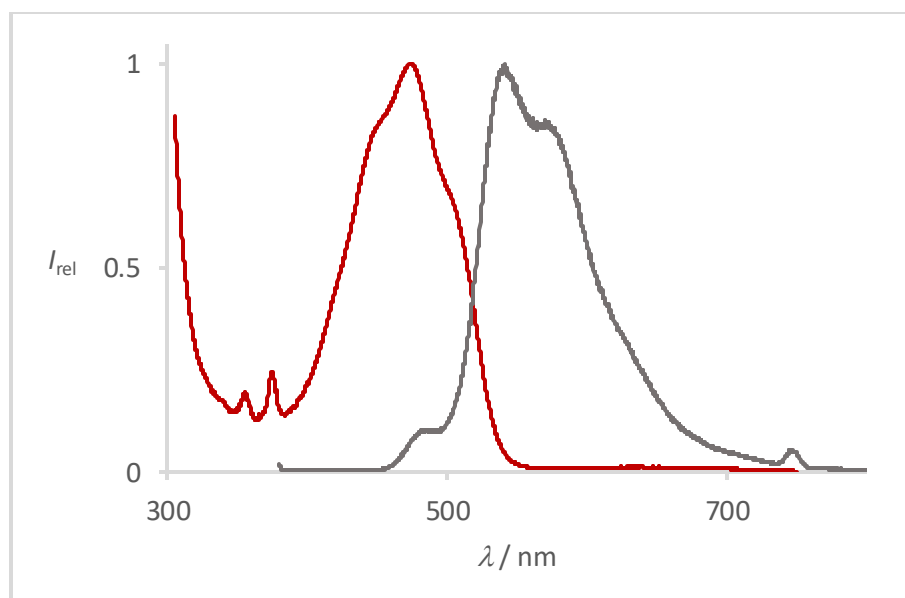


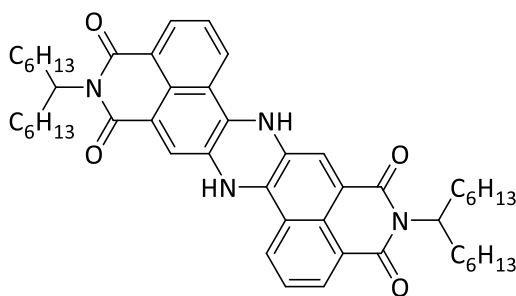
Figure 20: UV/Vis absorption (red) and fluorescence (grey) spectra of **48** in chloroform.

Conclusion

Anthracen-1,9-dicarboximid was shown to promptly react with most amines at comparably low temperature. However, in spite of the spontaneous reaction the rate determining step is the conversion of the intermediate into the final, oxidized fully aromatic compound. This requires the formal cleavage of a hydride ion. Reaction temperature did not seem to have a significant influence on the formation of the product. Some amines already reacted at room temperature and the product could be isolated and characterized. Unfortunately, all obtained compounds are unstable concerning UV-radiation limiting the applications as dyes. Chromatographic methods for purification failed as collected single fractions decomposed within minutes and exhibited multiple spots in thin layer chromatography, often with much smaller R_F -values than those of the initial fraction. This lability disables accurate optical measurements as the compound already decomposes during the investigation and prevents 10-aminoanthracen dicarboximides from serving as valuable fluorescent probes.

2.2.2.2 Transition Metal-Free Homo-Coupling Reactions of Anthracen- and Naphthalene Dicarboximides

Harsh conditions with elevated temperatures and strong basic conditions further enable metal-free C-C coupling reactions. Very careful exclusion of moisture and even oxygen allows a homo-coupling reaction of anthracene dicarboximide (**40**) at 120 °C. The resulting aceanthrene green (**49**) exists in two constitutional isomers, *cis* and *trans* (Scheme 17). The homo-coupling of **40** is described in literature^[55] applying a KOH melt at 240 °C. Yao *et al.* succeeded to apply Sakamoto's "Green Route" using KOtBu and DBN.^[60] Waiving DBN also leads to the product in yields comparable to literature. Direct comparison of the reaction with or without DBN under else same conditions demonstrated even better results omitting DBN. Thus, the uncertain role of DBN might get obsolete as it does not need to take part in the presented coupling reaction.



52

Scheme 18: Structure of 5,13-bis(tridecan-7-yl)-8,16-dihydrodiisoquinolino[5,4-*ab*:5',4'-*hi*]phenazine-4,6,12,14(5*H*,13*H*)-tetraone (**52**).

3-Aminonaphthalene dicarboximide **51** was converted to 5,13-bis(tridecan-7-yl)-8,16-dihydrodiisoquinolino[5,4-*ab*:5',4'-*hi*]phenazine-4,6,12,14(5*H*,13*H*)-tetraone (**52**) in a C-N-coupling reaction (likely following the same mechanism proposed above for 10-aminoanthracene dicarboximides), see Scheme 18. The yield was found to be 19%.

The optical properties of aceanthrene green (**49**) and dihydrophenazine **52** were studied in chloroform (Figure 21). The lateral extended π -system of aceanthrene green results in a bathochromic absorption maximum at nearly 700 nm. The position of the absorption and also fluorescence maxima is not strongly influenced by the isomeric constitution. The *trans*-derivative **49a** exhibits its strongest absorption at 694.6 nm whereas that of the *cis*-derivative **49b** is found at 694.2 nm. Smaller absorption bands are found at 419.4 nm ($I_{rel} = 0.15$) and 638.4 nm ($I_{rel} = 0.56$) for the *trans*-compound **49a** and 426.8 nm ($I_{rel} = 0.24$) and 645.2 nm ($I_{rel} = 0.59$) for the *cis*-analogue **49b**, respectively. Fluorescence maxima are detected at 730.0 nm (for **49a**) and 737.2 nm (for **49b**). The determination of the fluorescence quantum yield was carried out only for *cis*-aceanthrene green **49a** and equals $\Phi = 0.10$. For the same compound a fluorescence lifetime of 2.88 ns was found. Regarding the small fluorescence quantum yield, a natural decay of $\tau_n = 28.8$ ns has to be assumed according to equation (6). Hence, lateral expanded annulated aryls do not seem to be the choice for fast-decay fluorophores for opto-electronic purposes.

The shape of the absorption and fluorescence spectra of dihydrophenazine **52** are similar to those of *S*-13 (**1**). A slightly bathochromically shifted absorption can be observed. The spectrum displays maxima at 470.0 ($I_{rel} = 0.16$), 502.6 ($I_{rel} = 0.52$) and 540.6 nm ($I_{rel} = 1.00$). A

strong fluorescence with its maxima at 546.6 ($I_{\text{rel}} = 1.00$) and 592.5 nm ($I_{\text{rel}} = 0.29$) is detected with a fluorescence quantum yield of $\Phi = 0.76$. The fluorescence lifetime was found to be 3.77 ns and thus, considering the fluorescence quantum yield, slightly longer ($\tau_n = 4.96$ ns, calculated) than for perylene diimides ($\Phi > 0.99$, $\tau = 3.95$ ns).

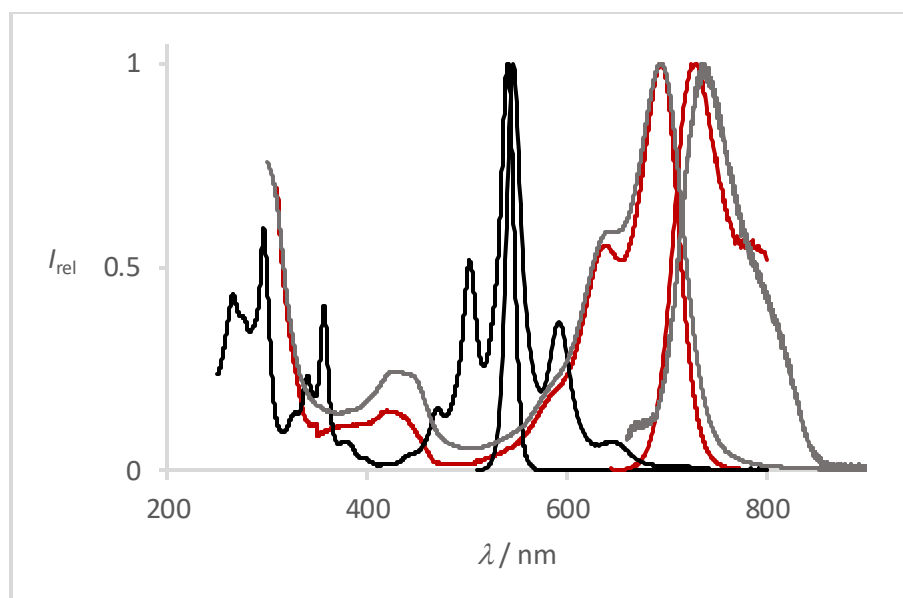


Figure 21: UV/Vis (left) and fluorescence (right) spectra of *trans*-aceanthrene green **49a** (red), *cis*-aceanthrene green **49b** (grey) and dihydrophenazine **52** (black) in chloroform.

Conclusion

The presented coupling reactions bear the huge advantage of transition-metal free conditions for C-C coupling reactions. On the downside, they are very limited in the scope of applications. Only small, well soluble carboximides resulted in any reaction. Anhydrides or simple arenes such as naphthalene did not take part under the applied conditions. Furthermore, only homo-coupling was observed. The conversion of *N*-(tridecan-7-yl)naphthalene-1,8-dicarboximide (**50**) with *N,N'*-bis(tridecan-7-yl)perylene-3,4-dicarboximide for a cross-coupling gave nothing but starting material. In this case, *Sakamoto* conditions are reported to work.^[34, 61] However, selected aryl-aryl-couplings succeeded in acceptable yields of up to 42%. In these cases standard procedures such as *Suzuki*-coupling require more steps and much more expensive reagents and thus, favors the described method for such reactions.

2.3

Concentration Dependency of the Fluorescence Lifetime: Long-Range Electromagnetic Molecular Interactions Indicated by the Process of Light Emission

H. Langhals, T. Schlücker, *Ger. Offen.* DE 102014006209.0 (Apr. 29th 2014).

The release of electromagnetic waves from matter is considered by several theoretical concepts^[62] where the wave-particle dualism^[63] is the most generally accepted. The absorption and emission of visible light from matter is generally attributed to local molecular processes, such as the fluorescence of electronically excited molecules. The induction of interactions with other dye molecules, known as exciton coupling,^[64] requires a comparably close contact and alters the UV/Vis spectrum in a characteristic way (Davidov splitting). The slightly longer-range dipole-dipole interactions are intensely studied by Förster^[65] and others^[66] by means of energy transfer processes (FRET)^[67] being damped with the sixth power of the distance. As a consequence, significant effects are described for distances below 5 nm. More distant dye molecules are estimated to be isolated and independent in operation. Further specific interactions beyond this limit were investigated by means of fluorescence lifetime spectroscopy.

Generally, alterations in concentration do not have an impact on the spectral constants in diluted solutions. The time constant of the fluorescent decay is also expected and generally accepted to be invariable. The generation of light is limited by the natural transition probability from the excited state of the molecule to the ground state. This probability of the release of electromagnetic waves is indicated by the fluorescence lifetime τ . There is a direct relation between the oscillator strength, the fluorescence lifetime and the fluorescence quantum yield according to fundamental work by Förster^[68] and others. The oscillator strength is proportional to the molar absorptivity for unaltered shapes of UV/Vis spectra. These correlations are expressed in equations (5) and (6) described in Chapter 1.1 in more detail.

$$k_r = \frac{1}{\tau_n} \cong 2.88 \text{ s}^{-1} \times 10^{-9} n^2 \frac{\int I(\sigma) d\sigma}{\int I(\sigma) \sigma^{-3} d\sigma} \int \frac{\varepsilon(\sigma)}{\sigma} d\sigma \quad (5)$$

$$\Phi = \frac{\tau}{\tau_n} \quad (6)$$

In diluted solution, aggregation and reabsorption can be neglected and the quantum yields are found to be independent on the concentration. Thus, the fluorescence lifetime only depends on the molar attenuation ε which is also constant for diluted concentrations. The correlation of the attenuation E from the molar absorptivity ε and the concentration c is given by equation (15). The attenuation E is defined as logarithmic quotient of the initial intensity of light I_0 and the measured intensity I for the respective wavelength after passing through the sample with a thickness of d in cm (usually 1 cm). According to *Lambert-Beer's law* (equation (15)), the extinction coefficient is invariable in diluted concentrations. Thus, the concentration c does not affect the extinction coefficient ε which in turn should correlate to a constant fluorescence lifetime t . Hence, there should be no theoretical reason to expect a dependency of the fluorescence lifetime on the concentration of the measured chromophore.

$$E = \lg \frac{I_0}{I} = \varepsilon c d \quad (15)$$

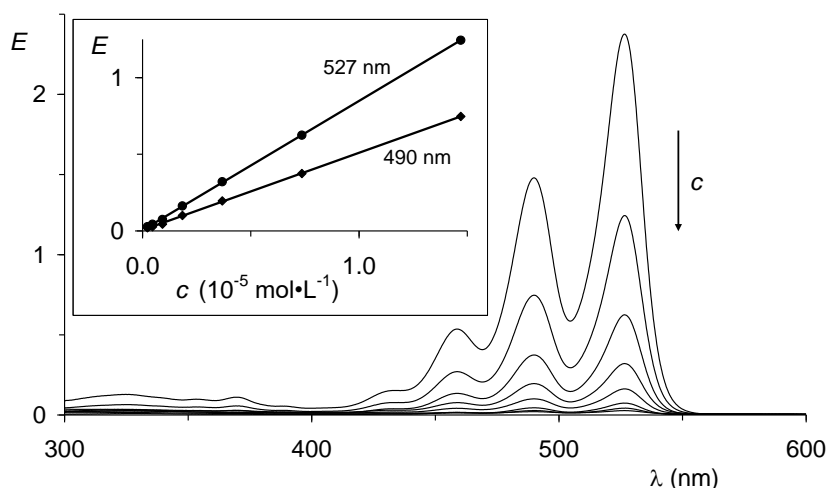


Figure 22: UV/Vis absorption spectra of **1** in chloroform with increasing dilution. Insert: Verification of Lambert-Beer's law by the linear correlation of the absorptivity E as a function of the concentration c ; circles: 527 nm, slope $0.810 \times 10^5 \text{ L mol}^{-1}$, standard deviation 0.0049, correlation number 0.99995, coefficient of determination 0.9999, 7 measurements) and diamonds: 490 nm (slope $0.504 \times 10^5 \text{ L mol}^{-1}$, standard deviation 0.0044, correlation number 0.99988, coefficient of determination 0.9998, 7 measurements).

We tested the validity of Lambert-Beer's law for *N,N'*-bis(tridecan-7-yl)perylene-3,4:9,10-tetracarboxylic diimide (**1**) and found both an invariance of the shape of the absorption spectrum concerning dilution and a perfect linear relation of the absorptivity with the molar concentration of **1** confirming the expectations made from theory.

Furthermore, we tested the invariance of the shape of the fluorescence spectrum of **1** with concentration and also found both, unaltered shapes of the fluorescence spectra and a linear correlation between the fluorescence intensity *I* and the molar concentration *c* until as low as $9 \times 10^{-10} \text{ mol L}^{-1}$ verifying a constant fluorescence quantum yield (Figure 23). This corresponds to literature^[69] where the linearity between the concentration and the fluorescence signal of some other perylene derivatives in a glassy matrix was confirmed down to a dilution of $10^{-13} \text{ mol L}^{-1}$.

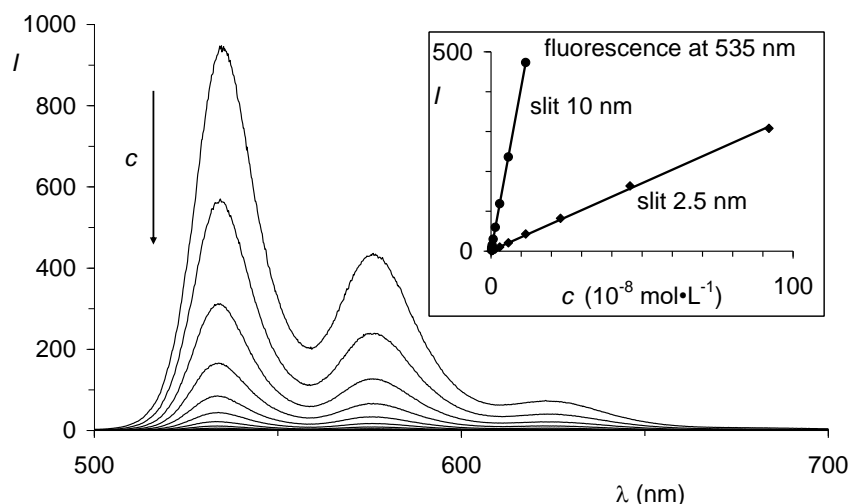


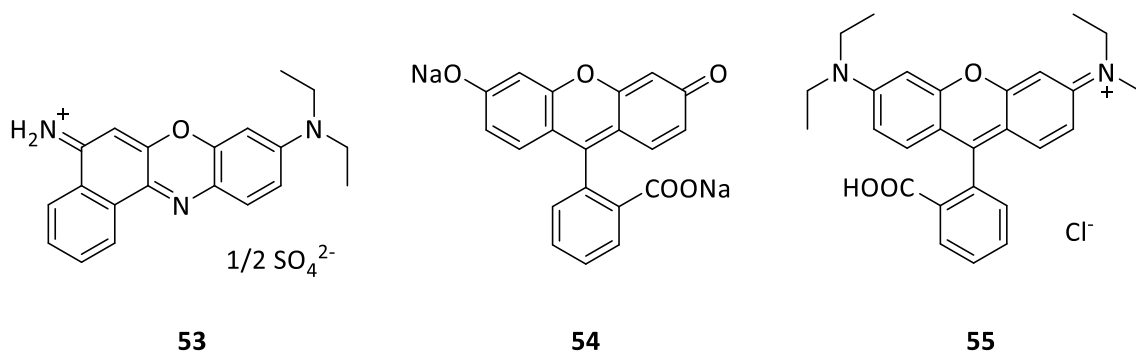
Figure 23: Fluorescence spectra of **1** in chloroform with optical excitation at 490 nm and increasing dilution. Insert: Linear correlation of the intensity of fluorescence as a function of the concentration of **1**; diamonds: Slit for excitation 2.5 nm (slope $3.38 \times 10^8 \text{ L mol}^{-1}$, standard deviation 3.1, correlation number 0.9995, coefficient of determination 0.9991, 11 measurements) and steeline, circles: Slit for excitation 10 nm (slope $4.11 \times 10^9 \text{ L mol}^{-1}$, standard deviation 0.33, correlation number 0.999998, coefficient of determination 0.999997, 8 measurements).

Thus, we conclude that there is no indication for any interactions caused by a possible direct contact of dye molecules such as in aggregates: There are operating isolated molecules even at the higher reported concentrations. Finally, the influence of the concentration on the refractive index of the solution was investigated. A value of $n_D^{20} = 1.444$ was measured for

Chloroform, that was successively substituted by a 10^{-4} M solution of **1** in chloroform. The variation amounted less than 0.002 which is within the range of the alteration caused by the temperature decrease due to evaporation. Furthermore, this leads to even higher concentrations exceeding the discussed range for optical measurements by far. Thus, the refractive index can be estimated as independent from the concentration for diluted solutions.

The fluorescence lifetime of a solution of **1** with a fluorescence quantum yield of $\Phi > 0.99$ in chloroform was measured at different concentrations. The fluorescence lifetime τ was found to be 5.00 ns in 2.5×10^{-5} molar solution. Remarkably, the fluorescence lifetimes of **1** decrease with further dilution and decreasing concentration c to reach 3.81 ns at 1.6×10^{-7} mol L $^{-1}$. The alterations of the fluorescence lifetime is far beyond any experimental error with 31% within the studied range. Long-range interactions of the dye molecules must be taken into account as a cause for the alterations of the fluorescence lifetime τ .

The investigation was extended to further highly fluorescent dyes as suitable probes for the investigation of the formation of electromagnetic waves. The well-studied, commonly used fluorophores Nile blue A sulfate (**53**), fluorescein (**54**) and rhodamine B (**55**) were investigated in different solvents. Moreover, the high inertness of **53-55** excludes any interference by unspecified chemical reactions in the required diluted solutions and their high photo stability allows the registration of spectra without photo bleaching.



Scheme 19: Chemical structures of the applied fluorophores **53-55**.

The fluorescence lifetime of **53** was reported^[70] to be independent of the concentration in the limits of 10^{-8} to 10^{-3} mol L⁻¹ in ethanol. In contrast, our measurements indicated a continuous decrease of fluorescence lifetime by 10% from 2.32 to 2.10 in a range of concentration from 2.2×10^{-5} to 5.6×10^{-7} mol·L⁻¹. Thus, we conclude that the effect of the dependence of the fluorescence lifetime on the concentration is not limited to **1** but more general valid for most highly fluorescent dyes. The rather small effect for **53** is attributed to the comparably small fluorescence quantum yield of 0.27^[71] caused by non-emitting relaxation processes. For further confirmation of the results, fluorescein (**54**, $\Phi = 0.93$)^[72] and rhodamine B (**55**), $\Phi = 0.49$ ^[73] were studied as well-known probes leading to the same observation. The fluorescence lifetimes of **54** in water (4.64 ns at 2.3×10^{-5} mol L⁻¹ to 4.00 ns at 6.0×10^{-8} mol L⁻¹, 16%) and **55** in ethanol (3.31 ns at 1.7×10^{-5} mol L⁻¹ to 2.89 ns at 5.9×10^{-8} mol L⁻¹, 15%) also display a distinct dependency on the concentration. The results are displayed in Figure 24 and summarized in Table 14.

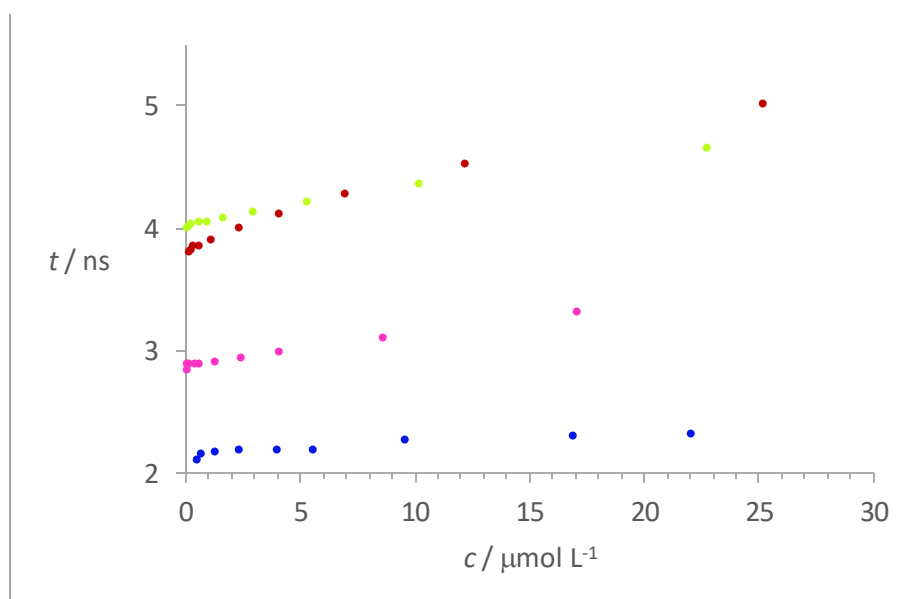


Figure 24: Concentration dependency of the fluorescence lifetime of fluorophores **1** (red), **53** (blue), **54** (green) and **55** (violet).

Dyes **1**, **53** and **55** were excited with a PC-510 laser. Fluorescein (**54**) samples were excited with PC-405 laser. Both light sources had 0.4 mW power and a maximum puls frequency of 80 MHz. The detection was realized at the respective fluorescence maximum of each dye.

Further investigation focussed on perylene diimide **1** exhibiting the most pronounced effect and Nile blue (**53**) due to the reported invariance of the fluorescence lifetime. For better comparability and more precise determinations, the exciting light source was changed to a tunable NKT-Laser SuperK Extreme EXB-4 from NKT Photonics A/S. The detection was set up using a monochromator of Edinburgh Instruments Ltd., a photomultiplier PMA-C 192-N-M and electronics PicoHarp 300 from PicoQuant GmbH. The following results are based on excitation wavelengths of 490 nm and 628 nm and detection wavelengths of 535 nm and 667 nm for **1** and **53**, respectively.

A dilution series of **1** within the same range as above was studied. The fluorescence lifetime displays very similar behaviour and excludes any artefacts depending on the instrument. The results are summarized in Table 14.

Table 14: Fluorescence lifetimes τ of **1** in chloroform depending on the concentration c and the calculated average molecular distance d , respectively. Fluorescence excitation at 490 nm and detection at 535 nm.

$c / 10^{-6} \text{ mol L}^{-1}$	τ / ns	d / nm
0.108	3.79	249
0.456	3.82	154
1.37	3.90	106
2.94	4.05	83
4.56	4.13	71
6.05	4.29	65
8.00	4.41	59
11.6	4.59	52
15.2	4.77	48
17.8	4.91	45
22.6	5.04	42

The general concentration-dependent interaction of molecules is well described by an equation developed for solvent effects.^[74] That equation was modified for the fluorescence lifetimes of **1** to obtain equation (16) where τ is the fluorescence lifetime of dye **1** at the concentration c and τ_0 the lifetime at infinite dilution. E_D and c^* are the parameters of the

equation where E_D is the slope of a correlation according to equation (16) and c^* the onset concentration where interactions become important.

$$\tau = E_D \ln\left(\frac{c}{c^*} + 1\right) + \tau_0 \quad (16)$$

Equation (16) describes the fluorescence lifetime of **1** as a function of the concentration c with high precision with a characteristic concentration c^* of 10^{-5} mol L⁻¹ corresponding to a molecular distance d of 50 nm; see Figure 25. As a consequence, long-range intermolecular interactions are made responsible for such alterations of the fluorescence lifetime. Even large mean molecular distances of more than 40 nm were spanned and effects were found until as high as about 250 nm. A direct interaction of the dye molecules with the electromagnetic field of the forming wave in its whole extension given by its wavelengths seems to be the most probable cause for the effect.

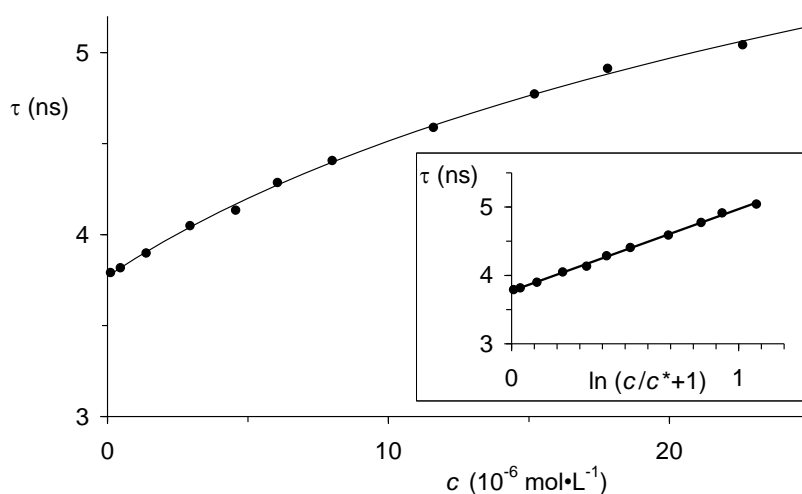


Figure 25: Dependence of the fluorescence lifetime τ of **1** in chloroform on the concentration c (circles; see Table 14). Insert: Linear correlation according to equation (8) ($E_D = 1.17$ ns, $c^* = 1.17 \cdot 10^{-5}$ mol L⁻¹ and $\tau_0 = 3.77$ ns), (standard deviation 0.015, correlation number 0.9992, coefficient of determination 0.9984, 11 measurements).

Same results were obtained for nile blue (**53**) in ethanol. The numbers are given in Table 15. The concentrations dependency as well as the validation of Lambert-Beer's law for **53** are shown in Figure 26.

Table 15: Fluorescence lifetimes τ of **53** in ethanol depending on the concentration c . Fluorescence excitation at 628 nm and detection at 667 nm.

$c / 10^{-6} \text{ mol L}^{-1}$	τ / ns
0.0581	3.79
0.107	3.82
0.377	3.90
1.09	4.05
4.58	4.13
14.1	4.29

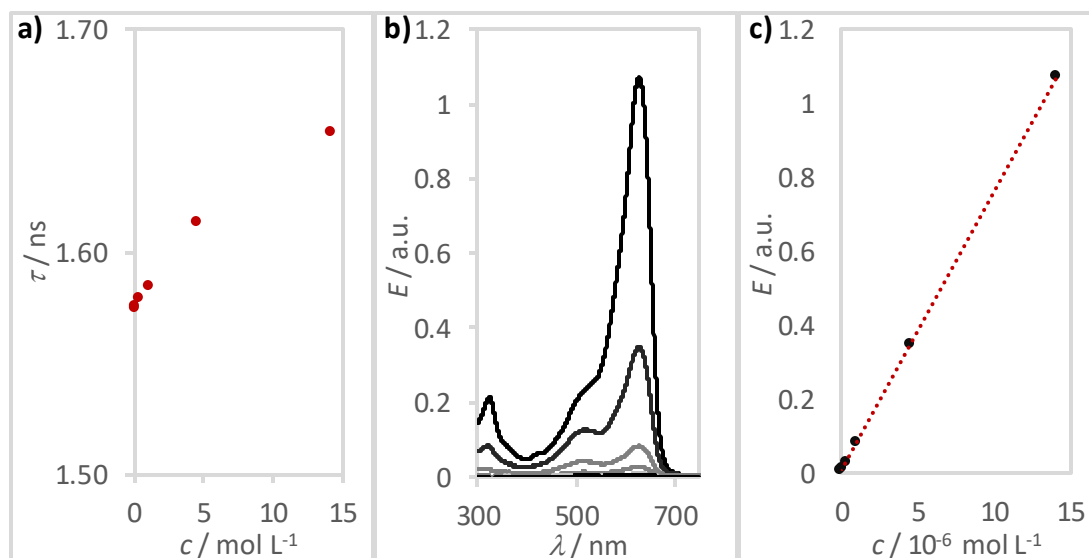


Figure 26: Optical properties of Nile blue (**53**) in ethanol. a) Concentration dependent fluorescence lifetime. b) Dilution series of **53** in ethanol. c) Linear correlation between concentration and absorptivity in agreement with *Lambert-Beer's law*.

To exclude possible near-range dye-dye interactions, i.e. by spontaneous aggregation, chromophore **1** was incorporated in poly(methyl methacrylate) (PMMA) nanoparticles. The particles were synthesized by Zgela^[75] and display optical properties comparable to those of *S-13* (**1**). The dye is statistically dispersed and covalently bond to the PMMA polymer

backbone. Thus, in contrast to solutions the free mobility of the single dye is inhibited and two chromophores attached to the same particle are more or less fixed in an invariant distance. Moreover, chromophores of two different particles are hindered from close contact by the bulky polymer chain. Five types of particles with different weight-average molecular weights resulting in average diameters of 200 - 300 nm and different doping grades from 25 – 300 ppm were dissolved in chloroform and their fluorescence lifetimes were studied in a dilution series. The obtained correspondence of the lifetime τ on the concentration (in this case attenuation as no molarity is possible for polymers) displays the same dependencies already described above (Figure 27). Even the doping grade is represented by the measured fluorescence lifetimes. The increasing values for very low concentrations are ascribed to autofluorescence of byproducts of PMMA (described detailed in Chapter 2.4.1)

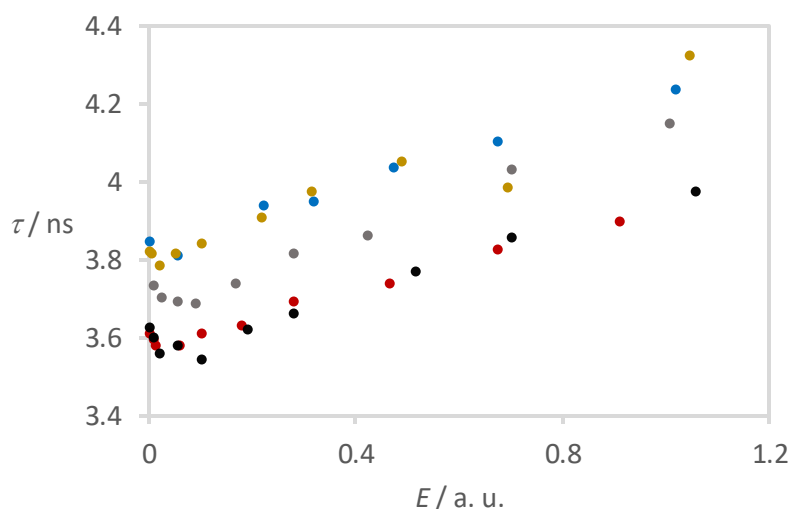


Figure 27: Dependency of the fluorescence lifetime τ of S-13(1) doped PMMA nanoparticles on the concentration (represented by attenuation E). Applied nanoparticles (rounded average values): 25 ppm 1, 200 nm (black); 25 ppm 1, 300 nm (red); 100 ppm 1, 200 nm (grey); 300 ppm 1, 200 nm (yellow); 300 ppm 1, 300 nm (blue).

There is no sign for short-range interactions due to the presented results. *Lamber-Beer's* law is valid for all studied solutions contradicting aggregation or exciton effects. Moreover, steric hindrance by extended polymer chains prevents from close dye-dye contact. Thus, the observed dependency of the fluorescence lifetime on the concentration is attributed to long-range interactions between the chromophores. Such interactions seem to be less important

for the absorption of light because neither the line-type nor the validity of Lambert-Beer's law were influenced by dilution as shown in Figures 22 and 26. The very short time of the process of light absorption proceeding in about 10^{-15} s acts like a flashlight concerning the orientation of the involved dye molecules where relaxation processes remain unimportant.

There are completely different conditions for the emission of light. The fluorescence lifetime of several ns is long enough to allow relaxation processes. Obviously, not only the electronically excited dye molecule (the "hot" molecule) is involved in the generation of the electromagnetic light wave, but also the neighbouring molecules in the electronic ground state (the "cold" molecules) and these interactions lead to a retardation of the evolution of light reported in Table 14. This effect resembles the function of Yagi-Uda antennae^[76] for radio-TV-transmission at UHF frequencies where there is one "hot" resonating dipole with dimensions of about $\lambda/2$ and further "cold" dipoles slightly off resonance parallel arranged in a ladder with distances of slightly more than $\lambda/10$. The dimensions of visible light waves with about half a micrometer are still macroscopic and may be treated in the same way. A realization of such arrangements was proposed for nano particles^[77] where $\lambda/2$ would extend to about 250 nm and relevant distances of the single "hot" molecule to the "cold" neighbours would be in the range of 50 nm. This value corresponds to that of c^* found in the correlation of Figure 25. As a consequence, the emission of light from electronically excited molecules seems to be a complex process where neighbours in the electronic ground state are involved in the formation of the finally propagating wave. At least, molecular electromagnetic interactions should not be treated as processes between the directly involved molecules, but the complete surrounding volume with a pattern of $\lambda/10$ and an extension in the dimension of the wavelengths or even more should be taken into account.

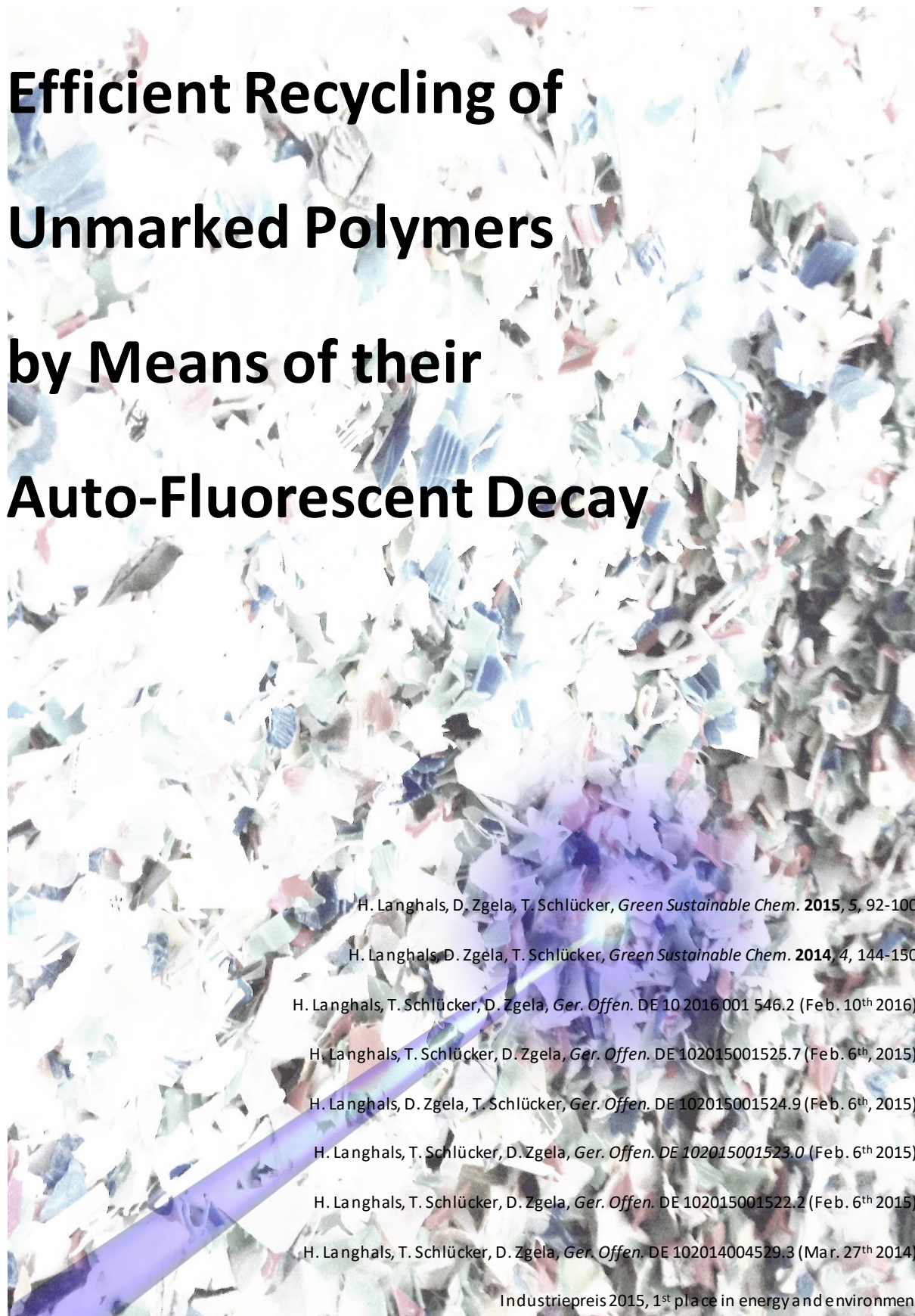
Conclusion

The process of emission of fluorescence light from electronically excited molecules seems to be extended in macroscopic dimensions such as $\lambda/2$ and does not remain localized to single molecules. Interactions of the excited molecules with surrounding non-excited ones prolong the fluorescence decay with decreasing inter-molecular distance and becomes important even for more than $\lambda/10$. An analogy to the Yagi-Uda antennae for UHF applications was established. The results may be important for the interpretation and construction of light-collecting and light-harvesting arrangements of chromophores. Reported measurements of

fluorescence lifetimes should be re-evaluated because of possible dependence of concentration. On the other hand, decay times can be precisely and efficiently measured even in optically inhomogeneous samples and allow a precise optical determination of the local concentration.

2.4

Efficient Recycling of Unmarked Polymers by Means of their Auto-Fluorescent Decay



- H. Langhals, D. Zgela, T. Schlücker, *Green Sustainable Chem.* **2015**, *5*, 92–100.
- H. Langhals, D. Zgela, T. Schlücker, *Green Sustainable Chem.* **2014**, *4*, 144–150.
- H. Langhals, T. Schlücker, D. Zgela, *Ger. Offen.* DE 10 2016 001 546.2 (Feb. 10th 2016).
- H. Langhals, T. Schlücker, D. Zgela, *Ger. Offen.* DE 102015001525.7 (Feb. 6th, 2015).
- H. Langhals, D. Zgela, T. Schlücker, *Ger. Offen.* DE 102015001524.9 (Feb. 6th, 2015).
- H. Langhals, T. Schlücker, D. Zgela, *Ger. Offen.* DE 102015001523.0 (Feb. 6th 2015).
- H. Langhals, T. Schlücker, D. Zgela, *Ger. Offen.* DE 102015001522.2 (Feb. 6th 2015).
- H. Langhals, T. Schlücker, D. Zgela, *Ger. Offen.* DE 102014004529.3 (Mar. 27th 2014).

Industriepreis 2015, 1st place in energy and environment

The fluorescence lifetimes of fluorophores depend on their environment. Interactions with surrounding molecules, the refractive index of the sample and even changes in concentration have impact on the fluorescent decay. This draws lifetime spectroscopical methods in the UV/Vis-region into the focus for applications in analyzing and sorting approaches. Unmarked polymers were investigated and proved to display a measurable fluorescence induced by UV radiation. The emission is traced back to impurities and additives or even byproducts evolving during the production process. This composition might lead to characteristic fluorescence spectra and lifetimes. For such applications, the effecting compounds within the analyzed material may not necessarily have to be identified. A distinct fluorescent decay at a constant detection wavelength would allow efficient recycling even of unmarked polymers.

2.4.1 Development of an Optical Method for the Recycling of Unmarked Polymers

Recycling of polymeric waste still presents a challenge in both, research and technology. There is a necessity for the development and improvement of efficient processes because of increasing amounts of waste caused by polymers ("plastic planet"). The pacific trash vortex, named Great Pacific Garbage Patch, is one of the most prominent and impressive examples for environmental pollution. Moreover, recycling of cheap plastic waste may open an economic source for organic materials. The majority of technical polymers are thermoplasts and melt and moulding again is attractive for their easy re-use. However, the immiscibility and incompatibility of organic polymers are therefore the main obstacles because lacking uniformity as low as 5% lowers the value of polymers appreciably and an even higher uniformity is required for high performance materials. Pure polymers for recycling may be collected in polymer-processing manufactories, however, the majority of collected material forms mixtures where an efficient sorting is required before processing. The machine-based recognition of polymers is a prerequisite for such processes where methods using the density or electrostatic properties were described.^[78] Optical methods are more attractive because of simple, stable and efficient technology where fluorescence is advantageous^[79] because of unproblematic light path and detection. The doping of polymers with fluorescent markers^[80] and their re-identification by the spectral resolution of their fluorescence in combination with a binary coding was described by *Langhals et al.*^[81] This demonstrated the efficiency of the application of fluorescence. However, there are two topics for a fundamental improvement.

First, only doped material can be recycled where the recycling has to be already targeted in the production of final products whereas undefined wastes cannot be recycled in this way. Second, the spectral resolution for every flake for recycling costs appreciable efforts for detection and signal processing. Fast optical processes such as lifetime spectroscopy for the sorting of undoped material would bring about an appreciable progress and would even allow working up deposited material.

The investigation of the recycling efficiency of fluorescence lifetime methods was concentrated on the technical polymers Luran® (styrene, polyacrylonitile copolymer from BASF), Delrin® (polyoxymethylene from DuPont) and Ultramid® (polyamide with glass fibre from BASF). The polymers were applied without further treatment. Fluorescence decays were measured with an Edinburgh Analytical Instruments CD900 and a tungsten flashlight nF900.

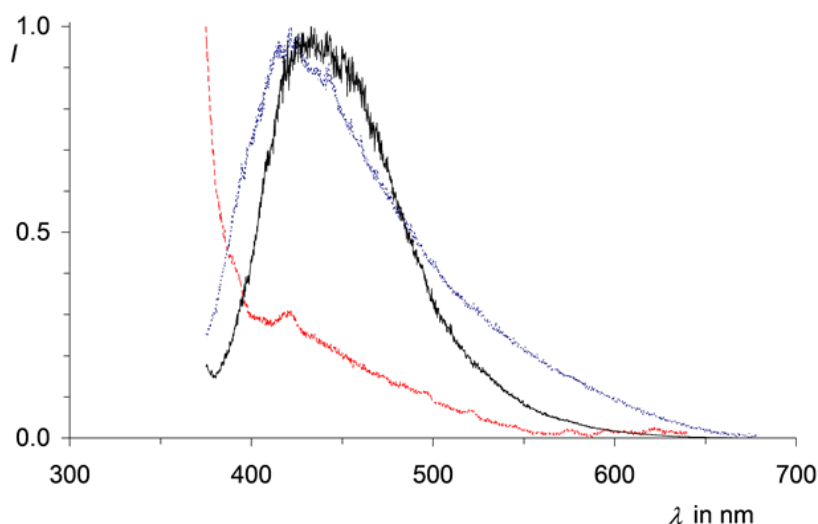


Figure 28: Fluorescence spectra of the auto fluorescence of Luran® (blue, dotted curve), Delrin® (red, dashed curve) and Ultramid® (black, solid curve) with optical excitation at 365 nm.

An appreciable strong auto fluorescence (Figure 28) of these technical materials was found for standard optical exciting at 365 nm where tungsten or mercury lamps and laser diodes (AlInGaN) may be applied as accessible light sources. Slight variations of the wavelengths of excitation do not alter the spectra significantly. The investigated polymers exhibit individual shapes of their auto fluorescence spectra. Hence, further investigation were executed using an excitation wavelength of 365 nm. These spectra already may be used for the identification and sorting of polymers by means of methods of pattern search. Thus, identification of

undoped material was successful, however, this requires still an appreciable effort of calculation and measuring time.

As an alternative, the fluorescence lifetimes of the auto fluorescence were investigated and found to be remarkable different for various polymers (Table 16). The fluorescence decay was evaluated by first order in time with the time constant τ . This represents a non-arithmetic average of a multi-exponential decay caused by several fluorescent species.

Less intense mono-exponential components (τ_2) were detected for longer lifetimes ($t > 12$ ns) as displayed in Figure 29. The decay curves can be easily splitted into two branches (τ for $t < 12$ ns, τ_2 for $t > 12$ ns) representing each a majority of the single components of the fluorescence lifetime. However, a mono-exponential interpretation is sufficient for the distinct identification by far. Factors of about two distinguish the decay times τ for Delrin[®], Ultramid[®] and Luran[®] allowing an unambiguous identification of the polymers. The decay curves of the auto fluorescence of the polymers are reported in Figure 29 and clearly indicate their pronounced differences. A simple logarithmic representation of the flat, right branch (represented by τ_2) of the decay curves is shown to exhibit mainly mono-exponential behavior.

Table 16: Fluorescence lifetimes of the studied polymers Luran[®], Delrin[®] and Ultramid[®].

Polymer	τ^a / ns	τ_2^b / ns
Luran [®]	3.53	5.78
Delrin [®]	0.74	8.42
Ultramid [®]	1.96	7.83

Excitation wavelength: 365 nm, detection wavelength: 460 nm. a) Mono-exponential evaluation of the fluorescence lifetime; b) Mono-exponential fluorescence lifetime of long-life components ($t > 12$ ns).

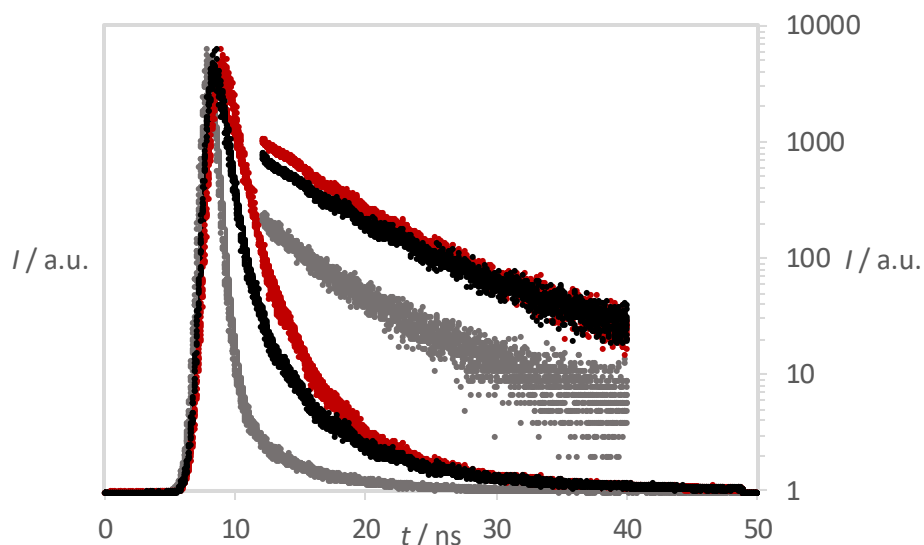


Figure 29: Fluorescence decay of polymers (excitation: 356 nm, detection: 460 nm) in linear(left) and logarithmic scales (right). Mono-exponentially fitted functions of decay as solid lines (mainly covered by actual measurement points). Fluorescence decay of Luran® (red), Delrin® (grey) and Ultramid® (black).

The presented method was further extended to polymers with higher volumes of production, such as poly ethylene (PE) or poly styrene (PS). The setup of the instrument was changed to a more intense light sources using a PC-405 laser with 405 nm and 0.4 mW, max. 80 MHz. The detection was realized with a PicoQuant FluTime 300 and a PicoQuant PicoHarp 300 TCSPC unit.

The preferred wavelengths for the detection of the fluorescence decays were located by means of lifetime dependent fluorescence spectroscopy. A fluorescence spectrum was recorded regarding all emissive components with lifetimes between 2 and 3 ns as well as between 4 and 100 ns (Figure 30) using the script depicted in Scheme 20 below. The maximum of the obtained spectrum was intended to be the detection maximum for lifetime determination to accent the slower components as those carrying the main information about the material. However, most reproducible results (within tolerance of $\pm 1\%$) were obtained for detection at 460 nm. All spectra display appreciable fluorescence at this wavelength thus, all fluorescence decays were detected at this experimentally found wavelength.

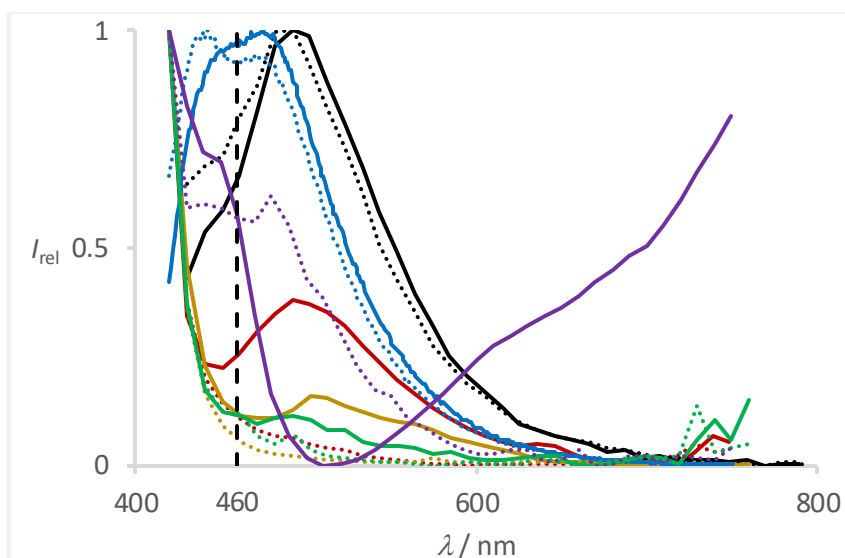


Figure 30: Time-resolved fluorescence spectra of selected polymers: HDPE (red), Delrin® (black), PC (yellow), PET (blue), PMMA (green) and Tectosil® (violet) Light curves represent the timeslots from 2 ns to 3 ns, solid curves those from 4 ns to 100 ns.

The actual script for the determination of time resolved emission spectra is given below and was applied in the PicpQuant operation software:

```
{ Data aquisition for TRES with Xe flash lamp }

{ block of variable definitions }
def
  StartWL : Float;
  StopWL : Float;
  DeltaWL : Float;
  WL : Float;
  i: Int;
  TimePerPoint : Float;
  Spectrum1: Curve; { Resulting time-gated Spectrum}
  Spectrum2: Curve; { Resulting time-gated Spectrum}
  TimeGate1First: Float;
  TimeGate1Last: Float;
  TimeGate2First: Float;
  TimeGate2Last: Float;
  ns: Float;
  us: Float;
  ms: Float;

{ program block }
exec
  { >> set the script aquisition parameters HERE << }
  Sample="SAMPLENAME";
  Solvent="SOLVENT";
  StartWL=420; { in nm }
  StopWL=750;
  DeltaWL=10;
  TimePerPoint=1; { in sec }

  ns = 1e-9;
  us = 1e-6;
  ms = 1e-3;
  TimeGate1First = 2.0 * ns;
  TimeGate1Last = 3.0 * ns;
  TimeGate2First = 4.0 * ns;
  TimeGate2Last = 100 * ns;
```

```

DETECTOR_1.DETShutterPos=FALSE;
Spectrum1.NumPoints = ((StopWL - StartWL)/ DeltaWL) + 1;
Spectrum2.NumPoints = ((StopWL - StartWL)/ DeltaWL) + 1;
for i = 0 to Spectrum1.NumPoints - 1 step 1
    Spectrum1.x[i] = StartWL + DeltaWL * i;
    Spectrum1.y[i] = 0;
    Spectrum1.Valid[i] = FALSE;

    Spectrum2.x[i] = StartWL + DeltaWL * i;
    Spectrum2.y[i] = 0;
    Spectrum2.Valid[i] = FALSE;
end;
i = 0;
for WL=StartWL to StopWL step DeltaWL
    DisplayStatus("Wavelength: " + WL + " nm (" + StartWL + " nm -> " + StopWL + " nm)");
    DETECTION_MONO.MCRGratingWavelength=WL*1E-9; { in meter }
    DETECTOR_1.DETShutterPos=TRUE;
    Histogram(TimePerPoint,-1);
    Spectrum1.y[i] = integral(crv[LastMeasCurveIndex] from TimeGate1First to TimeGate1Last);
    Spectrum1.Valid[i] = TRUE;
    Spectrum2.y[i] = integral(crv[LastMeasCurveIndex] from TimeGate2First to TimeGate2Last);
    Spectrum2.Valid[i] = TRUE;

    Spectrum1.y[i] = Spectrum1.y[i] / (crv[LastMeasCurveIndex].x[1] - crv[LastMeasCurveIndex].x[0] + 1e-30);
    Spectrum2.y[i] = Spectrum2.y[i] / (crv[LastMeasCurveIndex].x[1] - crv[LastMeasCurveIndex].x[0] + 1e-30);
    Plot(Spectrum1, 0); // second parameter = 0 for clearing the plot
    Plot(Spectrum2, -1); // second parameter < 0 for redrawing the plot
    i = i + 1;
end;
StoreAsSpectrum(Spectrum1);
StoreAsSpectrum(Spectrum2);
EXCITATION_ATTENUATOR.ACTPos=1;
DETECTOR_1.DETShutterPos=FALSE;
end.

```

Scheme 20: Determination of a time-resolved emission spectrum with custom time slots. The range from TimeGate1First to TimeGate1Last was set up for control of the short fluorescent components. The second time range in red considers all components with lifetimes of the excited state of more than 4 ns. The top limit of 100 ns is set to a value where all molecules are estimated to have already relaxed.

Fluorescence decays were obtained with a repetition rate of 20 MHz for a span of 10 s, slightly increased noise is obtained for a shortened accumulation time of 1.0 ms. Polymer material contains different unknown fluorophores in small concentration with the result of globally multi-exponential decays. The reported fluorescence lifetimes, hence the time constants for monoexponentially fitted decays, were obtained by exponential fitting (exponential tail fit) of the respective sections according to the equation (2) (Chapter 1.1) by means of the software FluoFit from PicoQuant. The shape of the laser pulse was neglected due to its small FWHM. A broad range of different values for τ between 0.2 until 5 ns is observed. The individual time constants shown in Figure 31 are as characteristic as fingerprints. Remarkably, the chemically very similar and otherwise difficult to discriminate types of polyethylene, LDPE (low-density polyethylene), HDPE (high-density polyethylene) and UHDPE (ultra- high-density polyethylene) can be unambiguously distinguished. This may be a consequence of different microscopic rigidities of these materials. Moreover, different methods of manufacturing such as PET for bottles and for PET plates or different types of silicones can be well categorized; see Figure 31. The various types of silicone adhesives result in distinguishable, however similar lifetimes τ . The availability of a further criterion for characterization would be of interest.

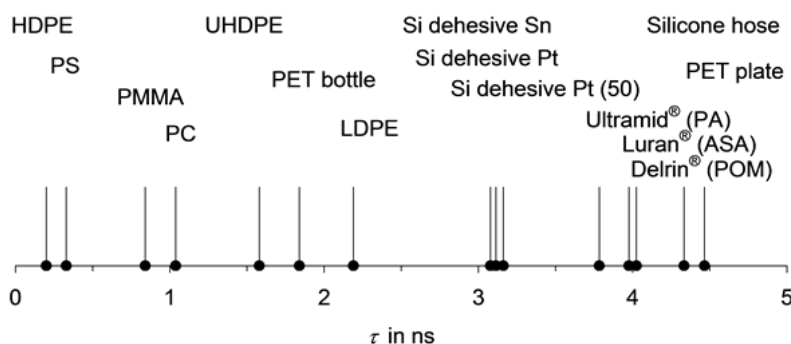


Figure 31: Fluorescence lifetimes τ in ns of technical polymers. Reproducibility is given within $\pm 1\%$.

Although the obtained data depend on the instrument and applied methods, a very good reproducibility allows identification of unmarked technical polymers. The mono-exponential decay dominates resulting in the quite well acceptable first order kinetics. However, there is at least a second fluorescent component in the decay process. Thus, the lifetimes τ from Figure 31 mean an averaging of both components depending on their relative contributions. The fluorescence decay was analyzed bi-exponentially and the two time constants τ_1 and τ_2 were

introduced. All three time constants τ , τ_1 and τ_2 are reported in Table 17. Bi-exponential analysis was realized by splitting the curve in two sections (Figure 32), a steep one (τ_1) representing the fast relaxation processes and a flat one (τ_2) describing the slower processes respectively. The decay time τ_1 was calculated within the period between 2 ns (t_{\max}) and 3 ns ($t_{\max+3}$) (Figure 32, black) relative to the maximum intensity and the decay time τ_2 (Figure 32, red) between 4 ns ($t_{\max+3}$) and 43 ns ($t_{\max+43}$) past the maximum. Thus, all values are relative and are not independent on the used analytical equipment. The advantage of this method is the independency of instrumental variation caused by fitting processes. More parameters do not lead to unequivocal reproducibility. Hence, a simplified method was evolved to ensure a best possible efficiency of identification and sorting.

Table 17: Time constants for the auto-fluorescence decay of technical polymers.

Polymeric material	τ^a / ns	τ_1^b / ns	τ_2^b / ns
Poly(methyl methacrylate) (PMMA)	0.841	0.124	3.669
Polystyrene (PS)	3.290	0.171	4.457
Polycarbonate (PC)	1.038	0.077	4.379
Polyethylene terephthalate (PET) bottle ^c	1.840	1.176	4.205
Polyethylene terephthalate (PET) plate	4.466	1.387	8.933
Polyethylene LDPE	2.190	0.456	4.655
Polyethylene HDPE	<0.2	0.155	4.238
Polyethylene UHDPE	1.580	0.217	4.932
Silicone Tectosil granulate		0.132	7.709
Silicone Tectosil foil		0.084	8.572
Silicone Dehesive Sn	3.078	1.432	6.825
Silicon Dehesive Pt	3.162	1.473	6.149
Silicone Dehesive Pt (50)	3.114	1.707	6.106
Silicone hose	4.333	1.793	8.180
Delrin (POM)	4.024	1.433	4.487
Luran (ASA)	3.976	1.199	4.259
Ultramid (PA)	3.784	1.145	4.313

a) Mono-exponential evaluation of the entire decay. Mono-exponential evaluation of short-life (τ_1) and long-life (τ_2) components separately.

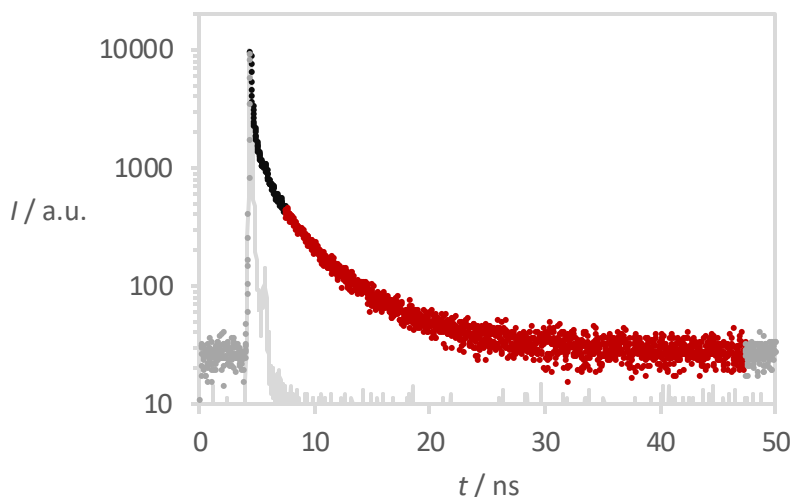


Figure 32: For determination of τ_1 and τ_2 the decay was split in two branches, one representing the short relaxation processes from t_{\max} to $t_{\max}+3$ (black). IRF (grey line) and non-relevant measuring points (light grey) are given for completion.

The two time constants τ_1 and τ_2 of the bi-exponential data evaluation allow a two-dimensional characterization of the polymers as is shown in Figure 33. Luran® is omitted for clearness because recording the very high value of τ_1 would compress the abscissa. The two-dimensional presentation of the fluorescence lifetimes τ_1 and τ_2 in Figure 33 allows a clear distinguishing of the analyzed polymers. Even for similar materials and supplements with close τ values (Figure 31) a discrimination is possible. It also becomes more distinct to distinguish as well between the widely applied polyethylenes LDPE, HDPE and UHDPE (filled circles) as between differently processed materials such as the silicone elastomer Tectosil® (triangles) and PET (squares). The differently processed silicone adhesives (diamonds) become more clearly separated where the applied catalyst for cross-linking (Sn or Pt) seems to influence predominantly τ_2 , whereas the addition of a hardener (Pt (50)) increases τ_1 . This corresponds to the very low values of τ_1 for the elastomer Tectosil®.

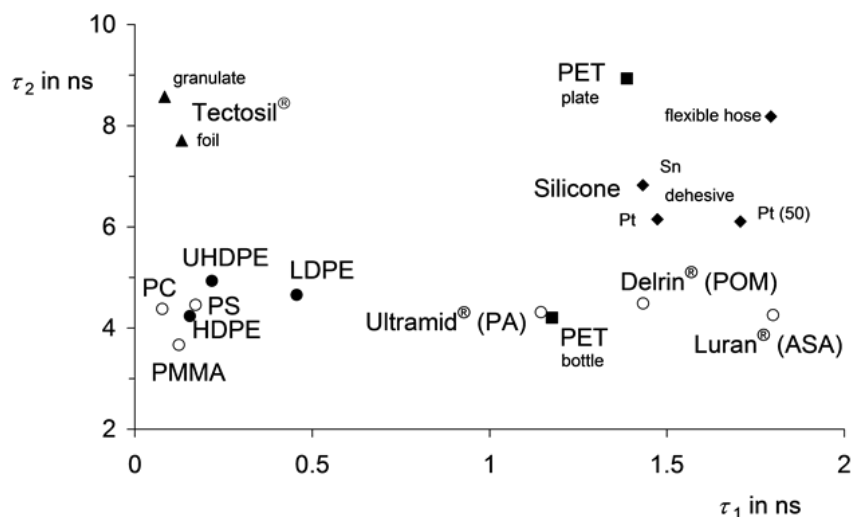


Figure 33: Two-dimensional characterization of polymers by means of their constants τ_1 and τ_2 attained by bi-exponential evaluation of the fluorescence decay. Filled circles: polyethylenes LDPE, HDPE and UHDPE; squares: PET; diamonds: Silicones; triangles: silicone elastomer Tectosil®.

Different manufacturing processes and physical conditions of the polymers such as in case of PE were proved to lead to characteristic fluorescence lifetimes. Besides these pre-use factors it is likely to also detect differences of the fluorescence decays caused by varied usage. PET is widely applied for both, for foodstuff such as bottles for water and soft drinks and for technical liquids such as the mineral oils diesel or engine oil. The latter lipophilic liquids can diffuse into the polymeric material such as a plasticizer and would be slowly released. As a consequence, PET for foodstuff must be carefully separated from the latter material. Such contaminations were simulated by the contact with the mineral oils diesel and engine oil for one week and subsequent purification of PET with alkaline detergents according to a technical standard procedure. The contaminated PET-Flakes were treated under stirring with a mixture of 3% aqueous NaOH (100 mL) and 15% aqueous sodiumdodecyl sulphate solution (SDS, 50 mL) at 85 °C for 2 h, washed with distilled water, dried in air at room temperature and then at 60 °C for 16 h. Figure 34 clearly indicates that a pre-treatment of PET results in a lowering of the fluorescence lifetime τ . This is most pronounced for diesel with low molecular weight and low viscosity and slightly less pronounced for engine oil with higher molecular weight and viscosity. This corresponds to observations with silicone dehesives and Tectosil® (Figure 33). A technical cleaning of the contaminated PET increases the fluorescence lifetime again, however, it does not reach the high value of the neat material by far. Even clean commercial recycling flakes exhibit a slightly diminished fluorescence lifetime.

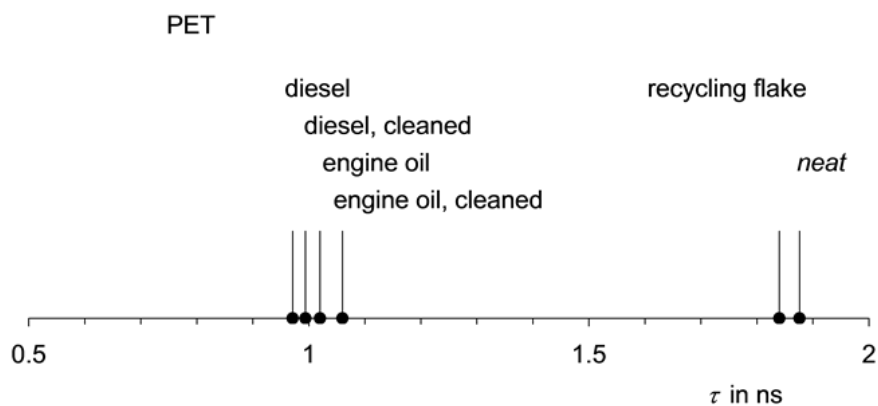


Figure 34: Fluorescence lifetimes τ of pre-treated PET; expanded range.

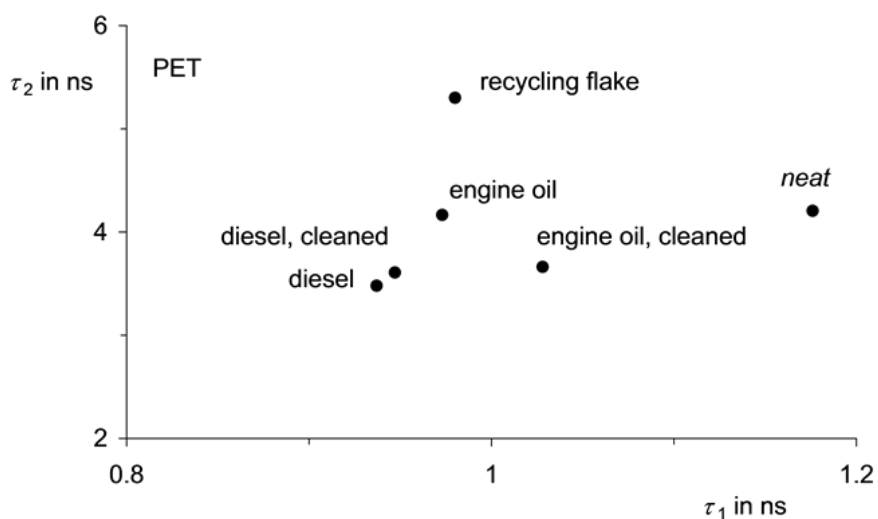


Figure 35: Two-dimensional characterization of PET with various pre-treatment by means of their constants τ_1 and τ_2 after bi-exponential evaluation of the fluorescence decay.

The detection of contaminations becomes more extended by means of the two-dimensional presentation of the fluorescence lifetimes τ_1 and τ_2 in Figure 35. The recycling flake with τ close to the neat material also given in Figure 34 becomes much more separated by τ_1 and τ_2 in Figure 35. The alterations by means of purifying exhibit different effects for diesel and engine oil. As a consequence, neat material can be well separated from contaminated and foodstuff pureness can be ensured after sorting by means of fluorescence lifetime analysis.

2.4.2 Studies on the Fluorescence of Ce(IV). A Universal Probe for Sorting Polymers

The fluorescence spectra of the studied polymers (Figure 30, above) exhibited various differences. However, a few small but distinct emission bands were found predominantly in the weakly fluorescent samples, most noticeable at 460, 480 and 717 nm. Additionally, the best reproducibility of determination of fluorescence lifetimes for most samples was observed at a detection wavelength of 460 nm. These results prompted to test for a universal fluorescent species that can be used as versatile probe in various polymers. Potential additives such as transition metal catalysts or fillers such as highly dispersed silica were investigated by means of fluorescence spectroscopy as film or in different solvents (Figure 36). The characteristic bands at 460, 480 and 720 nm were found to be also emitted by most technical silica materials such as Carb-o-sil© (Merck) and HDK® (Wacker).

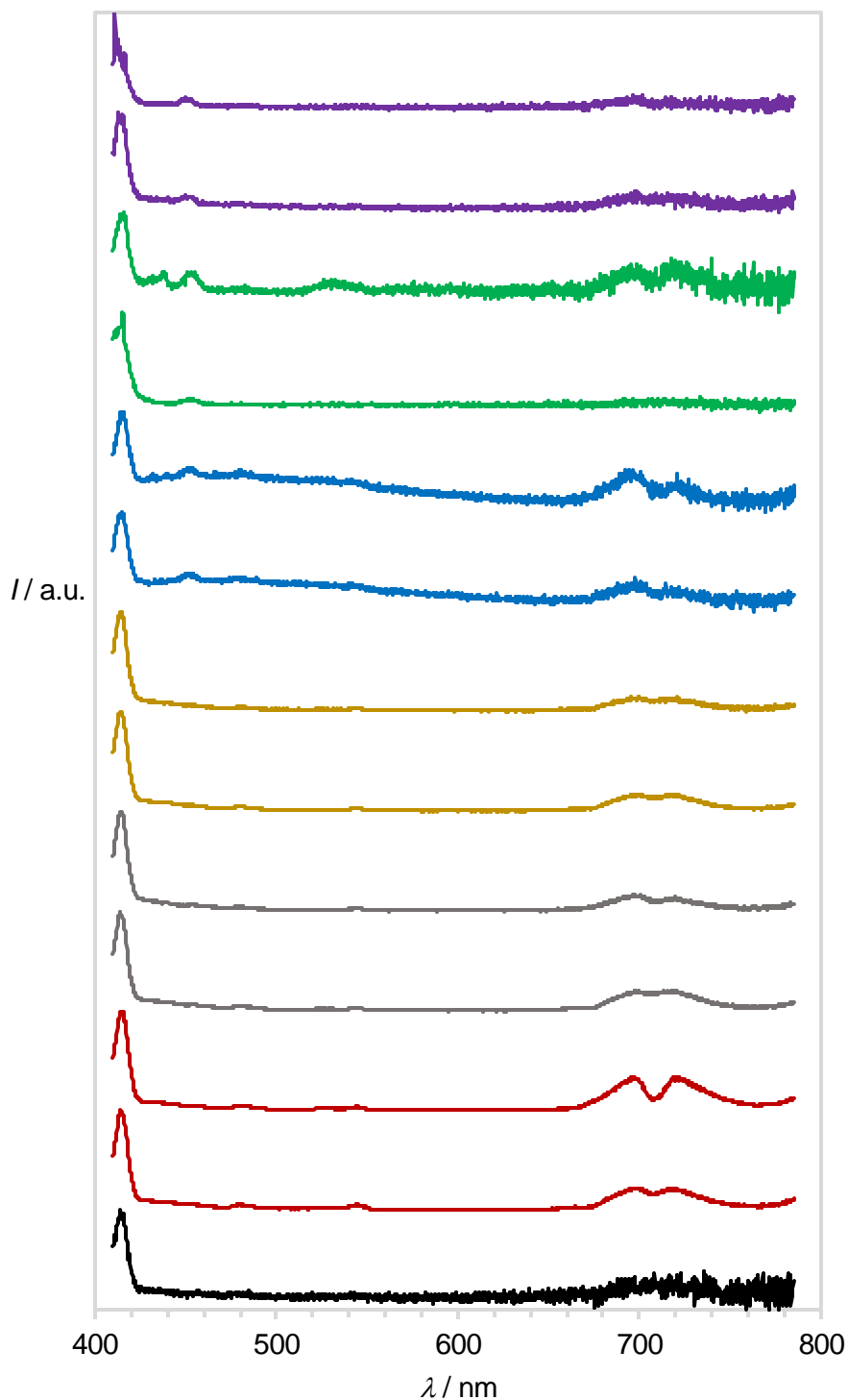


Figure 36: Fluorescence spectra of highly disperse silica excited at 405 nm. Colors indicate the applied dispersant: Neat film (red), water (grey), methanol (yellow), DMF (blue), toluene (green), hexane (violet). The top respective curve is for Cab-o-sil® from Merck (Acros), the accompanying bottom curve for HDK® H 15 from Wacker. The bottom black curve represents the spectrum of Ludox® from sigma aldrich, a highly pure aqueous silica standard for optical scattering.

The studied species exhibit similar fluorescence which indicates similar or even same fluorescent structures. Further fluorescence spectroscopy revealed cerium (IV) to be the potentially responsible compound. Fluorescence spectra of aqueous solutions of cerium(IV)sulfate were recorded and both, position and shape of the emission spectra were found to equal the measured peaks of the polymers and silica samples. The fluorescence spectra of cerium(IV)sulfate are reported in a dilution series to show the dependence of relative intensities on concentration. Spectra were recorded in aqueous solution with excitation at 405 nm and are given in Figure 37 and 38.

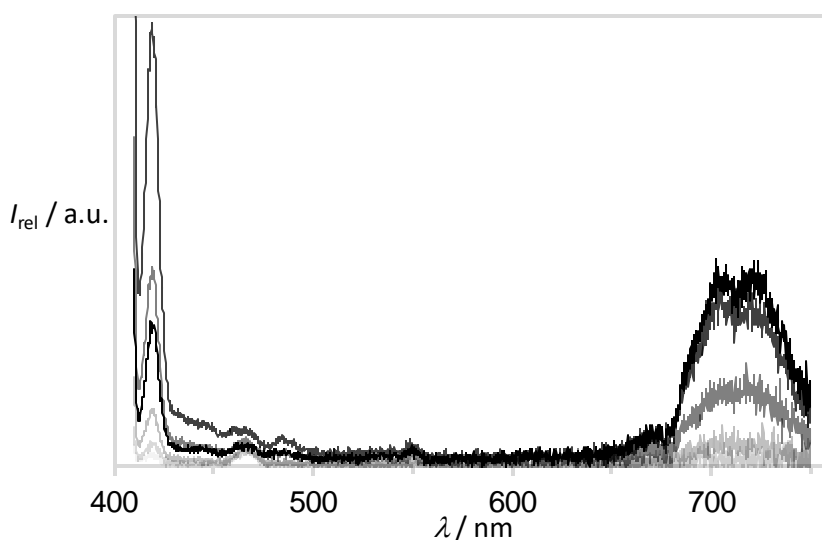


Figure 37: Fluorescence spectra of cerium(IV)sulfate in aqueous solution at different concentrations. Lighter colors represent lower concentration. The excitation wavelength was set to 405 nm.

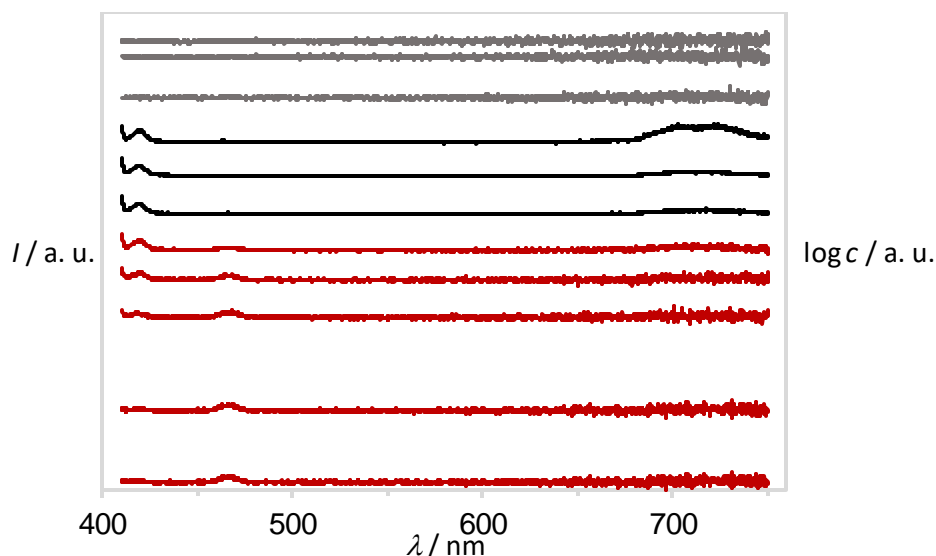


Figure 38: Correlation of relative fluorescence intensities and concentration of aqueous solutions of cerium(IV)sulfate. Very high concentrations completely quench fluorescence (grey). At lower concentrations (red) the relative intensity of the fluorescence band at 460 nm increases.

The peak at 460 nm was found to be most intense at low concentrations (Figure 38). Interestingly, Raman scattering of water is expected to occur at approx. 461 nm. However, the emission wavelength was found to be independent from the excitation wavelength and also the solvent (Figure 36). As a consequence, the detected emission was attributed to fluorescence processes. Regarding the case for polymers, this makes cerium(IV)sulfate the ideal versatile probe for recycling applications. Most unmarked polymers contain very small amounts of cerium (IV) and display most distinct, measurable fluorescence at 460 nm. The fluorescence decay in turn depends on environmental conditions and thus, leads to specific values which are characteristic for the polymer matrix material. Table 18 summarizes the fluorescence lifetimes of Cab-o-sil© and HDK® H 15 in different dispersants for a simulation of different environmental effect. Even in dispersion the fluorescence lifetimes was found to depend on surrounding conditions.

Table 18: Fluorescence lifetimes of different silica dispersions.

Silica type	τ_1^a / ns	τ_2^a / ns
HDK® H 15 in water	8.815	3.060
HDK® H 15 in methanol	8.709	3.116
HDK® H 15 in DMF	10.104	3.292
HDK® H 15 in toluene	8.550	2.692
HDK® H 15 in hexane	6.713	0.897
Cab-o-sil© in water	9.244	3.139
Cab-o-sil© in methanol	10.091	3.390
Cab-o-sil© in DMF	10.250	3.324
Cab-o-sil© in toluene	9.262	2.640
Cab-o-sil© in hexane		
Ludox© (in water)	5.686 ^b	

a) Excitation at 405 nm, detection at 460 nm. τ_1 and τ_2 were determined in bi-exponential tailfits starting from 3 ns after the intensity maximum with FluoFit software; b) No results could be generated by bi-exponential fitting of the decay. For comparability the mono-exponential value (in this case a non-arithmetic mean) is given.

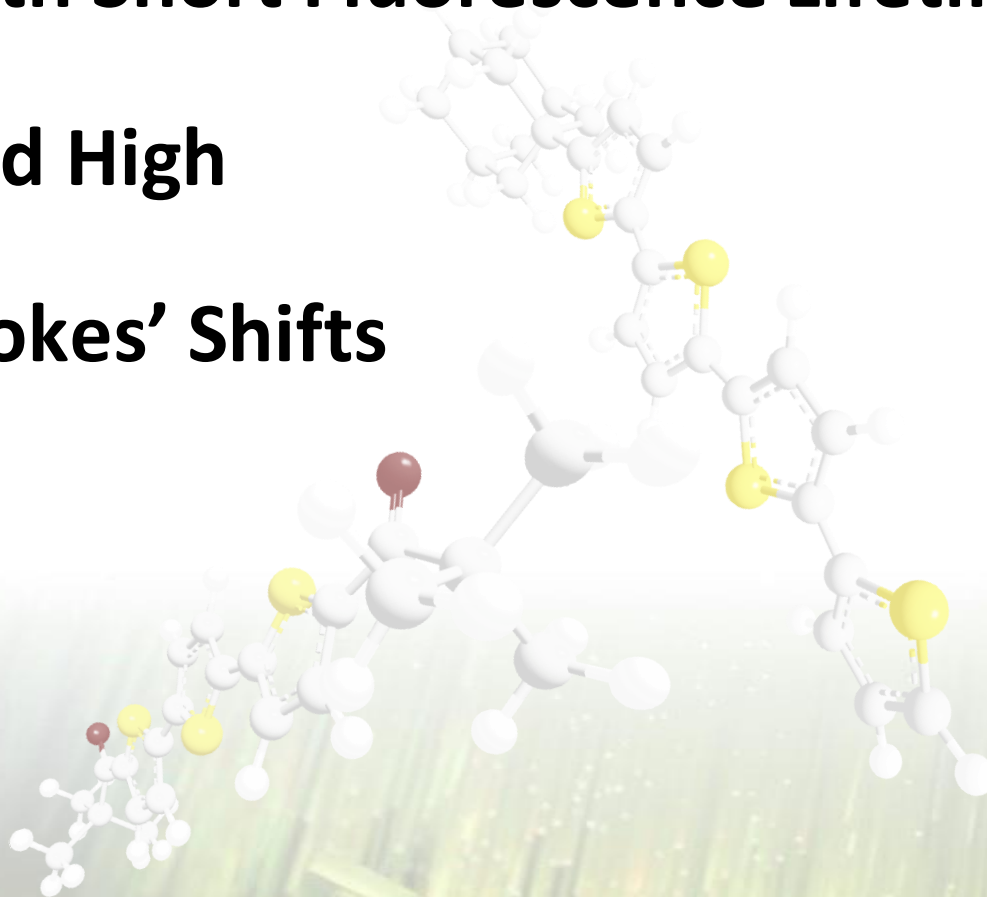
Conclusion

Technical polymers were efficiently identified by means of their auto-fluorescence lifetime. Mono-exponential evaluation allows reliable and reproducible values for sorting of unmarked batches of mixed polymers. Bi-exponential and pseudo bi-exponential analysis improves the accuracy and enables advanced classification. The additional information is useful for the discrimination of chemical similar materials such as LDPE, HDPE and UHDPE or even different processing or recognition of contaminants. This enables efficient sorting applications using UV or visible light. Easy signal processing, fast measurements and well-known detector technology draw the presented method in focus for high throughput recycling solutions. Cerium (IV) was found to be a versatile fluorescence probe which is already found in many technical polymers due to production techniques. The wide distribution of cerium allows the development of standardized procedures for the realization of light-based polymer sorting by means of fluorescence lifetime spectroscopy.

2.5

Synthesis and Characterization of Oligothiophenes

with Short Fluorescence Lifetimes and High Stokes' Shifts



T. Schlücker, V. Dhayalan, H. Langhals, C. Sämann, P. Knochel, *Asian J. Org. Chem.* **2015**, *4*, 763-769;

H. Langhals, T. Schlücker, PCT/EP2016/051211, *Ger. Offen.* DE 102015000815.3 (Jan. 21st, 2015).

H. Langhals, T. Schlücker, P. Knochel, *Ger. Offen.* DE 102014009757.9 (Jun. 26th 2014).

H. Langhals, P. Knochel, V. Dhayalan, T. Schlücker, C. Sämann, *Ger. Offen.* DE 102014009756.0 (Jun. 26th, 2014).

The fluorescent lifetime of a compound was shown to depend on several environmental effects, such as concentration or medium. However, only minor effects are obtained by variation of these factors. The main cause for fast or slow relaxation is chemical structure of the chromophore. A validity of equation (5) was found within same classes of dyes but there is no precise prediction of fluorescence lifetimes possible from only chemicals structure. The studies were expanded to repetitive oligomer structures such as oligoenes and oligothiophenes and fluorescence lifetimes of less than 1 ns were found frequently. On the basis of comparably stable oligothiophenes a series of highly soluble derivatives was developed with absorption maxima in the visible region.

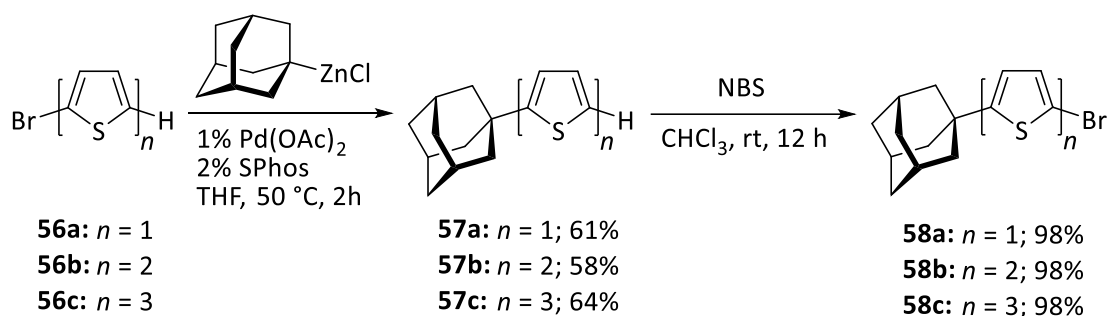
2.5.1 Adamantyl Substituted Oligothiophenes

The covering of increasing volumes in data processing draws optical systems such as the popular internet trans-continental cable lanes more and more into the focus of interest.^[68] Fluorescent materials are principally useful as frequency converters in optical devices or polymer optical fibers. However, their frequency of operating is fundamentally limited by the time constant of the fluorescence decay and one may ask how far this decay time can be shortened. According to Förster^[2] this time constant is indirectly proportional both to the fluorescence quantum yield and the oscillator strengths where the latter is interrelated with the molar absorptivity. Fluorescence decay times of about 4 ns were found in solution^[13] for highly fluorescent dyes with quantum yields close to 100% and high color strengths with molar absorptivities of about 100 000 such as for perylene dyes.^[27]

Shorter decay times in the sub-nano second region were found frequently for oligothiophenes^[82]. Particularly quaterthiophene displays fluorescence lifetimes of about 0.4 ns^[83] while its optical spectra matches the requirements given by commercially available inexpensive light sources (e.g. GaN-LEDs). Furthermore, when incorporated in polymers the emission spectrum fits the highly transparent spectral regions of the solid matrices (preferably poly(methyl methacrylate) (PMMA). However, the solubility^[84] in organic solvents and polymer materials is deficient for most applications. Herein, a new approach for increasing the solubility of oligothiophenes by the attachment of a bulky adamantyl group via Negishi cross-coupling reactions^[45,85] is reported briefly. The suitability of such oligothiophenes as

ultra-fast frequency converters for optical data processing is shown, particularly in polymer optical fibers.

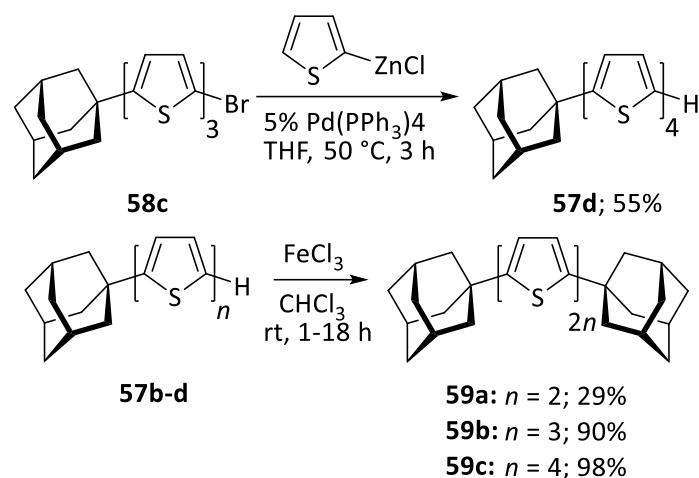
The preparation of fluorescent dyes for doped polymer optical fibers requests two key properties: a good solubility of the dye in the corresponding monomer and a high stability towards polymerization reactions. To increase the solubility, oligothiophenes were terminally capped with bulky substituents^[86] using 1-adamantyl moieties. With this system, radical side-reactions are impeded by avoiding hydrogen atoms in benzylic position.^[87] Moreover, the bridgehead nature^[88] of the 1-adamantyl group^[89] will also efficiently prevent from dealkylation of the terminal groups due to the bridgehead strain.^[90]



Scheme 21: Preparation of 1-adamantyl substituted oligothiophenes **57a-c** ($n=1-3$) via Negishi cross coupling reactions. Further bromination with NBS leads to the readily soluble 5-bromo oligothiophenes **58a-c**.

In literature,^[91] 1-adamantylzinc chloride was shown to react smoothly in a Pd-catalyzed *Negishi* cross-coupling with bromoaryl derivatives. According to Scheme 21, the brominated compounds **56a-c** were mono-alkylated with 1-adamantylzinc chloride using 1% Pd(OAc)₂ and 2% of the ligand SPhos, introduced by *Buchwald*^[92] as a catalytic system. 1-(Adamantyl)thiophenes **57a-c**, bearing 1-3 thiophene units respectively, have been prepared in 58-64% yield. The (1-adamantyl)thiophenes were brominated with NBS (CHCl₃, rt, 12 h, 98% yield) to obtain activated derivatives suitable for further reactions. The alkylated bromooligothiophenes **58a-c** display an excellent solubility in organic solvents, even for extended π -systems like the 5-(1-adamantyl)-5''-bromoterthiophene (**58c**). To shift the absorption wavelength into the visible the chromophore needs to be further extended (Scheme 22). The solubility of 5-bromoquaterthiophene is by far too poor for the following organometallic couplings. Thus, the highly soluble 5''-(1-adamantyl)-5-bromoterthiophene

57c was reacted with 2-thienylzinc chloride in the presence of 5% Pd(PPh₃)₄ (THF, 50 °C, 3 h). The prolongation by one thiophene unit leads to 5-(1-adamantyl)quaterthiophene (**57d**) in 55% yield.



Scheme 22: Preparation of higher homologues ($n=4,6,8$) of (1-adamantyl)oligothiophene. The well soluble mono-alkylated quaterthiophene **57d** was obtained via a Negishi cross-coupling reaction of 2-thienylzinc chloride with 5'-(1-adamantyl)-5-bromoterthiophene (**58c**). Treatment of mono-(1-adamantyl)oligothiophenes ($n=2-4$) with FeCl₃ leads to the respective mirror symmetrical coupling products **59a-c**.

Moreover, oligothiophenes **59a-c**, bearing two terminal adamantyl substituents and 4, 6 and 8 thiophene units, respectively, could be prepared by treatment of **57b-d** with FeCl₃. Whereas 5,5'-di(adamantan-1-yl)-2,2'-dithiophene could only be obtained in traces, the higher oligomers **59a-c** were prepared in yields up to 98%. While mono-substitution leads to readily soluble oligothiophenes **57a-d**, α,ω -capping with two 1-adamantyl moieties significantly decreases the solubility. The compounds **59a-c** exhibit an even lower solubility than the completely unsubstituted derivatives of oligothiophenes. Although impurities substantially promote their solubility in chloroform, once the compounds of type **59** are isolated, they become nearly insoluble in common solvents. Therefore, they might be useful as high performance fluorescent pigments.

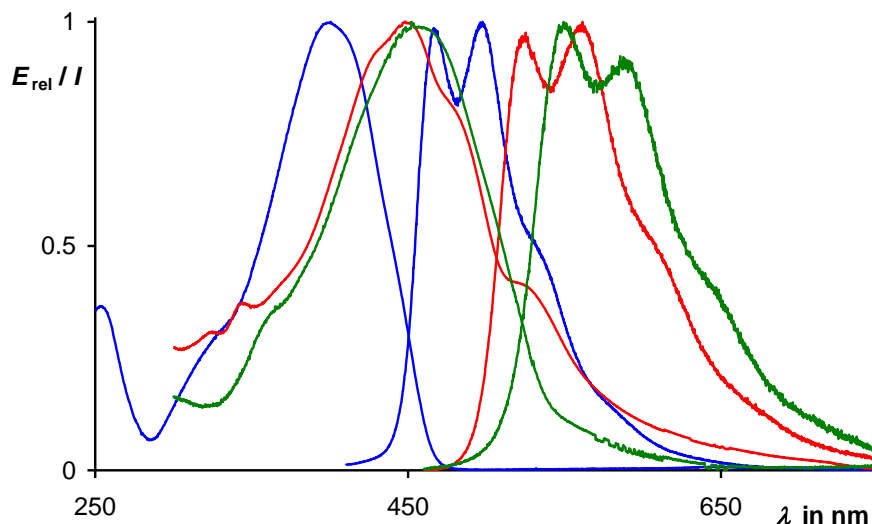


Figure 39: UV/Vis-Spectra in chloroform (for **59a**) or $C_2H_2Cl_4$ (for **59b-c**). **Blue 59a** ($n = 4$), **red 59b** ($n = 6$), **green 59c** ($n = 8$). Left absorption spectra with scale $E_{rel.}$, right fluorescence spectra with scale I .

For higher degrees of oligomerization, the absorption of light is successively shifted to longer wavelengths.^[93] The absorption maximum of **59a** ($n = 4$) is observed at 400.6 nm, it shifts to 448.2 nm for **59b** ($n = 6$) and 452.2 nm for **59c** ($n = 8$) (Figure 39). The molar absorptivities were determined to be 31900, 49000 and 64400 for oligothiophenes **59a-c**, respectively. An appreciable fluorescence is accompanied by a remarkably large Stokes' shift. The fluorescence maxima were found at 496.4 nm for **59a**, 561.6 nm for **59b** and 549.4 nm for **59c** (Table 19). Aggregation might take place for higher concentrations. The absorption spectrum exhibits a shoulder at about 520 nm for sexithiophene **59b**. This typically indicates *J*-type aggregation.^[94] However, the fluorescence quantum yields were found to be independent from the used concentrations smaller than 10^{-6} mol L^{-1} with values of about 0.20. The effect on the fluorescence efficiency might be too small to be detected beyond the limited accuracy of the measurement.

Table 19: Optical properties of (1-adamantyl)oligothiophenes.

	λ_{Abs}^a	λ_{Fluo}^b	ϵ^c	Φ^d	$\lambda_{Em}-\lambda_{Abs}^e$	$E_{Em}-E_{Fluo}^f$
4T^g	395.6	481.8	32100	0.21	86.2	0.561
57b	313.4	378.2	16000	0.04	64.8	0.678
57c	360.4	442.7	21400	0.12	82.3	0.640
57d	396.8	490.0	35600	0.43	93.2	0.596
59a	400.6	496.4	31900	0.20	95.8	0.597
59b	448.2	561.6	49000	0.20	113.4	0.559
59c	452.2	549.4 ^h	64400	0.21	97.2	0.485 ^h

a) Absorption maximum in nm; b) Fluorescence maximum in nm; c) Molar absorptivity; d) Fluorescence quantum yield; e) Stokes' shift (referred to total maxima) in nm; f) Stokes' shift (referred to total maxima) in eV; g) Experimental data of 2,2':5',2'':5'',2'''-quaterthiophene; h) The second maximum decreases relatively and therefore the values refer to the more intense one at lower wavelengths.

Whereas oligothiophenes of type **59** are of interest as fluorescent pigments, the soluble mono-substituted oligothiophenes of type **57** are practical for application in optical signal processing devices. Moreover, they exhibit remarkable optical properties. The absorption of **57b** ($n = 2$) displays its maximum at 313.4 nm in the UVB region, shifts to 360.4 nm in the UVA for **57c** ($n = 3$) and reaches the visible part of the spectrum at 396.8 nm for the new oligothiophene **57d** ($n = 4$) (Figure 40). As a consequence, the absorption spectrum can be adapted to various requirements by choosing the appropriate number of thiophene units. The molar absorptivities starting from 16000 for oligomer **57b**, increase with the number of thiophenes to 21400 for **57c** and high values of 35600 for **57d**. The fluorescence maxima were observed at 378.2 nm for **57b**, at 442.7 nm for **57c** in the visible and at 490.0 nm for oligomer **57d**. Fluorescence quantum yields were determined to be 4% for **57b**, 12% for **57c** as well as 43% for **57d**, respectively. Compared to the α,ω -capped quaterthiophene **59a** as well as the simple unsubstituted quaterthiophene^[83], the emission efficiency represented by the fluorescence quantum yield, of the mono-alkylated compound **57d** displays a more than two times higher value (Table 19). Thus, 5-(1-adamantyl)quaterthiophen (**57d**) is well suited for practical applications.

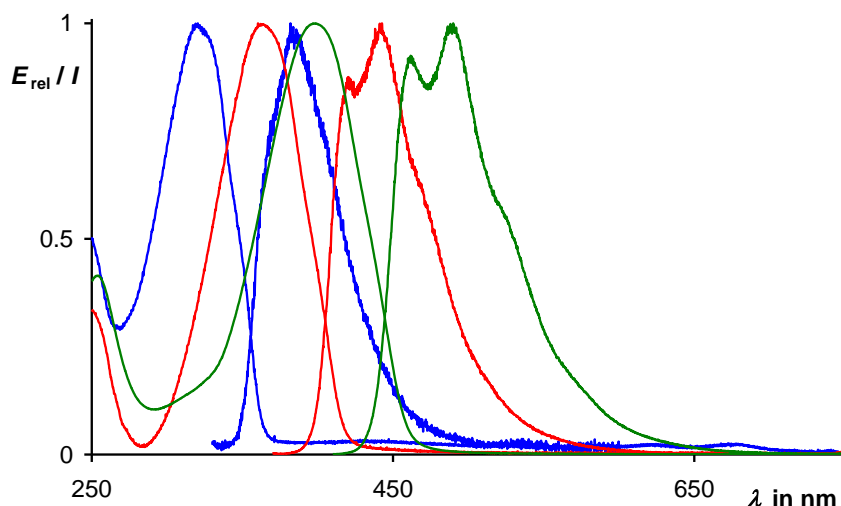


Figure 40: UV/Vis-Spectra in chloroform. Blue **57b** ($n = 2$), red **57c** ($n = 3$), green **57d** ($n = 4$). Left absorption spectra with scale $E_{rel.}$, right fluorescence spectra with scale I .

The combination of a large Stokes' shift, comparably strong fluorescence, ultra-short fluorescence decay and appreciable photo-stability makes particularly **57d** appropriate as fluorescent component in light collectors^[12] and frequency converters for optical data systems. Polymer optical fibers, doped with fluorescent dyes, can be applied in slip ring arrangements^[2] for the transmission of information. In dye doped light guides used in slip rings, the information is transmitted stepless and contactless from any position of the axis. Therefore, the fluorescent dye has to be dissolved within the polymeric fiber. The 1-adamantyl moiety confers not only high solubility in common organic solvents, it also avoids aggregation in most liquid monomers such as methyl methacrylate (MMA) in concentrations higher than 50 ppm. It is worth mentioning the tolerance of **57** towards standard polymerization reactions. 2-(1-Adamantyl)oligothiophene **57d** was dissolved in MMA that subsequently was polymerized with azobisisobutyronitrile (AIBN) at comparatively high temperatures up to 70 °C. The oligothiophene has exhibited no sign of decomposition or participation in radical processes. Combining this stability with high solubility should allow easy technical processing using the reported adamantyl oligothiophenes.

Oligothiophene **57d** exhibits a very short^[95] fluorescence decay of 0.39 ns in chloroform and 0.42 ns in polymethylmethacrylate (PMMA), respectively. With respect to the fluorescence decay as the limiting factor for optical frequencies of modulation, this allows a very high data throughput compared to known chromophores for this applications.

Obviously, the large Stokes' shift is advantageous as it avoids re-absorption within the light guide and thus reduces attenuation. Geometric relaxation processes that occur after the electronic excitation seem to be responsible for the increased Stokes' shift (Figure 41). The thiophene rings are planar in oligothiophenes and slightly twisted against each other with reported dihedral angles between 3 and 9°.^[96] A diminishing of the dihedral angle between the thiophene units and a shortening of the single bond between the rings are probable relaxation processes in the optically excited state leading to a bathochromically shifted fluorescence (compare to Section 2.4.1).

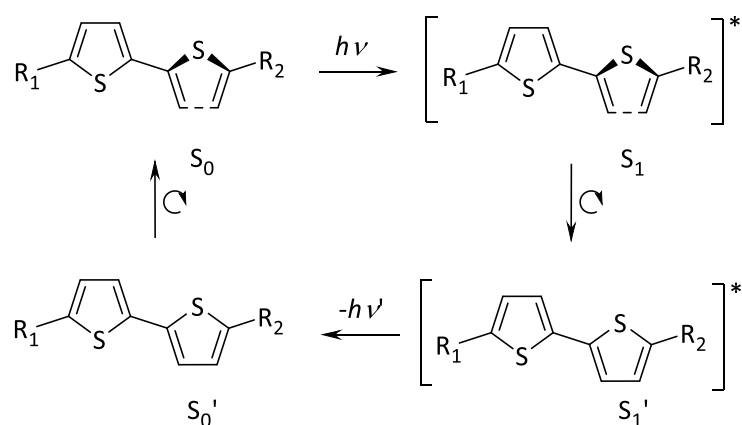


Figure 41: Schematic process causing the increased Stokes' shifts. i) Vertical transition by light absorption ($h\nu$) from the electronic ground state S_0 (top left) to reach the electronically excited state S_1 . ii) Relaxation to a geometrically more favorable, energetically lower excited state S_1' . iii) Bathochromically shifted fluorescence ($-h\nu'$) from S_1' to S_0' . iv) Relaxation to the energetically more favored initial state from S_0' to S_0 .

In solution β -alkylation further increases the Stokes' shift by decreasing the conjugation in the ground state leading to shorter absorption wavelengths while displaying nearly same fluorescence properties.^[97] In contrast, bulky substituents in these positions would strongly suppress the dynamics in polymer glass matrices. Moreover, extinction values and fluorescence quantum yields decrease with steric hindrance due to reduced π -electron delocalization.

Hence, a rod-like compound enables the best possible molecular dynamics between the polymer chains. Furthermore, the total size of the fluorophores should be as small as possible to prevent light scattering processes within the light guide. Thus, the common substitution of oligothiophenes in position 3 and 4 was avoided and the introduction of solubilizing moieties limited to the 5-positions of the oligothiophenes respecting the described application. The discussed dynamic process was first developed for perylene-based dyes^[41] but appears to be adaptable to other chromophores. Theoretical calculations for oligothiophenes support the proposed mechanism.^[98]

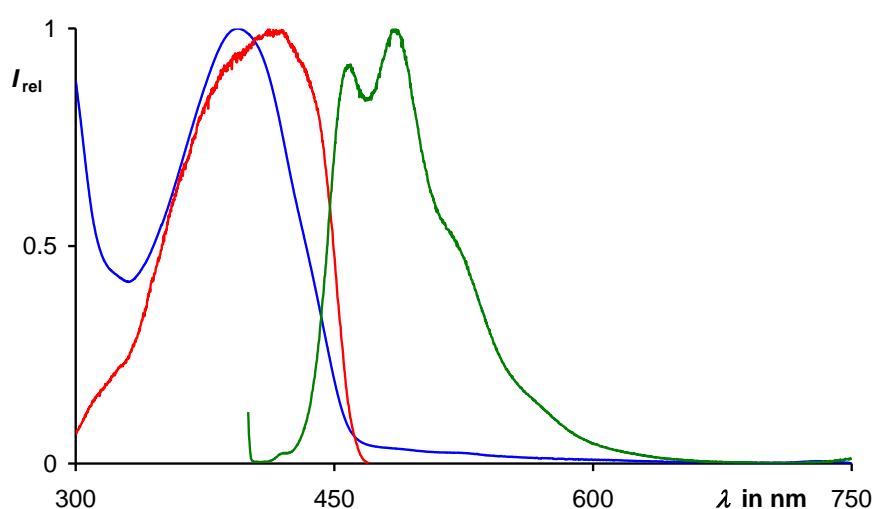


Figure 42: UV/Vis-Spectrum (blue), fluorescence excitation spectrum (red) and fluorescence spectrum (green) of **57d** in solid PMMA. Absorption spectrum with scale E_{rel} , Fluorescence spectra with scale I .

As intended, the optical properties of **57d** are not affected considerably by the local environment of the 2-(1-adamantyl)quaterthiophene (**57d**). The global geometry of the molecules seems to be only slightly influenced and the Stokes' shift remains nearly unaltered in a solid glass matrix of PMMA (Figure 42). Furthermore, neither the fluorescence lifetime (0.39 ns in CHCl_3 , 0.42 ns in PMMA), nor the absorption and fluorescence properties displays significant dependence (Figure 43). The respective fluorescence quantum yield (0.43 in CHCl_3 , 0.48 in PMMA) also remain mainly unaffected. This enables a multitude of different variations, i.e. the used polymer, for application as fluorescent dye in optical data processing.

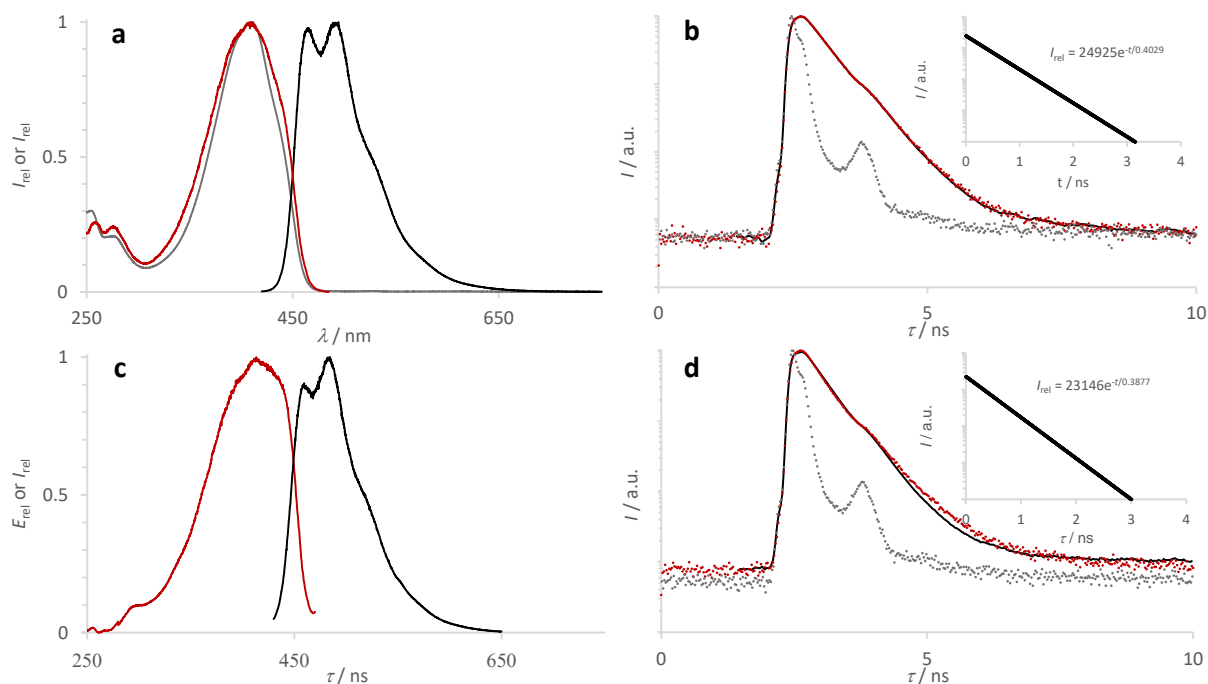


Figure 43: Comparison of optical spectra of **57d**. a) Absorption (grey), fluorescence excitation (red) and fluorescence (black) spectra in chloroform; b) Fluorescence lifetime in chloroform. Excitation pulse (grey), decay (red) and mono-exponential deconvolution fit (black). Insert: Logarithmic decay; c) Fluorescence excitation (red) and fluorescence (black) spectra in PMMA; b) Fluorescence lifetime in PMMA. Excitation pulse (grey), decay (red) and mono-exponential deconvolution fit (black). Insert: Logarithmic decay.

Conclusion

5-(1-adamantyl)oligothiophenes **57a-d** were readily prepared by cross-coupling reactions. Whereas the homo-coupling products **59a-c** behave as pigments, mono-substitution with the 1-adamantyl moiety confers **57a-d** an excellent solubility in most organic solvents. These compounds, particularly the 5-(1-adamantyl)quaterthiophene **57d**, exhibit remarkable optical properties in solution and in solid PMMA like an increased Stokes' shift and high fluorescence quantum yields. This makes them interesting for applications in frequency converting systems. Focussing on the very fast fluorescence decay of 0.39 ns of **57d**, these properties may allow using this substance as a highly soluble fluorescent dye in high throughput optical signal processing units exceeding the benchmark of 1 GBit/s.

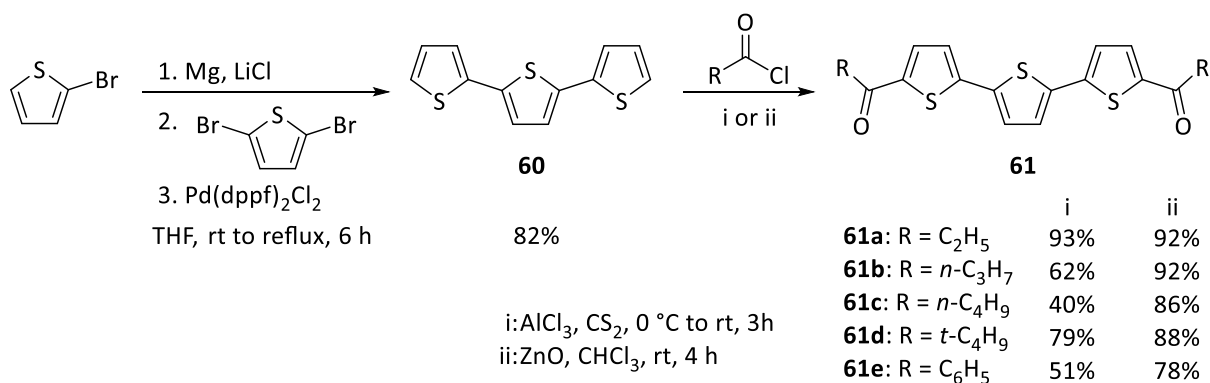
2.5.2 Alkyl and Aryl Substituted Oligothiophenes

2-Alkyloligothiophenes such as the 5-(1-adamantyl)quaterthiophene **57d** presented above exhibits high chemical stability and can be added to radical polymerization reactions without any sign of decomposition. However, long-term exposure to light, particularly to exciting wavelengths, leads to considerable photo bleaching. For application in optical data processing a high stability towards photons is essential for long-life components. Thus, the focus was laid on more electron deficient oligothiophenes. Terminal substitution with electron withdrawing moieties should not only increase the stability, moreover, variation of these groups offers a viable option for the spectral adaption, particularly to common light sources such as GaN-diodes with emission wavelengths in the region of 405 nm.

Electron withdrawing moieties cause a bathochromic shift of the absorption of oligothiophenes^[99]. To reach visible regions of more than 400 nm, the synthesis of less soluble quaterthiophenes can be avoided and replaced by the more readily accessible terthiophenes. A simple and efficient synthesis of terminal bisketo-2,2'-terthiophenes was targeted. The positions 3 and 4 were left unsubstituted for supporting molecular dynamics of the excited states. Furthermore, a rod-like shape causes less defects in the glassy structure of the polymer, preferably poly(methyl methacrylate) (PMMA) to realize minimal scattering of the guided light. Carbonyl derivatives such as the diacetyl terthiophene^[100] were sparingly investigated. Only the poorly soluble carboxylic acid and some esters were reported more detailed^[101].

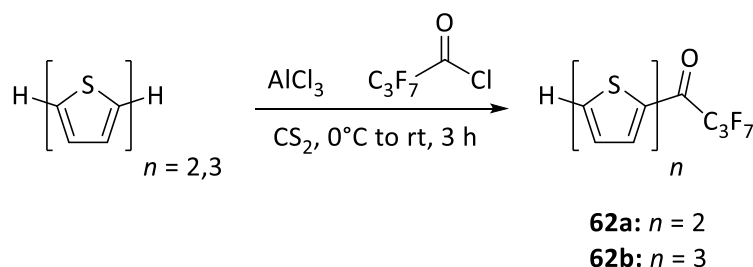
Synthesis was started with readily available mono- and dibromo thiophene to carry out a double *Kumada* coupling reaction, shown in Scheme 23. Using 0.2 mol% of Pd(dppf)Cl₂ as catalyst led to a very satisfying yield of 82%. The resulting terthiophene **60** was isolated and treated with acyl chlorides in *Friedel-Crafts* reactions to obtain the respective terminal bisketones **61a-e**. Two different conditions were applied. One was following a standard procedure using an excess of water-free aluminum chloride as Lewis acid in carbon disulphide.^[102] An alternative route applied simple solid zinc oxide in sub-stoichiometric amounts (0.25 equivalent per reactive center). The catalytic potency of zinc oxide is already described for few reactions^[103] however, in most cases activated species such as nanorods^[104], nanoparticles^[105] or hollow spheres^[106] had to be prepared previously or the method was

restricted to solvent free conditions^[107]. The electron rich terthiophene reacts using half an equivalent of low-cost plain powder of zinc oxide to obtain the (terthiophenediyl)bisketones **61a-e** in yields clearly exceeding those of the AlCl₃ approach. Further advantages of the ZnO-pathway are the application of more convenient solvents such as chloroform and the prevention of the formation of byproducts. The reduced activity of ZnO results only in product and starting material which can easily be recovered.



Scheme 23: Synthesis of ([2,2':5',2''-terthiophene]-5,5''-diyl)bisketones **61a-e** under two different conditions.

To further decrease the electron density in the chromophore extension with perfluoroalkylacyl chlorides^[108] was investigated. Using ZnO as Lewis acid led to no significant reaction. However, the reaction could be catalyzed with AlCl₃ in CS₂ but stopped at the stage of mono substitution due to the influence of the desactivating perfluoroketo group. The monosubstituted derivatives **62a-b** (Scheme 24) were obtained.



Scheme 24: Synthesis of bi- and terthienylheptafluorobutanone **62a-b**.

The bisketones **61a-e** form highly fluorescent yellow solutions in chloroform. Compound **61a** absorbs at 406.2 nm, the more electron donating substituents of **61b-c** cause a slight bathochromic shift to 409.4 nm and 410.2 nm for **61d**, respectively. The fluorescence spectra are stronger structured than the absorption spectra and an appreciable Stokes' shift is found for all derivatives. An extension of the conjugated system for the phenyl derivative **61e** causes a further shift to longer wavelengths to 422.4 nm in absorption and 510.4 nm in fluorescence, the large Stokes' shift remains nearly similar. The perfluoroketones **62a-b** also display a bathochromic shift of both, absorption and fluorescence. Dithiophene **62a** absorbs close to the visible region of light at 384.0 nm and exhibits its emission maximum at 447.7 nm. The fluorescence quantum yield of 0.62 is remarkably high for blue-emitting organic dyes^[109]. The terthiophene derivative **62b** appears intensively yellow with maxima of absorption at 432.2 nm and fluorescence at 528.8 nm, respectively.

Table 20: Ketoterthiophenes **61** and **62**. Spectroscopic measurements in chloroform.

Dye	% Yield	$\lambda_{\text{abs}}^{[a]}$	$\lambda_{\text{fluo}}^{[b]}$	$\epsilon^{[c]}$	$\Phi^{[d]}$	$\tau^{[e]}$	$\lambda_{\text{fluo}} - \lambda_{\text{abs}}^{[f]}$	$E_{\text{abs}} - E_{\text{fluo}}^{[g]}$
61a	92 (93) ^[h]	406.2	490.4	45 300	0.52	0.391	84.2	0.527
61b	92 (62) ^[h]	409.4	491.2	39 800	0.39	0.388	81.8	0.505
61c	86 (40) ^[h]	409.4	494.3	41 200	0.50	0.402	85.2	0.526
61d	88 (79) ^[h]	410.2	494.3	43 800	0.54	0.403	84.1	0.505
61e	78 (51) ^[h]	421.8	510.4 ^[i]	42 400	0.40	0.407	88.6	0.507
62a	30 ^[h]	384.0	447.7	23 300	0.62	1.453	63.7	0.459
62b	18 ^[h]	432.2	528.8	42 200	0.47	2.496	96.6	0.524

a) Absorption maximum in nm; b) Fluorescence maximum in nm; c) Molar absorptivity; d) Fluorescence quantum yield; e) Fluorescence lifetime in ns; f) Stokes' shift (referred to total maxima) in nm; g) Stokes' shift (referred to total maxima) in eV; h) Application of aluminum chloride; i) Second maximum (Irel = 0.97) for comparability.

The optical properties of terthiophendiyl bisketones **61a-e** are comparable to those of 5-alkylated quaterthiophenes. The remarkably short fluorescence lifetimes of about 0.4 ns observed for quaterthiophenes can also be found in all discussed derivatives of type **61**; see Table 20 and insert of Figure 44. Remarkably, the monoketone **62b** exhibits a five times prolonged fluorescence lifetime of 2.05 ns. As a consequence, the very short fluorescence lifetime of **61a-e** seems to be neither a characteristic property of the basic structure of the

terthiophene, nor a consequence of the attached perfluoroalkyls. Even alkyl substituents which mainly affect the π -electrons of the chromophore by induction strongly influence the fluorescence lifetimes of similar chromophores. Fluorescence lifetimes of more than 1 ns are also described for monoketo di- and terthiophenes.^[103b]

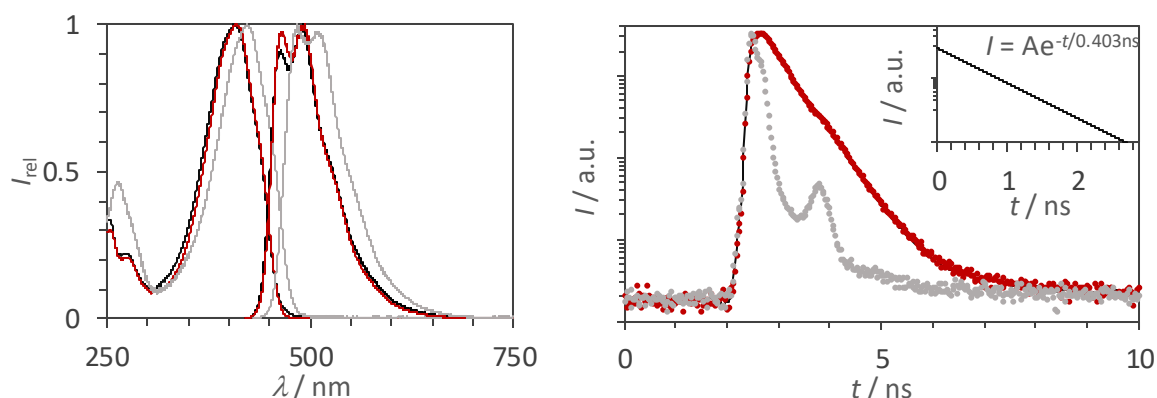


Figure 44: Left: Absorption (right) and fluorescence (left) spectra of **61a** (black), **61d** (red) and **61e** (grey) in chloroform; Right: Fluorescence lifetime of **61d** in chloroform. IRF (grey), fluorescence decay (red), deconvolutional fit (black). Insert: Exponential fit of **61d** resulting in a fluorescence lifetime of 0.403 ns.

The stability of bisketo-terthiophenes exceed that of the alkylated species. No sign of decomposition could be detected for the bisketon derivative **61d**, whereas alkylquaterthiophene **57d** exhibits decreasing fluorescence quantum yields after exposure to sunlight for several months. This difference is further confirmed by the energies (DFT B3LYP 6-311**G) of the respective HOMO^[110] with values of -6.022 eV for **61d** compared to -5.277 eV for **57d**. A difference of 0.745 eV represents higher stability towards photo oxidation in the order of about one magnitude.

Quantum chemical calculations (DFT B3LYP 6-311**G and CAM 6-311**G) propose a complete planar structure for both, ground state and excited state and is shown in Figure 45, left. HOMO and LUMO are shown in Figure 45, right. However, crystallographic data presented in Figure 46 exhibit slightly twisted rings with dihedral angles of 9.53 and 10.53°, respectively. These results agree with literature confirming the assumed mechanism which is made responsible for the increased Stokes' shift.^[96]

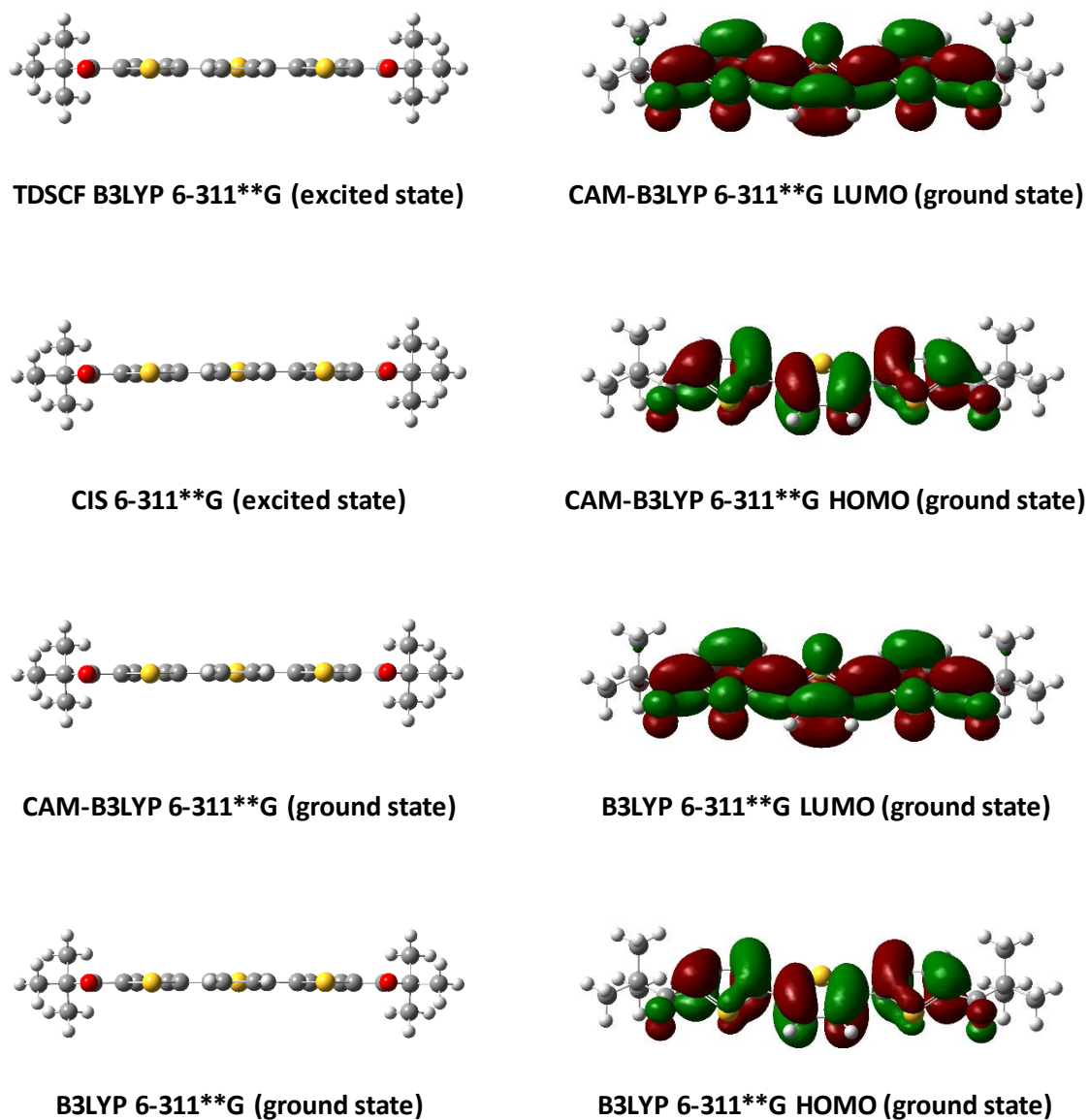


Figure 45: Quantumchemical calculations of **61d** (B3LYP 6-311**G and CAM-B3LYP 6-311**G). Left: Planar structure of the electronic ground state (bottom) and the electronically excited state (top) in either of the applied methods. Right: Calculated HOMO and LUMO of **61d**.

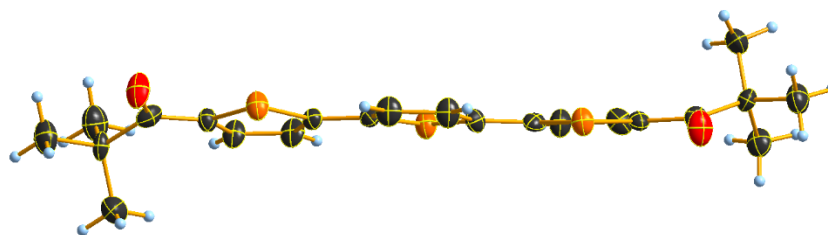


Figure 46: Crystal structure of terthiophenediyl bisketone **61d**. The thiophene units are twisted to each other with dihedral angles of about 10°.

The bisketones **61a-e** are of general interest for data processing due to their short fluorescence lifetimes, their high lightfastness and comparably high fluorescence quantum yields. Furthermore, they can be efficiently synthesised and chemically purified. Particularly dye **61d** is attractive for such applications because there are no enolisable hydrogen atoms inhibiting side reactions. The high solubility of all derivatives (increasing from **61a** to **61d**) enables easy processing of polymer fibers. The phenyl derivative **61e** is an alternative if more bathochromic spectra are required and proves the potential of the synthetic method to achieve arylated oligothiophenes.

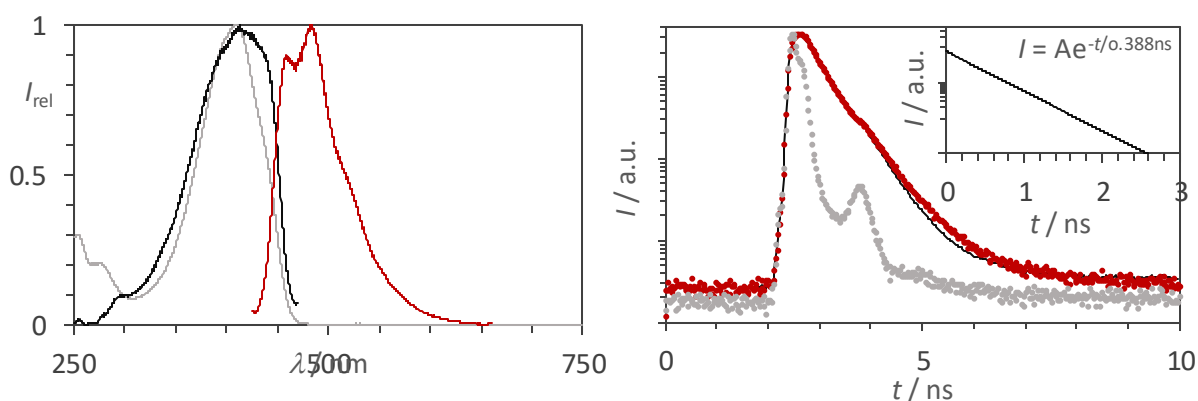


Figure 47: Left: Absorption (in chloroform, grey), fluorescence excitation (in PMMA, black) and fluorescence (in PMMA, red) spectra of **61d**; Right: Fluorescence lifetime of **61d** in PMMA fiber. IRF (grey), fluorescence decay (red), deconvolutional fit (black). Insert: Exponential fit of **61d** in PMMA resulting in a fluorescence lifetime of 0.388 ns.

PMMA is a preferred organic polymer for fibre optics because of its low absorptivity where there is even a spectral window with very low optical damping of yellow light. As a consequence, **61d** was incorporated into PMMA to study the optical properties. The chemical inertness of **61d** allows a dissolution in monomeric MMA and subsequent radical polymerisation without any measureable destructive effect to the dye. The fluorescence and fluorescence excitation spectra of **61d** in a PMMA fiber (Figure 48) are reported in Figure 47. A comparison of the fluorescence excitation of **61d** in PMMA with the absorption spectrum in solution indicates a bathochromic shift in the polymer and slightly diminishes the Stokes' shift compared with the liquid phase. This is attributed to limited dynamic processes in solid glass structures. However, there is still a very good spectral separation. The total width of the absorption spectrum determines the reabsorption and in both, solution and solid matrix, the baseline is reached at approximately the same values.



Figure 48: PMMA fluorescent optical fiber (FOF) with 35 ppm of **61d**.

The versatility of the ZnO-catalyzed Friedel-Crafts acylation enables simple access to various thiophene derivatives with selectively binding groups for bio marker applications. The small fluorescent lifetime of **61a-e** and **62a-b** also bears an additional advantage for bio imaging methods. Background emission caused by bio molecules can be repressed by exploiting the combination of small fluorescent lifetimes and comparably efficient quantum yields. The high intensity of the fluorescence of **61a-e** and **62a-b** in the first nanosecond dominates over most background interference. Vice versa, commonly used markers usually display average lifetimes of 3-4 ns and could be detected simultaneously in the period starting from a few nanoseconds after the excitation.

Conclusion

Terthiophene could efficiently be substituted by means of Friedel-Craft acylation for the preparation of appreciable chemically and photostable diketones. The reaction was performed under very simple conditions using sub-stoichiometric amounts of zinc oxide as catalytic Lewis acid. Starting from brominated thiophenes the presented compounds could be obtained in two steps in very good yields. The final materials are considerably fluorescent with quantum yields of about 0.50 and exhibit large Stokes' shifts. Their very short fluorescence lifetimes of about 0.4 ns remain persistent in a glassy matrix of poly(methyl methacrylate). This fast decay in combination with large Stokes' shifts and high fluorescence quantum yields make the dyes of special interest for GBit optical data processing such as in fiber optics.

3 Summary

Various fluorescent carboximides and oligothiophene derivatives were synthesized and analyzed in terms of their optical properties. Particularly the fluorescence lifetimes were investigated and compared to each other regarding applied physical correlations and equations. The validity of these concepts was partially confirmed. However, no comparison was possible across the frontiers of different classes of chromophores.

Studies on the fluorescence lifetime of linear perylene diimide multichromophores confirmed the concept of superelevation of the molecular attenuation coefficient caused by intramolecular exciton interactions on the example of dichromophore **9**. This in turn effects the fluorescence lifetime to decrease. The preparation of such dyads was partially successful. Poor solubility of higher oligomers such as **13** impedes both, good synthetic access and even adequate optical analysis due to aggregation. An approach to introduce solubilizing alkyl groups via the linker was prevented by competing reactions, mainly metal exchange. The obtained results agree with literature.

The better accessibility of smaller annulated arenes such as naphthalene dicarboximides enabled various options for substitution to obtain a series of 4-arylnaphthalimides. The main focus was on electron rich aryls to provide two physical features, intra-molecular dynamics and a high polarity enabling intra-molecular charge transfer. A remarkably high positive solvatochromism of fluorescence was found for some species such as **27** exceeding 150 nm. The absorption properties remained nearly unaffected by the applied solvent. Hence, high Stokes' shifts of more than 200 nm (1.5 eV) were observed for some derivatives such as **25-28**. The solvatochromism was evaluated according to the concepts of *Dimroth* and *Reichardt*, *Brooker*, *Kawski*, *Kamlet*, *Taft* and *Abboud* and *Catalán* with best results for the first approach. The results were compared to TICT-theory (twist induced charge transfer) and found to be subject to a comparable mechanism. However, the investigated 4-arylnaphthalimides exhibit much higher fluorescence quantum yields. Thus, an intermolecular planarization between the electron rich aryl moiety and the electron withdrawing naphthalimide group was proposed to be responsible for the large Stokes' shifts in combination with a pronounced intramolecular

charge transfer. This suggests the exact opposite of the TICT concept where orthogonalization is assumed. The lack of fluorescence in comparable sterically fixed orthogonal compounds such as the dimethylated 4-arylnaphthalimide **32** affirms this presumption. The theoretical concepts were attested with means of quantum chemical calculation which also suggest a planarization of the chromophore subunits in combination with a distinct charge transfer. This interplay of geometric and electronic effects results in highly fluorescent compounds such as **24** and **27** with easily adjustable emission spectra controlled by medium effects. This provides very large Stokes' shifts exceeding 200 nm (approx. 1.6 eV) being of interest for various applications such as for frequency converters, fluorescence optical fibers and highly tunable light sources.

In further investigations anthraceneimide was also substituted with electron rich functional groups. Amines appear to readily react with *N*-(tridecan-7yl)anthracene-1,9-dicarboximide **40**. Various representatives of simple amines were added to **40** and a sudden change of the color was observed. The amines form a σ -adduct with the anthraceneimide resulting in a brilliant color indicating for a single substance. Dilution or quenching causes the collapse of this adduct in some cases and starting material is recovered. In most approaches a *C-N* bond was established and *N*-substituted (10-amino)anthracene imides **41-47** were obtained. The products displayed moderate fluorescence and a pronounced lability towards exposure to sunlight. These compounds were analyzed by UV/Vis absorption and fluorescence spectroscopy, however further methods failed due to their high photo-sensitivity.

Anthracene-1,9-dicarboximide **40** exhibited homo coupling after treatment with potassium *tert*-butoxide at elevated temperatures under transition metal-free conditions. In contrast to *Sakamoto's* observations on naphthalimides the reaction was found to take place even without the addition of a second base such as 1,5-Diazabicyclo[4.3.0]non-5-ene (DBN). Interestingly, the formation of *cis* or *trans* derivatives could be influenced by the used solvent where toluene and xylene favored the *trans* derivative **49a** and DEE favored the respective *cis* derivative **49b**. The same reaction strategy was applied to *N*-(tridecan-7-yl)naphthalene-1,8-dicarboxylic imide **50** to obtain the corresponding perylene imide **1** in 43% yield. Amination of the naphthalimide in position 3 enabled analogue *C-N*-coupling to yield 5,13-bis(tridecan-7-yl)-8,16-dihydrodiisoquinolino[5,4-*ab*:5',4'-*hi*]phenazine-4,6,12,14(5*H*,13*H*)-tetraone (**52**) in 19%.

Investigation of the fluorescence lifetime of perylene diimide **1** revealed a strong dependence of the actually measured decay on the concentration. However, no such effects were observed for the fluorescence quantum yield in the respective concentrations. Opposed to quenching effects, an increase of the fluorescence quantum yield by a factor of up to 1.5 was found for higher concentrations. The experiments were expanded to well-known fluorophores such as fluorescein (**54**) or rhodamine B (**55**) and led to the same results. The linear correlation of attenuation and concentration given by *Lambert-Beer's* law was verified and no inconsistencies to this theory were found. Neither viscosity nor refractive indices were measurably influenced in the respective range of dilution. The results imply to not consider fluorescence lifetime for a constant as done in literature. Moreover, all equations regarding fluorescence lifetime that are presented in this work do not include concentration as an unknown quantity. Long-range interactions between the highly separated (up to 250 nm in average) fluorophores seem to be responsible for a temporal stabilization of the excited state. The emitted light wave is of macroscopic dimensions and thus, not localized to a single molecule. Analogously to Yagi-Uda antenna for UHF applications the excited molecule might interact with the surrounding molecules and result in a kind of stabilizing resonance which prolongs the lifetime of the excited state.

Not only concentration varies the fluorescence lifetime of chromophores. Environmental influences such as the refractive index mentioned above also have a strong impact. Polymers were found to display a weak but detectable auto-fluorescence. Even unmarked technical, aliphatic polymers such as polyethylene can be irradiated with light pulses and identified by distinct fluorescent decays. These decays exhibit multi-exponential behavior which can be used to ensure an unequivocal fingerprint of the time-resolved fluorescence. The high reliability even expands to distinguish between contaminated and mainly pure polymers. The method of using light enables sorting of recycling material by means of well-known technology in very high repetition frequencies. Cerium (IV) was found to be a universal probe found in most technical products. The wide distribution of cerium allows standardized procedures for the identification of polymers and draws fluorescence lifetime analysis into the focus of industrial plastic recycling solutions.

The implementation of fluorophores into polymers is generally interesting for opto-electronic applications. In optical slip rings a fluorescent dye is incorporated into a glassy polymer matrix, preferably poly(methyl methacrylate) (PMMA). Short lifetimes of the excited state enable high pulse frequencies and thus, high data transmission rates. In contrast to most fluorescent dyes with appreciable quantum yields, α - ω -oligothiophenes exhibit very short fluorescence lifetimes of about 1 ns. The poor solubility of higher oligomers with absorption maxima in the visible range ($n \geq 4$) was increased by organometallic substitution with 1-adamantyl moieties in position 5. The mono-alkylated derivatives display high solubility in the monomeric methyl methacrylate and (adamantyl)quaterthiophene **57d** was implemented into a PMMA fiber. The optical properties characterized by a high Stokes' shift and a short fluorescence lifetime of 0.4 ns match the requirements for data transmission in slip ring arrangements.

For better accessibility and higher long-term stability at the same time, the degree of oligomerization was decreased to 3. To shift the absorption maximum into the visible region where low-cost and fast light sources are available (GaN laser diodes with emission maxima at about 405 nm) the terthiophenes were terminally substituted with alkyl-keto groups. The reactions were realized in zinc oxide-mediated *Friedel-Crafts* acylations where the applied *Lewis'* acid led to higher yields compared to classic approaches such as with aluminum chloride. The obtained α , ω -bisketones **61a-e** display similar optical spectra compared to **57d** and also the short fluorescence lifetime of 0.4 ns remains unaltered. The considerably fluorescent terthiophenes **61a-e** exhibit fluorescence quantum yields of about 0.50 and large Stokes' shifts that avoid re-absorption within the fiber. Thus, *tert*-butyl derivative **61d** was incorporated into a PMMA fiber to be tested in prototype stage for high speed data processing with rates of more than 1 GBit s⁻¹.

4 Experimental Section

4.1 General Working Techniques

All reactions carried out under argon atmosphere were performed using *Schlenk* technique in flame-dried ($T > 300\text{ }^{\circ}\text{C}$) glassware applying medium vacuum of less than 10^{-2} mbar (1 Pa). Syringes for the transfer of anhydrous solvents or reagents were purged with argon prior to use. THF was continuously refluxed over sodium and freshly distilled from sodium benzophenone ketyl under nitrogen. All remaining solvents attributed “dry” were purchased in 98+% purity and dried and distilled according to standard procedures. Yields refer to isolated compounds estimated to be >98% pure as determined by ^1H NMR (27 $^{\circ}\text{C}$) and/or capillary GC. Chemical shifts are reported as δ -values in ppm relative to the solvent peak. NMR spectra were recorded in deuterated solvents (>99%). For the characterization of the observed signal multiplicities the following abbreviations were used: s (singlet), d (doublet), t (triplet), q (quartet), dd (doublet of a doublet), ddd (doublet of a doublet of a doublet), dt (doublet of triplet), tt (triplet of triplet), m (multiplet) and br (broad signal). Column chromatography was performed using silica (SiO_2) (0.040 – 0.063 mm or 0.63 – 0.200 mm particle size) from Merck and aluminum oxide (activity as indicated) from Merck. All reagents were obtained from commercial sources with > 95% purity and used without further purification if not indicated otherwise. Masses and quantities are given with 3 valid digits or less respecting the limitations of the accuracy of instruments. Fluorescence spectra were obtained by excitation at the respective absorption maximum (> 320 nm) if not noted otherwise. Fluorescence quantum yields were determined according to literature.^[111]

4.2 Analytical Methods and Instruments

IR-Spectra: Perkin Elmer Spektrum B XII FT-IR System

NMR spectroscopy: Varian Vnmrs 600 (600 MHz), Varian Mercury 200 (200 MHz)

UV/Vis-Spectra: Varian Cary 5000

Fluorescence spectra: Varian Cary Eclipse

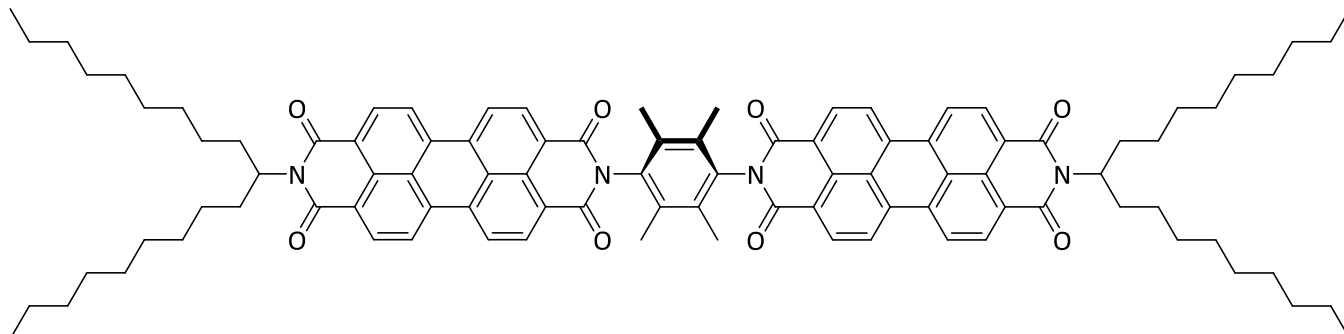
Fluorescence lifetimes: PicoQuant FluoTime 300, PicoQuant PicoHarp 300, PC-405 and PC-510 laser with 0.4 mW power and a puls frequency of 80 MHz; Edinburgh Analytical Instruments CD900, nF900 tungsten flashlight; NKT-Laser SuperK Extreme EXB-4 from NKT Photonics A/S, monochromator from Edinburgh Instruments Ltd., photomultiplier PMA-C 192-N-M and electronics PicoHarp 300 from PicoQuant GmbH. Fluorescence lifetimes were obtained by exponential fitting of the deconvoluted fluorescence decays with a resulting resolution of up to 8 ps;

Mass spectrometry: Finnigan MAT 95

Elemental analysis: Elementar vario EL, Elementar vario microcube.

Fluorescence quantum yields were determined according to literature.^[8001]

4.3.1 9,9'-(2,3,5,6-Tetramethyl-1,4-phenylene)bis(2-(nonadecan-10-yl)anthra[2,1,9-def:6,5,10-d'e'f']diisoquinoline-1,3,8,10(2H,9H)-tetraone) (9)



1,4-Diamino-2,3,5,6-tetramethylbenzene (**10**) (41.1 mg, 0.250 mmol), *N*-(nonadecan-10-yl)perylene-3,4-dicarboximide-9,10-dicarboxylic anhydride (**11b**) (164 mg, 0.250 mmol) and zinc acetate (6.9 mg, 0.038 mmol, 15 mol%) were treated with imidazole (approx. 2.0 g) and heated to 140 °C under nitrogen flow. The molten reaction mixture was stirred at that temperature for 5 h and quenched still hot with 25 mL of 2 M hydrochloric acid. The suspension was neutralized with potassium carbonate to a *pH*-value of 7 and filtrated. The residue was purified via threefold column chromatography on silica (eluents: 1st: chloroform, 3rd fraction; 2nd: chloroform/methanol 10:1, 1st fraction, 3rd: chloroform/methanol 40:1, 1st fraction) to obtain an intensively red solid.

Yield: 85 mg (0.059 mmol, 47%).

***R_f*-value (CHCl₃/MeOH 40:1):** 0.75.

m. p.: >250 °C.

¹H NMR (600 MHz, CDCl₃): δ = 8.76-8.67 (m, 16 H, CH_{aryl}), 5.20-5.16 (m, 2 H, NCH), 2.26-2.15 (m, 4 H, β -CH₂), 2.04 (s, 12 H, CH₃) 1.90-1.82 (m, 4 H, β -CH₂) 1.51-1.21 (m, 56 H, CH₂), 0.82 ppm (t, ³*J* = 7.2 Hz, 12 H, ω -CH₃).

UV/Vis (CHCl₃): λ_{\max} (*E_{rel}*) = 261.0, (0.40), 460.4 (0.20), 492.2 (0.54), 529.6 nm (1.00).

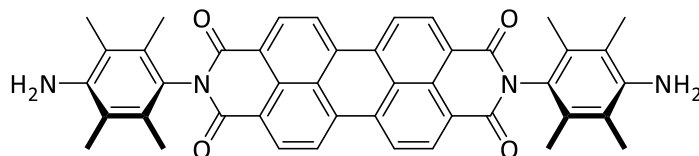
Fluorescence (CHCl₃, λ_{Exc} = 492.2 nm): λ_{\max} (*I_{rel}*) = 536.0 (1.00), 577.9 nm (0.41).

Fluorescence quantum yield (CHCl_3 , $\lambda_{\text{Ex}} = 492.2 \text{ nm}$, $E_{492.2 \text{ nm}/1 \text{ cm}} = 0.027$, reference: *N,N'*-Bis(tridecan-7-yl)perylene-3,4:9,10-tetracarboxylic bisimide with $\Phi = 1.00$): 0.99.

MS (FAB⁺): m/z (%) = 1444 (0.54) [$M+H^+$].

MS (MALDI): m/z = 1441.7 [$M-H^+$].

4.3.2 2,9-Bis(4-amino-2,3,5,6-tetramethylphenyl)anthra[2,1,9-def:6,5,10-d'e'f']diisoquinoline-1,3,8,10(2*H*,9*H*)-tetraone (12)



Perylene-3,4:9,10-tetracarboxylic anhydride (**5**) (1.00 g, 2.55 mmol), 1,4-diamino-2,3,5,6-tetramethylbenzene (**10**) (2.05 g, 12.7 mmol, 5 eq.) and zinc acetate were treated with imidazole (approx. 10 g) and heated to 140 °C under nitrogen flow. The molten reaction mixture was stirred at that temperature for 4 h and quenched still hot with 75 mL of 2 M hydrochloric acid. The resulting suspension was filtrated and washed with further 75 mL of 2 M hydrochloric acid. The residual solid was dried at 110 C for 1 d to obtain the dark red product.

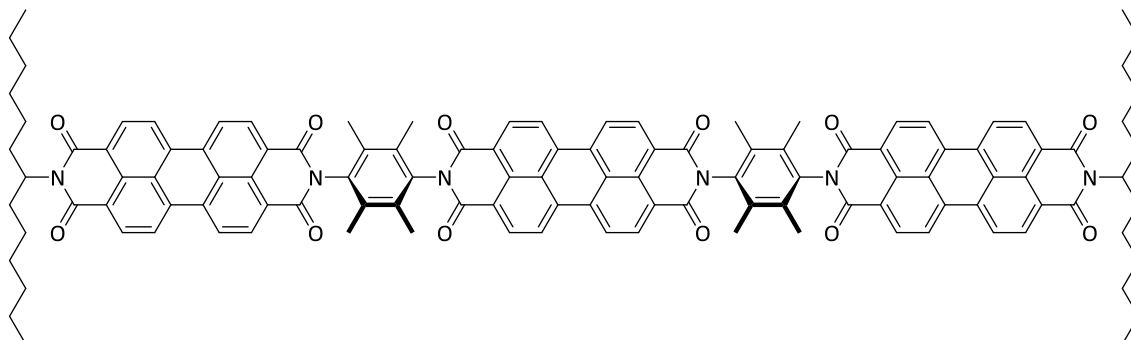
Yield: 1.67 g (2.44 mmol, 96%).

m. p.: >250 °C.

MS (70 eV, EI): m/z (%) = 684 (41) [M^+], 537 (17) [$M^+ - C_{10}H_{13}N$], 390 (51) [$M^+ - C_{20}H_{26}N_2$].

MS (MALDI): m/z = 683.7 [M^+], 537.0 [$M^+ - C_{10}H_{13}N$].

4.3.3 9,9'-((1,3,8,10-Tetraoxo-1,3,8,10-tetrahydroanthra[2,1,9-def:6,5,10-d'e'f']diisoquinoline-2,9-diyl)bis(2,3,5,6-tetramethyl-4,1-phenylene))bis(2-(tridecan-7-yl)anthra[2,1,9-def:6,5,10-d'e'f']diisoquinoline-1,3,8,10(2H,9H)-tetraone) (13)



N,N'-Bis-(4-amino-2,3,4,5-tetramethylphenyl)perylene-3,4:9,10-tetracarboxylic imide (**12**) (20.4 mg, 0.0296 mmol) and *N,N'*-bis(tridecan-7-yl)perylene-3,4-dicarboximide-9,10-dicarboxylic anhydride (**11a**) (84.3 mg, 0.147 mmol, 5 eq.) were dissolved in 0.5 mL of quinoline and stirred at 220 °C for 6 h. The reaction mixture was quenched with 15 mL of half concentrated hydrochloric acid and filtrated. The residue was dried at 110 °C overnight and purified via repeated column chromatography (silica, chloroform/methanol 7:1). The 1st fraction was collected each time to obtain a red solid.

Yield: 3.7 mg (0.0021 mmol, 7%).

***R_f*-value (CHCl₃/MeOH 7:1):** 0.60.

m. p.: >250 °C.

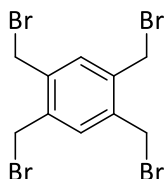
UV/Vis (CHCl₃): λ_{\max} (E_{rel}) = 261.4 (0.66), 490.8 (0.62), 527.2 nm (1.00), 589.0 (0.09).

UV/Vis (EtOAc): λ_{\max} (E_{rel}) = 483.8 (0.63), 519.0 nm (1.00).

Fluorescence (CHCl₃, λ_{Exc} = 490.8 nm): λ_{\max} (I_{rel}) = 534.8 (1.00), 577.6 nm (0.50).

Fluorescence quantum yield (CHCl₃, λ_{Ex} = 490.8 nm, $E_{490.8 \text{ nm}/1 \text{ cm}}$ = 0.122, reference: *N,N'*-Bis(tridecan-7-yl)perylene-3,4:9,10-tetracarboxylic bisimide with Φ = 1.00): 0.86.

MS (MALDI): m/z = 1794 [$M-H^+$].

4.3.4 1,2,4,5-Tetrakis(bromomethyl)benzene (15)

N-Bromosuccinimide (71.2 g, 400 mmol, 4 eq.) was dissolved in 300 mL of dichloromethane. After addition of 1,2,4,5-tetramethylbenzene (**14**) (13.4 g, 100 mmol), the reaction mixture was stirred at 50 °C under reflux and exposed to UV-radiation (254 nm, 366 nm, 3 W each) for 22 h. Subsequently, the reaction mixture was filtrated and washed with 200 mL of dichloromethane. The residue was treated with 150 mL of methanol and stirred at room temperature overnight. After further filtration the residue was collected and dried at 80 °C for 1 d. The colorless product was obtained as powder.

Yield: 20.7 g (45.8 mmol, 46%).

m. p.: 162 °C.

IR (ATR): $\tilde{\nu}$ = 3020, 2974, 1503, 1453, 1443, 1435, 1306, 1229, 1208 (s), 1085, 909, 898, 797 cm^{-1} .

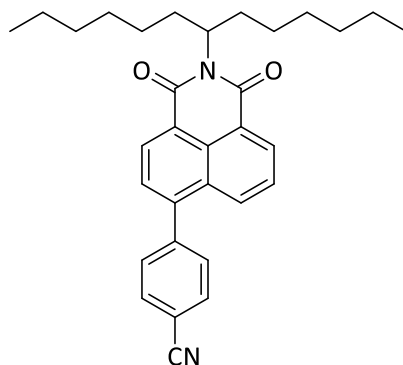
$^1\text{H NMR}$ (400 MHz, CDCl_3): δ = 7.37 (s, 2 H, CH_{aryl}), 4.69 ppm (s, 8 H, CH_2).

MS (70 eV, EI): m/z (%) = 450 (6) [M^+], 369 (100) [$M^+ - \text{Br}$], 290 (24) [$M^+ - 2 \text{ Br}$], 211 (37) [$M^+ - 3 \text{ Br}$], 130 (31) [$M^+ - 4 \text{ Br}$].

HRMS (EI, $\text{C}_{10}\text{H}_{10}\text{Br}_4$): m/z = calc. 445.7516, found 445.7519, Δ = +0.3 mmu.

Elemental analysis $\text{C}_{10}\text{H}_{10}\text{Br}_4$ (449.8 g mol^{-1}): calc. C: 26.70, H: 2.24, Br: 71.06;
found C: 26.88, H: 2.23, Br: 70.35.

4.4.1.1 6-(4-Cyanophenyl)-2-(tridecan-7-yl)-1H-benzo[de]isoquinoline-1,3(2H)-dione (30)



A dry argon flushed *Schlenk*-flask was charged with potassium hexacyanidoferrate(II) ($K_4Fe(CN)_6$, 128 mg, 0.348 mmol, 2.0 equiv.), potassium carbonate (K_2CO_3 , 72.1 mg, 0.522 mmol, 3.0 equiv.) and [1,1'-bis(diphenylphosphino)ferrocene]dichloro-palladium(II) ($Pd(dppf)Cl_2$, 12.7 mg, 0.0174 mmol, 10 mol%). A solution of 2-(tridecan-7-yl)-6-(4-iodophenyl)-1H-benzo-[de]isoquinoline-1,3(2H)-dione (**33**) (101 mg, 0.174 mmol) in 1.7 mL of dry *N,N*-dimethylformamide was added at room temperature under argon. The reaction mixture was stirred at 100 °C for 4 h, allowed to cool down and the solvent was removed under reduced pressure. The crude residue was treated with 15 mL of sat. aq. NH_4Cl solution and extracted with chloroform (3 x 15 mL). Purification by column chromatography (silica, *iso*-hexane/ $CHCl_3$ = 1:1) obtained compound **30** as bright yellow oil.

Yield: 54.9 mg (0.114 mmol, 66%).

R_f -value (*iso*-hexane/ $CHCl_3$ 1:1): 0.40.

IR (ATR): $\tilde{\nu}$ = 2923, 2855, 1699, 1656, 1588, 1465, 1397, 1349, 1327, 1238, 1179, 1103, 844, 784, 759 cm^{-1} .

1H NMR (600 MHz, $CDCl_3$): δ = 8.71-8.60 (br s, 2 H), 8.36 (dd, $^3J = 8.5$ Hz, $^4J = 1.0$ Hz, 1 H), 7.89 (d, $^3J = 8.4$ Hz, 2 H), 7.78 (d, $^3J = 7.5$ Hz, 1 H), 7.77-7.73 (m, 1 H), 7.67 (d, $^3J = 8.4$ Hz, 2 H), 5.23-5.18 (m, 1 H, NCH), 2.30-2.23 (m, 2 H, β - CH_2), 1.89-1.82 (m, 2 H, β - CH_2), 1.37-1.20 (m, 16 H, 8 x CH_2), 0.84 ppm (t, $^3J = 7.1$ Hz, 6 H).

^{13}C NMR (100 MHz, CDCl_3): δ = 165.67, 165.49, 164.58, 164.41, 146.08, 140.64, 138.49, 132.32, 131.81, 131.40, 131.02, 130.70, 130.08, 129.10, 128.02, 127.56, 127.12, 123.83, 123.10, 122.77, 122.05, 54.70, 32.60, 31.94, 29.41, 27.09, 22.76, 14.21 ppm.

UV/Vis (CHCl_3): λ_{max} (ϵ) = 366.4 nm (23700).

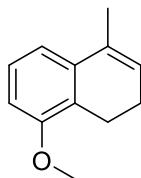
Fluorescence (CHCl_3): λ_{max} = 447.4 nm.

Fluorescence quantum yield (CHCl_3 , λ_{Ex} = 366.4 nm, $E_{366.4 \text{ nm}/1 \text{ cm}}$ = 0.073, reference: *N,N'*-Bis(tridecan-7-yl)perylene-3,4:9,10-tetracarboxylic bisimide with $\Phi = 1.00$): 0.54.

MS (70 eV, EI): m/z (%) = 480 (2) [M^+], 299 (17).

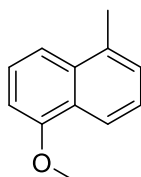
HRMS (EI, $\text{C}_{32}\text{H}_{36}\text{N}_2\text{O}_2$): m/z = calc. 480.2777, found 480.2773, Δ = -0.4 mmu.

4.4.1.2 8-Methoxy-4-methyl-1,2-dihydronaphthalene (precursor of 28)



A solution of 5-methoxy-1,1-dimethyl-1,2,3,4-tetrahydronaphthalene (1.27 g, 6.61 mmol) in 7 mL of chloroform was treated with triethylamine (735 mg, 1.01 mL, 727 mmol, 1.1 eq.) and 4-toluenesulfonyl chloride (1.39 g, 7.27 mmol, 1.1 eq.) at room temperature. The reaction mixture was stirred at 65 °C for 2 h. After cooling down to room temperature 10 mL of water were added and stirred for 10 min. The organic layer was separated from the aqueous layer which was further extracted with chloroform (2 x 10 mL). The combined organic layers were washed with saturated sodium carbonate solution (2 x 15 mL) and dried over magnesium sulfate. The crude product was obtained after evaporation of the volatiles and directly converted in the next reaction.

4.4.1.3 1-Methoxy-5-methylnaphthalene (precursor of 28)



Crude 8-methoxy-4-methyl-1,2-dihydronaphthalene (6.61 mmol) was dissolved in 7 mL of toluene and 2,3,5,6-tetrachlorocyclohexa-2,5-diene-1,4-dione (24.4 g, 9.92 mmol, 1.5 eq.) was added at room temperature. Subsequently, the reaction mixture was stirred at 130 °C for 2 h, cooled to room temperature and treated with 20 mL of water. The organic layer was separated and the aqueous layer was extracted with chloroform (2 x 30 mL). The combined organic layers were washed with water (2 x 50 mL), dried over magnesium sulfate and evaporated. The residual oil was purified via column chromatography (silica, *iso*-hexane/ethyl acetate 10:1) to obtain a colorless oil in the first fraction which crystallizes within several hours.

Yield: 393 mg (2.28 mmol, 35% after 2 steps).

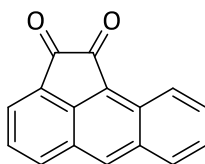
***R_f*-value (*iso*-hexane/EtOAc 10:1):** 0.30.

¹H NMR (400 MHz, CD₂Cl₂): δ = 8.12 (dd, ³*J* = 7.2 Hz, ⁴*J* = 2.6 Hz, 1 H), 7.58 (d, ³*J* = 8.5 Hz, 1 H), 7.44 (dd, ³*J* = 8.5 Hz, ³*J* = 7.7 Hz, 1 H), 7.38-7.32 (m, 2 H), 6.87 (d, ³*J* = 7.6 Hz, 1 H), 4.00 (s, 3 H, OCH₃), 2.67 ppm (s, 3 H, CH₃).

¹³C NMR (100 MHz, CDCl₃): δ = 155.9, 134.0, 133.6, 127.1, 125.6, 125.6, 124.7, 120.0, 116.3, 103.7, 55.5, 19.5 ppm.

MS (70 eV, EI): *m/z* (%) = 172 (100) [*M*⁺], 157 (32) [*M*⁺ - CH₃], 129 (34).

HRMS (EI, C₁₂H₁₂O): *m/z* = calc. 172.0888, found 172.0877, Δ = -1.1 mmu.

4.4.2.1 Aceanthrylene-1,2-dione (**38**)

Anthracene (**37**) (10 g, 56.1 mmol) is dissolved in 75 mL of carbon disulfide and cooled to 0 °C. Under argon atmosphere oxalyl chloride (25.0 mL, 37.0 g, 291 mmol, 5.2 eq.) is added. Subsequently, aluminum chloride (7.48 g, 56.1 mmol, 1 eq.) is added and a dark, viscous mass forms. The reaction mixture is stirred at 0 °C for 2 h and then diluted with further 75 mL of carbon disulfide. Again aluminum chloride (7.48 g, 56.1 mmol, 1 eq.) is added and stirred at room temperature for further 24 h. After addition of 200 mL of 2 M hydrochloric acid the carbon disulfide is removed at 60 °C at atmosphere pressure. The residual suspension is filtrated, washed with water and treated with a 3% potassium carbonate solution (2 x stirred at 70 °C for 30 minutes each). After filtration a yellow to orange solid is obtained.

Yield: 8.95 g (38.5 mmol, 69%).

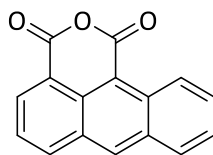
m. p.: 223 °C.

IR (ATR): $\tilde{\nu}$ = 1729, 1697 (s), 1573, 1085, 751 (s), 740 cm^{-1} .

^1H NMR (400 MHz, DMSO): δ = 9.81 (s, 1 H), 8.96 (d, 3J = 8.0 Hz, 1 H), 8.51 (d, 3J = 7.8 Hz, 1 H), 8.38 (d, 3J = 8.1 Hz, 1 H), 8.05 (d, 3J = 7.8 Hz, 1 H), 7.90 (t, 3J = 8.0 Hz, 1 H), 7.84 (t, 3J = 8.0 Hz, 1 H), 7.75 ppm (d, 3J = 7.8 Hz, 1 H).

^{13}C NMR (100 MHz, CDCl_3): δ = 188.38, 187.52, 145.60, 124.03, 132.34, 130.52, 129.97, 128.12, 127.90, 127.58, 127.28, 126.46, 123.47, 122.91, 121.39 ppm.

MS (70 eV, EI): m/z (%) = 232 (49) [M^+], 204 (93) [$M^+ - \text{CO}$], 176 (100) [$M^+ - \text{C}_2\text{O}_2$].

4.4.2.2 1*H*,3*H*-Dibenzo[*de,h*]isochromene-1,3-dione (39)

Aceanthrylene-1,2-dione (**38**) (8.13 g, 35.0 mmol) is dissolved in 175 mL of dioxane and treated with 50 mL of a 2 M sodium hydroxide solution. Subsequently, hydrogen peroxide 30% (40.8 mL, 45.3 g, 400 mmol) is added dropwise to the stirred reaction mixture over a period of 15 min. The reaction is quenched with 175 mL of water and treated with 350 mL of 2 M sulfuric acid and stirred overnight. The suspension is filtrated and the residue is washed with 2 M sulfuric acid. The solid is dissolved in 1 L of 3 M potassium hydroxide and the solution is filtrated. The filtrate is acidified with concentrated hydrochloric acid until no further precipitation occurs. The precipitate is collected by filtration to obtain an orange solid.

Yield: 7.17 g (28.9 mmol, 83%).

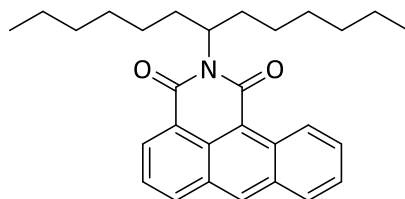
m. p.: 281 °C.

¹H NMR (400 MHz, DMSO): δ = 9.71 (d, ³*J* = 11.8 Hz, 1 H), 8.97 (s, 1 H), 8.76 (d, ³*J* = 11.8 Hz, 1 H), 8.47 (d, ³*J* = 8.2 Hz, 1 H), 8.18 (d, ³*J* = 8.2 Hz, 1 H), 7.92 (m, 1 H), 7.78 (m, 1 H), 7.72 ppm (m, 1 H).

¹³C NMR (100 MHz, CDCl₃): δ = 161.32, 160.75, 138.91, 137.22, 135.69, 133.34, 132.71, 132.33, 131.10, 130.94, 129.06, 127.34, 126.56, 125.53, 119.29, 111.85 ppm.

MS (70 eV, EI): *m/z* (%) = 248 (100) [*M*⁺], 204 (72) [*M*⁺ – CO₂], 176 (70) [*M*⁺ – C₂O₃].

HRMS (EI, C₁₆H₈O₃): *m/z* = calc. 248.0473, found 248.0513, Δ = +4.0 mmu.

4.4.2.3 2-(Tridecan-7-yl)-1*H*-dibenzo[*de,h*]isoquinoline-1,3(2*H*)-dione (40)

1*H*,3*H*-Dibenzo[*de,h*]isochromene-1,3-dione (**39**) (2.48 g, 10.0 mmol), zinc acetate (367 mg, 2.00 mmol, 20 mol%) and imidazole (20.0 g) are placed under argon and UV-exclusion. 7-Aminotridecane (3.99 g, 20.0 mmol, 2 eq.) is added the the reaction mixture is stirred at 140 °C for 4 h. The reaction is quenched with 300 mL of half concentrated hydrochloric acid and extracted with chloroform (3 x 200 mL). The solvent is removed and the residue is purified via column chromatography (silica, chloroform) under light exclusion to obtain a yellow solid.

Yield: 3.72 mg (8.66 mmol, 87%).

***R_f*-value (CHCl₃):** 0.90.

m. p.: 247 °C.

¹H NMR (400 MHz, CDCl₃): δ = 9.99 (d, ³*J* = 9.3 Hz, 1 H), 8.85 (s, 1 H), 8.75 (m, 1 H), 8.38-8.35 (m, 1 H), 8.14 (dd, ³*J* = 8.4 Hz, ⁴*J* = 1.3 Hz, 1 H), 7.88-7.77 (m, 1 H), 7.75 (dd, ³*J* = 8.3 Hz, ⁴*J* = 7.0 Hz, 1 H), 7.67-7.62 (m, 1 H), 5.29 (m, 1 H, CHN), 2.33-2.26 (m, 2 H, β -CH₂), 1.93-1.87 (m, 2 H, β -CH₂), 1.39-1.19 (m, 16 H, CH₂), 0.81 ppm (t, ³*J* = 7.1 Hz, 6 H, CH₃).

¹³C NMR (100 MHz, CDCl₃): δ = 134.60, 132.61, 131.03, 129.71, 128.82, 128.56, 127.01, 126.37, 125.51, 77.19, 76.98, 76.77, 32.56, 29.25, 26.99, 22.56, 14.01 ppm.

UV/Vis (CHCl₃): λ_{\max} (ϵ) = 435.2 nm (1200).

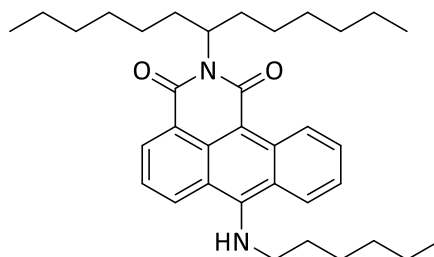
Fluorescence (CHCl₃): λ_{\max} (*I*_{rel}) = 482.5 (1.00), 512.8 nm (0.90).

MS (70 eV, EI): *m/z* (%) = 429 (15) [*M*⁺], 344 (3) [*M*⁺ - C₆H₁₃], 247 () [*M*⁺ - C₁₃H₂₆].

HRMS (EI, C₂₉H₃₅NO₂): *m/z* = calc. 429.2668, found 429.2661, Δ = -0.7 mmu.

Elemental analysis C₂₉H₃₅NO₂ (429.6 g mol⁻¹): calc. C: 81.08, H: 8.21, N: 3.26;
found C: 80.93, H: 7.90, N: 3.37.

4.4.2.4 7-(Hexylamino)-2-(tridecan-7-yl)-1H-dibenzo[de,h]isoquinoline-1,3(2H)-dione (41)



2-(Tridecan-7-yl)-1H-dibenzo[de,h]isoquinoline-1,3(2H)-dione (**40**) (43 mg, 0.10 mmol) was dissolved in 1-Aminohexane (1.5 mL, 11 mmol). The reaction took place under light exclusion at room temperature and without solvent or stirring. After 24 h the reaction was stopped by removing the excessive amine in medium vacuum. The crude product was purified via column chromatography (silica, chloroform) to obtain a red solid.

Yield: 26 mg (0.049 mmol, 49%).

R_f-value (CHCl₃): 0.45.

¹H NMR (400 MHz, CDCl₃): δ = 10.10-9.90 (m, 1 H), 8.85-8.45 (m, 2 H), 8.25-8.07 (m, 1 H), 7.88-7.48 (m, 3 H), 5.33-5.26 (m, 1 H, CHN), 2.40-2.15 (m, 2 H, β -CH₂), 2.00-1.76 (m, 2 H, β -CH₂), 1.83-1.70 (m, 2 H, CH₂, NCH₂), 1.45-1.14 (m, 24 H), 0.88-0.84 (m, 3 H, CH₃) 0.80 ppm (t, ³J = 7.7 Hz, 6 H, CH₃).

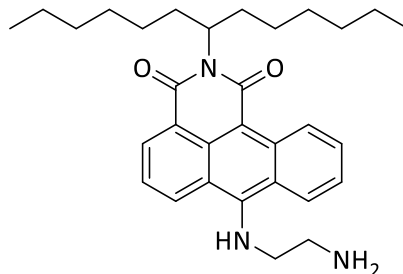
UV/Vis (CHCl₃): λ_{max} (E_{rel}) = 360.6 (0.26), 380.4 (0.39), 445.0 (0.61), 469.0 (0.81), 515.4 nm (1.00).

Fluorescence (CHCl₃): λ_{max} = 614.0 nm.

Fluorescence quantum yield (CHCl₃, λ_{Ex} = 515.4 nm, $E_{515.4 \text{ nm}/1 \text{ cm}}$ = 0.347, reference: *N,N'*-Bis(tridecan-7-yl)perylene-3,4:9,10-tetracarboxylic bisimide with Φ = 1.00): 0.11.

MS (70 eV, EI): m/z (%) = 528 (93) [M^+], 346 (100) [$M^+ - C_{13}H_{26}$], 275 (20).

HRMS (EI, C₃₅H₃₄N₂O₂): m/z = calc. 528.3716, found 528.3727, Δ = +1.1 mmu.

4.4.2.5 7-((2-Aminoethyl)amino)-2-(tridecan-7-yl)-1H-dibenzo[de,h]isoquinoline-1,3(2H)-dione (42)

2-(Tridecan-7-yl)-1H-dibenzo[de,h]isoquinoline-1,3(2H)-dione (**40**) (43 mg, 0.10 mmol) was dissolved in 1,2-diaminoethane (1.5 mL, 23 mmol). The reaction took place under light exclusion at room temperature and without solvent or stirring. After 4 d the reaction was stopped by removing the excessive amine in medium vacuum. The crude product was purified via column chromatography (silica, chloroform) to obtain a violet solid.

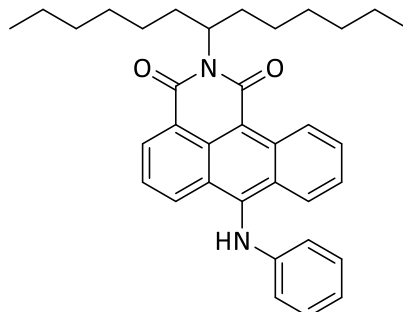
Yield: 8.1 mg (0.017 mmol, 17%).

R_f-value (CHCl₃): 0.30.

UV/Vis (CHCl₃): λ_{max} = 509.4 nm.

Fluorescence (CHCl₃): λ_{max} = 583.1 nm.

MS (70 eV, EI): m/z (%) = 487 (8) [M^+].

4.4.2.6 7-(Phenylamino)-2-(tridecan-7-yl)-1*H*-dibenzo[*de,h*]isoquinoline-1,3(2*H*)-dione (43)

2-(Tridecan-7-yl)-1*H*-dibenzo[*de,h*]isoquinoline-1,3(2*H*)-dione (**40**) (43 mg, 0.10 mmol) was dissolved in aniline (1.5 mL, 16 mmol). The reaction took place under light exclusion at room temperature and without solvent or stirring. After 6 d the reaction was stopped by removing the excessive amine in medium vacuum. The crude product was purified via column chromatography (silica, chloroform) to obtain a red solid.

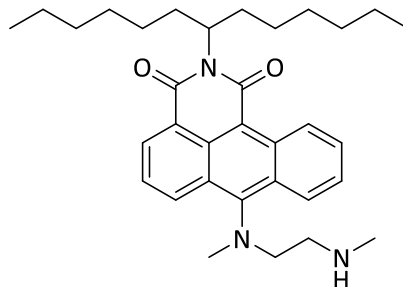
Yield: 4 mg (0.008 mmol, 8%).

***R_F*-value (CHCl₃):** 0.50.

UV/Vis (CHCl₃): λ_{max} = 343.2 nm.

MS (70 eV, EI): m/z (%) = 520 (55) [M^+], 328 (100) [$M^+ - C_{13}H_{26}$].

4.4.2.7 7-(Methyl(2-(methylamino)ethyl)amino)-2-(tridecan-7-yl)-1H-dibenzo[de,h]isoquinoline-1,3(2H)-dione (44)



2-(Tridecan-7-yl)-1H-dibenzo[de,h]isoquinoline-1,3(2H)-dione (**40**) (43 mg, 0.10 mmol) was dissolved in *N,N'*-dimethyl-1,2-diaminoethane (1.5 mL, 14 mmol). The reaction took place under light exclusion at room temperature and without solvent or stirring. After 4 d the reaction was stopped by removing the excessive amine in medium vacuum. The crude product was purified via column chromatography (silica, chloroform) to obtain a red solid.

Yield: 3 mg (0.006 mmol, 6%).

***R_f*-value (CHCl₃):** 0.40.

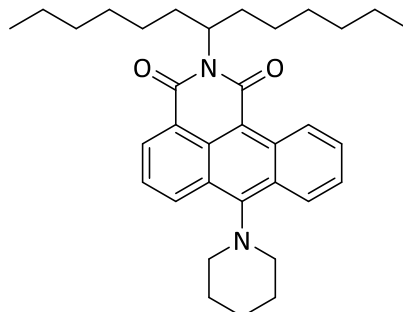
UV/Vis (CHCl₃): λ_{max} (E_{rel}) = 364.0 (0.31), 383.4 (0.64), 445.0 (0.61), 470.0 nm (1.00).

Fluorescence (CHCl₃): λ_{max} (I_{rel}) = 488.0 (0.60), 518.4 nm (1.00).

Fluorescence quantum yield (CHCl₃, λ_{Ex} = 470.0 nm, $E_{470.0 \text{ nm}/1 \text{ cm}}$ = 0.223, reference: *N,N'*-Bis(tridecan-7-yl)perylene-3,4:9,10-tetracarboxylic bisimide with $\Phi = 1.00$): 0.02.

MS (70 eV, EI): m/z (%) = 515 (100) [M^+], 332 (95) [$M^+ - \text{C}_{13}\text{H}_{27}$], 236 (83).

4.4.2.8 7-(Piperidin-1-yl)-2-(tridecan-7-yl)-1*H*-dibenzo[*de,h*]isoquinoline-1,3(2*H*)-dione (45)



2-(Tridecan-7-yl)-1*H*-dibenzo[*de,h*]isoquinoline-1,3(2*H*)-dione (**40**) (43 mg, 0.10 mmol) was dissolved in piperidine (1.5 mL, 15 mmol). The reaction took place under light exclusion at room temperature and without solvent or stirring. After 6 d the reaction was stopped by removing the excessive amine in medium vacuum. The crude product was purified via column chromatography (silica, *iso*-hexane/ethyl acetate 9:1) to obtain a red solid.

Yield: 11 mg (0.021 mmol, 21%).

***R_F*-value (*iso*-hexane/EtOAc 9:1):** 0.35.

UV/Vis (CHCl₃): λ_{max} (E_{rel}) = 364.0 (0.29), 382.4 (0.57), 445.0 (0.61), 486.2 nm (1.00).

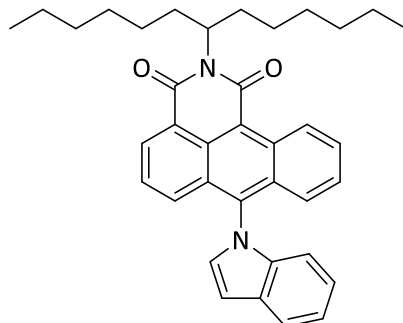
Fluorescence (CHCl₃): λ_{max} = 591.2 nm.

Fluorescence quantum yield (CHCl₃, λ_{Ex} = 486.2 nm, $E_{486.2 \text{ nm}/1 \text{ cm}}$ = 0.228, standard: *N,N'*-Bis(tridecan-7-yl)perylene-3,4:9,10-tetracarboxylic bisimide with $\Phi = 1.00$): 0.04.

MS (70 eV, EI): m/z (%) = 512 (9) [M^+], 330 (7) [$M^+ - C_{13}H_{26}$], 236 (100).

HRMS (EI, C₃₄H₄₄N₂O₂): m/z = calc. 512.3403, found 512.3383, Δ = -2.0 mmu.

4.4.2.9 7-(1*H*-Indol-1-yl)-2-(tridecan-7-yl)-1*H*-dibenzo[*de,h*]isoquinoline-1,3(2*H*)-dione (46)



Potassium-*tert*-butoxide (1.37 g, 13.1 mmol, 10 eq.) was sublimed and placed in a 2-neck round bottom flask under argon atmosphere. Toluene (2.0 mL) was added through a septum and the suspension was heated to 120 °C under reflux. Once the temperature was reached, a solution of *N*-(tridecan-7-yl)anthracene-1,9-dicarboximide (**40**) and indole (771 mg, 6.58 mmol, 5 eq.) in 3 mL of toluene was added under strict exclusion of air and moisture. The reaction mixture was stirred at 120 °C for 1.5 h and subsequently quenched by addition of 10 mL of 2 M hydrochloric acid. After cooling down to room temperature the layers were separated and the aqueous one was extracted with chloroform (3 x 30 mL). The combined organic layers were dried over magnesium sulfate and evaporated. The crude product was purified via threefold column chromatography on silica (eluents: 1st: chloroform, 2nd fraction; 2nd: chloroform/methanol 7:1, 2nd fraction, 3rd: chloroform, 2nd fraction). The obtained orange solid was again purified by chromatography on aluminum oxide with chloroform. The 2nd fraction turned out to be pure product and formed orange crystals after evaporation of the solvent.

Yield: 324 mg (0.595 mmol, 45%).

***R_f*-value (CHCl₃):** 0.40.

m. p.: >250 °C.

IR (ATR): $\tilde{\nu}$ = 2921, 2853, 1782 (s), 1628 (s), 1561 (s), 1538, 1455, 1424, 1406, 1342, 1218 cm⁻¹.

^1H NMR (400 MHz, CDCl_3): δ = 10.08 (d, 3J = 8.7 Hz, 1 H, H-8), 8.81-8.67 (m, 2 H, H-3', H-2), 8.28 (d, 3J = 8.7 Hz, 1 H, H-4), 8.08 (d, 3J = 8.7 Hz, 1 H, H-5), 7.80 (t, 3J = 8.1 Hz, 1 H, H-7), 7.61 (t, 3J = 8.3 Hz, 1 H, H-6'), 7.55 (dd, 3J = 7.0 Hz, 3J = 8.6 Hz, 1 H, H-3), 7.47-7.42 (m, 2 H, H-6, H-2'), 7.36-7.32 (m, 1 H, H-5'), 7.12-7.05 (m, 2 H, H-4', H-7'), 5.34 (m, 1 H, NCH), 2.42-2.28 (m, 2 H, β - CH_2), 1.97-1.88 (m, 2 H, β - CH_2), 1.28-1.18 (m, 16 H, CH_2), 0.82 ppm (t, 3J = 6.9 Hz, 6 H, CH_3).

^{13}C NMR (100 MHz, CDCl_3): δ = 140.59, 135.80, 134.35, 133.54, 132.68, 130.50, 129.29, 128.94, 128.67, 128.46, 126.90, 125.95, 125.48, 124.96, 123.05, 120.78, 119.96, 112.59, 11.45, 32.62, 31.76, 29.28, 27.00, 22.57, 14.01 ppm.

UV/Vis (CHCl_3): λ_{max} (ϵ) = 271.2 (56600), 452.8 (8200), 651.0 nm (3600).

Fluorescence (CHCl_3): λ_{max} = 580.1 nm.

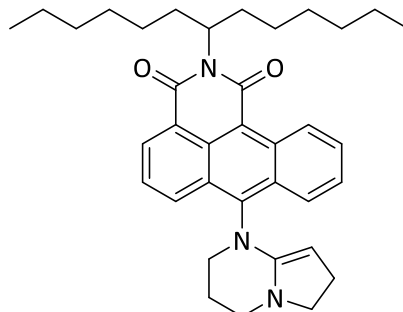
Fluorescence quantum yield (CHCl_3 , λ_{Ex} = 452.8 nm, $E_{452.8 \text{ nm}/1 \text{ cm}}$ = 0.014, reference: *N,N'*-Bis(tridecan-7-yl)perylene-3,4:9,10-tetracarboxylic bisimide with Φ = 1.00): 0.12.

MS (70 eV, EI): m/z (%) = 544 (34) [M^+], 362 (100) [$M^+ - \text{C}_{13}\text{H}_{26}$].

HRMS (EI, $\text{C}_{37}\text{H}_{40}\text{N}_2\text{O}_2$): m/z = calc. 544.3090, found 544.3083, Δ = -0.7 mmu.

Elemental analysis $\text{C}_{37}\text{H}_{40}\text{N}_2\text{O}_2$ (544.7 g mol $^{-1}$): calc. C: 81.58, H: 7.40, N: 5.14;
found C: 81.46, H: 7.51, N: 5.15.

4.4.2.10 7-(3,4,6,7-Tetrahydropyrrolo[1,2-*a*]pyrimidin-1(2*H*)-yl)-2-(tridecan-7-yl)-1*H*-dibenzo[*de,h*]isoquinoline-1,3(2*H*)-dione (47)



A solution of 2-(Tridecan-7-yl)-1*H*-dibenzo[*de,h*]isoquinoline-1,3(2*H*)-dione (**40**) (110 mg, 0.270 mmol) in 1 mL of DMF was added to 1,5-Diazabicyclo[4.3.0]non-5-en (384 mg, 3.10 mmol) at room temperature and left aside without stirring at room temperature for 3 d. The volatiles were removed in medium vacuum and the residue was purified via column chromatography (silica, chloroform/methanol 50:1) to obtain a blue solid. The yield was not determined because no single fraction could be isolated.

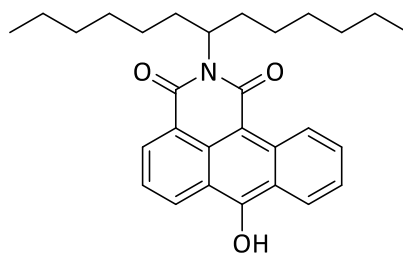
UV/Vis (CHCl₃): λ_{\max} (E_{rel}) = 368.2 (0.28), 418.2 (0.10), 565.6 (0.68), 603.0 nm (1.00).

Fluorescence (CHCl₃): λ_{\max} (I_{rel}) = 618.1 (1.00), 667.8 nm (0.25).

Fluorescence quantum yield (CHCl₃, λ_{Ex} = 607.8 nm, $E_{607.8 \text{ nm}/1 \text{ cm}}$ = 0.0351, reference: *N,N'*-Bis(tridecan-7-yl)perylene-3,4:9,10-tetracarboxylic bisimide with $\Phi = 1.00$): 0.96.

MS (70 eV, EI): m/z (%) = 551 (40) [M^+], 369 (50) [$M^+ - C_{13}H_{27}$].

HRMS (EI, C₃₆H₄₅N₃O₂): m/z = calc. 551.3512, found 551.3168, Δ = -34.4 mmu.

4.4.2.11 7-Hydroxy-2-(tridecan-7-yl)-1H-dibenzo[de,h]isoquinoline-1,3(2H)-dione (48)

Freshly sublimed potassium-*tert*-butoxide (112 mg, 1.00 mmol, 10 eq.) was placed under argon atmosphere and suspended in 0.2 mL of dry toluene. The suspension was heated to 120 °C and a solution of 2-(tridecan-7-yl)-1H-dibenzo[de,h]isoquinoline-1,3(2H)-dione (**40**) (43.0 mg, 0.100 mmol) in 0.3 mL of dry toluene was added. The reaction mixture instantly turned dark red and was stirred at 120 °C for 30 min, cooled to room temperature, treated with 10 mL of 2 M hydrochloric acid and extracted with chloroform (3 x 20 mL). The crude product was purified via column chromatography (silica, chloroform) under light exclusion to obtain a red solid.

Yield: 25 mg (0.056 mmol, 56%).

R_F-value (CHCl₃): 0.20.

m. p.: 113 °C (decomposition)

IR (ATR): $\tilde{\nu}$ = 3333, 2954, 2923, 2855, 1676 (s), 1601, 1551, 1456, 1398, 1316 (s), 1282, 1262, 1261, 1223, 1172, 1120, 1013, 874, 787, 738, 707 (s), 681 cm⁻¹.

¹H NMR (400 MHz, CDCl₃): δ = 10.20-9.80 (s, br, 1 H), 9.20-7.40 (m, 6 H), 5.45-5.20 (m, 1 H, CHN), 2.69-2.44 (m, 2 H, β -CH₂), 2.41-2.18 (m, 2 H, β -CH₂), 1.52-1.05 (m, 16 H, CH₂), 1.05-0.75 ppm (m, 6 H, CH₃).

UV/Vis (CHCl₃): λ_{\max} (E_{rel}) = 354.8 (0.19), 374.8 (0.25), 473.2 nm (1.00).

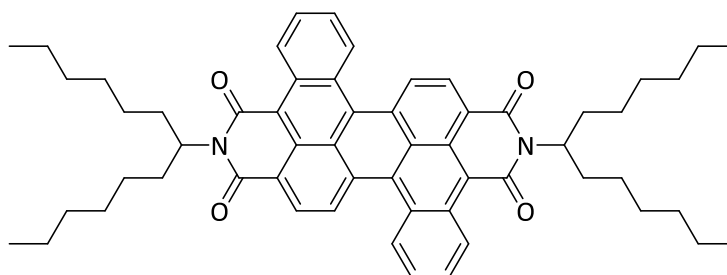
Fluorescence (CHCl₃): λ_{\max} (I_{rel}) = 541.0 (1.00), 565.8 nm (0.85).

Fluorescence quantum yield (CHCl₃, λ_{Ex} = 374.8 nm, $E_{374.8 \text{ nm}/1 \text{ cm}}$ = 0.0317, reference: *N,N'*-Bis(tridecan-7-yl)perylene-3,4:9,10-tetracarboxylic bisimide with Φ = 1.00): 0.30.

MS (70 eV, EI): m/z (%) = 545 (17) [M^+], 263 (100) [$M^+ - C_{13}H_{26}$].

HRMS (EI, $C_{29}H_{35}NO_3$): m/z = calc. 445.2617, found 445.2591, Δ = -2.6 mmu.

4.4.2.12 2,9-Di(tridecan-7-yl)tetrapheno[8,9-*ab*]benzo[5,6,7-*def*:10,11,12-*d'e'f'*]diisoquinoline-1,3,8,10(2*H*,9*H*)-tetraone (49a)



Freshly sublimed potassium-*tert*-butoxide (90.0 mg, 0.800 mmol, 8 eq.) was placed in a 2-neck flask under argon atmosphere and suspended in 0.5 mL of dry toluene. A solution of 2-(tridecan-7-yl)-1*H*-dibenzo[*de,h*]isoquinoline-1,3(2*H*)-dione (**40**) (43.0 mg, 0.100 mmol) in 0.5 mL of dry toluene was added. The reaction mixture was heated to 120 °C and stirred for 30 min, treated with 20 mL of 2 M hydrochloric acid when hot, cooled to room temperature and extracted with chloroform (3 x 30 mL). The crude product was purified via column chromatography (silica, chloroform) to obtain a green solid.

Yield: 18 mg (0.21 mmol, 42%).

R_f -value ($CHCl_3$): 0.80.

m. p.: >250 °C.

1H NMR (600 MHz, $CDCl_3$): δ = 10.01 (d, 3J = 9.0 Hz, 2 H), 8.98-8.80 (m, 4 H), 8.69-8.55 (m, 4 H) 8.11 ppm (t, 3J = 6.9 Hz, 2 H).

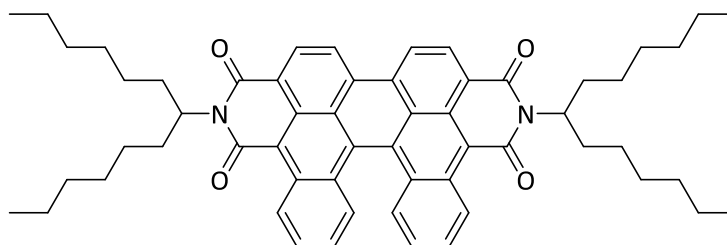
UV/Vis ($CHCl_3$): λ_{max} (E_{rel}) = 419.4 (0.15), 638.4 (0.56), 694.6 nm (1.00).

Fluorescence (CHCl₃): λ_{\max} = 730.0 nm.

MS (FAB): m/z (%) = 856 (45) [$M+H^+$], 855 (37) [M^+], 674 (74) [$M^+ - C_{13}H_{26}$]

HRMS (FAB, C₅₈H₆₆N₂O₄): m/z = calc. 854.5023, found 854.5005, Δ = -1.8 mmu.

4.4.2.13 2,9-di(Tridecan-7-yl)tetrapheno[5,6,7-*def*]isoquinoline[10,11,12-*d'e'f'*']([7,8- α ,*b*]benzoisoquinoline-1,3,8,10(2*H*,9*H*)-tetraone (49b)



Freshly sublimed potassium-*tert*-butoxide (1.12 g, 10.0 mmol, 10 eq.) was placed in a 2-neck flask under argon atmosphere and suspended in 2.0 mL of dry bis(2-ethoxyethyl) ether. The suspension was heated to 130 °C and a solution of 2-(tridecan-7-yl)-1*H*-dibenzo[*de,h*]isoquinoline-1,3(2*H*)-dione (**40**) (430 mg, 1.00 mmol) in 3.0 mL of dry bis(2-ethoxyethyl) ether was added. The reaction mixture was stirred at 130 °C for 30 min, treated with 200 mL of 2 M hydrochloric acid when hot, cooled to room temperature and extracted with chloroform (3 x 100 mL). The crude product was purified via twofold column chromatography (silica, 1st: chloroform, 2nd: toluene) to obtain a green solid.

Yield: 66.0 mg (0.771 mmol, 15%).

R_f-value (CHCl₃): 0.80.

m. p.: >250 °C.

¹H NMR (200 MHz, CDCl₃): δ = 9.82-9.77 (m, 2 H), 8.92-8.72 (m, 4 H), 7.81-7.33, (m, 6 H), 5.36-5.24 (m, 2 H, CHN), 2.39-2.33 (m, 4 H, β -CH₂), 1.96-1.93 (m, 4 H, β -CH₂), 1.36-1.24 (m, 32 H, CH₂), 0.83 ppm (t, 12 H, ³J = 7.2 Hz, CH₃).

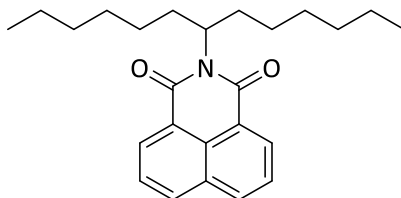
UV/Vis (CHCl₃): λ_{\max} (E_{rel}) = 425.2 (0.24), 649.4 (0.59), 694.2 nm (1.00).

Fluorescence (CHCl₃): λ_{\max} = 737.2 nm.

Fluorescence quantum yield (CHCl₃, λ_{Ex} = 650.0 nm, $E_{650.0 \text{ nm}/1 \text{ cm}}$ = 0.0286, reference: *N,N'*-Bis(tridecan-7-yl)perylene-3,4:9,10-tetracarboxylic bisimide with Φ = 1.00): 0.10.

MS (70 eV, EI): m/z (%) = 855 (100) [M^+], 673 (10) [$M^+ - C_{13}H_{27}$], 490 (26) [$M^+ - C_{26}H_{54}$].

4.4.2.14 2-(Tridecan-7-yl)-1*H*-benzo[*de*]isoquinoline-1,3(2*H*)-dione (50)



Naphthalene-1,8-dicarboxylic anhydride (0.991 g, 5.00 mmol), 7-aminotridecane (1.40 g, 7.00 mmol, 1.4 eq.), zinc acetate (92.0 mg, 0.500 mmol, 10 mol%) and imidazole (7 g) are heated to 140 °C under nitrogen. The reaction mixture was stirred at 140 °C for 4 h and then treated with 100 mL of 2 M hydrochloric acid at about 80 °C. The suspension was extracted with chloroform (2 x 100 mL). The combined organic layers were washed with water (1 x 50 mL), dried over magnesium sulfate, evaporated and purified via column chromatography (silica, chloroform) to obtain a colorless oil as first fraction.

Yield: 1.71 g (4.52 mmol, 90%).

R_f -value (CHCl₃): 0.90.

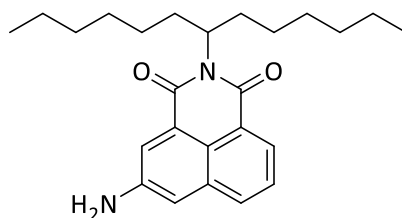
IR (ATR): $\tilde{\nu}$ = 2948, 292, 2854, 1699 (s), 1656 (s), 1627, 1587, 1512, 1464, 1458, 1369, 1373, 1337 (s), 1263, 1236 (s), 1200, 1178, 1139, 1089, 1927, 980, 907, 844, 779 (s), 727, 666 cm⁻¹.

$^1\text{H NMR}$ (400 MHz, CDCl_3): δ = 8.57 (d, 3J = 8.1 Hz, 2 H, H-2, H-7), 8.19 (d, 3J = 8.4 Hz, 2 H, H-4, H-5), 7.74 (t, 3J = 7.7 Hz, 2 H, H-3, H-6), 5.70 (tt, 3J = 5.8 Hz, 3J = 9.4 Hz, 1 H, CHN), 2.27-2.19 (m, 2 H, β - CH_2), 1.86-1.80 (m, 2 H, β - CH_2), 1.35-1.16 (m, 16 H, CH_2), 0.81 ppm (t, 3J = 7.1 Hz, 6 H, CH_3).

MS (70 eV, EI): m/z (%) = 379 (8) [M^+], 198 (100) [$M^+ - \text{C}_{13}\text{H}_{27}$].

HRMS (EI, $\text{C}_{25}\text{H}_{33}\text{NO}_2$): m/z = calc. 379.2511, found 379.25,6 Δ = -0.5 mmu.

4.4.2.15 5-Amino-2-(tridecan-7-yl)-1H-benzo[de]isoquinoline-1,3(2H)-dione (51)



2-(Tridecan-7-yl)-1H-benzo[de]isoquinoline-1,3(2H)-dione (**50**) (1.31 g, 3.46 mmol) is dissolved in 3.7 mL of concentrated sulfuric acid (96%) and slowly treated with a mixture of fuming nitric acid (> 90%, 0.261 g, 4.15 mmol,) and concentrated sulfuric acid (96%, 0.407 g, 4.15 mmol). The temperature was kept below 40 °C controlled by dropwise addition. After complete addition the reaction mixture was stirred at 45 °C for 1 h. Subsequently, the resulting solution was poured into 50 mL of ice water and extracted with chloroform (3 x 100 mL). The combined organic layers were washed with water (1 x 100 mL), dried over magnesium sulfate and evaporated to obtain the nitrated species. This intermediate was dissolved in 45 mL of concentrated acetic acid. Addition of stannous(II)chloride (6.25 g, 27.7 mmol, 8 eq.) was followed by addition of 15 mL of concentrated hydrochloric acid. The reaction mixture was stirred at 60 °C for 2 h and consecutively cooled down to room temperature and treated with 200 mL of water. The *pH*-value was adjusted to 5-6 with sodium carbonate and the aqueous suspension was extracted with chloroform (3 x 150 mL). The combined organic layers were dried over magnesium sulfate and evaporated. The crude product was purified via column chromatography (silica, chloroform) to obtain a yellow oil as the first fraction.

Yield: 1.08 mg (2.74 mmol, 79%).

***R_f*-value (CHCl₃):** 0.35.

IR (ATR): $\tilde{\nu}$ = 3456, 3365, 3252, 2953, 2923, 2855, 1693, 1620 (s), 1598, 1578 (s), 1523, 1445, 1396, 1360, 1339 (s), 1299, 1236, 1179, 1140, 1117, 1083, 1013, 988, 909, 861, 818, 779, 760, 748, 724, 666, 629 cm⁻¹.

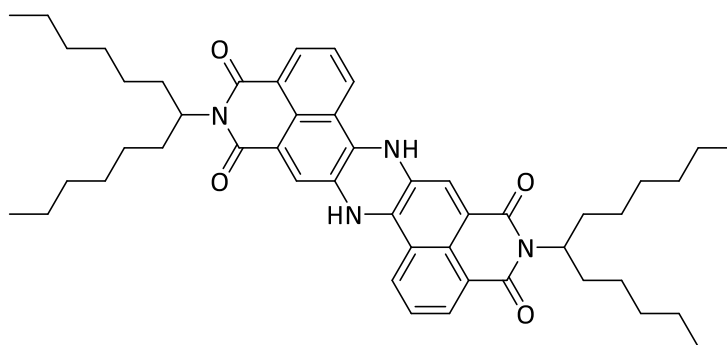
¹H NMR (600 MHz, CDCl₃): δ = 8.16 (d, ⁴*J* = 1.9 Hz, 1 H), 8.07 (d, ⁴*J* = 2.4 Hz, 1 H), 8.02 (dd, ³*J* = 8.4 Hz, ⁴*J* = 1.0 Hz, 1 H), 7.66 (dd, ³*J* = 8.3 Hz, ³*J* = 7.2 Hz, 1 H), 7.39 (m, 1 H), 5.205.13 (m, 1 H, CHN), 4.23 (s, br, 2 H, NH₂), 2.27-2.17 (m, 2 H, β -CH₂), 1.84-1.75 (m, 2 H, β -CH₂), 1.35-1.15 (m, 16 H, CH₂), 0.82 ppm (t, ³*J* = 7.1 Hz, 6 H, CH₃).

¹³C NMR (150 MHz, CDCl₃): δ = 164.5, 164.3, 145.4, 134.3, 133.7, 132.5, 132.1, 128.1, 127.5, 127.4, 122.5, 114.7, 54.6, 32.4, 31.7, 29.2, 26.9, 22.6, 14.0 ppm.

MS (70 eV, EI): *m/z* (%) = 394 (14) [*M*⁺], 212 (100) [*M*⁺ - C₁₃H₂₆].

HRMS (EI, C₂₅H₃₄N₂O₂): *m/z* = calc. 394.2620, found 394.2612, Δ = -0.8 mmu.

4.4.2.16 5,13-Di(tridecan-7-yl)-8,16-dihydrodiisoquinolino[5,4-*ab*:5',4'-*hi*]phenazine-4,6,12,14(5*H*,13*H*)-tetraone (52)



Freshly sublimed potassium-*tert*-butoxide (224 mg, 2.00 mmol, 8 eq.) was placed in a 2-neck flask under argon atmosphere and suspended in 1.0 mL of dry toluene. A solution of 5-amino-

2-(tridecan-7-yl)-1*H*-benzo[*de*]isoquinoline-1,3(2*H*)-dione (**51**) (99.0 mg, 0.250 mmol) in 1.5 mL of dry toluene was added. The reaction mixture was stirred at 120 °C for 30 min, treated with 20 mL of 2 M hydrochloric acid when hot, cooled to room temperature and extracted with chloroform (3 x 30 mL). The crude product was purified via column chromatography (silica, chloroform) to obtain a red solid.

Yield: 19 mg (0.024 mmol, 19%).

***R*_F-value (CHCl₃/MeOH 7:1):** 0.85.

m. p.: 268 °C.

IR (ATR): $\tilde{\nu}$ = 2922, 2853, 2360, 2338, 1674 (s), 1643, 1590, 1534, 1489, 1462, 1415, 1328, 1266 (s), 1228, 1195, 1161, 888, 794, 746, 668, 655, 634, 608 cm⁻¹.

¹H NMR (600 MHz, CDCl₃): δ = 11.88 (s, 2 H, NH), 8.28-8.19 (m, 2 H, H-3, H-11), 7.65 (d, ³*J* = 7.8 Hz, 2 H, H-1, H-9), 7.37 (t, ³*J* = 7.7 Hz, 2 H, H-2, H-10), 7.05-6.98 (m, 2 H, H-7, H-15), 5.25-5.10 (m, 2 H, CHN), 2.26-2.14 (m, 4 H, β -CH₂), 1.88-1.79 (m, 4 H, β -CH₂), 1.38-1.11 (m, 32 H, CH₂), 0.82 ppm (t, ³*J* = 7.0 Hz, 12 H, CH₃).

UV/Vis (CHCl₃): λ_{\max} (ϵ) = 470.0 (11400), 502.6 (37200), 540.6 nm (71500).

Fluorescence (CHCl₃): λ_{\max} (*I*_{rel}) = 546.6 (1.00), 592.5 nm (0.29).

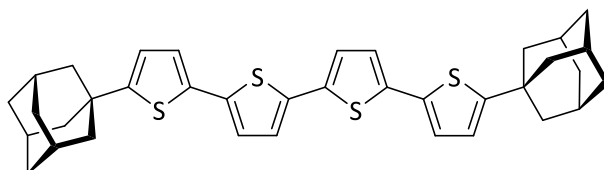
Fluorescence quantum yield (CHCl₃, λ_{Ex} = 502.6 nm, $E_{502.6 \text{ nm}/1 \text{ cm}}$ = 0.0266, reference: *N,N'*-Bis(tridecan-7-yl)perylene-3,4:9,10-tetracarboxylic bisimide with Φ = 1.00): 0.76.

MS (70 eV, EI): *m/z* (%) = 785 (11) [*M*⁺], 603 (5) [*M*⁺ - C₁₃H₂₆], 420 (17) [*M*⁺ - C₂₆H₅₅].

HRMS (EI, C₅₀H₆₄N₄O₄): *m/z* = calc. 784.4928, found 784.4912, Δ = -1.6 mmu.

Elemental analysis C₅₀H₆₄N₄O₄ (785.1 g mol⁻¹): calc. C: 76.49, H: 8.22, N: 7.14;
found C: 75.70, H: 7.90, N: 7.10.

4.5.1.1 5,5''-Di(adamantan-1-yl)-2,2':5',2'':5'',2'''-quaterthiophene (59a)



5-(Adamantyl-1-yl)-2,2'-dithiophene (98.7 mg, 0.328 mmol) was dissolved in chloroform (1.0 mL) and treated with ferrous(III)chloride (79.9 mg, 0.493 mmol). The reaction mixture was stirred at room temperature (25 °C) for 18 h. Chloroform was evaporated, the residue suspended in 2 M hydrochloric acid (5 mL), stirred for 2 h, and washed with 2 M hydrochloric acid (100 mL) and water (20 mL). The solid was dissolved in chloroform (100 mL) and filtrated, evaporated and again suspended in a mixture of *iso*-hexane/ethyl acetate 9:1 (20 mL). After filtration, the residue was purified by flash chromatography (silica gel, *iso*-hexane/chloroform 1:1) to obtain a yellow solid.

Yield: 28.1 mg (0.0469 mmol, 29%).

***R_f*-value (*iso*-hexane/EtOAc 9:1):** 0.25.

m. p.: >250 °C.

IR (ATR): $\tilde{\nu}$ = 2899, 2846, 1507, 1447, 1356, 1342, 1314, 1258, 1216, 1183, 1164, 1100, 1100, 1066, 1002, 975, 880, 826, 808, 788, 684, 667 cm⁻¹.

UV/Vis (CHCl₃): λ_{\max} (ϵ) = 400.6 nm (31900).

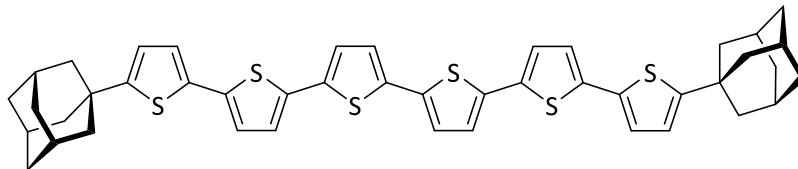
Fluorescence (CHCl₃): λ_{\max} (I_{rel}) = 466.4 (0.98), 496.4 (1.00) nm.

Fluorescence quantum yield (CHCl₃, λ_{Ex} = 400.6 nm, $E_{400.6 \text{ nm}/1 \text{ cm}}$ = 0.0176, reference: Tetramethyl perylene-3,4:9,10-tetracarboxylate with $\Phi = 1.00$): 0.20.

MS (70 eV, EI): m/z (%) = 598 (100) [M^+], 541 (8), 328 (5), 299 (5), 135 (11).

HRMS (EI, C₃₆H₃₈S₄): m/z = calc. 598.1856, found 598.1865, Δ = +0.9 mmu.

4.5.1.2 5,5''''-Di(adamantan-1-yl)-2,2':5',2'':5'',2''':5''',2''''':5''''',2''''''-sexithiophene (59b)



5-(Adamantyl-1-yl)-2,2':5',2''-terthiophene (18.0 mg, 0.0470 mmol) was dissolved in chloroform (0.5 mL) and treated with ferrous(III)chloride (11.4 mg, 0.0706 mmol). The reaction mixture was stirred at room temperature (25 °C) for 1 h under exclusion of water (CaCl₂). 1 M hydrochloric acid (3 mL) was added. After stirring overnight the precipitate was filtered and suspended in ethanol, stirred for 1 h, filtered again and washed with ethanol (50 mL). The product was dried at 110 °C for 2 d and obtained as orange solid.

Yield: 16.2 mg (0.0212 mmol, 90%).

m. p.: >250 °C.

IR (ATR): $\tilde{\nu}$ = 3061, 2896, 2845, 1737, 1499, 1439, 1364, 1354, 1341, 1313, 1253, 1217, 1188, 1157, 1100, 1070, 1001, 973, 934, 905, 876, 843, 822, 809, 787, 778, 737, 678 cm⁻¹.

UV/Vis (C₂H₂Cl₄): λ_{\max} (ϵ) = 448.2 nm (49000).

Fluorescence (C₂H₂Cl₄): λ_{\max} (I_{rel}) = 525.2 (0.98), 561.6 nm (1.00).

Fluorescence quantum yield (C₂H₂Cl₄, λ_{Ex} = 448.2 nm, $E_{448.2 \text{ nm}/1 \text{ cm}}$ = 0.0178, reference: Tetramethyl perylene-3,4:9,10-tetracarboxylate with Φ = 1.00): 0.20.

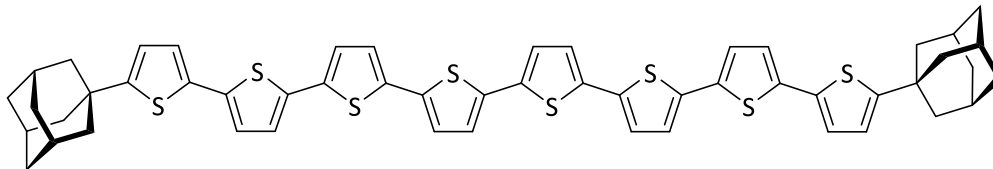
MS (70 eV, EI): m/z (%) = 762 (100) [M^+], 628 (7), 381 (11), 324 (8).

HRMS (EI, C₄₄H₄₂S₆): m/z = calc. 762.1611, found 762.1610, Δ = -0.1 mmu.

Elemental analysis C₄₄H₄₂S₆ (763.2 g mol⁻¹): calc. C: 69.25, H: 5.55, S: 25.21;
found C: 69.79, H: 5.58, S: 24.66.

AAS: Fe: 0.000%.

**4.5.1.3 5,5'-Di(adamantan-1-yl)-
2,2':5',2'':5'',2''':5''',2''':5''''',2''''':5''''',2''''':5''''',2''''':5''''',2''''':5''''',2''''':5'''''-octithiophene (59c)**



5-(Adamantyl-1-yl)-2,2':5',2'':5'',2'''-quaterthiophene (42.4 mg, 0.0912 mmol) was dissolved in chloroform (1.5 mL) and treated with ferrous(III)chloride (22.2 mg, 0.137 mmol). The reaction mixture was stirred at room temperature (25 °C) for 24 h. Water (2 mL) and 2 M hydrochloric acid (2 mL) were added. After stirring overnight the precipitate was filtered and suspended in ethanol (5 mL), stirred for 3 h, filtered again and washed with ethanol (100 mL). The product was dried at 110 °C for 1 d and obtained as red solid.

Yield: 41.3 mg (0.0446 mmol, 98%).

m. p.: >250 °C.

IR (ATR): $\tilde{\nu}$ = 3060, 2896, 2843, 2358, 2337, 1497, 1439, 1434, 1341, 1313, 1216, 1099, 1070, 1001, 973, 877, 842, 821, 786, 778, 736, 681, 667 cm^{-1} .

UV/Vis (C₂H₂Cl₄): λ_{max} (ϵ) = 452.2 nm (64400).

Fluorescence (C₂H₂Cl₄): λ_{max} (I_{rel}) = 549.4 (1.00), 565.6 nm (0.92).

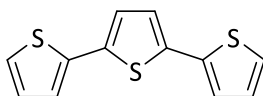
Fluorescence quantum yield (C₂H₂Cl₄, λ_{Ex} = 452.2 nm, $E_{452.2 \text{ nm}/1 \text{ cm}}$ = 0.00859, reference: Tetramethyl perylene-3,4:9,10-tetracarboxylate with $\Phi = 1.00$): 0.21.

MS (70 eV, EI): m/z (%) = 926 (54) [M^+], 464 (24), 268 (21), 256 (22).

HRMS (EI, C₅₂H₄₆S₈): m/z = calc. 926.1365, found 926.1380, Δ = +1.5 mmu.

AAS: Fe: 0.007%.

4.5.2.1 2,2':5',2''-Terthiophene (60)



Lithium chloride (2.67 g, 63.0 mmol, 3.15 eq.) and magnesium turnings (1.53 g, 63.0 mmol, 3.15 eq.) were placed in a 2-neck flask and flame dried. 30 mL of dry THF were added under argon and the suspension was treated with a solution of 2-bromothiophene (9.78 g, 60.0 mmol, 3 eq.) in 20 mL of THF at room temperature. The reaction mixture was heated to 65 °C and stirred at this temperature for 2 h. In a second dry 2-neck flask 2,5-dibromothiophene (4.84 g, 20.0 mmol) was dissolved in 20 mL of THF and slowly treated with the freshly prepared *Grignard* reagent at 0 °C under argon atmosphere. [1,1'-Bis(diphenylphosphino)ferrocene]dichloropalladium(II) was added and the reaction mixture was stirred at room temperature for 1 h and at 65 °C for subsequent 3 h. The resulting intensively green mixture was cooled to room temperature and quenched with 50 mL of saturated aqueous ammonium chloride. Extraction with chloroform (3 x 75 mL) was followed by evaporation and the crude product was purified via twofold column chromatography (silica, 1st: *iso*-hexane/chloroform 12:1, 2nd: *iso*-hexane) to obtain a slightly yellow oil which crystallizes within several hours to form brown needles.

Yield: 4.07 g (16.4 mmol, 82%).

***R_f*-value (*iso*-hexane):** 0.50.

¹H NMR (200 MHz, CD₂Cl₂): δ = 7.27 (dd, ³*J* = 5.0 Hz, ⁴*J* = 1.1 Hz, 2 H), 7.22 (dd, ³*J* = 3.6 Hz, ⁴*J* = 1.1 Hz, 2 H), 7.12 (s, 2 H), 7.05 ppm (dd, ³*J* = 5.0 Hz, ³*J* = 3.6 Hz, 2 H).

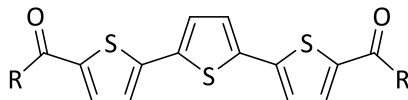
¹³C NMR (150 MHz, CDCl₃): δ = 136.92, 136.10, 127.88, 124.54, 124.27, 123.69 ppm.

MS (70 eV, EI): *m/z* (%) = 248 (100) [*M*⁺], 171 (7), 127 (7).

HRMS (EI, C₁₂H₈S₃): *m/z* = calc. 247.9788, found 247.9765, Δ = -2.3 mmu.

Elemental analysis C₁₂H₈S₃ (248.4 g mol⁻¹): calc. C: 58.03, H: 3.25, S: 38.72;
found C: 57.81, H: 3.49, S: 38.98.

4.5.2.2 General procedure for the preparation of 1,1'-([2,2':5',2''-terthiophene]-5,5''-diyl)bisketones (61-62)



Route 1:

In a dry glass apparatus flushed with argon, 2,2':5',2''-terthiophene (**60**) (62.1 mg, 0.250 mmol) was dissolved in 1.0 mL of carbon disulfide, stirred, cooled to 0 °C and treated with 10 eq of the respective acyl chloride (2.50 mmol) and 2.5 eq of aluminum chloride (83.3 mg, 0.625 mmol). The reaction mixture instantly turned red and was allowed to warm to rt. After 1 h as well as after 2 h, additional 2.5 eq aluminum chloride were added each. After an overall reaction time of 3 h the remaining volatiles were evaporated, the residue was treated with 5 mL of a solution of saturated ammonium chloride and extracted with chloroform (2 x 10 mL). After evaporation of the solvent, the crude product was purified by column chromatography (respective conditions given below) and filtrated through neutral aluminum oxide.

Yields:

61a: 93% (83.8 mg, 0.233 mmol)

61b: 62% (60.2 mg, 0.155 mmol)

61c: 40% (42.1 mg, 0.101 mmol)

61d: 79% (82.5 mg, 0.198 mmol)

61e: 51% (58.2 mg, 0.128 mmol)

62a: 30% (27.2 mg, 0.0751 mmol)

62b: 18% (20.0 mg, 0.0450 mmol)

Route 2:

2,2':5',2''-Terthiophene (**60**) (62.1 mg, 0.250 mmol) was dissolved in 1.0 mL of chloroform. Zinc oxide (31.1 mg, 50% (w/w)) was added and the stirred suspension was treated with 8 eq of the respective acyl chloride (2.00 mmol) at rt. The reaction mixture turned purple and was allowed to react for 4 h at rt. Subsequently, the volatiles were removed at reduced pressure. The residue was treated with 5 mL of sat. aqueous sodium carbonate solution and extracted with chloroform (2 x 10 mL). The combined organic layers were washed with sat. aqueous sodium carbonate (1 x 10 mL) and water (1 x 10 mL). The solvent was evaporated and the crude product was purified by column chromatography (respective conditions given below) and filtrated through neutral aluminum oxide.

Yields:

61a: 92 % (82.6 mg, 0.229 mmol)

61b: 92% (89.4 mg, 0.229 mmol)

61c: 86% (89.6 mg, 0.216 mmol)

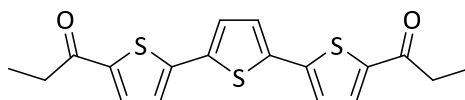
61d: 88% (91.7 mg, 0.220 mmol)

61e: 78% (89 mg, 0.0195 mmol)

62a: < 5%

62b: < 5%

4.5.2.3 1,1'-[(2,2':5',2''-Terthiophene)-5,5''-diyl]bis(propan-1-on) (61a)



Purification: Silica, chloroform/*iso*-hexane 2:1.

***R_f*-value (CHCl₃/*iso*-hexane 2:1):** 0.65.

m. p.: 222 °C.

IR (ATR): $\tilde{\nu}$ = 2977, 2938, 2877, 1655 (s), 1507, 1441, 1412, 1378, 1354, 1254, 1221, 1086, 1060, 912, 882, 854, 787 (vs), 744, 724, 666 cm⁻¹.

¹H NMR (400 MHz, CD₂Cl₂): δ = 7.63 (d, ³*J* = 4.0 Hz, 2 H), 7.29 (s, 2 H), 7.24 (d, ³*J* = 4.0 Hz, 2 H), 2.92 (q, ³*J* = 7.3 Hz, 4 H), 1.21 ppm (t, ³*J* = 7.3 Hz, 6 H).

¹³C NMR (100 MHz, CD₂Cl₂): δ = 133.0, 127.0, 125.2, 32.7, 8.8 ppm.

UV/Vis (CHCl₃): λ_{\max} (ϵ) = 406.2 nm (45300).

Fluorescence (CHCl₃): λ_{\max} (*I*_{rel}) = 463.3 (0.91), 490.4 nm (1.00).

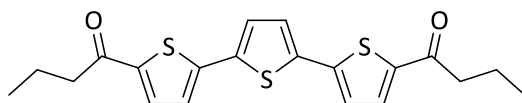
Fluorescence quantum yield (CHCl₃, λ_{Ex} = 406.2 nm, $E_{406.2 \text{ nm}/1 \text{ cm}}$ = 0.0248, reference: Tetramethyl perylene-3,4:9,10-tetracarboxylate with Φ = 1.00): 0.52.

MS (70 eV, EI): *m/z* (%) = 360 (85) [*M*⁺], 331 (100) [*M*⁺ – C₂H₅], 303 (16) [*M*⁺ – C₃H₅O], 259 (42).

HRMS (EI, C₁₈H₁₆O₂S₃): *m/z* = calc. 360.0312, found 360.0314, Δ = +0.2 mmu.

Elemental analysis C₁₈H₁₆O₂S₃ (360.5 g mol⁻¹): calc. C: 59.97, H: 4.47, S: 26.68;
found C: 60.20, H: 4.53, S: 26.82.

4.5.2.4 1,1'-[(2,2':5',2''-Terthiophene)-5,5''-diyl]bis(butan-1-on) (61b)



Purification: Silica, chloroform/*iso*-hexane 2:1.

***R_F*-value (CHCl₃/*iso*-hexane 2:1):** 0.70.

m. p.: 225 °C.

IR (ATR): $\tilde{\nu}$ = 3294, 3063, 2959, 2933, 2872, 2668, 1654 (s), 1506, 1483, 1464, 1439 (s), 1407, 1370, 1326, 1306, 1289, 1253, 1211 (s), 1113, 1077, 1067, 1038, 957, 901, 878, 856, 817, 792 (s), 757, 749, 674 cm⁻¹.

¹H NMR (400 MHz, CD₂Cl₂): δ = 7.62 (d, ³*J* = 4.0 Hz, 2 H), 9.29 (s, 2 H), 7.24 (d, ³*J* = 4.0 Hz, 2 H), 2.86 (t, ³*J* = 7.3 Hz, 4 H), 1.76 (h, ³*J* = 7.4 Hz, 4 H), 1.00 ppm (t, ³*J* = 7.4 Hz, 6 H).

¹³C NMR (100 MHz, CD₂Cl₂): δ = 193.4, 144.5, 143.8, 137.6, 133.1, 127.0, 125.2, 41.3, 18.75, 14.17 ppm.

UV/Vis (CHCl₃): λ_{\max} (ϵ) = 409.4 nm (39800).

Fluorescence (CHCl₃): λ_{\max} (*I*_{rel}) = 465.2 (0.98), 491.2 nm (1.00).

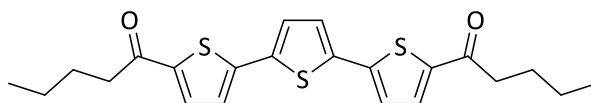
Fluorescence quantum yield (CHCl₃, λ_{Ex} = 409.4 nm, $E_{409.4 \text{ nm/1 cm}}$ = 0.042, reference: Tetramethyl perylene-3,4:9,10-tetracarboxylate with Φ = 1.00): 0.39.

MS (70 eV, EI): *m/z* (%) = 388 (11) [*M*⁺], 345 (91), 273.01 (42).

HRMS (EI, C₂₀H₂₀O₂S₃): *m/z* = calc. 388.0625, found 388.0626, Δ = +0.1 mmu.

Elemental analysis C₂₀H₂₀O₂S₃ (388.1 g mol⁻¹): calc. C: 61.82, H: 5.19, S: 24.75;
found C: 61.75, H: 5.06, S: 25.16.

4.5.2.5 1,1'-[(2,2':5',2''-Terthiophene)-5,5''-diyl]bis(pentan-1-on) (61c)



Purification: Silica, chloroform/*iso*-hexane 1:1.

***R_f*-value (CHCl₃/*iso*-hexane 1:1):** 0.50.

m. p.: 208 °C.

IR (ATR): $\tilde{\nu}$ = 2960, 2929, 2872, 1655, 1507, 1464, 1445, 1409, 1380, 1347, 1259, 1209, 1088, 1016 (s), 930, 858, 789 (s), 751, 735, 701, 673 cm⁻¹.

¹H NMR (400 MHz, CD₂Cl₂): δ = 7.62 (d, ³*J* = 4.0 Hz, 2 H), 7.29 (s, 2 H), 7.24 (d, ³*J* = 4.0 Hz, 2 H), 2.88 (t, ³*J* = 7.3 Hz, 4 H), 1.75-1.67 (m, 4 H), 1.52-1.37 (m, 4H), 0.96 ppm (t, ³*J* = 7.3 Hz, 6 H).

¹³C NMR (100 MHz, CD₂Cl₂): δ = 193.5, 144.5, 143.7, 137.5, 133.1, 127.0, 125.2, 39.2, 27.4, 23.0, 14.2, 1.3 ppm.

UV/Vis (CHCl₃): λ_{\max} (ϵ) = 409.4 nm (34700).

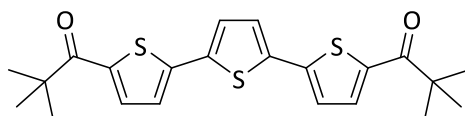
Fluorescence (CHCl₃): λ_{\max} (*I*_{rel}) = 464.2 (0.98), 491.2 nm (1.00).

Fluorescence quantum yield (CHCl₃, λ_{Ex} = 409.4 nm, $E_{409.4 \text{ nm}/1 \text{ cm}}$ = 0.0421, reference: Tetramethyl perylene-3,4:9,10-tetracarboxylate with Φ = 1.00): 0.71.

MS (70 eV, EI): *m/z* = 416.02 [*M*⁺], 374.00 [*M*⁺ - C₃H₆], 331.98 [*M*⁺ - C₆H₁₂], 316.97 [*M*⁺ - C₇H₁₅].

HRMS (EI, C₂₂H₂₄O₂S₃): *m/z* = calc. 416.0933, found 416.0934, Δ = +0.1 mmu.

4.5.2.6 1,1'-[(2,2':5',2''-Terthiophene)-5,5''-diyl]bis(2,2-dimethylpropan-1-on) (61d)



Purification: Silica, chloroform/*iso*-hexane 2:1.

***R_f*-value (CHCl₃/*iso*-hexane 2:1):** 0.80.

m. p.: 206 °C.

IR (ATR): $\tilde{\nu}$ = 2968, 1633 (s), 1506, 1466, 1436 (s), 1363, 1327, 1278, 1196, 1175, 1065, 1024, 914, 854, 820, 792 (s), 748 cm⁻¹.

¹H NMR (400 MHz, CD₂Cl₂): δ = 7.69 (d, ³*J* = 4.1 Hz, 2 H), 7.24 (s, 2 H), 7.18 (d, ³*J* = 4.0 Hz, 2 H), 1.41 ppm (s, 18 H).

¹³C NMR (100 MHz, CD₂Cl₂): δ = 199.0, 143.7, 141.7, 137.3, 133.3, 126.8, 124.7, 44.4, 28.69 ppm.

UV/Vis (CHCl₃): λ_{\max} (ϵ) = 410.2 nm (43800).

Fluorescence (CHCl₃): λ_{\max} (*I_{rel}*) = 465.6 (0.98), 494.3 nm (1.00).

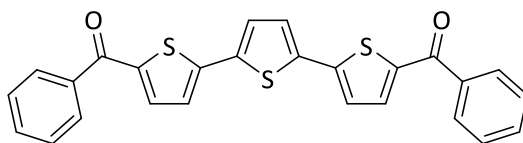
Fluorescence quantum yield (CHCl₃, λ_{Ex} = 410.2 nm, $E_{410.2 \text{ nm}/1 \text{ cm}}$ = 0.0246, reference: Tetramethyl perylene-3,4:9,10-tetracarboxylate with Φ = 1.00): 0.54.

MS (70 eV, EI): *m/z* = 416.07 [*M*⁺], 359.03 [*M*⁺ – C₄H₉], 331.05 [*M*⁺ – C₅H₉O].

HRMS (EI, C₂₂H₂₄O₂S₃): *m/z* = cal. 416.0933, found 416.0930, Δ = -0.3 mmu.

Elemental analysis C₂₂H₂₄O₂S₃ (416.6 g mol⁻¹): calc. C: 63.42, H: 5.81, S: 23.09;
found C: 62.04, H: 5.91, S: 20.60.

4.5.2.7 1,1'-([2,2':5',2''-Terthiophene]-5,5''-diyl)bis(phenylmethanon) (61e)



Purification: Silica, chloroform/*iso*-hexane 2:1.

***R_f*-value (CHCl₃/*iso*-hexane 2:1):** 0.75.

m. p.: 218 °C.

IR (ATR): $\tilde{\nu}$ = 3057, 1612 (s), 1597, 1574, 1503, 1446, 1435 (s), 1425, 1360, 1340, 1317, 1293 (s), 1219, 1178, 1137, 1074, 1058, 1022, 999, 973, 925, 906, 886, 854, 827, 812, 791 (s), 711 (s), 699 (s), 691 (s), 669, 653 (s) cm⁻¹.

¹H NMR (600 MHz, CD₂Cl₂): δ = 7.86 (dd, ³*J* = 8.3 Hz, ⁴*J* = 1.3 Hz, 4 H, *o*-H), 7.65-7.61 (m, 2 H, *p*-H), 7.58 (d, ³*J* = 4.0 Hz, 2 H), 7.54 (t, ³*J* = 7.6 Hz, 4 H, *m*-H), 7.37 (s, 2 H), 7.30 ppm (d, ³*J* = 4.0 Hz, 2 H).

¹³C NMR (150 MHz, CD₂Cl₂): δ = 188.0, 145.4, 143.0, 138.5, 137.7, 136.3, 132.9, 129.5, 129.1, 127.4, 125.3 ppm.

UV/Vis (CHCl₃): λ_{\max} (ϵ) = 421.8 nm (42400).

Fluorescence (CHCl₃): λ_{\max} (*I*_{rel}) = 484.3 (1.00), 510.6 nm (0.97).

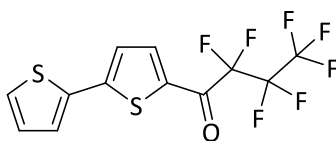
Fluorescence quantum yield (CHCl₃, λ_{Ex} = 421.8 nm, $E_{421.8 \text{ nm}/1 \text{ cm}}$ = 0.067, reference: Tetramethyl perylene-3,4,9,10-tetracarboxylate with Φ = 1.00): 0.40.

MS (70 eV, EI): *m/z* (%) = 456 (100) [*M*⁺], 379 (14) [*M*⁺ - C₆H₅], 351 (7) [*M*⁺ - C₇H₅O].

HRMS (EI, C₂₆H₁₆O₂S₃): *m/z* = calc. 456.0312, found 456.0308, Δ = -0.4 mmu.

Elemental analysis C₂₆H₁₆O₂S₃ (456.6 g mol⁻¹): calc. C: 68.39, H: 3.53, S: 21.06;
found C: 67.02, H: 3.95, S: 21.21.

4.5.2.8 1-([2,2'-Bithiophen]-5-yl)-2,2,3,3,4,4,4-heptafluorbutan-1-on (62a)



Purification: Silica, *iso*-hexane/chloroform 3:1.

***R_f*-value (*iso*-hexane/CHCl₃ 3:1):** 0.30.

m. p.: 58 °C.

IR (ATR): $\tilde{\nu}$ = 3118, 1663 (s), 1540, 1502, 1442 (s), 1208 (s), 1117 (s), 1079, 958, 936, 843, 799 (s), 705 (s), 694 (s) cm⁻¹.

¹H NMR (400 MHz, CD₂Cl₂): δ = 7.91-7.88 (m, 1 H), 7.48-7.47 (m, 2 H), 7.31 (d, ³*J* = 4.2 Hz, 1 H), 7.14-7.12 ppm (m, 1 H).

¹³C NMR (100 MHz, CD₂Cl₂): δ = 151.6, 138.9, 136.3, 136.1, 129.3, 129.5, 128.2, 126.2 ppm.

¹⁹F NMR (376 MHz, CD₂Cl₂): δ = -80.67 (t, *J* = 9.1 Hz, 1H), -115.66 – -115.83 (m), -126.17 (s) ppm.

UV/Vis (CHCl₃): λ_{\max} (ϵ) = 384.0 nm (23300).

Fluorescence (CHCl₃): λ_{\max} = 447.7 nm.

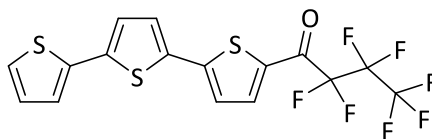
Fluorescence quantum yield (CHCl₃, λ_{Ex} = 384.0 nm, $E_{384.0 \text{ nm}/1 \text{ cm}}$ = 0.0418, reference: Tetramethyl perylene-3,4,9,10-tetracarboxylate with Φ = 1.00): 0.62.

MS (70 eV, EI): *m/z* = 361.93 [*M*⁺], 329.95, 193.04 [*M*⁺ – C₃F₇], 165.05 [*M*⁺ – C₄F₇O].

HRMS (EI, C₁₂H₆F₇OS₂ for *M*+H⁺): *m/z* = calc. 362.9742, found 362.9746, Δ = +0.4 mmu.

Elemental analysis C₁₂H₆F₇OS₂ (362.3 g mol⁻¹): calc. C:39.78, H: 1.39, S: 17.70;
found C: 40.49, H: 1.95, S: 19.04.

4.5.2.9 1-([2,2':5',2''-Terthiophen]-5-yl)-2,2,3,3,4,4,4-heptafluorbutan-1-on (62b)



Purification: Silica, *iso*-hexane.

R_f -value (*iso*-hexane): 0.35.

m. p.: 107 °C.

IR (ATR): $\tilde{\nu}$ = 1663 (s), 1500, 1449, 1433, 1344, 1228 (s), 1208 (s), 1171, 1119, 1069, 968, 938, 823, 793 (s), 787 (s), 750, 698 (s) cm^{-1} .

^1H NMR (800 MHz, CD_2Cl_2): δ = 7.90-7.89 (m, 1 H), 7.40 (d, 3J = 3.8 Hz, 1 H), 7.34 (dd, 3J = 5.1 Hz, 4J = 1.1 Hz, 1 H), 7.30 (d, 3J = 4.2 Hz, 1 H), 7.29 (dd, 3J = 3.6 Hz, 4J = 1.1 Hz, 1 H), 7.20 (d, 3J = 3.9 Hz, 1 H), 7.08 ppm (dd, 3J = 5.1 Hz, 3J = 3.6 Hz, 1 H).

^{13}C NMR (201 MHz, CD_2Cl_2): δ = 175.2, 150.9, 141.0, 138.7, 136.6, 135.9, 134.1, 128.7, 126.5, 125.6, 125.5 ppm.

UV/Vis (CHCl_3): λ_{max} (ϵ) = 432.2 nm (42200).

Fluorescence (CHCl_3): λ_{max} = 528.8 nm.

Fluorescence quantum yield (CHCl_3 , λ_{Ex} = 432.2 nm, $E_{432.2 \text{ nm}/1 \text{ cm}}$ = 0.0470, reference: Tetramethyl perylene-3,4:9,10-tetracarboxylate with Φ = 1.00): 0.47.

MS (70 eV, EI): m/z = 443.80 [M^+], 274.97 [$M^+ - \text{C}_3\text{F}_7$].

HRMS (EI, $\text{C}_{16}\text{H}_7\text{F}_7\text{OS}_3$): m/z = calc. 443.9547, found 443.9539, Δ = -0.8 mmu.

Elemental analysis $\text{C}_{16}\text{H}_7\text{F}_7\text{OS}_3$ (444.4 g mol^{-1}): calc. C: 43.24, H: 1.59, S: 21.64;
found C: 43.19, H: 2.27, S: 23.27.

4.6 Preparation of Solid Poly(methyl methacrylate) Samples

4.6.1 Standard Polymerization Reaction for the Preparation of Dye-Doped Poly(methyl methacrylate) (PMMA)

The respective dye was dissolved in freshly distilled methyl methacrylate (MMA, about 20 g) in concentrations of 5 to 200 ppm. Azobisisobutyronitrile (AIBN) (200 ppm (m/m) referring to MMA) was added and stirred at 25 °C for 30 min. The solution was filtered into a form determining the shape of the product and the filtrate polymerized at 70 °C for 2.5 h followed by 5-7 d at 45 °C to obtain dye-doped poly(methyl methacrylate).

4.6.2 Preparation of Dye-Doped Poly(methyl methacrylate) (PMMA) Films

About 1 g of poly(methyl methacrylate; Acros, M_w :33000 g mol⁻¹) was dissolved in the 20-fold amount (m/m) of toluene overnight under stirring. After filtration, the solution was treated with the respective dye (50 ppm (m/m)) and stirred until complete dissolution. A second filtration was followed by drop-coating the filtrate on glass (approx. 10 x 10 x 1 mm, silica glass). One drop from a *Pasteur* pipette per sample was placed in the middle of the carrier and left aside at room temperature on a plane and even surface for at least 6 h. The resulting samples displayed thicknesses of about 0.2 mm and were measured as obtained on the glass surface.

5 References

- [1] M. Hilbert, P. López, *Science* **2011**, *332*, 60-65.
- [2] O. Ziemann, J. Krauser, P. E. Zamzow, W. Daum, *POF-Handbuch Optische Kurzstreckenübertragung*, 2nd ed., Springer-Verlag Berlin Heidelberg **2007**.
- [3] S. Gogouvitis, K. Konstanteli, S. Waldschmidt, G. Kousiouris, G. Katsaros, A. Menychtas, D. Kyriazis, T. Varvarigou, *Future Gener. Comp. Sy.* **2012**, *28*, 193–209.
- [4] a) R. Visbal, M. C. Gimeno, *Chem. Soc. Rev.* **2014**, *43*, 3551-3574; b) H. Nakanotani, T. Higuchi, T. Furukawa, K. Masui, K. Morimoto, M. Numata, H. Tanaka, Y. Sagara, T. Yasuda, C. Adachi, *Nat. Commun.* **2014**, *5*, 4016.
- [5] a) H. Sirringhaus, *Adv. Mat.* **2014**, *26*, 1319-1335; b) H. E. Katz, A. J. Lovinger, J. Johnson, C. Kloc, T. Slegrist, W. Li, Y.-Y. Lin, A. Dodabalapur, *Nature* **2000**, *404*, 478-481; c) T. Bourgeteau, D. Tondelier, B. Geffroy, R. Brisse, S. Campidelli, R. Cornut, B. Jusselme, *J. Mat. Chem. A* **2016**, *4*, 4831-4839.
- [6] <https://de.statista.com/infografik/3553/anteil-von-glasfaseranschluesen-in-der-der-oecd/>; accessed on Aug. 23rd 2016.
- [7] a) C. Emslie, *J. Mat. Sci.* **1988**, *23*, 2281-2293; b) J. Zubia, J. Arrue, *Opt. Fiber Tech.* **2001**, 101-140.
- [8] I. Möllers, D. Jäger, R. Gaudino, A. Nocivelli, H. Kragl, O. Ziemann, N. Weber, T. Koonen, C. Lezzi, A. Bluschke, S. Randel, *IEEE Commun. Mag.* **2009**, *47*, 58–68.
- [9] a) D. Siebler, P. Rohwetter, R. Brusenbach, R. Plath, *Porcedia Eng.* **2015**, *120*, 845-848; b) K. Kalli, D. J. Webb, *Adv. Fiber Opt.* **2011**, 345-388.
- [10] a) T. H. Nguyen, S. A. Hardwick, T. Sun, K. T. V. Kenneth, *IEEE Sens. J.* **2012**, *12*, 255-260; b) M. R. Shortreed, S. Dourado, R. Kopelman, *Sensor Actuat. B-Chem.* **1997**, 8-12; c) C. Preininger, I. Klimant, O. S. Wolfbeis, *Anal. Chem.* **1994**, *66*, 1841-1846.
- [11] P. K. Mohanty, S. R. Dugad, S. K. Gupta, *Rev. Sci. Instrum.* **2012**, *83*, 043301/1-043301/10.
- [12] a) H. Langhals, *Nachr. Chem. Tech. Lab.* **1980**, *28*, 716-718; *Chem. Abstr.* **1981**, *95*, R9816q; b) S. Knabe, N. Soleimani, T. Markvart, G. H. Bauer, *Phys. Status Solidi RRL* **2010**, *4*, 118-120.
- [13] a) T. Förster, *Umwandlung der Anregungsenergie in W. Foerst (Herausg.), 2. Internationales Farbensymposium:Optische Anregung organischer Systeme. Aufnahme und Umwandlung von Lichtenergie durch Farbstoffe und die Einflüsse des Mediums*, p. 516, Verlag Chemie GmbH, Weinheim **1966**; *Chem. Abstr.* **1967**, *67*, 103925;

- [14] J. R. Lakowicz, *Principles of Fluorescence Spectroscopy*, 3rd ed., Springer, New York **2006**.
- [15] a) K. Jahn, V. Buschmann, C. Hille, *Sci. Rep.* **2015**, *5*, 14334; b) X. Dong, L. Wei, Y. Su, Z. Li, H. Geng, C. Yanga, Y. Zhang, *J. Mater. Chem. C* **2015**, *3*, 2798-2801.
- [16] International Union of Pure and Applied Chemistry (IUPAC), *Compendium of Chemical Terminology*, 2nd ed., **1997**.
- [17] a) W. König, *J. Prakt. Chem.* **1925**, *112*, 1-36; b) W. Ismailsky, *Dissertation*, **1913**, Univ. Dresden.
- [18] G. G. Stokes, *Phil. Trans. R. Soc.* **1852**, *142*, 463-562.
- [19] S. J. Strickler, R. A. Berg, *J. Chem. Phys.* **1962**, *37*, 814-822.
- [20] a) S. R. Phillips, L. J. Wilson, R. F. Borkman, *Curr. Eye Res.* **1986**, *5*, 611-619; b) X. Peng, D. R. Draney, W. M. Volcheck, *Proc. SPIE* **2006**, 6097; c) R. Weissleder, C. H. Tung, U. Mahmood, A. Bogdanov, *Nat. Biotechnol.* **1999**, *17*, 375-378.
- [21] a) L. Mangolini, E. Thimsen, U. Kortshagen, *Nano Lett.* **2005**, *5*, 655-659; b) G. Beane, K. Boldt, N. Kirkwood, P. Mulvaney, *J. Phys. Chem. C* **2014**, *118*, 18079-18086; c) V. C. Gupta, N. Chaudhary, R. Srivastava, G. D. Sharma, R. Bhardwaj, S. Chand, *J. Am. Chem. Soc.* **2011**, *133*, 9960-9963; d) G. G. Stokes, *Phil. Trans. R. Soc.* **1953**, *143*, 385-396.
- [22] a) E. J. Noga, P. Udomkusonsri, *Vet Pathol.* **2012**, *39*, 726-731; b) D. Slate, T. P. Algeo, K. M. Nelson, R. B. Chipman, D. Donovan, J. D. Blanton, M. Niezgodna, C. E. Rupprecht, J. M. Bethony, *PLoS Negl. Trop. Dis.* **2009**, *3*, e549.
- [23] a) A. Guillemette, *J. Pharmacie* **1835**, *21*, 172-178; b) W. H. Perkin, *J. Chem. Soc.* **1868**, *21*, 53-63; c) F. J. Duarte, L. S. Liao, K. M. Vaeth, A. M. Miller, *J. Opt. A: Pure Appl. Opt.* **2006**, *8*, 172-174; d) U. S. Weber, B. Steffen, C. P. Siegers, *Res. Commun. Mol. Pathol. Pharmacol.* **1998**, *99*, 193-206.
- [24] a) B. Mujumdar, A. Ernst, S. R. Mujumdar, C. J. Lewis, A. S. Waggoner, *Bioconjugate Chem.* **1993**, *4*, 105-111; b) K. Umezawa, A. Matsui, Y. Nakamura, D. Citterio, K. Suzuki, *Chem. Eur J.* **2009**, *15*, 1096-1106.
- [25] T. Eicher, S. Hauptmann, A. Speicher, *The Chemistry of Heterocycles: Structures, Reactions, Synthesis, and Applications*, p. 442, 3rd ed., John Wiley & Sons **2013**.
- [26] a) F. G. Prendergast, K. G. Mann, *Biochem.* **1978**, *17*, 3448-3453; b) R. Y. Tsien, *Ann. Rev. Biochem.* **1998**, *67*, 509-544.
- [27] a) H. Langhals, *Helv. Chim. Acta* **2005**, *88*, 1309-1343; b) H. Langhals, *Chromophores for picoscale optical computers in K. Sattler (ed.), Fundamentals of picoscience*, p. 705, Taylor & Francis Inc. CRC Press Inc., Boca Roca/US **2013**; ISBN : 9781466505094; c) Demmig, H. Langhals, *Chem. Ber.* **1988**, *121*, 225-230.

- [28] H. Langhals, L. B.-Å. Johansson, *J. Chem. Soc. Faraday Trans.* **1998**, *94*, 2919-2922.
- [29] H. Langhals, S. Demmig, H. Huber, *Spectrochim. Acta* **1988**, *44A*, 1189-1193.
- [30] a) H. Langhals, A. J. Esterbauer, A. Walter, E. Riedle, I. Pugliesi, *J. Am. Chem. Soc.* **2010**, *132*, 16777-16782; b) P. Kölle, I. Pugliesi, H. Langhals, R. Wilcken, A. Esterbauer, R. de Vivie-Riedle, E. Riedle, *Phys. Chem. Chem. Phys.* **2015**, *17*, 25061-25072; c) H. Langhals, S. Poxleitner, O. Krotz, T. Pust, A. Walter, *Eur. J. Org. Chem.* **2008**, 4559-4562.
- [31] a) T. Förster, *Ann. Phys.* **1948**, *437*, 55-75; b) H. Edelhoich, L. Brand, M. Wilchek, *Biochem.* **1967**, *6*, 547-559; c) A. N. Bader, E. G. Hofman, J. Voortman, P. M. P. Van Bergen En Henegouwen, H. C. Gerritsen, *Biophys. J.* **2009**, *97*, 2613-2622.
- [32] H. Langhals, W. Jona, *Angew. Chem. Int. Ed.* **1998**, *37*, 952-955.
- [33] a) J. R. Lakowicz, G. Weber, *Biochemistry* **1973**, *12*, 4161-4170; b) H. Yang, G. Luo, P. Karnchanaphanurach, T.-M. Louie, I. Rech, S. Cova, L. Xun, X. S. Xie, *Science* **2003**, *302*, 262-266; c) U. Resch-Genger, M. Grabolle, S. Cavaliere-Jaricot, R. Nitschke, T. Nann, *Nat. Methods* **2008**, *5*, 763-775; d) M. Y. Berezin, S. Achilefu, *Chem. Rev.* **2010**, *110*, 2641-2684.
- [34] a) L. I. Smith, *Org. Synth.* **1930**, *10*, 40-42; b) H. Langhals, A. Walter, E. Rosenbaum, L. B.-A. Johansson, *Phys. Chem. Chem. Phys.* **2011**, *13*, 11055-11059.
- [35] H. Langhals, S. Demmig, T. Potrawa, *J. Prakt. Chem.* **1991**, *333*, 733-748.
- [36] H. Langhals, A. Hofer, *J. Org. Chem* **2011**, *78*, 5889-5897.
- [37] a) G. Scheibe, *Angew. Chem.* **1937**, *50*, 212-219; b) E. E. Jelley, *Nature* **1937**, *139*, 631-631; c) F. Würthner, T. E. Kaiser, C. R. Saha-Möllner, *Angew. Chem. Int. Ed.* **2011**, *50*, 3376-3410.
- [38] a) V. Grignard, *Compt. Rend.* **1900**, *130*, 1322-1325; M. B. Smith, J. March, *Advanced Organic Reactions, Mechanisms and Structure*, 6th ed., Wiley-Interscience, New York **2007**.
- [39] H. Kawai, T. Umehara, K. Fujiwara, T. Tsuji, T. Suzuki, *Angew. Chem. Int. Ed.* **2006**, *45*, 4281-4286.
- [40] a) A. J. Kennedy, T. P. Mathews, Y. Kharel, S. D. Field, M. L. Moyer, J. E. East, J. D. Houck, K. R. Lynch, T. L. Macdonald, *J. Med. Chem.* **2011**, *54*, 3524-3548; b) S. Araki, Y. Butsugan, *J. Chem. Soc. Perkin Trans. 1* **1984**, 969-972; c) E. L. Stangeland, T. Sammakia, *Tetrahedron* **1997**, *53*, 16503-16510.
- [41] H. Langhals, A. Hofer, *J. Org. Chem.* **2012**, *77*, 9585-9592.

- [42] a) W. Rettig, *Angew. Chem. Int. Ed.* **1986**, *25*, 971-988; b) D. Oesch, N. W. Luedtke, *Chem. Commun.* **2015**, *51*, 12641-12644; c) Z. H. Guo, Z.-X. Jin, J.-Y. Wang, J. Pei, *Chem. Commun.* **2014**, *50*, 6088-6090; d) S. Chevreux, R. Paulino Neto, C. Allain, K. Nakatani, P. Jacques, I. Ciofini, G. Lemerrier, *Phys. Chem. Chem. Phys.* **2015**, *17*, 7639-7642; e) R. Ghosh, A. Nandi, D. K. Palit, *Phys. Chem. Chem. Phys.* **2016**, *18*, 7661-7671; f) H. Tanaka, K. Shizu, H. Nakanotani, C. Adachi, *Chem. Mater.* **2013**, *25*, 3766-3771.
- [43] a) I. A. Zhmyreva, V. V. Zelinskii, V. P. Kolobkov, N. D. Krasnitskaya, *Dokl. Akad. Nauk. SSSR* **1959**, *129*, 1089; *Chem. Abstr.* **1961**, *55*, 141336; b) K. Schwetlick, *Kinetic methods for studying reaction mechanisms*, p. 165, VEB Deut. Verlag Wiss., Berlin **1971**; *Chem. Abstr.* **1972**, *77*, 79990; c) C. Reichardt, T. Welton, *Solvents and Solvent Effects in Organic Chemistry*; 4th ed.; Wiley-VCH: Weinheim **2011**; ISBN 3-527-26805-7.
- [44] a) N. Miyaoura, A. Suzuki, *Chem. Rev.* **1995**, *95*, 2457-2483; b) N. Miyaoura, K. Yamada, A. Suzuki, *Tetrahedron Lett.* **1979**, *20*, 3437-3440; c) J. H. Kirchhoff, M. R. Netherton, I. D. Hill, G. C. Fu, *J. Am. Chem. Soc.* **2002**, *124*, 13662-13663.
- [45] a) D. Haas, J. M. Hammann, R. Greiner and P. Knochel, *ACS Catalysis* **2016**, *6*, 1540-1552; b) E.-i. Negishi, L. F. Valente and M. Kobayashi, *J. Am. Chem. Soc.* **1980**, *102*, 3298-3299; c) E.-i. Negishi, *Acc. Chem. Res.* **1982**, *15*, 340-348; d) A. de Meijere and F. Diederich, *Metal-Catalyzed Cross-Coupling Reactions*, Wiley-VCH, Weinheim, **2004**.
- [46] a) N. Barl, V. Werner, C. Saemann, P. Knochel, *Heterocycles* **2014**, *88*, 827-844; b) A. Krasovskiy, P. Knochel, *Angew. Chem. Int. Ed.* **2004**, *43*, 3333-3336.
- [47] a) K. Dimroth, C. Reichardt, T. Siepmann, F. Bohlmann, *Liebigs Ann. Chem.* **1963**, *661*, 1-37; b) C. Reichardt, *Angew. Chem. Int. Ed.* **1965**, *4*, 29-40; c) C. Reichardt, R. Müller, *Liebigs Ann. Chem.* **1976**, 1937-1952; d) C. Reichardt, *Pure Appl. Chem.* **2008**, *80*, 1415-1432; e) V. G. Machado, R. I. Stock, C. Reichardt, *Chem. Rev.* **2014**, *114*, 10429-10475; f) J. P. Cerón-Carrasco, D. Jacquemin, C. Laurence, A. Planchat, C. Reichardt, K. Sraïdi, *J. Phys. Org. Chem.* **2014**, *27*, 512-518; g) M. Afri, H. E. Gottlieb, A. A. Frimer, *Canad. J. Chem.* **2014**, *92*, 128-134; h) T. Etienne, C. Michaux, A. Monari, X. Assfeld, E. A. Perpète, *Dyes Pigments* **2014**, *100*, 24-31.
- [48] L. G. S. Brooker, A. C. Craig, D. W. Heseltine, P. W. Jenkins, L. L. Lincoln, *J. Am. Chem. Soc.* **1965**, *87*, 2443-2450.
- [49] N. B. Chapman, J. Shorter (Eds.), *Correlation Analysis in Chemistry - Recent Advances*, Plenum Press: New York, London, **1978**; ISBN 0-306-31068-6.
- [50] A. Kawski, P. Bojarski, B. Kukliński, *Chem. Phys. Lett.* **2008**, *463*, 410-412.
- [51] J.-L. M. Abboud, R. W. Taft, M. J. Kamlet, *J. Chem. Soc. Perkin Trans. II* **1985**, 815-819.
- [52] J. Catalán, *J. Phys. Chem. B* **2009**, *113*, 5951-5960.

References

- [53] C. Cao, X. Liu, Q. Qiao, M. Zhao, W. Yin, D. Mao, H. Zhang, Z. Xu, *Chem. Commun.* **2014**, 50, 15811-15814.
- [54] H. Langhals, S. Christian, A. Hofer, *J. Org. Chem.* **2013**, 78, 9883-9891.
- [55] H. Langhals, G. Schönmann, K. Polborn, *Chem. Eur. J.* **2008**, 14, 5290-5303.
- [56] a) R. Eberhardt, S. Löbbecke, B. Neidhardt, C. Reichardt, *Liebigs Ann./Recueil* **1997**, 1195-1199; b) C. Reichardt, *Chem. Rev.* **1994**, 94, 2319-2358; c) C. Reichardt, *Green Chem.* **2005**, 7, 339-351; d) C. Reichardt, G. Schäfer, *Liebigs Ann.* **1995**, 1579-1582.
- [57] a) I. G. Farbenindustrie AG, *Brit. Patent* GB 402309 (Mar 24, **1933**); *Chem. Abstr.*, **1934**, 28, 27267; b) Gevaert PhotoProducten N.V. (inv. W. K. Koerber, F. L. Schouteden) *Ger. Patent* DE 1108560 (June 6, **1957**); *Chem. Abstr.* **1962**, 56, 32447; c) B.M. Krasovitskii, D. G. Pereyaslova, E. G. Yushko, G. V. Tatsii, *Monokrist. Stsintill. Org. Lyuminafory* **1967**, 1, 92; *Chem. Abstr.* **1968**, 69, 60030.
- [58] b) C. McGill, A. Rappa, *Adv. Heterocycl. Chem.* **1988**, 44, 1-79.
- [59] a) A. E. Chichibabin, O. A. Zeide, *Zhur. Russ. Fiz. Khim. Obshch (J. Russ. Phys. Chem. Soc.)* **1914**, 46, 1216-1236; b) R. A. Abramovitch, F. Helmer, J. G. Saha, *Can. J. Chem.* **1965**, 43, 725-731; c) M. Wozniak, H.C. van der Plas, *J. Heterocycl. Chem.* **1978**, 15, 731-736.
- [60] a) J. H. Yao, C. Chi, J. Wu, K.-P. Loh, *Chem. Eur. J.* **2009**, 15, 9299-9302; b) S. Moez, *Dissertation* **2011**, LMU München.
- [61] A. M. Walter, *Dissertation* **2011**, LMU München.
- [62] A. A. Martínez, *Phys. perspect.* **2004**, 5, 4-28.
- [63] a) A. Einstein, *Zürich. Physik. Z.* **1910**, 10, 817-826; b) A. Einstein, *Über die Entwicklung unserer Anschauungen über das Wesen und die Konstitution der Strahlung*, in: 81. *Versammlung Deutscher Naturforscher und Ärzte zu Salzburg*, **1909**.
- [64] a) A. S. Davydov, *Zhur. Eksptl. i Teoret. Fiz.* **1948**, 18, 210-218; *Chem. Abstr.* **1949**, 43, 24604; b) A. S. Davydov, *Theory of molecular excitations*, Transl. H. Kasha, M. Oppenheimer Jr., McGraw-Hill, New York **1962**.
- [65] a) T. Förster, *Naturwiss.* **1946**, 33, 166-175; *Chem. Abstr.* **1947**, 41, 36668; b) T. Förster, *Ann. Phys.* 1948, 6(2), 55-75; *Chem. Abstr.* **1949**, 43, 31172. c) T. Förster, *Z. Elektrochem.* **1949**, 53, 93-99; *Chem. Abstr.* **1949**, 43, 33629; d) T. Förster, *Zeitschr. Naturforsch.* **1949**, 4a, 321-327; *Chem. Abstr.* **1950**, 44, 43074.
- [66] J. B. Perrin, *Fluorescence et radiochimie Conseil de Chemie*. 2nd ed., Solvay, Paris, 1924, Gauthier & Villar. pp 322-398; *Chem. Abstr.* **1926**, 20, 29565.
- [67] R. M. Clegg, *Reviews in Fluorescence* **2006**, (C. D. Geddes, J. R. Lakowicz, eds.), Springer US, New York, **2006**; DOI 10.1007/0-387-33016-X_1, ISBN 978-0-387-29342-4.

- [68] T. Förster, *Fluoreszenz organischer Verbindungen*, Göttingen, Vandenhoeck & Ruprecht, **1951**; *Chem. Abstr.* **1951**, 45, 26285.
- [69] C. Aubert, J. Fünfschilling, I. Zschokke-Gränacher, H. Langhals, *Zeitschr. Analyt. Chem.* **1985**, 320, 361-364.
- [70] a) J. Jose, K. Burgess, *Tetrahedron* **2006**, 62, 11021–11037; b) http://en.wikipedia.org/wiki/Nile_blue Nile blue. (July 8, **2014**).
- [71] R. Sens, K. H. Drexhage, *J. Lumin.* **1981**, 24-25, 709-712.
- [72] R. Sjöback, J. Nygren, M. Kubista, *Spectrochim. Acta A* **1995**, 51, L7-L21.
- [73] K. G. Casey, E. L. Quitevis, *J. Phys. Chem.* **1988**, 92, 6590–6594.
- [74] H. Langhals, *Angew. Chem. Int. Ed.* **1982**, 21, 724-733.
- [75] D. Zgela, *Dissertation*, LMU München, **2015**.
- [76] a) H. Yagi, *Proc. of the IRE* **1928**, 16, 715-740; b) K. Rothammel, *Antennenbuch*. 5th ed., Telekosmos Verlag, Stuttgart **1976**.
- [77] a) J. Li, A. Salandrino, N. Engheta, *Phys. Rev. B* **2007**, 76, 245403-245407; b) J. Li, A. Salandrino, N. Engheta, *Phys. Rev. B* **2009**, 79, 195104.
- [78] a) E. Nemeth, G. Schubert, V. Albrecht, F. Simon, *Aufbereitungs-Technik* **2005**, 46, 35-46; b) E. Nemeth, F. Simon, V. Albrecht, G. Schubert, *Ger. Patent No. 102004024754 B3*; *Chemical Abstracts* **2004**, 144, 392348; c) U. Gohs, V. Albrecht, K. Husemann, E. Reinsch, R. Schuenemann, F. Simon, *Ger. Offen. No. DE 102007055765 A1*; *Chemical Abstracts* **2009**, 151, 57663.
- [79] a) E. C. Corbet, J. G. Frey, R. I. Groce, P. J. Hendra, *Plast. Rubber Compos. Process. Appl.* **1994**, 21, 5-11; b) S. Rafi Ahmad, *Assem. Autom.* **2000**, 20, 58-65; c) M. K. Alam, S. L. Stanton, G. A. Hebner, *J. Spectrosc.* **1994**, 9, 31-39; d) D. M. Scott, *Meas. Sci. Technol.* **1995**, 6, 156-159; e) S. F. Hubbard, R. A. Potyrailo, P. Schottland, V. Thomas, *US Patent No. 2005/0095715 (2003)*; *Chem. Abstr.* **2005**, 142, 412287.
- [80] S. F. Hubbard, R. A. Potyrailo, P. Schottland, V. Thomas, *PCT Int. Appl., WO 2003006965 A1 20030123 (2003)*; *Chem. Abstr.* **2005**, 138, 107667.
- [81] a) H. Langhals, T. Schmid, M. Herman, M. Zwiener, A. Hofer, *Int. J. Environ. Eng.* **2013**, 7, 124-132; b) H. Langhals, T. Schmid, M. Herman, M. Zwiener, A. Hofer, *Ger. Offen. DE 102012012772.3*; *Chemical Abstracts* **2014**, 160, 63983.

- [82] a) G. Schopf, G. Koßmehl, *Polythiophenes: Electrically Conductive Polymers*, Springer, Berlin **1997**, ISBN 3-540-61483-4; ISBN 0-387-61483-4; b) A. J. Heeger, N. S. Sariciftci, E. B. Namdas, *Semiconducting and Metallic Polymers*, Oxford University Press, Oxford, 2010; ISBN 978-0-19-852864-7; c) D. Fichou, *Handbook of Oligo- and Polythiophenes*, Wiley-VCH, Weinheim **1999**, ISBN 3-527-29445-7. d) M. Weidelenner, C. D. Wessendorf, J. Hanisch, E. Ahlswede, G. Goetz, M. Linden, G. Schulz, E. Mena-Osteritz, A. Mishra, P. Baeuerle, *Chem. Commun.* **2013**, 49, 10865-10867; e) T. Keisuke, K. Masayoshi, K. Mutsumi, *ACS applied materials & interfaces* **2012**, 4, 6289-6294; f) S. E. Koh, C. Risko, D. A. da Silva Filho, O. Kwon, A. Facchetti, J.-L. Bredas, T. J. Marks, M. A. Ratner, *Adv. Funct. Mater.* **2008**, 18, 332-340.
- [83] R. S. Becker, J. Seixas de Melo, A. L. Maçanita, F. Elisei, *J. Phys. Chem.* **1996**, 100, 18683.
- [84] a) H. Dong, X. Fu, J. Liu, Z. Wang, W. Hu, Wenping, *Adv. Mater.* **2013**, 25, 6158-6183; b) D. M. DeLongchamp, R. J. Kline, D. A. Fischer, L. J. Richter, M. F. Toney, *Adv. Mater.* **2011**, 23, 319-337.
- [85] a) A. Krasovskiy, V. Malakhov, A. Gavryushin, P. Knochel, *Angew. Chem., Int. Ed.* **2006**, 45, 6040-6044; b) T. D. Blümke, F. M. Piller; P. Knochel, *Chem. Commun.* **2010**, 46, 4082-4084.
- [86] a) T. Otani, M. Hachiya, D. Hashizume, T. Matsuo, K. Tamao, *Chem. Asian J.* **2011**, 6, 350-354; b) Y. Shibata, T. Kono, N. Komura, Y. Yoshida, *Org. Electron.* **2013**, 14(4), 1073-1080; c) T. Inubushi, Y. Hattori, Y. Yamanoi, H. Nishihara, *J. Org. Chem.* **2014**, 79, 2974-2979; d) Y.-X. Peng, T. Tao, X.-X. Wang, B.-B. Ma, K. Zhang, W. Huang, *Chem. Asian J.* **2014**, 9, 3593-3603; e) M. Lu, S. Nagamatsu, Y. Yushida, M. Chikamatsu, R. Azumi, K. Yase, *Chem. Lett.* **2010**, 39, 60-61.
- [87] a) H. Hock, H. Kropf, *Angew. Chem.* **1957**, 69, 313-321; b) H. Hock, S. Lang, *Ber. dtsh. chem. Ges. B* **1944**, 77B, 257-264; *Chem. Abstr.* **1945**, 39, 22122; c) H.-J. Arpe, K. Weissermel, *Industrielle Organische Chemie: Bedeutende Vor- und Zwischenprodukte*, 6. Ed., Wiley-VCH, New York, **2007**, pp. 418.
- [88] a) P. D. Bartlett, L. H. Knox, *J. Am. Chem. Soc.* **1939**, 61, 3184-3192; b) U. Schöllkopf, *Angew. Chem.* **1960**, 72, 147-159; c) R. C. Fort, P. v. R. Schleyer in H. Hart, G. J. Karabatsos, *Advances in Alicyclic Chemistry*, **1966**, 1; d) R. C. Fort in G. A. Olah, P. v. R. Schleyer, *Carbonium Ions*, J. Wiley-Interscience, New York, **1973**, Vol. IV, pp. 1783.
- [89] a) W. Hoek, J. Strating, H. Wynberg, *Rec. Trav. Chim. Pays-Bas* **1966**, 85, 1045-1053; b) S. Brase, B. Waegell, A. De Meijere, *Synthesis* **1998**, 148-152; c) V. V. Kovalev, Y. N. Luzikov, Y. I. Savel'ev, *Neftekhimiya* **1989**, 29, 628-643.
- [90] H. Langhals, C. Rüchardt, *Chem. Ber.* **1981**, 114, 3831-3854.
- [91] C. Sämann, V. Dhayalan, P. Schreiner, P. Knochel, *Org. Lett.* **2014**, 16, 2418-2421.
- [92] J. E. Milne, S. L. Buchwald, *J. Am. Chem. Soc.* **2004**, 126, 13028-13032.

- [93] a) S. L. Bondarev, I. I. Ivanov, Y. N. Romashin, O. G. Kulinkovich, *Zh. Prikl. Spektrosk.* **1992**, *56*, 739-744; *Chem. Abstr.* **1992**, *117*, 180817; b) J. Gierschner, H.-G. Mack, H.-J. Egelhaaf, S. Schweizer, B. Doser, D. Oelkrug, *Synth. Met.* **2003**, *138*, 311-315; c) D. Wasserberg, P. Marsal, S. C. J. Meskers, R. A. J. Janssen, D. Beljonne, *J. Phys. Chem. B* **2005**, *109*, 4410-4415.
- [94] a) S. Ellinger, U. Ziener, U. Thewalt, K. Landfester, M. Möller, *Chem. Mater.* **2007**, *19*(5), 1070-1075; b) M. Kirkus, L. Wang, S. Mothy, D. Beljonne, J. Cornil, R. A. J. Janssen, S. C. J. Meskers, *J. Phys. Chem. A* **2012**, *116*, 7927-7936; c) J. Mizuguchi, *J. Imaging Sci. Technol.* **2002**, *46*, 257-261; d) J. Mizuguchi, *J. Phys. Chem. A* **2000**, *104*, 1817-1821.
- [95] a) J. C. Horne, G. J. Blanchard, E. LeGoff, *J. Am. Chem. Soc.* **1995**, *117*, 9551-9558; b) H. Tang, L. Zhu, Y. Harima, K. Yamashita, K. L. Kazuo, N. A. Kyung, M. Ishikawa, *J. Chem. Soc., Perkin 2* **2000**, 1976-1979.
- [96] a) F. Van Bolhuis, H. Wynberg, *Synth. Met.* **1989**, *30*, 381-389; b) C. Y. Yang, Y. Yang, *Mol. Cryst. Liq. Cryst.* **1995**, *270*, 113-122; c) L. Antolini, G. Horowitz, F. Kouki, F. Garnier, *Adv. Mater.* **1998**, *10*, 382-385; d) G. Horowitz, B. Bachet, A. Yassar, P. Lang, F. Demanze, J.-L. Fave, F. Garnier, *Chem. Mater.* **1996**, *7*, 1337-1341.
- [97] a) N. DiCésare, M. Belletête, A. Donat-Bouillud, M. Leclerc, G. Durocher, *Macromolecules* **1998**, *31*, 6289-6296; b) N. DiCésare, M. Belletête, A. Donat-Bouillud, M. Leclerc, G. Durocher, *J. Lumin.* **1999**, *81*, 111-125.
- [98] F. Costanzo, D. Tonelli, G. Scalmani, J. Cornil, *Polymer* **2006**, *47*, 6692-6697.
- [99] (a) R. H. Abu-Eittah, F. A. Al-Sugeir, *Bull. Chem. Soc. Jpn.* **1985**, *58*, 2126-2132; b) J.-Y. Balandier, F. Quist, C. Amato, S. Bouzakraoui, J. Cornil, S. Sergeyev, Y. Geerts, *Tetrahedron* **2010**, *66*, 9560-9572; c) F. Effenberger, F. Würthner, F. Steybe, *J. Org. Chem.* **1995**, *60*, 2082-2091; d) P. Garcia, J. M. Pernaut, P. Hapiot, V. Wintgens, P. Valat, F. Garnier, D. Delabouglise, *J. Phys. Chem.* **1993**, *97*, 513-516; e) S. Li, J. Yan, C.-Z. Li, F. Liu, M. Shi, H. Chen, T. P. Russell, *J. Mater. Chem. A* **2016**, *4*, 3777-3783; f) T. Vikramaditya, M. Saisudhakar, K. Sumithra, *J. Mol. Struct.* **2015**, *1081*, 114-123.
- [100] a) H. Wynberg, A. Bantjes, *J. Am. Chem. Soc.* **1960**, *82*, 1447-1450; b) M. A. Hempenius, B. M. W. Langeveld-Voss, J. A. H. van Haare, R. A. J. Janssen, S. S. Sheiko, J. P. Spatz, M. Möller, E. W. Meijer, *J. Am. Chem. Soc.* **1998**, *120*, 2798-2804; c) J. Kagan, S. K. Arora, A. Üstünoğlu, *J. Org. Chem.* **1983**, *48*, 4076-4078.
- [101] M. Treiber, S. Giebeler, T. Lessing, T. J. J. Müller, *Organ. Biomol. Chem.* **2013**, *11*, 3541-3552.
- [102] a) S. Joshi, R. M. Patel, P.M. Patel, *J. Polym. Res.* **2003**, *10*(4), 235-239; b) W. E. Truce, C. W. Vriesen, *J. Am. Chem. Soc.* **1953**, *75*, 5032-5036.
- [103] a) S. M. Hosseini, S. Hashem, *J. Org. Chem.* **2004**, *69*(20), 6953-6956; b) V. Lukeš, M. Danko, A. Andicsová, P. Hrdlovič, D. Végh, *Synt. Met.* **2013**, *165*, 17-26.

- [104] M. Hosseini-Sarvari, M. Tavakolian, *Appl. Cat. A* **2012**, 441-442, 65-71.
- [105] a) S. J. T. Rezaei, M. R. Nabid, S. Z. Hosseini, M. Abedi, *Synth. Commun.* **2012**, 42(10), 1432-1444. (b) M. Raula, M. H. Rashid, T. K. Paira, E. Dinda, T. K. Mandal, *Langmuir* **2010**, 26, 8769-8782.
- [106] S. Ashoka, P. Chithaiah, K. V. Thipperudraiah, G. T. Chandrappa, *Inorg. Chim. Acta* **2010**, 363(13), 3442-3447.
- [107] M. H. Sarvari, H. Sharghi, *J. Org. Chem.* **2004**, 69, 6953-6956.
- [108] S. Portnoy, H. Gisser, *J. Org. Chem.* **1967**, 233-234.
- [109] a) D. Karthik; K.R. Justin Thomas; J.-H. Jou, S. Kumar, Y.-L. Chen; Y.-C. Jou, *RCS Advances* **2015**, 5, 8727-8738; b) S. N. Lee, S. J. Lee, Y. K. Kim, D. M. Shin, *Mol. Cryst. Liq. Cryst.* **2013**, 581, 59-69; c) K. H. Lee, S. O. Kim, S. Kang, J. Y. Lee, K. S. Yook, J. Y. Lee, S. S. Yoon, *J. Org. Chem.* **2012**, 77, 2748-2755.
- [110] a) G. Schnurpfeil, A. K. Sobbi, W. Spiller, H. Kliesch, D. Wöhrle, *J. Porphyrins Phthalocyanines* **1997**, 1, 159-167; b) K. Yoshida, M. Nakamura, Y. Kazue, N. Tachikawa, S. Tsuzuki, S. Seki, K. Dokko, M. Watanabe, *J. Am. Chem. Soc.* **2011**, 133, 13121-13129.
- [111] H. Langhals, J. Karolin, L. B.-Å. Johansson, *J. Chem. Soc. Faraday Trans.* **1998**, 94, 2919-2922.

Images:

- p. 15 Prism: <https://globalleadershipprograms.files.wordpress.com/2012/08/prisma.jpg>, accessed on Oct. 3rd 2016.
- p. 69 Waves: http://static.nautil.us/2895_6b8b8e3bd6ad94b985c1b1f1b7a94cb2.jpg, accessed on Oct. 6th 2016.
- p. 81 Polymer flakes: http://www.instituteofmaking.org.uk/assets/_files/uploads/IMG_5867.jpg, accessed on Oct. 3rd 2016
Laser: <http://i.imgur.com/mq0TZxJ.jpg>, accessed on Oct. 6th 2016.
- p. 99 Registered Jacks: <http://newatlas.com/optical-fiber-throughput-breakthrough/30038>; accessed on Oct. 5th 2016.